Gamma-Ray Bursts

Contents

1 Topics **187**

2 Participants **189**
2.1 ICRANet participants 189
2.2 Past collaborators 189
2.3 Ongoing collaborations 191
2.4 Students 192

3 Selected publications before 2005 **195**
3.1 Refereed journals 195
3.2 Conference proceedings 202

4 Publications (2005–2023) **207**
4.1 Refereed journals 207
4.2 Conference proceedings 250

1 Topics

- GRB classification in different families with different progenitor systems.
- "Genuine short" GRBs: Possible identifications and selection effects
- The observed spectra of the P-GRBs.
- GRB prompt emission spectra below 5 keV: challenges for future missions.
- Interpretation of the ultra high energy emission from GRBs observed by Fermi, AGILE and MAGIC.
- Analysis of different families of progenitors for GRBs with different energetics.
- GRBs at redshift $z > 6$.
- GRBs originating from a multiple collapse.
- Emission from newly born neutron stars, or "neo neutron stars" (νNS).
- Induced Gravitational Collapse process for GRBs associated with supernovae.
- Redshift estimators for GRBs with no measured redshift.
- Binary Driven Hypernovae (BdHNe) as progenitor of GRBs via Induced Gravitational Collapse.
- GRB light curves as composed of different episodes.
- "Cosmic Matrix" for GRBs.
- GRB X-Ray Flares and Gamma-Ray Flares.

- GRB afterglow theory consistent with the mildly relativistic velocities inferred from the observations.
- Extended thermal emission components in GRBs.
- GRBs from merging white dwarfs.
- "Inner engine" of GRB emission.
- Quantized emission in GRBs.
- Redshift distribution of all different GRB families.
- Observations of early X-ray afterglow emission in high-redshift GRBs: implications for the νNS-rise.

2 Participants

2.1 ICRANet participants

- David Arnett
- Carlo Luciano Bianco
- Massimo Della Valle
- Li Liang
- Rahim Moradi
- Jorge Armando Rueda Hernandez
- Remo Ruffini
- Narek Sahakyan
- Gregory Vereshchagin
- Yu Wang
- She-Sheng Xue

2.2 Past collaborators

- Andrey Baranov
- Maria Grazia Bernardini (OAB, Italy)
- Joao Braga (INPE, Brazil)
- Sabrina Casanova (MPIK, Germany)

- Letizia Caito
- Pascal Chardonnet (Université de Savoie, France)
- Guido Chincarini (Università di Milano “Bicocca”, Italy)
- Demetrios Christodoulou (ETH Zurich, Switzerland)
- Alessandra Corsi (INAF-IASF Roma, Italy)
- Valeri Chechetkin
- Maria Giovanna Dainotti
- Thibault Damour (IHES, France)
- Maxime Enderli
- Walter Ferrara
- Federico Fraschetti (CEA Saclay, France)
- Roberto Guida
- Vahe Gurzadyan (Yerevan Physics Institute, Armenia)
- Wen-Biao Han
- Milos Kovacevic
- Massimiliano Lattanzi (Oxford Astrophysics, UK)
- Vincenzo Liccardo
- Hendrik Ludwig
- Marco Muccino
- Nino Panagia
- Barbara Patricelli (Pisa University, Italy)
- Elena Pian
- Giovanni Battista Pisani

- Giuliano Preparata (Università di Milano, Italy)
- Daria Primorac
- Jay D. Salmonson (Livermore Lab, USA)
- Vineeth Valsan
- Jim Wilson (Livermore Lab, USA)

2.3 Ongoing collaborations

- Alexey Aksenov (ITEP, Russia)
- Lorenzo Amati (INAF-IASF Bologna, Italy)
- Ulisses Barres de Almeida (CBPF, Brazil)
- Laura Marcela Becerra Bayona (Universidad Industrial de Santander, Colombia)
- Riccardo Belvedere (ICRANet-Rio, Brazil)
- Sandip Kumar Chakrabarti (S.N. Bose National Centre and Indian Centre for Space Physics, India)
- Christian Cherubini (Università Campus Biomedico, Italy)
- Alessandro Chieffi (INAF-IASF Roma, Italy)
- Stefano Covino (OAB, Italy)
- Gustavo de Barros (UFRJ, Brazil)
- Simonetta Filippi (Università Campus Biomedico, Italy)
- Filippo Frontera (Università di Ferrara, Italy)
- Chris Fryer (Los Alamos National Laboratories, USA).
- Dafne Guetta (OAR, Italy)
- Cristiano Guidorzi (OAB, Italy)

- Stanislav Kelner (MEPhI, Russia, and MPIK, Germany)
- Marco Limongi (OAR, Italy)
- Clovis Maia (University of Brasilia, Brazil)
- Vanessa Mangano (INAF-IASF Palermo, Italy)
- Marco Marongiu (INAF - Cagliari Observatory and University of Ferrara, Italy)
- Grant Mathews (University of Notre Dame, USA)
- Taghi Mirtorabi (Alzahra University, Tehran, Iran)
- Ana Virginia Penacchioni (INPE, Brazil)
- Luis Juracy Rangel Lemos (Fundação Universidade Federal do Tocantins, Brazil)
- Felix Ryde (KTH Royal Institute of Technology, Stockholm, Sweden)
- Soroush Shakeri (Isfahan University of Technology, Iran)
- Ivan Siutsou (ICRANet-Rio, Brazil)
- Bing Zhang (University of Nevada, USA)
- Susanna Vergani (Dunsink Observatory, Ireland)
- Francesco Vissani (INFN, Italy)
- Elena Zaninoni (ICRANet-Rio, Brazil)

2.4 Students

- Yerlan Aimuratov (IRAP PhD, Kazakhstan)
- Stefano Campion (IRAP PhD, Italy)
- Yen-Chen Chen (IRAP-PhD, China-Taiwan)
- Mile Karlika (IRAP PhD, Croatia)

- Ronaldo V. Lobato (IRAP-PhD, Brazil)
- J. David Melon Fuksman (IRAP PhD, Argentina)
- Jose Fernando Rodriguez Ruiz (IRAP PhD, Colombia)
- Shurui Zhang (JIRA PhD, China)

3 Selected publications before 2005

3.1 Refereed journals

1. D. Christodoulou, R. Ruffini; "Reversible Transformations of a Charged Black Hole"; Physical Review D, 4, 3552 (1971).

   A formula is derived for the mass of a black hole as a function of its "irreducible mass", its angular momentum, and its charge. It is shown that 50% of the mass of an extreme charged black hole can be converted into energy as contrasted with 29% for an extreme rotating black hole.

2. T. Damour, R. Ruffini; "Quantum electrodynamical effects in Kerr-Newman geometries"; Physical Review Letters, 35, 463 (1975).

   Following the classical approach of Sauter, of Heisenberg and Euler and of Schwinger the process of vacuum polarization in the field of a "bare" Kerr-Newman geometry is studied. The value of the critical strength of the electromagnetic fields is given together with an analysis of the feedback of the discharge on the geometry. The relevance of this analysis for current astrophysical observations is mentioned.

3. G. Preparata, R. Ruffini, S.-S. Xue; "The dyadosphere of black holes and gamma-ray bursts"; Astronomy & Astrophysics, 338, L87 (1999).

   The "dyadosphere" has been defined as the region outside the horizon of a black hole endowed with an electromagnetic field (abbreviated to EMBH for "electromagnetic black hole") where the electromagnetic field exceeds the critical value, predicted by Heisenberg & Euler for $e^{\pm}$ pair production. In a very short time ($\sim O(\hbar/mc^2)$) a very large number of pairs is created there. We here give limits on the EMBH parameters leading to a Dyadosphere for $10M_{\odot}$ and $10^5 M_{\odot}$ EMBH's, and give as well the pair densities as functions of the radial coordinate. We here assume that the pairs reach thermodynamic equilibrium with a photon gas and estimate the average energy per pair as a function of the EMBH mass. These data give the initial conditions for the analysis of an enormous pair-electromagnetic-pulse or "P.E.M. pulse" which naturally leads to relativistic expansion. Basic energy requirements for gamma ray bursts (GRB), including GRB971214 recently observed at z=3.4, can be accounted for by processes occurring in the dyadosphere. In this letter we do not address the problem of forming either the EMBH or the dyadosphere: we establish some inequalities which must be satisfied during their formation process.

4. R. Ruffini, J.D. Salmonson, J.R. Wilson, S.-S. Xue; "On the pair electromagnetic pulse of a black hole with electromagnetic structure"; Astronomy & Astrophysics, 350, 334 (1999).

   We study the relativistically expanding electron-positron pair plasma formed by the process of vacuum polarization around an electromagnetic black hole (EMBH). Such processes can occur for EMBH's with mass all the way up to $6 \times 10^5 M_\odot$. Beginning with a idealized model of a Reissner-Nordstrom EMBH with charge to mass ratio $\xi = 0.1$, numerical hydrodynamic calculations are made to model the expansion of the pair-electromagnetic pulse (PEM pulse) to the point that the system is transparent to photons. Three idealized special relativistic models have been compared and contrasted with the results of the numerically integrated general relativistic hydrodynamic equations. One of the three models has been validated: a PEM pulse of constant thickness in the laboratory frame is shown to be in excellent agreement with results of the general relativistic hydrodynamic code. It is remarkable that this precise model, starting from the fundamental parameters of the EMBH, leads uniquely to the explicit evaluation of the parameters of the PEM pulse, including the energy spectrum and the astrophysically unprecedented large Lorentz factors (up to 6×10^3 for a $10^3 M_\odot$ EMBH). The observed photon energy at the peak of the photon spectrum at the moment of photon decoupling is shown to range from 0.1 MeV to 4 MeV as a function of the EMBH mass. Correspondingly the total energy in photons is in the range of 10^{52} to 10^{54} ergs, consistent with observed gamma-ray bursts. In these computations we neglect the presence of baryonic matter which will be the subject of forthcoming publications.

5. R. Ruffini, J.D. Salmonson, J.R. Wilson, S.-S. Xue; "On the pair-electro magnetic pulse from an electromagnetic black hole surrounded by a baryonic remnant"; Astronomy & Astrophysics, 359, 855 (2000).

   The interaction of an expanding Pair-Electromagnetic pulse (PEM pulse) with a shell of baryonic matter surrounding a Black Hole with electromagnetic structure (EMBH) is analyzed for selected values of the baryonic mass at selected distances well outside the dyadosphere of an EMBH. The dyadosphere, the region in which a super critical field exists for the creation of e+e- pairs, is here considered in the special case of a Reissner-Nordstrom geometry. The interaction of the PEM pulse with the baryonic matter is described using a simplified model of a slab of constant thickness in the laboratory frame (constant-thickness approximation) as well as performing the integration of the general relativistic hydrodynamical equations. Te validation of the constant-thickness approximation, already presented in a previous paper Ruffini et al. (1999) for a PEM pulse in vacuum, is here generalized to the presence of baryonic matter. It is found that for a baryonic shell of mass-energy less than 1% of the total energy of the dyadosphere, the constant-thickness approximation is in excellent agreement with full general relativistic computations. The approximation breaks down for larger values of the baryonic shell mass, however such cases are of less interest for observed Gamma Ray Bursts (GRBs). On the basis of numerical computations of the slab model for PEM pulses, we describe (i) the properties of relativistic evolution of a PEM pulse colliding with a baryonic shell; (ii) the details of the expected emission energy and observed temperature of the associated GRBs for a given value of the EMBH mass; $10^3 M_\odot$, and for baryonic mass-energies in the range 10^{-8} to 10^{-2} the total energy of the dyadosphere.

6. C.L. Bianco, R. Ruffini, S.-S. Xue; "The elementary spike produced by a pure e+e- pair-electromagnetic pulse from a Black Hole: The PEM Pulse"; Astronomy & Astrophysics, 368, 377 (2001).

   In the framework of the model that uses black holes endowed with electromagnetic structure (EMBH) as the energy source, we study how an elementary spike appears to the detectors. We consider the simplest possible case of a pulse produced by a pure e^+e^- pair-electro-magnetic plasma, the PEM pulse, in the absence of any baryonic matter. The resulting time profiles show a *Fast-Rise-Exponential-Decay* shape, followed by a power-law tail. This is obtained without any special fitting procedure, but only by fixing the energetics of the process taking place in a given EMBH of selected mass, varying in the range from 10 to 10^3 $M_\odot$ and considering the relativistic effects to be expected in an electron-positron plasma gradually reaching transparency. Special attention is given to the contributions from all regimes with Lorentz γ factor varying from $\gamma = 1$ to $\gamma = 10^4$ in a few hundreds of the PEM pulse travel time. Although the main goal of this paper is to obtain the elementary spike intensity as a function of the arrival time, and its observed duration, some qualitative considerations are also presented regarding the expected spectrum and on its departure from the thermal one. The results of this paper will be comparable, when data will become available, with a subfamily of particularly short GRBs not followed by any afterglow. They can also be propedeutical to the study of longer bursts in presence of baryonic matter currently observed in GRBs.

7. R. Ruffini, C.L. Bianco, P. Chardonnet, F. Fraschetti, S.-S. Xue; "Relative spacetime transformations in Gamma-Ray Bursts"; The Astrophysical Journal, 555, L107 (2001).

   The GRB 991216 and its relevant data acquired from the BATSE experiment and RXTE and Chandra satellites are used as a prototypical case to test the theory linking the origin of gamma ray bursts (GRBs) to the process of vacuum polarization occurring during the formation phase of a black hole endowed with electromagnetic structure (EMBH). The relative space-time transformation paradigm (RSTT paradigm) is presented. It relates the observed signals of GRBs to their past light cones, defining the events on the worldline of the source essential for the interpretation of the data. Since GRBs present regimes with unprecedently large Lorentz γ factor, also sharply varying with time, particular attention is given to the constitutive equations relating the four time variables: the comoving time, the laboratory time, the arrival time at the detector, duly corrected by the cosmological effects. This paradigm is at the very foundation of any possible interpretation of the data of GRBs.

8. R. Ruffini, C.L. Bianco, P. Chardonnet, F. Fraschetti, S.-S. Xue; "On the interpretation of the burst structure of Gamma-Ray Bursts"; The Astrophysical Journal, 555, L113 (2001).

   Given the very accurate data from the BATSE experiment and RXTE and Chandra satellites, we use the GRB 991216 as a prototypical case to test the EMBH theory linking the origin of the energy of GRBs to the electromagnetic energy of black holes. The fit of the afterglow fixes the only two free parameters of the model and leads to a new paradigm for the interpretation of the burst structure, the IBS paradigm. It leads as well to a reconsideration of the relative roles of the afterglow and burst in GRBs by defining two new phases in this complex phenomenon: a) the injector phase, giving rise to the proper-GRB (P-GRB), and b) the beam-target phase, giving rise to the extended afterglow peak emission (E-APE) and to the afterglow. Such differentiation leads to a natural possible explanation of the bimodal distribution of GRBs observed by BATSE. The agreement with the observational data in regions extending from the horizon of the EMBH all the way out to the distant observer confirms the uniqueness of the model.

9. R. Ruffini, C.L. Bianco, P. Chardonnet, F. Fraschetti, S.-S. Xue; "On a possible Gamma-Ray Burst-Supernova time sequence"; The Astrophysical Journal, 555, L117 (2001).

   The data from the Chandra satellite on the iron emission lines in the afterglow of GRB 991216 are used to give further support for the EMBH theory, which links the origin of the energy of GRBs to the extractable energy of electromagnetic black holes (EMBHs), leading to an interpretation of the GRB-supernova correlation. Following the relative space-time transformation (RSTT) paradigm and the interpretation of the burst structure (IBS) paradigm, we introduce a paradigm for the correlation between GRBs and supernovae. The following sequence of events is shown as kinematically possible and consistent with the available data: a) the GRB-progenitor star P_1 first collapses to an EMBH, b) the proper GRB (P-GRB) and the peak of the afterglow (E-APE) propagate in interstellar space until the impact on a supernova-progenitor star P_2 at a distance $\leq 2.69 \times 10^{17}$ cm, and they induce the supernova explosion, c) the accelerated baryonic matter (ABM) pulse, originating the afterglow, reaches the supernova remnants 18.5 hours after the supernova explosion and gives rise to the iron emission lines. Some considerations on the dynamical implementation of the paradigm are presented. The concept of induced supernova explosion introduced here specifically for the GRB-supernova correlation may have more general application in relativistic astrophysics.

10. R. Ruffini, C.L. Bianco, P. Chardonnet, F. Fraschetti, S.-S. Xue; "On the physical processes which lie at the bases of time variability of GRBs"; Il Nuovo Cimento B, 116, 99 (2001).

    The relative-space-time-transformation (RSTT) paradigm and the interpretation of the burst-structure (IBS) paradigm are applied to probe the origin of the time variability of GRBs. Again GRB 991216 is used as a prototypical case, thanks to the precise data from the CGRO, RXTE and Chandra satellites. It is found that with the exception of the relatively inconspicuous but scientifically very important signal originating from the initial "proper gamma ray burst" (P-GRB), all the other spikes and time variabilities can be explained by the interaction of the accelerated-baryonic-matter pulse with inhomogeneities in the interstellar matter. This can be demonstrated by using the RSTT paradigm as well as the IBS paradigm, to trace a typical spike observed in arrival time back to the corresponding one in the laboratory time. Using these paradigms, the identification of the physical nature of the time variablity of the GRBs can be made most convincingly. It is made explicit the dependence of a) the intensities of the afterglow, b) the spikes amplitude and c) the actual time structure on the Lorentz gamma factor of the accelerated-baryonic-matter pulse. In principle it is possible to read off from the spike structure the detailed density contrast of the interstellar medium in the host galaxy, even at very high redshift.

11. R. Ruffini, C.L. Bianco, P. Chardonnet, F. Fraschetti, S.-S. Xue; "On the structures in the afterglow peak emission of gamma ray bursts"; The Astrophysical Journal, 581, L19 (2002).

    Using GRB 991216 as a prototype, it is shown that the intensity substructures observed in what is generally called the "prompt emission" in gamma ray bursts (GRBs) do originate in the collision between the accelerated baryonic matter (ABM) pulse with inhomogeneities in the interstellar medium (ISM). The initial phase of such process occurs at a Lorentz factor $\gamma \sim 310$. The crossing of ISM inhomogeneities of sizes $\Delta R \sim 10^{15}$ cm occurs in a detector arrival time interval of ~ 0.4 s implying an apparent superluminal behavior of $\sim 10^5 c$. The long lasting debate between the validity of the external shock model vs. the internal shock model for GRBs is solved in favor of the first.

12. R. Ruffini, C.L. Bianco, P. Chardonnet, F. Fraschetti, S.-S. Xue; "On the structure of the burst and afterglow of Gamma-Ray Bursts I: the radial approximation"; International Journal of Modern Physics D, 12, 173 (2003).

    We have recently proposed three paradigms for the theoretical interpretation of gamma-ray bursts (GRBs). (1) The relative space-time transformation (RSTT) paradigm emphasizes how the knowledge of the entire world-line of the source from the moment of gravitational collapse is a necessary condition in order to interpret GRB data. (2) The interpretation of the burst structure (IBS) paradigm differentiates in all GRBs between an injector phase and a beam-target phase. (3) The GRB-supernova time sequence (GSTS) paradigm introduces the concept of *induced supernova explosion* in the supernovae-GRB association. In the introduction the RSTT and IBS paradigms are enunciated and illustrated using our theory based on the vacuum polarization process occurring around an electromagnetic black hole (EMBH theory). The results are summarized using figures, diagrams and a complete table with the space-time grid, the fundamental parameters and the corresponding values of the Lorentz gamma factor for GRB 991216 used as a prototype. In the following sections the detailed treatment of the EMBH theory needed to understand the results of the three above letters is presented. We start from the considerations on the dyadosphere formation. We then review the basic hydrodynamic and rate equations, the equations leading to the relative space-time transformations as well as the adopted numerical integration techniques. We then illustrate the five fundamental eras of the EMBH theory: the self acceleration of the e^+e^- pair-electromagnetic plasma (PEM pulse), its interaction with the baryonic remnant of the progenitor star, the further self acceleration of the e^+e^- pair-electroma--gnetic radiation and baryon plasma (PEMB pulse). We then study the approach of the PEMB pulse to transparency, the emission of the proper GRB (P-GRB) and its relation to the "short GRBs". Particular attention is given to the free parameters of the theory and to the values of the thermodynamical quantities at transparency. Finally the three different regimes of the afterglow are described within the fully radiative and radial approximations: the ultrarelativistic, the relativistic and the nonrelativistic regimes. The best fit of the theory leads to an unequivocal identification of the "long GRBs" as extended emission occurring at the afterglow peak (E-APE). The relative intensities, the time separation and the hardness ratio of the P-GRB and the E-APE are used as distinctive observational test of the EMBH theory and the excellent agreement between our theoretical predictions and the observations are documented. The afterglow power-law indexes in the EMBH theory are compared and contrasted with the ones in the literature, and no beaming process is found for GRB 991216. Finally, some preliminary results relating the observed time variability of the E-APE to the inhomogeneities in the interstellar medium are presented, as well as some general considerations on the EMBH formation. The issue of the GSTS paradigm will be the object of a forthcoming publication and the relevance of the iron-lines observed in GRB 991216 is shortly reviewed. The general conclusions are then presented based on the three fundamental parameters of the EMBH theory: the dyadosphere energy, the baryonic mass of the remnant, the interstellar medium density. An in depth discussion and comparison of the EMBH theory with alternative theories is presented as well as indications of further developments beyond the radial approximation, which will be the subject of paper II in this series. Future needs for specific GRB observations are outlined.

13. R. Ruffini, C.L. Bianco, P. Chardonnet, F. Fraschetti, V. Gurzadyan, S.-S. Xue; “On the instantaneous spectrum of gamma ray bursts”; International Journal of Modern Physics D, 13, 843 (2004).

    A theoretical attempt to identify the physical process responsible for the afterglow emission of Gamma-Ray Bursts (GRBs) is presented, leading to the occurrence of thermal emission in the comoving frame of the shock wave giving rise to the bursts. The determination of the luminosities and spectra involves integration over an infinite number of Planckian spectra, weighted by appropriate relativistic transformations, each one corresponding to a different viewing angle in the past light cone of the observer. The relativistic transformations have been computed using the equations of motion of GRBs within our theory, giving special attention to the determination of the equitemporal surfaces. The only free parameter of the present theory is the “effective emitting area” in the shock wave front. A self consistent model for the observed hard-to-soft transition in GRBs is also presented. When applied to GRB 991216 a precise fit $\left(\chi^2 \simeq 1.078\right)$ of the observed luminosity in the 2–10 keV band is obtained. Similarly, detailed estimates of the observed luminosity in the 50–300 keV and in the 10–50 keV bands are obtained.

3.2 Conference proceedings

1. R. Ruffini; “Beyond the critical mass: The dyadosphere of black holes”; in “Black Holes and High Energy Astrophysics”, H. sato, N. Sugiyama, Editors; p. 167; Universal Academy Press (Tokyo, Japan, 1998).

   The “dyadosphere” (from the Greek word “duas-duados” for pairs) is here defined as the region outside the horizon of a black hole endowed with an electromagnetic field (abbreviated to EMBH for “electromagnetic black hole”) where the electromagnetic field exceeds the critical value, predicted by Heisenberg and Euler for e^+e^- pair production. In a very short time ($\sim O(\hbar/mc^2)$), a very large number of pairs is created there. I give limits on the EMBH parameters leading to a Dyadosphere for $10M_\odot$ and $10^5M_\odot$ EMBH’s, and give as well the pair densities as functions of the radial coordinate. These data give the initial conditions for the analysis of an enormous pair-electromagnetic-pulse or “PEM-pulse” which naturally leads to relativistic expansion. Basic energy requirements for gamma ray bursts (GRB), including GRB971214 recently observed at $z = 3.4$, can be accounted for by processes occurring in the dyadosphere.

2. R. Ruffini, C.L. Bianco, P. Chardonnet, F. Fraschetti, L. Vitagliano, S.-S. Xue; "New perspectives in physics and astrophysics from the theoretical understanding of Gamma-Ray Bursts"; in "COSMOLOGY AND GRAVITATION: Xth Brazilian School of Cosmology and Gravitation; 25th Anniversary (1977-2002)", Proceedings of the Xth Brazilian School on Cosmology and Gravitation, Mangaratiba, Rio de Janeiro (Brazil), July - August 2002, M. Novello, S.E. Perez Bergliaffa, Editors; AIP Conference Proceedings, 668, 16 (2003).

   If due attention is given in formulating the basic equations for the Gamma-Ray Burst (GRB) phenomenon and in performing the corresponding quantitative analysis, GRBs open a main avenue of inquiring on totally new physical and astrophysical regimes. This program is very likely one of the greatest computational efforts in physics and astrophysics and cannot be actuated using shortcuts. A systematic approach is needed which has been highlighted in three basic new paradigms: the relative space-time transformation (RSTT) paradigm, the interpretation of the burst structure (IBS) paradigm, the GRB-supernova time sequence (GSTS) paradigm. From the point of view of fundamental physics new regimes are explored: (1) the process of energy extraction from black holes; (2) the quantum and general relativistic effects of matter-antimatter creation near the black hole horizon; (3) the physics of ultrarelativisitc shock waves with Lorentz gamma factor $\gamma > 100$. From the point of view of astronomy and astrophysics also new regimes are explored: (i) the occurrence of gravitational collapse to a black hole from a critical mass core of mass $M \gtrsim 10M_{\odot}$, which clearly differs from the values of the critical mass encountered in the study of stars "catalyzed at the endpoint of thermonuclear evolution" (white dwarfs and neutron stars); (ii) the extremely high efficiency of the spherical collapse to a black hole, where almost 99.99% of the core mass collapses leaving negligible remnant; (iii) the necessity of developing a fine tuning in the final phases of thermonuclear evolution of the stars, both for the star collapsing to the black hole and the surrounding ones, in order to explain the possible occurrence of the "induced gravitational collapse". New regimes are as well encountered from the point of view of nature of GRBs: (I) the basic structure of GRBs is uniquely composed by a proper-GRB (P-GRB) and the afterglow; (II) the long bursts are then simply explained as the peak of the afterglow (the E-APE) and their observed time variability is explained in terms of inhomogeneities in the interstellar medium (ISM); (III) the short bursts are identified with the P-GRBs and the crucial information on general relativistic and vacuum polarization effects are encoded in their spectra and intensity time variability. A new class of space missions to acquire information on such extreme new regimes are urgently needed.

3. R. Ruffini, C.L. Bianco, P. Chardonnet, F. Fraschetti, S.-S. Xue; "The EMBH Model in GRB 991216 and GRB 980425"; in Proceedings of "Third Rome Workshop on Gamma-Ray Burst in the Afterglow Era", 17-20 September 2002; M. Feroci, F. Frontera, N. Masetti, L. Piro, Editors; ASP Conference Series, 312, 349 (2004).

   This is a summary of the two talks presented at the Rome GRB meeting by C.L. Bianco and R. Ruffini. It is shown that by respecting the Relative Space-Time Transformation (RSTT) paradigm and the Interpretation of the Burst Structure (IBS) paradigm, important inferences are possible: a) in the new physics occurring in the energy sources of GRBs, b) on the structure of the bursts and c) on the composition of the interstellar matter surrounding the source.

4. M.G. Bernardini, C.L. Bianco, P. Chardonnet, F. Fraschetti, R. Ruffini, S.-S. Xue; "A New Astrophysical 'Triptych': GRB030329/SN2003dh/ URCA-2"; in "GAMMA-RAY BURSTS: 30 YEARS OF DISCOVERY", Proceedings of the Los Alamos "Gamma Ray Burst Symposium", Santa Fe, New Mexico, 8 – 12 September 2003, E.E. Fenimore, M. Galassi, Editors; AIP Conference Proceedings, 727, 312 (2004).

   We analyze the data of the Gamma-Ray Burst/Supernova GRB030329/ SN2003dh system obtained by HETE-2, R-XTE, XMM and VLT within our theory for GRB030329. By fitting the only three free parameters of the EMBH theory, we obtain the luminosity in fixed energy bands for the prompt emission and the afterglow. Since the Gamma-Ray Burst (GRB) analysis is consistent with a spherically symmetric expansion, the energy of GRB030329 is $E = 2.1 \times 10^{52}$ erg, namely $\sim 2 \times 10^{3}$ times larger than the Supernova energy. We conclude that either the GRB is triggering an induced-supernova event or both the GRB and the Supernova are triggered by the same relativistic process. In no way the GRB can be originated from the supernova. We also evidence that the XMM observations, much like in the system GRB980425/SN1998bw, are not part of the GRB afterglow, as interpreted in the literature, but are associated to the Supernova phenomenon. A dedicated campaign of observations is needed to confirm the nature of this XMM source as a newly born neutron star cooling by generalized URCA processes.

5. F. Fraschetti, M.G. Bernardini, C.L. Bianco, P. Chardonnet, R. Ruffini, S.-S. Xue; "The GRB980425-SN1998bw Association in the EMBH Model"; in "GAMMA-RAY BURSTS: 30 YEARS OF DISCOVERY", Proceedings of the Los Alamos "Gamma Ray Burst Symposium", Santa Fe, New Mexico, 8 – 12 September 2003, E.E. Fenimore, M. Galassi, Editors; AIP Conference Proceedings, 727, 424 (2004).

   Our GRB theory, previously developed using GRB 991216 as a prototype, is here applied to GRB 980425. We fit the luminosity observed in the 40–700 keV, 2–26 keV and 2–10 keV bands by the BeppoSAX satellite. In addition the supernova SN1998bw is the outcome of an "induced gravitational collapse" triggered by GRB 980425, in agreement with the GRB-Supernova Time Sequence (GSTS) paradigm. A further outcome of this astrophysically exceptional sequence of events is the formation of a young neutron star generated by the SN1998bw event. A coordinated observational activity is recommended to further enlighten the underlying scenario of this most unique astrophysical system.

6. A. Corsi, M.G. Bernardini, C.L. Bianco, P. Chardonnet, F. Fraschetti, R. Ruffini, S.-S. Xue; "GRB 970228 Within the EMBH Model"; in "GAMMA-RAY BURSTS: 30 YEARS OF DISCOVERY", Proceedings of the Los Alamos "Gamma Ray Burst Symposium", Santa Fe, New Mexico, 8 – 12 September 2003, E.E. Fenimore, M. Galassi, Editors; AIP Conference Proceedings, 727, 428 (2004).

   We consider the gamma-ray burst of 1997 February 28 (GRB 970228) within the ElectroMagnetic Black Hole (EMBH) model. We first determine the value of the two free parameters that characterize energetically the GRB phenomenon in the EMBH model, that is to say the dyadosphere energy, $E_{dya} = 5.1 \times 10^{52}$ ergs, and the baryonic remnant mass M_B in units of E_{dya}, $B = M_B c^2 / E_{dya} = 3.0 \times 10^{-3}$. Having in this way estimated the energy emitted during the beam-target phase, we evaluate the role of the InterStellar Medium (ISM) number density (n_{ISM}) and of the ratio $\mathcal{R}$ between the effective emitting area and the total surface area of the GRB source, in reproducing the observed profiles of the GRB 970228 prompt emission and X-ray (2-10 keV energy band) afterglow. The importance of the ISM distribution three-dimensional treatment around the central black hole is also stressed in this analysis.

4 Publications (2005–2023)

4.1 Refereed journals

1. R. Ruffini, C.L. Bianco, P. Chardonnet, F. Fraschetti, V. Gurzadyan, S.-S. Xue; "Emergence of a filamentary structure in the fireball from GRB spectra"; International Journal of Modern Physics D, 14, 97 (2005).

   It is shown that the concept of a fireball with a definite filamentary structure naturally emerges from the analysis of the spectra of Gamma-Ray Bursts (GRBs). These results, made possible by the recently obtained analytic expressions of the equitemporal surfaces in the GRB afterglow, depend crucially on the single parameter R describing the effective area of the fireball emitting the X-ray and gamma-ray radiation. The X-ray and gamma-ray components of the afterglow radiation are shown to have a thermal spectrum in the co-moving frame of the fireball and originate from a stable shock front described self-consistently by the Rankine-Hugoniot equations. Precise predictions are presented on a correlation between spectral changes and intensity variations in the prompt radiation verifiable, e.g., by the Swift and future missions. The highly variable optical and radio emission depends instead on the parameters of the surrounding medium. The GRB 991216 is used as a prototype for this model.

2. R. Ruffini, M.G. Bernardini, C.L. Bianco, P. Chardonnet, F. Fraschetti, V. Gurzadyan, M. Lattanzi, L. Vitagliano, S.-S. Xue; "Extracting energy from black holes: 'long' and 'short' GRBs and their astrophysical settings"; Il Nuovo Cimento C, 28, 589 (2005).

   The introduction of the three interpretational paradigms for Gamma-Ray Bursts (GRBs) and recent progress in understanding the X- and gamma-ray luminosity in the afterglow allow us to make assessments about the astrophysical settings of GRBs. In particular, we evidence the distinct possibility that some GRBs occur in a binary system. This subclass of GRBs manifests itself in a "tryptich": one component formed by the collapse of a massive star to a black hole, which originates the GRB; a second component by a supernova and a third one by a young neutron star born in the supernova event. Similarly, the understanding of the physics of quantum relativistic processes during the gravitational collapse makes possible precise predictions about the structure of short GRBs.

3. M.G. Bernardini, C.L. Bianco, P. Chardonnet, F. Fraschetti, R. Ruffini, S.-S. Xue; "Theoretical interpretation of luminosity and spectral properties of GRB 031203"; The Astrophysical Journal, 634, L29 (2005).

   The X-ray and gamma-ray observations of the source GRB 031203 by INTEGRAL are interpreted within our theoretical model. In addition to a complete spacetime parameterization of the GRB, we specifically assume that the afterglow emission originates from a thermal spectrum in the comoving frame of the expanding baryonic matter shell. By determining the two free parameters of the model and estimating the density and filamentary structure of the ISM, we reproduce the observed luminosity in the 20-200 keV energy band. As in previous sources, the prompt radiation is shown to coincide with the peak of the afterglow, and the luminosity substructure is shown to originate in the filamentary structure of the ISM. We predict a clear hard-to-soft behavior in the instantaneous spectra. The time-integrated spectrum over 20 s observed by INTEGRAL is well fitted. Despite the fact that this source has been considered "unusual", it appears to us to be a normal low-energy GRB.

4. R. Ruffini, M.G. Bernardini, C.L. Bianco, P. Chardonnet, F. Fraschetti, S.-S. Xue; Evidence for isotropic emission in GRB991216; Advances in Space Research, 38, 1291 (2006).

   The issue of the possible presence or absence of jets in GRBs is here re-examined for GRB991216. We compare and contrast our theoretically predicted afterglow luminosity in the 2–10 keV band for spherically symmetric versus jetted emission. At these wavelengths the jetted emission can be excluded and data analysis confirms spherical symmetry. These theoretical fits are expected to be improved by the forthcoming data of the Swift mission.

5. R. Ruffini, M.G. Bernardini, C.L. Bianco, P. Chardonnet, F. Fraschetti, R. Guida, S.-S. Xue; "GRB 050315: A step toward understanding the uniqueness of the overall GRB structure"; The Astrophysical Journal, 645, L109 (2006).

Using the Swift data of GRB 050315, we are making progress toward understanding the uniqueness of our theoretically predicted gamma-ray burst (GRB) structure, which is composed of a proper GRB (P-GRB), emitted at the transparency of an electron-positron plasma with suitable baryon loading, and an afterglow comprising the so-called prompt emission due to external shocks. Thanks to the Swift observations, the P-GRB is identified, and for the first time we can theoretically fit detailed light curves for selected energy bands on a continuous timescale ranging over 106 s. The theoretically predicted instantaneous spectral distribution over the entire afterglow is presented, confirming a clear hard-to-soft behavior encompassing, continuously, the "prompt emission" all the way to the latest phases of the afterglow.

6. C.L. Bianco, L. Caito, R. Ruffini; "Theoretical interpretation of GRB 011121"; Il Nuovo Cimento B, 121, 1441 (2006).

   GRB011121 is analyzed as a prototype to understand the "flares" recently observed by Swift in the afterglow of many GRB sources. Detailed theoretical computation of the GRB011121 light curves in selected energy bands are presented and compared and contrasted with observational BeppoSAX data.

7. R. Ruffini, M.G. Bernardini, C.L. Bianco, P. Chardonnet, F. Fraschetti, R. Guida, S.-S. Xue; "GRB 050315: A step toward the uniqueness of the overall GRB structure"; Il Nuovo Cimento B, 121, 1367 (2006).

   Using the *Swift* data of GRB 050315, we progress on the uniqueness of our theoretically predicted Gamma-Ray Burst (GRB) structure as composed by a proper-GRB (P-GRB), emitted at the transparency of an electron-positron plasma with suitable baryon loading, and an afterglow comprising the so called "prompt emission" as due to external shocks. Thanks to the *Swift* observations, we can theoretically fit detailed light curves for selected energy bands on a continuous time scale ranging over 10^6 seconds. The theoretically predicted instantaneous spectral distribution over the entire afterglow confirms a clear hard-to-soft behavior encompassing, continuously, the "prompt emission" all the way to the latest phases of the afterglow. Consequences of the instrumental threshold on the definition of "short" and "long" GRBs are discussed.

8. M.G. Bernardini, C.L. Bianco, L. Caito, P. Chardonnet, A. Corsi, M.G. Dainotti, F. Fraschetti, R. Guida, R. Ruffini, S.-S. Xue; GRB970228 as a prototype for short GRBs with afterglow; Il Nuovo Cimento B, 121, 1439 (2006).

GRB970228 is analyzed as a prototype to understand the relative role of short GRBs and their associated afterglows, recently observed by Swift and HETE-II. Detailed theoretical computation of the GRB970228 light curves in selected energy bands are presented and compared with observational BeppoSAX data.

9. M.G. Dainotti, M.G. Bernardini, C.L. Bianco, L. Caito, R. Guida, R. Ruffini; "GRB060218 and GRBs associated with Supernovae Ib/c"; Astronomy & Astrophysics, 471, L29 (2007).

   Context: The *Swift* satellite has given continuous data in the range 0.3–150 keV from 0 s to 10^6 s for GRB060218 associated with SN2006aj. This Gamma-Ray Burst (GRB) which has an unusually long duration ($T_{90} \sim 2100$ s) fulfills the Amati relation. These data offer the opportunity to probe theoretical models for GRBs connected with Supernovae (SNe).
   Aims: We plan to fit the complete γ- and X-ray light curves of this long duration GRB, including the prompt emission, in order to clarify the nature of the progenitors and the astrophysical scenario of the class of GRBs associated with SNe Ib/c.
   Methods: We apply our "fireshell" model based on the formation of a black hole, giving the relevant references. It is characterized by the precise equations of motion and equitemporal surfaces and by the role of thermal emission.
   Results: The initial total energy of the electron-positron plasma $E_{e^\pm}^{tot} = 2.32 \times 10^{50}$ erg has a particularly low value, similar to the other GRBs associated with SNe. For the first time, we observe a baryon loading $B = 10^{-2}$ which coincides with the upper limit for the dynamical stability of the fireshell. The effective CircumBurst Medium (CBM) density shows a radial dependence $n_{cbm} \propto r^{-\alpha}$ with $1.0 \lesssim \alpha \lesssim 1.7$ and monotonically decreases from 1 to 10^{-6} particles/cm^3. This behavior is interpreted as being due to a fragmentation in the fireshell. Analogies with the fragmented density and filling factor characterizing Novae are outlined. The fit presented is particularly significant in view of the complete data set available for GRB060218 and of the fact that it fulfills the Amati relation.
   Conclusions: We fit GRB060218, usually considered as an X-Ray Flash (XRF), as a "canonical GRB" within our theoretical model. The smallest possible black hole, formed by the gravitational collapse of a neutron star in a binary system, is consistent with the especially low energetics of the class of GRBs associated with SNe Ib/c. We provide the first evidence for a fragmentation in the fireshell. This fragmentation is crucial in explaining both the unusually large T_{90} and the consequently inferred abnormally low value of the CBM effective

density.

10. M.G. Bernardini, C.L. Bianco, L. Caito, M.G. Dainotti, R. Guida, R. Ruffini; "GRB970228 and a class of GRBs with an initial spikelike emission"; Astronomy & Astrophysics, 474, L13 (2007).

    Context: The discovery by *Swift* and HETE-2 of an afterglow emission associated possibly with short GRBs opened the new problematic of their nature and classification. This issue has been further enhanced by the observation of GRB060614 and by a new analysis of the BATSE catalog which led to the identification of a new class of GRBs with "an occasional softer extended emission lasting tenths of seconds after an initial spikelike emission".
    Aims: We plan a twofold task: a) to fit this new class of "hybrid" sources within our "canonical GRB" scenario, where all GRBs are generated by a "common engine" (i.e. the gravitational collapse to a black hole); b) to propose GRB970228 as the prototype of the above mentioned class, since it shares the same morphology and observational features.
    Methods: We analyze *Beppo*SAX data on GRB970228 within the "fireshell" model and we determine the parameters describing the source and the CircumBurst Medium (CBM) needed to reproduce its light curves in the 40–700 keV and 2–26 keV energy bands.
    Results: We find that GRB970228 is a "canonical GRB", like e.g. GRB050315, with the main peculiarity of a particularly low average density of the CBM $\langle n_{cbm} \rangle \sim 10^{-3}$ particles/cm^3. We also simulate the light curve corresponding to a rescaled CBM density profile with $\langle n_{cbm} \rangle = 1$ particle/cm^3. From such a comparison it follows that the total time-integrated luminosity is a faithful indicator of the nature of GRBs, contrary to the peak luminosity which is merely a function of the CBM density.
    Conclusions: We call attention on discriminating the short GRBs between the "genuine" and the "fake" ones. The "genuine" ones are intrinsically short, with baryon loading $B \lesssim 10^{-5}$, as stated in our original classification. The "fake" ones, characterized by an initial spikelike emission followed by an extended emission lasting tenths of seconds, have a baryon loading $10^{-4} \lesssim B \leq 10^{-2}$. They are observed as such only due to an underdense CBM consistent with a galactic halo environment which deflates the afterglow intensity.

11. R. Guida, M.G. Bernardini, C.L. Bianco, L. Caito, M.G. Dainotti, R. Ruffini; "The Amati relation in the "fireshell" model"; Astronomy & Astrophysics, 487, L37 (2008).

Context: The cosmological origin of gamma-ray bursts (GRBs) has been firmly established, with redshifts up to $z = 6.29$. They are possible candidates for use as "distance indicators" for testing cosmological models in a redshift range hardly achievable by other cosmological probes. Asserting the validity of the empirical relations among GRB observables is now crucial for their calibration.
Aims: Motivated by the relation proposed by Amati and collaborators, we look within the "fireshell" model for a relation between the peak energy E_p of the νF_ν total time-integrated spectrum of the afterglow and the total energy of the afterglow E_{aft}, which in our model encompasses and extends the prompt emission.
Methods: The fit within the fireshell model, as for the "canonical" GRB050315, uses the complete arrival time coverage given by the Swift satellite. It is performed simultaneously, self-consistently, and recursively in the four BAT energy bands (15–25 keV, 25–50 keV, 50–100 keV, and 100-150 keV), as well as in the XRT one (0.2–10 keV). It uniquely determines the two free parameters characterizing the GRB source, the total energy $E^{e^\pm}_{tot}$ of the $e^\pm$ plasma and its baryon loading B, as well as the effective CircumBurst Medium (CBM) distribution. We can then build two sets of "gedanken" GRBs varying the total energy of the electron-positron plasma $E^{e^\pm}_{tot}$ and keeping the same baryon loading B of GRB050315. The first set assumes the one obtained in the fit of GRB050315 for the effective CBM density. The second set assumes instead a constant CBM density equal to the average value of the GRB050315 prompt phase.
Results: For the first set of "gedanken" GRBs we find a relation $E_p \propto (E_{aft})^a$, with $a = 0.45 \pm 0.01$, whose slope strictly agrees with the Amati one. Such a relation, in the limit $B \to 10^{-2}$, coincides with the Amati one. Instead, no correlation is found in the second set of "gedanken" GRBs.
Conclusions: Our analysis excludes the proper GRB (P-GRB) from the prompt emission, extends all the way to the latest afterglow phases, and is independent of the assumed cosmological model, since all "gedanken" GRBs are at the same redshift. The Amati relation, on the other hand, includes the P-GRB, focuses only on the prompt emission, being therefore influenced by the instrumental threshold that fixes the end of the prompt emission, and depends on the assumed cosmology. This might explain the intrinsic scatter observed in the Amati relation.

12. L. Caito, M.G. Bernardini, C.L. Bianco, M.G. Dainotti, R. Guida, R. Ruffini; "GRB060614: a "fake" short GRB from a merging binary system"; Astronomy & Astrophysics, 489, 501 (2009).

Context: GRB060614 observations by VLT and by Swift have infringed the traditionally accepted gamma-ray burst (GRB) collapsar scenario that purports the origin of all long duration GRBs from supernovae (SN). GRB060614 is the first nearby long duration GRB clearly not associated with a bright Ib/c SN. Moreover, its duration ($T_{90} \sim 100$ s) makes it hardly classifiable as a short GRB. It presents strong similarities with GRB970228, the prototype of a new class of "fake" short GRBs that appear to originate from the coalescence of binary neutron stars or white dwarfs spiraled out into the galactic halo. *Aims*: Within the "canonical" GRB scenario based on the "fireshell" model, we test if GRB060614 can be a "fake" or "disguised" short GRB. We model the traditionally termed "prompt emission" and discriminate the signal originating from the gravitational collapse leading to the GRB from the process occurring in the circumburst medium (CBM). *Methods*: We fit GRB060614 light curves in Swift's BAT ($15-150$ keV) and XRT ($0.2-10$ keV) energy bands. Within the fireshell model, light curves are formed by two well defined and different components: the proper-GRB (P-GRB), emitted when the fireshell becomes transparent, and the extended afterglow, due to the interaction between the leftover accelerated baryonic and leptonic shell and the CBM. *Results*: We determine the two free parameters describing the GRB source within the fireshell model: the total $e^\pm$ plasma energy ($E_{tot}^{e^\pm} = 2.94 \times 10^{51}$erg) and baryon loading ($B = 2.8 \times 10^{-3}$). A small average CBM density $\sim 10^{-3}$ particles/cm^3 is inferred, typical of galactic halos. The first spikelike emission is identified with the P-GRB and the following prolonged emission with the extended afterglow peak. We obtain very good agreement in the BAT ($15-150$ keV) energy band, in what is traditionally called "prompt emission", and in the XRT ($0.2-10$ keV) one. *Conclusions*: The *anomalous* GRB060614 finds a natural interpretation within our canonical GRB scenario: it is a "disguised" short GRB. The total time-integrated extended afterglow luminosity is greater than the P-GRB one, but its peak luminosity is smaller since it is deflated by the peculiarly low average CBM density of galactic halos. This result points to an old binary system, likely formed by a white dwarf and a neutron star, as the progenitor of GRB060614 and well justifies the absence of an associated SN Ib/c. Particularly important for further studies of the final merging process are the temporal structures in the P-GRB down to 0.1 s.

13. M.G. Bernardini, C.L. Bianco, L. Caito, M.G. Dainotti, R. Guida, R. Ruffini; "GRB970228 in the "canonical GRB" scenario"; Journal of the Korean Physical Society, 56, 1575 (2010).

Within the "fireshell" model, we define a "canonical GRB" light curve with two sharply different components: the proper-GRB (P-GRB), emitted when the optically thick fireshell of an electron-positron plasma originating from the phenomenon reaches transparency, and the afterglow, emitted due to the collision between the remaining optically thin fireshell and the circumburst medium (CBM). On the basis of the recent understanding of GRB970228 as the prototype for a new class of GRBs with "an occasional softer extended emission lasting tenths of seconds after an initial spikelike emission", we outline our "canonical GRB" scenario, originating from the gravitational collapse to a black hole, with special emphasis on the discrimination between "genuine" and "fake" short GRBs. Furthermore, we investigate how the GRB970228 analysis provides a theoretical explanation for the apparent absence of such a correlation for the GRBs belonging to this new class.

14. L. Caito, M.G. Bernardini, C.L. Bianco, M.G. Dainotti, R. Guida, R. Ruffini; "GRB060614: a preliminary result"; Journal of the Korean Physical Society, 56, 1579 (2010).

    The explosion of GRB 060614 produced a deep break in the GRB scenario and opened new horizons of investigation because it can't be traced back to any traditional scheme of classification. In fact, it manifests peculiarities both of long bursts and of short bursts, and above all, it is the first case of a long-duration near GRB without any bright Ib/c associated Supernova. We will show that, in our canonical GRB scenario, this "anomalous" situation finds a natural interpretation and allows us to discuss a possible variation in the traditional classification scheme, introducing a distinction between "genuine" and "fake" short bursts.

15. M.G. Dainotti, M.G. Bernardini, C.L. Bianco, L. Caito, R. Guida, R. Ruffini; "The astrophysical trypthic: GRB, SN and URCA can be extended to GRB060218?"; Journal of the Korean Physical Society, 56, 1588 (2010).

    The *Swift* satellite has given continuous data in the range 0.3–150 keV from 0 s to 10^6 s for GRB060218 associated with SN2006aj. This GRB is the fourth GRB spectroscopically associated with SNe after the cases of GRB980425-SN1998bw, GRB031203-SN2003lw, GRB 030329-SN2003dh. It has an unusually long duration ($T_{90} \sim 2100$ s). These data offer the opportunity to probe theoretical models for Gamma-Ray Bursts (GRBs) connected with Supernovae (SNe). We plan to fit the complete γ- and X-ray light curves of this long duration GRB, including the prompt emission, in order to clarify the nature of the progenitors and the astrophysical scenario of the class of GRBs associated to SNe Ib/c. We apply our "fireshell" model based on the formation of a black hole, giving the relevant references. The initial total energy of the electron-positron plasma $E^{tot}_{e^\pm} = 2.32 \times 10^{50}$ erg has a particularly low value similarly to the other GRBs associated with SNe. For the first time we observe a baryon loading $B = 10^{-2}$ which coincides with the upper limit for the dynamical stability of the fireshell. The effective CircumBurst Medium (CBM) density shows a radial dependence $n_{cbm} \propto r^{-\alpha}$ with $1.0 \lesssim \alpha \lesssim 1.7$ and monotonically decreases from 1 to 10^{-6} particles/cm^3. Such a behavior is interpreted as due to a fragmentation in the fireshell. Such a fragmentation is crucial in explaining both the unusually large T_{90} and the consequently inferred abnormal low value of the CBM effective density. We fit GRB060218, usually considered as an X-Ray Flash (XRF), as a "canonical GRB" within our theoretical model. The smallest possible black hole, formed by the gravitational collapse of a neutron star in a binary system, is consistent with the especially low energetics of the class of GRBs associated with SNe Ib/c. We present the URCA process and the connection between the GRBs associated with SNe extended also to the case of GRB060218.

16. L. Izzo, M.G. Bernardini, C.L. Bianco, L. Caito, B. Patricelli, R. Ruffini; "GRB 090423 at Redshift 8.1: a Theoretical Interpretation"; Journal of the Korean Physical Society, 57, 551 (2010).

    GRB 090423 is the farthest gamma ray burst ever observed, with a redshift of about 8.1. We present within the fireshell scenario a complete analysis of this GRB. We model the prompt emission and the first rapid flux decay of the afterglow emission as being to the canonical emission of the interaction in the interval $0 \leq t \leq 440$ s by using accelerated baryonic matter with the circumburst medium. After the data reduction of the Swift data in the BAT (15 - 150 keV) and XRT (0.2 - 10 keV) energy bands, we interpret the light curves and the spectral distribution in the context of the fireshell scenario. We also confirm in this source the existence of a second component, a plateau phase, as being responsible for the late emission in the X-ray light curve. This extra component originates from the fact that the ejecta have a range of the bulk Lorentz Γ factor, which starts to interact each other ejecta at the start of the plateau phase.

17. L. Caito, L. Amati, M.G. Bernardini, C.L. Bianco, G. De Barros, L. Izzo, B. Patricelli, R. Ruffini; "GRB 071227: an additional case of a disguised

short burst”; Astronomy & Astrophysics, 521, A80 (2010).

Context: Observations of gamma-ray bursts (GRBs) have shown an hybridization between the two classes of long and short bursts. In the context of the fireshell model, the GRB light curves are formed by two different components: the *proper* GRB (P-GRB) and the extended afterglow. Their relative intensity is linked to the fireshell baryon loading B. The GRBs with P-GRB predominance are the short ones, the remainders are long. A new family of *disguised* short bursts has been identified: long bursts with a protracted low instantaneous luminosity due to a low density CircumBurst Medium (CBM). In the 15–150 keV energy band GRB 071227 exhibits a short duration (about 1.8s) spike-like emission followed by a very soft extended tail up to one hundred seconds after the trigger. It is a faint ($E_{iso} = 5.8 \times 10^{50}$) nearby GRB ($z = 0.383$) that does not have an associated type Ib/c bright supernova (SN). For these reasons, GRB 071227 has been classified as a short burst not fulfilling the Amati relation holding for long burst. *Aims:* We check the classification of GRB 071227 provided by the fireshell model. In particular, we test whether this burst is another example of a *disguised* short burst, after GRB 970228 and GRB 060614, and, for this reason, whether it fulfills the Amati relation. *Methods:* We simulate GRB 071227 light curves in the *Swift* BAT 15–50 keV bandpass and in the XRT (0.3–10 keV) energy band within the fireshell model. *Results:* We perform simulations of the tail in the 15–50 keV bandpass, as well as of the first part of the X-ray afterglow. This infers that: $E_{tot}^{e^\pm} = 5.04 \times 10^{51}$ erg, $B = 2.0 \times 10^{-4}$, $E_{P-GRB}/E_{aft} \sim 0.25$, and $\langle n_{cbm} \rangle = 3.33$ particles/cm^3. These values are consistent with those of “long duration” GRBs. We interpret the observed energy of the first hard emission by identifying it with the P-GRB emission. The remaining long soft tail indeed fulfills the Amati relation. *Conclusions:* Previously classified as a short burst, GRB 071227 on the basis of our analysis performed in the context of the fireshell scenario represents another example of a *disguised* short burst, after GRB 970228 and GRB 060614. Further confirmation of this result is that the soft tail of GRB 071227 fulfills the Amati relation.

18. M.G. Bernardini, C.L. Bianco, L. Caito, L. Izzo, B. Patricelli, R. Ruffini; “Analysis of GRB060607A within the fireshell model: prompt emission, X-ray flares and late afterglow phase”; Astronomy & Astrophysics, submitted to.

Context: GRB060607A is a very distant ($z = 3.082$) and energetic event ($E_{iso} \sim 10^{53}$ erg). Its main peculiarity is that the peak of the near-infrared (NIR) afterglow has been observed with the REM robotic telescope. This NIR peak has been interpreted as the afterglow onset within the fireball forward shock model, and the initial Lorentz gamma factor of the emitting system has been inferred. *Aims*: We analyze GRB060607A within the fireshell model. We emphasize the central role of the prompt emission in determining the initial Lorentz gamma factor of the extended afterglow and we interpret the X-ray flares as produced by the interaction of the optically thin fireshell with overdense CircumBurst Medium (CBM) clumps. *Methods*: We deal only with the Swift BAT and XRT observations, that are the basic contribution to the GRB emission and that are neglected in the treatment adopted in the current literature. The numerical modeling of the fireshell dynamics allows to calculate all its characteristic quantities, in particular the exact value of the Lorentz gamma factor at the transparency. *Results*: We show that the theoretically computed prompt emission light curves are in good agreement with the observations in all the *Swift* BAT energy bands as well as the spectra integrated over different time intervals. The flares observed in the decaying phase of the X-ray afterglow are also reproduced by the same mechanism, but in a region in which the typical dimensions of the clumps are smaller than the visible area of the fireshell and most energy lies in the X-ray band due to the hard-to-soft evolution. *Conclusions*: We show that it is possible to obtain flares with $\Delta t/t$ compatible with the observations when the three-dimensional structure of the CBM clumps is duly taken into account. We stop our analysis at the beginning of the X-ray plateau phase, since we suppose this originates from the instabilities developed in the collision between different subshells within a structured fireshell.

19. G. de Barros, M. G. Bernardini, C.L. Bianco, L. Caito, L. Izzo, B. Patricelli, R. Ruffini; "On the nature of GRB 050509b: a disguised short GRB"; Astronomy & Astrophyscs, 529, A130 (2011)

    Context: GRB 050509b, detected by the *Swift* satellite, is the first case where an X-ray afterglow has been observed associated with a short gamma-ray burst (GRB). Within the fireshell model, the canonical GRB light curve presents two different components: the proper-GRB (P-GRB) and the extended afterglow. Their relative intensity is a function of the fireshell baryon loading parameter B and of the CircumBurst Medium (CBM) density (n_{CBM}). In particular, the traditionally called short GRBs can be either "genuine" short GRBs (with $B \lesssim 10^{-5}$, where the P-GRB is energetically predominant) or "disguised" short GRBs (with $B \gtrsim 3.0 \times 10^{-4}$ and $n_{CBM} \ll 1$, where the extended afterglow is energetically predominant). *Aims*: We verify whether GRB 050509b can be classified as a “genuine” short or a “disguised” short GRB, in the fireshell model. *Methods*: We investigate two alternative scenarios. In the first, we start from the assumption that this GRB is a “genuine” short burst. In the second attempt, we assume that this GRB is a “disguised” burst. *Results*: If GRB 050509b were a genuine short GRB, there should initially be very hard emission which is ruled out by the observations. The analysis that assumes that this is a disguised short GRB is compatible with the observations. The theoretical model predicts a value of the extended afterglow energy peak that is consistent with the Amati relation. *Conclusions*: GRB 050509b cannot be classified as a “genuine” short GRB. The observational data are consistent with a “disguised” short GRB classification, i.e., a long burst with a weak extended afterglow “deflated” by the low density of the CBM. We expect that all short GRBs with measured redshifts are disguised short GRBs because of a selection effect: if there is enough energy in the afterglow to measure the redshift, then the proper GRB must be less energetic than the afterglow. The Amati relation is found to be fulfilled only by the extended afterglow excluding the P-GRB.

20. L. Caito, M.G. Bernardini, C.L. Bianco, L. Izzo, B. Patricelli, R. Ruffini; “GRB 071227: another disguised short burst”; International Journal of Modern Physics D, 20, 1931 (2011).

Observations of Gamma-ray Bursts (GRBs) put forward in the recent years have revealed, with increasing evidence, that the historical classification between long and short bursts has to be revised. Within the Fireshell scenario, both short and long bursts are canonical bursts, consisting of two different phases. First, a Proper-GRB (P-GRB), that is the emission of photons at the transparency of the fireshell. Then, the Extended Afterglow, multiwavelength emission due to the interacion of the baryonic remnants of the fireshell with the CircumBurst Medium (CBM). We discriminate between long and short bursts by the amount of energy stored in the first phase with respect to the second one. Within the Fireshell scenario, we have introduced a third intermediate class: the disguised GRBs. They appear like short bursts, because their morphology is characterized by a first, short, hard episode and a following deflated tail, but this last part — coincident with the peak of the afterglow — is energetically predominant. The origin of this peculiar kind of sources is inferred to a very low average density of the environment (of the order of 10^{-3}). After GRB 970228 and GRB 060614, we find in GRB 071227 a third example of disguised burst.

21. L. Izzo, M.G. Bernardini, C.L. Bianco, L. Caito, B. Patricelli, L.J. Rangel Lemos, R. Ruffini; "GRB 080916C and the high-energy emission in the fireshell scenario"; International Journal of Modern Physics D, 20, 1949 (2011).

    In this paper we discuss a possible explanation for the high energy emission (up to $\sim$ GeV) seen in GRB 080916C. We propose that the GeV emission is originated by the collision between relativistic baryons in the fireshell after the transparency and the nucleons located in molecular clouds near the burst site. This collision should give rise pion production, whose immediate decay provides high energy photons, neutrinos and leptons. Using a public code (SYBILL) we simulate these relativistic collisions in their simple form, so that we can draw our preliminar results in this paper. We will present moreover our hypothesis that the delayed onset of this emission identifies in a complete way the P-GRB emission.

22. B. Patricelli, M.G. Bernardini, C.L. Bianco, L. Caito, L. Izzo, R. Ruffini, G. Vereshchagin; "A new spectral energy distribution of photons in the fireshell model of GRBs"; International Journal of Modern Physics D, 20, 1983 (2011).

    The analysis of various Gamma-Ray Bursts (GRBs) having a low energetics (an isotropic energy $E_{iso} \lesssim 10^{53}$ ergs) within the fireshell model has shown how the $N(E)$ spectrum of their prompt emission can be reproduced in a satisfactory way by a convolution of thermal spectra. Nevertheless, from the study of very energetic bursts ($E_{iso} \lesssim 10^{54}$ ergs) such as, for example, GRB 080319B, some discrepancies between the numerical simulations and the observational data have been observed. We investigate a different spectrum of photons in the comoving frame of the fireshell in order to better reproduce the spectral properties of GRB prompt emission within the fireshell model. We introduce a phenomenologically modified thermal spectrum: a thermal spectrum characterized by a different asymptotic power-law index in the low energy region. Such an index depends on a free parameter α, so that the pure thermal spectrum corresponds to the case $\alpha = 0$. We test this spectrum by comparing the numerical simulations with the observed prompt emission spectra of various GRBs. From this analysis it has emerged that the observational data can be correctly reproduced by assuming a modified thermal spectrum with $\alpha = -1.8$.

23. A.V. Penacchioni, R. Ruffini, L. Izzo, M. Muccino, C.L. Bianco, L. Caito, B. Patricelli, L. Amati; "Evidence for a proto-black hole and a double

astrophysical component in GRB 101023"; Astronomy & Astrophysics, 538, A58 (2012).

Context: It has been recently shown that GRB 090618, observed by AGILE, Coronas Photon, Fermi, Konus, Suzaku and Swift, is composed of two very different components: episode 1, lasting 50 s, shows a thermal plus power-law spectrum with a characteristic temperature evolving in time as a power law; episode 2 (the remaining 100 s) is a canonical long GRB. We have associated episode 1 to the progenitor of a collapsing bare core leading to the formation of a black hole: what was defined as a "proto black hole". *Aims*: In precise analogy with GRB 090618 we aim to analyze the 89s of the emission of GRB 101023, observed by Fermi, Gemini, Konus and Swift, to see if there are two different episodes: the first one presenting a characteristic black-body temperature evolving in time as a broken power law, and the second one consistent with a canonical GRB. *Methods*: To obtain information on the spectra, we analyzed the data provided by the GBM detector onboard the Fermi satellite, and we used the heasoft package XSPEC and RMFIT to obtain their spectral distribution. We also used the numerical code GRBsim to simulate the emission in the context of the fireshell scenario for episode 2. *Results*: We confirm that the first episode can be well fit by a black body plus power-law spectral model. The temperature changes with time following a broken power law, and the photon index of the power-law component presents a soft-to-hard evolution. We estimate that the radius of this source increases with time with a velocity of $1.5 \times 10^4 km/s$. The second episode appears to be a canonical GRB. By using the Amati and the Atteia relations, we determined the cosmological redshift, $z \sim 0.9 \pm 0.084(stat.) \pm 0.2(sys.)$. The results of GRB 090618 are compared and contrasted with the results of GRB 101023. Particularly striking is the scaling law of the soft X-ray component of the afterglow. *Conclusions*: We identify GRB 090618 and GRB 101023 with a new family of GRBs related to a single core collapse and presenting two astrophysical components: a first one related to the proto-black hole prior to the process of gravitational collapse (episode 1), and a second one, which is the canonical GRB (episode 2) emitted during the formation of the black hole. For the first time we are witnessing the process of a black hole formation from the instants preceding the gravitational collapse up to the GRB emission. This analysis indicates progress towards developing a GRB distance indicator based on understanding the P-GRB and the prompt emission, as well as the soft X-ray behavior of the late afterglow.

24. R. Negreiros, R. Ruffini, C. L. Bianco, J. A. Rueda; "Cooling of young

neutron stars in GRB associated to supernovae"; Astronomy & Astrophysics, 540, A12 (2012).

Context: The traditional study of neutron star cooling has been generally applied to quite old objects such as the Crab Pulsar (957 years) or the central compact object in Cassiopeia A (330 years) with an observed surface temperature $\sim 10^6$ K. However, recent observations of the late ($t = 10^8$–10^9 s) emission of the supernovae (SNe) associated to GRBs (GRB-SN) show a distinctive emission in the X-ray regime consistent with temperatures $\sim 10^7$–10^8 K. Similar features have been also observed in two Type Ic SNe SN 2002ap and SN 1994I that are not associated to GRBs. *Aims*: We advance the possibility that the late X-ray emission observed in GRB-SN and in isolated SN is associated to a hot neutron star just formed in the SN event, here defined as a neo-neutron star. *Methods*: We discuss the thermal evolution of neo-neutron stars in the age regime that spans from ~ 1 minute (just after the proto-neutron star phase) all the way up to ages < 10–100 yr. We examine critically the key factor governing the neo-neutron star cooling with special emphasis on the neutrino emission. We introduce a phenomenological heating source, as well as new boundary conditions, in order to mimic the high temperature of the atmosphere for young neutron stars. In this way we match the neo-neutron star luminosity to the observed late X-ray emission of the GRB-SN events: URCA-1 in GRB980425-SN1998bw, URCA-2 in GRB030329-SN2003dh, and URCA-3 in GRB031203-SN2003lw. *Results*: We identify the major role played by the neutrino emissivity in the thermal evolution of neo-neutron stars. By calibrating our additional heating source at early times to $\sim 10^{12}$–10^{15} erg/g/s, we find a striking agreement of the luminosity obtained from the cooling of a neo-neutron stars with the prolonged ($t = 10^8$–10^9 s) X-ray emission observed in GRB associated with SN. It is therefore appropriate a revision of the boundary conditions usually used in the thermal cooling theory of neutron stars, to match the proper conditions of the atmosphere at young ages. The traditional thermal processes taking place in the crust might be enhanced by the extreme high-temperature conditions of a neo-neutron star. Additional heating processes that are still not studied within this context, such as e^+e^- pair creation by overcritical fields, nuclear fusion, and fission energy release, might also take place under such conditions and deserve further analysis. *Conclusions*: Observation of GRB-SN has shown the possibility of witnessing the thermal evolution of neo-neutron stars. A new campaign of dedicated observations is recommended both of GRB-SN and of isolated Type Ic SN.

25. L. Izzo, R. Ruffini, A.V. Penacchioni, C.L. Bianco, L. Caito, S.K. Chakrabarti, J.A. Rueda, A. Nandi, B. Patricelli; "A double component in GRB 090618: a proto-black hole and a genuinely long gamma-ray burst"; Astronomy & Astrophysics, 543, A10 (2012).

    Context: The joint X-ray and gamma-ray observations of GRB 090618 by very many satellites offer an unprecedented possibility of testing crucial aspects of theoretical models. In particular, they allow us to test (a) in the process of gravitational collapse, the formation of an optically thick e+e.-baryon plasma self-accelerating to Lorentz factors in the range $200 < \Gamma < 3000$; (b) its transparency condition with the emission of a component of 10^{53-54} baryons in the TeV region and (c) the collision of these baryons with the circumburst medium (CBM) clouds, characterized by dimensions of 10^{15-16} cm. In addition, these observations offer the possibility of testing a new understanding of the thermal and power-law components in the early phase of this GRB. *Aims*: We test the fireshell model of GRBs in one of the closest ($z = 0.54$) and most energetic ($E_{iso} = 2.90 \times 10^{53}$ erg) GRBs, namely GRB 090618. It was observed at ideal conditions by several satellites, namely *Fermi*, *Swift*, Konus-WIND, AGILE, RT-2, and Suzaku, as well as from on-ground optical observatories. *Methods*: We analyzed the emission from GRB 090618 using several spectral models, with special attention to the thermal and power-law components. We determined the fundamental parameters of a canonical GRB within the context of the fireshell model, including the identification of the total energy of the e^+e^- plasma, E_{tot}^{e+e-}, the proper GRB (P-GRB), the baryon load, the density and structure of the CBM. *Results*: We find evidence of the existence of two different episodes in GRB 090618. The first episode lasts 50 s and is characterized by a spectrum consisting of a thermal component, which evolves between $kT = 54$ keV and $kT = 12$ keV, and a power law with an average index $\gamma = 1.75 \pm 0.04$. The second episode, which lasts for ~ 100 s, behaves as a canonical long GRB with a Lorentz gamma factor at transparency of $\Gamma = 495$, a temperature at transparency of 29.22 keV and with a characteristic size of the surrounding clouds of $R_{cl} \sim 10^{15-16}$ cm and masses of $\sim 10^{22-24}$ g. *Conclusions*: We support the recently proposed two-component nature of GRB 090618, namely, episode 1 and episode 2, with a specific theoretical analysis.We furthermore illustrate that episode 1 cannot be considered to be either a GRB or a part of a GRB event, but it appears to be related to the progenitor of the collapsing bare core, leading to the formation of the black hole, which we call a "proto-black hole". Thus, for the first time, we are witnessing the process of formation of a black hole from the phases just preceding the gravitational collapse all the way up to the GRB emission.

26. B. Patricelli, M.G. Bernardini, C.L. Bianco, L. Caito, G. De Barros, L. Izzo, R. Ruffini, G.V. Vereshchagin; "Analysis of GRB 080319B and GRB 050904 within the Fireshell Model: Evidence for a Broader Spectral Energy Distribution"; The Astrophysical Journal, 756, 16 (2012).

    The observation of GRB 080319B, with an isotropic energy $E_{iso} = 1.32 \times 10^{54}$ erg, and GRB 050904, with $E_{iso} = 1.04 \times 10^{54}$ erg, offers the possibility of studying the spectral properties of the prompt radiation of two of the most energetic Gamma Ray Bursts (GRBs). This allows us to probe the validity of the fireshell model for GRBs beyond 10^{54} erg, well outside the energy range where it has been successfully tested up to now (10^{49}–10^{53} erg). We find that in the low energy region, the prompt emission spectra observed by *Swift* BAT reveals more power than theoretically predicted. The opportunities offered by these observations to improve the fireshell model are outlined in this paper. One of the distinguishing features of the fireshell model is that it relates the observed GRB spectra to the spectrum in the comoving frame of the fireshell. Originally, a fully radiative condition and a comoving thermal spectrum were adopted. An additional power-law in the comoving thermal spectrum is required due to the discrepancy of the theoretical and observed light curves and spectra in the fireshell model for GRBs 080319B and 050904. A new phenomenological parameter α is correspondingly introduced in the model. We perform numerical simulations of the prompt emission in the *Swift* BAT bandpass by assuming different values of α within the fireshell model. We compare them with the GRB 080319B and GRB 050904 observed time-resolved spectra, as well as with their time-integrated spectra and light curves. Although GRB 080319B and GRB 050904 are at very different redshifts (z=0.937 and z=6.29 respectively), a value of $\alpha = -1.8$ leads for both of them to a good agreement between the numerical simulations and the observed BAT light curves, time-resolved and time-integrated spectra. Such a modified spectrum is also consistent with the observations of previously analyzed less energetic GRBs and reasons for this additional agreement are given. Perspectives for future low energy missions are outlined.

27. M. Muccino, R. Ruffini, C.L. Bianco, L. Izzo, A.V. Penacchioni; "GRB 090227B: The missing link between the genuine short and long GRBs"; The Astrophysical Journal, 763, 125 (2013).

The time-resolved spectral analysis of GRB 090227B, made possible by the *Fermi*-GBM data, allows to identify in this source the missing link between the genuine short and long GRBs. Within the Fireshell model of the Gamma-Ray Bursts (GRBs) we predict genuine short GRBs: bursts with the same inner engine of the long bursts but endowed with a severely low value of the Baryon load, $B \lesssim 5 \times 10^{-5}$. A first energetically predominant emission occurs at the transparency of the e^+e^- plasma, the Proper-GRB (P-GRB), followed by a softer emission, the extended afterglow. The typical separation between the two emissions is expected to be of the order of 10^{-3} – 10^{-2} s. We identify the P-GRB of GRB 090227B in the first 96 ms of emission, where a thermal component with the temperature $kT = (517 \pm 28)$ keV and a flux comparable with the non thermal part of the spectrum is observed. This non thermal component as well as the subsequent emission, where there is no evidence for a thermal spectrum, is identified with the extended afterglow. We deduce a theoretical cosmological redshift $z = 1.61 \pm 0.14$. We then derive the total energy $E^{tot}_{e^+e^-} = (2.83 \pm 0.15) \times 10^{53}$ ergs, the Baryon load $B = (4.13 \pm 0.05) \times 10^{-5}$, the Lorentz Γ factor at transparency $\Gamma_{tr} = (1.44 \pm 0.01) \times 10^4$, and the intrinsic duration $\Delta t' \sim 0.35$ s. We also determine the average density of the CircumBurst Medium (CBM), $\langle n_{CBM} \rangle = (1.90 \pm 0.20) \times 10^{-5}$ particles/cm^3. There is no evidence of beaming in the system. In view of the energetics and of the Baryon load of the source, as well as of the low interstellar medium and of the intrinsic time scale of the signal, we identify the GRB progenitor as a binary neutron star. From the recent progress in the theory of neutron stars, we obtain masses of the stars $m_1 = m_2 = 1.34 M_\odot$ and their corresponding radii $R_1 = R_2 = 12.24$ km and thickness of their crusts ~ 0.47 km, consistent with the above values of the Baryon load, of the energetics and of the time duration of the event.

28. A.V. Penacchioni, R. Ruffini, C.L. Bianco, L. Izzo, M. Muccino, G.B. Pisani, J.A. Rueda; "GRB 110709B in the induced gravitational collapse paradigm"; Astronomy & Astrophysics, 551, A133 (2013).

    Context: GRB 110709B is the first source for which *Swift* BAT triggered twice, with a time separation of ~ 10 minutes. The first emission (called here Episode 1) goes from 40 s before the first trigger up to 60 s after it. The second emission (hereafter Episode 2) goes from 35 s before the second trigger to 100 s after it. These features reproduce the ones of GRB 090618, which has been recently interpreted within the Induced Gravitational Collapse paradigm (IGC). In line with this paradigm we assume the progenitor to be a close binary system composed of a core of an evolved star and a Neutron Star (NS). The evolved star explodes as a Supernova (SN) and ejects material that is partially accreted by the NS. We identify this process with Episode 1. The accretion process brings the NS over its critical mass, thus gravitationally collapsing to a BH. This process leads to the GRB emission, Episode 2. The double trigger has given for the first time the possibility to have a coverage of the X-ray emission observed by XRT both prior to and during the prompt phase of GRB 110709B. *Aims*: We analyze the spectra and time variability of Episode 1 and 2 and compute the relevant parameters of the binary progenitor, as well as the astrophysical parameters both in the SN and the GRB phase in the IGC paradigm. *Methods*: We perform a time-resolved spectral analysis of Episode 1 by fitting the spectrum with a blackbody (BB) plus a power-law (PL) spectral model. From the BB fluxes and temperatures of Episode 1 and the luminosity distance d_L, we evaluate the evolution with time of the radius of the BB emitter, associated here to the evolution of the SN ejecta. We analyze Episode 2 within the Fireshell model, identifying the Proper-GRB (P-GRB) and simulating the light curve and spectrum. We establish the redshift to be $z = 0.75$, following the phenomenological methods by Amati, by Yonetoku and by Grupe, and our analysis of the late X-ray afterglow. It is most remarkable that the determination of the cosmological redshift on the ground of the scaling of the late X-ray afterglow, already verified in GRB 090618 and GRB 101023, is again verified by this analysis. *Results*: We find for Episode 1 a temperature of the BB component that evolves with time following a broken PL, with the slope of the PL at early times $\alpha = 0$ (constant function) and the slope of the PL at late times $\beta = -4 \pm 2$. The break occurs at $t = 41.21$ s. The total energy of Episode 1 is $E^{(1)}_{iso} = 1.42 \times 10^{53}$ erg. The total energy of Episode 2 is $E^{(2)}_{iso} = 2.43 \times 10^{52}$ erg. We find at transparency a Lorentz factor $\Gamma \sim 1.73 \times 10^2$, laboratory radius of 6.04×10^{13} cm, P-GRB observed temperature $kT_{P-GRB} = 12.36$ keV, baryon load $B = 5.7 \times 10^{-3}$ and P-GRB energy of $E_{P-GRB} = 3.44 \times 10^{50}$ erg. We find a remarkable coincidence of the cosmological redshift by the scaling of the XRT data and with three other phenomenological methods. *Conclusions*: We interpret GRB 110709B as a member of the IGC sources, together with GRB 970828, GRB 090618 and GRB 101023. The existence of the XRT data during the prompt phase of the emission of GRB 110709B (Episode 2) offers an unprecedented tool for improving the diagnostic of GRBs emission.

29. G.B. Pisani, L. Izzo, R. Ruffini, C.L. Bianco, M. Muccino, A.V. Penacchioni, J.A. Rueda, Y. Wang; "Novel distance indicator for gamma-ray bursts associated with supernovae"; Astronomy & Astrophysics, 552,

L5 (2013).

Context: In recent years it has been proposed that the temporal coincidence of a Gamma Ray Burst (GRB) and a type Ib/c supernova (SN) can be explained by the concept of Induced Gravitational Collapse (IGC) of a Neutron Star (NS) to a Black Hole (BH) by accretion of matter ejected by a SN Ib/c. This scenario reveals a possible common behavior in the late time X-ray emission of this subclass of GRBs. *Aims*: We want to test if such a common behavior can actually be present in the sources belonging to this GRB sub-class and if this may lead to a redshift estimator for these sources. *Methods*: We build a sample of GRBs belonging to this sub-class, and we rescale the X-ray light curves of all of them both in time and in flux to a common cosmological redshift. *Results*: We found that the X-ray light curves of all the GRBs of the sample with a measured redshift present a common late time behavior when rescaled to a common redshift $z = 1$. We then use this result to estimate the redshift of the GRBs of the sample with no measured redshift. *Conclusions*: The common behavior in the late decay of the X-ray light curves of the GRBs of the sample points to a common physical mechanism in this particular phase of the GRB emission, possibly related to the SN process. This scenario may represent an invaluable tool to estimate the redshift of GRBs belonging to this sub-class of events. More GRBs are therefore needed in order to enlarge the subclass and to make more stringent constraints on the redshift estimates performed with this method for GRBs pertaining to this class.

30. C.L. Bianco, M. G. Bernardini, L. Caito, G. De Barros, L. Izzo, M. Muccino, B. Patricelli, A.V. Penacchioni, G.B. Pisani, R. Ruffini; "The canonical GRB scenario"; Il Nuovo Cimento C, 36 s01, 21 (2013).

    The canonical GRB scenario implied by the fireshell model is briefly summarized.

31. A.V. Penacchioni, R. Ruffini, L. Izzo, M. Muccino, C.L. Bianco, L. Caito, B. Patricelli; "Evidences for a double component in the emission of GRB 101023"; Il Nuovo Cimento C, 36 s01, 117 (2013).

    In this work we present the results of the analysis of GRB 101023 in the fireshell scenario. Its redshift is not known, so we attempted to infer it from the Amati Relation, obtaining $z = 0.9$. Its light curve presents a double emission, which makes it very similar to the already studied GRB 090618. We called each part Episode 1 and Episode 2. We performed a time-resolved spectral analysis with RMFIT using different spectral models, and fitted the light curve with a numerical code integrating the fireshell equations of motion. We used Fermi GBM data to build the light curve, in particular the second NaI detector, in the range (8.5–1000 keV). We considered different hypotheses regarding which part of the light curve could be the GRB and performed the analysis of all of them. We noticed a great variation of the temperature with time in the first episode, as well as almost no variation of the progenitor radius. We found that the first emission does not match the requirements for a GRB, while the second part perfectly agrees with being a canonical GRB, with a P-GRB lasting 4 s.

32. M. Muccino, R. Ruffini, C.L. Bianco, L. Izzo, A.V. Penacchioni, G.B. Pisani; "GRB 090510: A Disguised Short Gamma-Ray Burst with the Highest Lorentz Factor and Circumburst Medium"; The Astrophysical Journal, 772, 62 (2013).

    GRB 090510, observed both by Fermi and AGILE satellites, is the first bright short-hard Gamma-Ray Burst (GRB) with an emission from the keV up to the GeV energy range. Within the Fireshell model, we interpret the faint precursor in the light curve as the emission at the transparency of the expanding e^+e^- plasma: the Proper-GRB (P-GRB). From the observed isotropic energy we assume a total plasma energy $E^{tot}_{e^+e^-} = (1.10 \pm 0.06) \times 10^{53}$erg and derive a Baryon load $B = (1.45 \pm 0.28) \times 10^{-3}$ and a Lorentz factor at transparency $\Gamma_{tr} = (6.7 \pm 1.6) \times 10^2$. The main emission $\sim$ 0.4s after the initial spike is interpreted as the extended afterglow, due to the interaction of the ultrarelativistic baryons with the CircumBurst Medium (CBM). Using the condition of fully radiative regime, we infer a CBM average spherically symmetric density of $\langle n_{CBM} \rangle = (1.85 \pm 0.14) \times 10^3$ particles/cm^3, one of the highest found in the Fireshell model. The value of the filling factor, $1.5 \times 10^{-10} \leq \mathcal{R} \leq 3.8 \times 10^{-8}$, leads to the estimate of filaments with densities $n_{fil} = n_{CBM}/\mathcal{R} \approx (10^6 - 10^{14})$ particles/cm^3. The sub-MeV and the MeV emissions are well reproduced. When compared to the canonical GRBs with $\langle n_{CBM} \rangle \approx 1$ particles/cm^3 and to the disguised short GRBs with $\langle n_{CBM} \rangle \approx 10^{-3}$ particles/cm^3, the case of GRB 090510 leads to the existence of a new family of bursts exploding in an over-dense galactic region with $\langle n_{CBM} \rangle \approx 10^3$ particles/cm^3. The joint effect of the high Γ_{tr} and the high density compresses in time and "inflates" in intensity the extended afterglow, making it appear as a short burst, which we here define as "disguised short GRB by excess". The determination of the above parameters values may represent an important step towards the explanation of the GeV emission.

33. R. Ruffini, M. Muccino, C.L. Bianco, M. Enderli, L. Izzo, M. Kovacevic, A.V. Penacchioni, G.B. Pisani, J.A. Rueda, Y. Wang; "On Binary Driven Hypernovae and their nested late X-ray emission"; Astronomy & Astrophysics, 565, L10 (2014).

    Context: The induced gravitational collapse (IGC) paradigm addresses the very energetic (10^{52}–10^{54} erg) long gamma-ray bursts (GRBs) associated to supernovae (SNe). Unlike the traditional "collapsar" model, an evolved FeCO core with a companion neutron star (NS) in a tight binary system is considered as the progenitor. This special class of sources, here named "binary driven hypernovae" (BdHNe), presents a composite sequence composed of four different episodes with precise spectral and luminosity features.
    Aims: We first compare and contrast the steep decay, the plateau, and the power-law decay of the X-ray luminosities of three selected BdHNe (GRB 060729, GRB 061121, and GRB 130427A). Second, to explain the different sizes and Lorentz factors of the emitting regions of the four episodes, for definiteness, we use the most complete set of data of GRB 090618. Finally, we show the possible role of r-process, which originates in the binary system of the progenitor.
    Methods: We compare and contrast the late X-ray luminosity of the above three BdHNe. We examine correlations between the time at the starting point of the constant late power-law decay t_a^*, the average prompt luminosity $\langle L_{iso} \rangle$, and the luminosity at the end of the plateau L_a. We analyze a thermal emission ($\sim$ 0.97–0.29 keV), observed during the X-ray steep decay phase of GRB 090618.
    Results: The late X-ray luminosities of the three BdHNe, in the rest-frame energy band 0.3–10 keV, show a precisely constrained "nested" structure. In a space-time diagram, we illustrate the different sizes and Lorentz factors of the emitting regions of the three episodes. For GRB 090618, we infer an initial dimension of the thermal emitter of $\sim 7 \times 10^{12}$ cm, expanding at $\Gamma \approx 2$. We find tighter correlations than the Dainotti-Willingale ones.
    Conclusions: We confirm a constant slope power-law behavior for the late X-ray luminosity in the source rest frame, which may lead to a new distance indicator for BdHNe. These results, as well as the emitter size and Lorentz factor, appear to be inconsistent with the traditional afterglow model based on synchrotron emission from an ultra-relativistic ($\Gamma \sim 10^2$–10^3) collimated jet outflow. We argue, instead, for the possible role of r-process, originating in the binary system, to power the mildly relativistic X-ray source.

34. R. Ruffini, L. Izzo, M. Muccino, G.B. Pisani, J.A. Rueda, Y. Wang, C. Barbarino, C.L. Bianco, M. Enderli, M. Kovacevic; "Induced gravitational collapse at extreme cosmological distances: the case of GRB 090423"; Astronomy & Astrophysics, 569, A39 (2014).

    Context: The induced gravitational collapse (IGC) scenario has been introduced in order to explain the most energetic gamma ray bursts (GRBs), $E_{iso} = 10^{52} - 10^{54}$ erg, associated with type Ib/c supernovae (SNe). It has led to the concept of binary-driven hypernovae (BdHNe) originating in a tight binary system composed by a FeCO core on the verge of a SN explosion and a companion neutron star (NS). Their evolution is characterized by a rapid sequence of events: 1) The SN explodes, giving birth to a new NS (νNS). The accretion of SN ejecta onto the companion NS increases its mass up to the critical value; 2) The consequent gravitational collapse is triggered, leading to the formation of a black hole (BH) with GRB emission; 3) A novel feature responsible for the emission in the GeV, X-ray, and optical energy range occurs and is characterized by specific power-law behavior in their luminosity evolution and total spectrum; 4) The optical observations of the SN then occurs.
    Aims: We investigate whether GRB 090423, one of the farthest observed GRB at $z = 8.2$, is a member of the BdHN family.
    Methods: We compare and contrast the spectra, the luminosity evolution, and the detectability in the observations by *Swift* of GRB 090423 with the corresponding ones of the best known BdHN case, GRB 090618.
    Results: Identification of constant slope power-law behavior in the late X-ray emission of GRB 090423 and its overlapping with the corresponding one in GRB 090618, measured in a common rest frame, represents the main result of this article. This result represents a very significant step on the way to using the scaling law properties, proven in Episode 3 of this BdHN family, as a cosmological standard candle.
    Conclusions: Having identified GRB 090423 as a member of the BdHN family, we can conclude that SN events, leading to NS formation, can already occur already at $z = 8.2$, namely at 650 Myr after the Big Bang. It is then possible that these BdHNe originate stem from 40-60 $M_{\odot}$ binaries. They are probing the Population II stars after the completion and possible disappearance of Population III stars.

35. M. Muccino, C.L. Bianco, L. Izzo, Y. Wang, M. Enderli, M. Kovacevic, G.B. Pisani, A.V. Penacchioni, R. Ruffini; "The Genuine Short GRB 090227B and the Disguised by Excess GRB 090510"; Gravitation and

Cosmology, 20, 197 (2014).

GRB 090227B and GRB 090510, traditionally classified as short gamma-ray Bursts (GRBs), indeed originate from different systems. For GRB 090227B we inferred a total energy of the e^+e^- plasma $E^{tot}_{e^+e^-} = (2.83 \pm 0.15) \times 10^{53}$ erg, a baryon load of $B = (4.1 \pm 0.05) \times 10^{-5}$, and a CircumBurst Medium (CBM) average density $\langle n_{CBM} \rangle = (1.90 \pm 0.20) \times 10^{-5}$ cm^{-3}. From these results we have assumed the progenitor of this burst to be a symmetric neutron stars (NSs) merger with masses $m = 1.34 M_\odot$, radii $R = 12.24$ km. GRB 090510, instead, has $E^{tot}_{e^+e^-} = (1.10 \pm 0.06) \times 10^{53}$ erg, $B = (1.45 \pm 0.28) \times 10^{-3}$, implying a Lorentz factor at transparency of $\Gamma = (6.7 \pm 1.7) \times 10^2$, which are characteristic of the long GRB class, and a very high CBM density, $\langle n_{CBM} \rangle = (1.85 \pm 0.14) \times 10^3$ cm^{-3}. The joint effect of the high values of Γ and of $\langle n_{CBM} \rangle$ compresses in time and "inflates" in intensity in an extended afterglow, making appear GRB 090510 as a short burst, which we here define as "disguised short GRB by excess" occurring an overdense region with 10^3 cm^{-3}.

36. M. Muccino, C.L. Bianco, L. Izzo, Y. Wang, M. Enderli, G.B. Pisani, A.V. Penacchioni, R. Ruffini; "Two short bursts originating from different astrophysical systems: The genuine short GRB 090227B and the disguised short GRB 090510 by excess"; Journal of the Korean Physical Society, 65, 865 (2014).

    GRB 090227B and GRB 090510 are two gamma-ray bursts (GRBs) traditionally classified as short bursts. The major outcome of our analysis is that they indeed originate from different systems. In the case of GRB 090227B, from the inferred values of the total energy of the e^+e^- plasma, $E^{tot}_{e^+e^-} = (2.83 \pm 0.15) \times 10^{53}$ erg, the engulfed baryonic mass M_B, expressed as $B = M_B c^2 / E^{tot}_{e^+e^-} = (4.1 \pm 0.05) \times 10^{-5}$, and the circumburst medium (CBM) average density, $\langle n_{CBM} \rangle = (1.90 \pm 0.20) \times 10^{-5}$ cm^{-3}, we have assumed the progenitor of this burst to be a symmetric neutron star (NS) merger with masses $m = 1.34 M_\odot$, radii $R = 12.24$ km, and crustal thicknesses of ~ 0.47 km. In the case of GRB 090510, we have derived the total plasma energy, $E^{tot}_{e^+e^-} = (1.10 \pm 0.06) \times 10^{53}$ erg, the Baryon load, $B = (1.45 \pm 0.28) \times 10^{-3}$, and the Lorentz factor at transparency, $\Gamma = (6.7 \pm 1.7) \times 10^2$, which are characteristic of the long GRB class, as well as a very high CBM density, $\langle n_{CBM} \rangle = (1.85 \pm 0.14) \times 10^3$ cm^{-3}. The joint effect of the high values of Γ and $\langle n_{CBM} \rangle$ compresses in time and "inflates" in intensity the extended afterglow, making GRB 090510 appear to be a short burst, which we here define as a "disguised short GRB by excess", occurring in an overdense region with 10^3 cm^{-3}.

37. R. Ruffini, Y. Wang, M. Kovacevic, C.L. Bianco, M. Enderli, M. Muccino, A.V. Penacchioni, G.B. Pisani, J. Rueda; "GRB 130427A and SN 2013cq: A Multi-wavelength Analysis of An Induced Gravitational Collapse Event"; The Astrophysical Journal, 798, 10 (2015).

    We have performed our data analysis of the observations by *Swift*, *NuStar* and *Fermi* satellites in order to probe the induced gravitational collapse (IGC) paradigm for GRBs associated with supernovae (SNe), in the "terra incognita" of GRB 130427A. We compare and contrast our data analysis with those in the literature. We have verified that the GRB 130427A conforms to the IGC paradigm by examining the power law behavior of the luminosity in the early 10^4 s of the XRT observations. This has led to the identification of the four different episodes of the "binary driven hypernovae" (BdHNe) and to the prediction, on May 2, 2013, of the occurrence of SN 2013cq, duly observed in the optical band on May 13, 2013. The exceptional quality of the data has allowed the identification of novel features in *Episode 3* including: a) the confirmation and the extension of the existence of the recently discovered "nested structure" in the late X-ray luminosity in GRB 130427A, as well as the identification of a spiky structure at 10^2 s in the cosmological rest-frame of the source; b) a power law emission of the GeV luminosity light curve and its onset at the end of *Episode 2*; c) different Lorentz Γ factors for the emitting regions of the X-ray and GeV emissions in this *Episode 3*. These results make it possible to test the details of the physical and astrophysical regimes at work in the BdHNe: 1) a newly born neutron star and the supernova ejecta, originating in *Episode 1*, 2) a newly formed black hole originating in *Episode 2*, and 3) the possible interaction among these components, observable in the standard features of *Episode 3*.

38. M. Muccino, R. Ruffini, C.L. Bianco, M. Enderli, M. Kovacevic, L. Izzo, A.V. Penacchioni, G.B. Pisani, J.A. Rueda, Y. Wang; "On binary driven hypernovae and their nested late X-ray emission"; Astronomy Reports, 59, 581 (2015).

    The induced gravitational collapse (IGC) paradigm addresses energetic (10^{52}–10^{54} erg), long gamma-ray bursts (GRBs) associated to supernovae (SNe) and proposes as their progenitors tight binary systems composed of an evolved FeCO core and a companion neutron star (NS). Their emission is characterized by four specific episodes: Episode 1, corresponding to the on-set of the FeCO

SN explosion and the accretion of the ejecta onto the companion NS; Episode 2, related the collapse of the companion NS to a black hole (BH) and to the emission of a long GRB; Episode 3, observed in X-rays and characterized by a steep decay, a plateau phase and a late power-law decay; Episode 4, corresponding to the optical SN emission due to the ^{56}Ni decay. We focus on Episode 3 and we show that, from the thermal component observed during the steep decay of the prototype GRB 090618, the emission region has a typical dimension of $\sim 10^{13}$ cm, which is inconsistent with the typical size of the emitting region of GRBs, e.g., $\sim 10^{16}$ cm. We propose, therefore, that the X-ray afterglow emission originates from a spherically symmetric SN ejecta expanding at $\Gamma \sim 2$ or, possibly, from the accretion onto the newly formed black hole, and we name these systems "binary driven hypernovae" (BdHNe). This interpretation is alternative to the traditional afterglow model based on the GRB synchrotron emission from a collimated jet outflow, expanding at ultra-relativistic Lorentz factor of $\Gamma \sim 10^2 - 10^3$ and originating from the collapse of a single object. We show then that the rest-frame energy band 0.3–10 keV X-ray luminosities of three selected BdHNe, GRB 060729, GRB 061121, and GRB 130427A, evidence a precisely constrained "nested" structure and satisfy precise scaling laws between the average prompt luminosity, $< L_{iso} >$, and the luminosity at the end of the plateau, L_a, as functions of the time at the end of the plateau. All these features extend the applicability of the "cosmic candle" nature of Episode 3. The relevance of r-process in fulfilling the demanding scaling laws and the nested structure are indicated.

39. R. Ruffini, J.A. Rueda, C. Barbarino, C. L. Bianco, H. Dereli, M. Enderli, L. Izzo, M. Muccino, A.V. Penacchioni, G.B. Pisani, Y. Wang; "Induced Gravitational Collapse in the BATSE era: the case of GRB 970828"; Astronomy Reports, 59, 626 (2015).

    Following the recently established "Binary-driven HyperNova" (BdHN) paradigm, we here interpret GRB 970828 in terms of the four episodes typical of such a model. The "Episode 1", up to 40 s after the trigger time t_0, with a time varying thermal emission and a total energy of $E_{iso,1st} = 2.60 \times 10^{53}$ erg, is interpreted as due to the onset of an hyper-critical accretion process onto a companion neutron star, triggered by the companion star, an FeCO core approaching a SN explosion. The "Episode 2", observed up t_0+90 s, is interpreted as a canonical gamma ray burst, with an energy of $E^{e^+e^-}_{tot} = 1.60 \times 10^{53}$ erg, a baryon load of $B = 7 \times 10^{-3}$ and a bulk Lorentz factor at transparency of $\Gamma = 142.5$. From this Episode 2, we infer that the GRB exploded in an environment with a large average particle density $\langle n \rangle \approx 10^3$ particles/cm^3 and dense clouds characterized by typical dimensions of $(4 \div 8) \times 10^{14}$ cm and $\delta n/n \sim 10$. The "Episode 3" is identified from t_0+90 s all the way up to 10^{5-6} s: despite the paucity of the early X-ray data, typical in the BATSE, pre-Swift era, we find extremely significant data points in the late X-ray afterglow emission of GRB 970828, which corresponds to the ones observed in all BdHNe sources. The "Episode 4", related to the Supernova emission, does not appear to be observable in this source, due to the presence of darkening from the large density of the GRB environment, also inferred from the analysis of the Episode 2.

40. Y. Wang, R. Ruffini, M. Kovacevic, C.L. Bianco, M. Enderli, M. Muccino, A.V. Penacchioni, G.B. Pisani, J.A. Rueda; "Predicting supernova associated to gamma-ray burst 130427a"; Astronomy Reports, 59, 667 (2015).

    Binary systems constituted by a neutron star and a massive star are not rare in the universe. The Induced Gravitational Gamma-ray Burst (IGC) paradigm interprets Gamma-ray bursts as the outcome of a neutron star that collapses into a black hole due to the accretion of the ejecta coming from its companion massive star that underwent a supernova event. GRB 130427A is one of the most luminous GRBs ever observed, of which isotropic energy exceeds 10^{54} erg. And it is within one of the few GRBs obtained optical, X-ray and GeV spectra simultaneously for hundreds of seconds, which provides an unique opportunity so far to understand the multi-wavelength observation within the IGC paradigm, our data analysis found low Lorentz factor blackbody emission in the Episode 3 and its X-ray light curve overlaps typical IGC Golden Sample, which comply to the IGC mechanisms. We consider these findings as clues of GRB 130427A belonging to the IGC GRBs. We predicted on GCN the emergence of a supernova on May 2, 2013, which was later successfully detected on May 13, 2013.

41. R. Ruffini, M. Muccino, M. Kovacevic, F.G. Oliveira, J.A. Rueda, C.L. Bianco, M. Enderli, A.V. Penacchioni, G.B. Pisani, Y. Wang, E. Zaninoni; "GRB 140619B: a short GRB from a binary neutron star merger leading to black hole formation"; The Astrophysical Journal, 808, 190 (2015).

    We show the existence of two families of short GRBs, both originating from the merger of binary neutron stars (NSs): family-1 with $E_{iso} < 10^{52}$ erg, leading to a massive NS as the merged core, and family-2 with $E_{iso} > 10^{52}$ erg, leading to a black hole (BH). Following the identification of the prototype

GRB 090227B, we present the details of a new example of family-2 short burst: GRB 140619B. From the spectral analysis of the early ~ 0.2 s, we infer an observed temperature $kT = (324 \pm 33)$ keV of the e^+e^--plasma at transparency (P-GRB), a theoretically derived redshift $z = 2.67 \pm 0.37$, a total burst energy $E^{tot}_{e^+e^-} = (6.03 \pm 0.79) \times 10^{52}$ erg, a rest-frame peak energy $E_{p,i} = 4.7$ MeV, and a baryon load $B = (5.52 \pm 0.73) \times 10^{-5}$. We also estimate the corresponding emission of gravitational waves. Two additional examples of family-2 short bursts are identified: GRB 081024B and GRB 090510, remarkable for its well determined cosmological distance. We show that marked differences exist in the nature of the afterglows of these two families of short bursts: family-2 bursts, leading to BH formation, consistently exhibit high energy emission following the P-GRB emission; family-1 bursts, leading to the formation of a massive NS, should never exhibit high energy emission. We also show that both the families fulfill an $E_{p,i}$–E_{iso} relation with slope $\gamma = 0.59 \pm 0.07$ and a normalization constant incompatible with the one for long GRBs. The observed rate of such family-2 events is $\rho_0 = \left(2.1^{+2.8}_{-1.4}\right) \times 10^{-4}\mathrm{Gpc}^{-3}\mathrm{yr}^{-1}$.

42. R. Ruffini, Y. Aimuratov, C.L. Bianco, M. Enderli, M. Kovacevic, R. Moradi, M. Muccino, A.V. Penacchioni, G.B. Pisani, J.A. Rueda, Y. Wang; "Induced gravitational collapse in FeCO Core-Neutron star binaries and Neutron star-Neutron star binary mergers"; International Journal of Modern Physics A, 30, 1545023 (2015).

    We review the recent progress in understanding the nature of gamma-ray bursts (GRBs). The occurrence of GRB is explained by the Induced Gravitational Collapse (IGC) in FeCO Core-Neutron star binaries and Neutron star-Neutron star binary mergers, both processes occur within binary system progenitors. Making use of this most unexpected new paradigm, with the fundamental implications by the neutron star (NS) critical mass, we find that different initial configurations of binary systems lead to different GRB families with specific new physical predictions confirmed by observations.

43. R. Ruffini, M. Muccino, Y. Aimuratov, C.L. Bianco, C. Cherubini, M. Enderli, M. Kovacevic, R. Moradi, A.V. Penacchioni, G.B. Pisani, J.A. Rueda, Y. Wang; "GRB 090510: A genuine short-GRB from a binary neutron star coalescing into a Kerr-Newman black hole"; The Astrophysical Journal, 831, 178 (2016).

    In a new classification of merging binary neutron stars (NSs) we separate short gamma-ray bursts (GRBs) in two sub-classes. The ones with $E_{\rm iso} \lesssim 10^{52}$ erg coalesce to form a massive NS and are indicated as short gamma-ray flashes (S-GRFs). The hardest, with $E_{\rm iso} \gtrsim 10^{52}$ erg, coalesce to form a black hole (BH) and are indicated as genuine short-GRBs (S-GRBs). Within the fireshell model, S-GRBs exhibit three different components: the P-GRB emission, observed at the transparency of a self-accelerating baryon-e^+e^- plasma; the prompt emission, originating from the interaction of the accelerated baryons with the circumburst medium; the high-energy (GeV) emission, observed after the P-GRB and indicating the formation of a BH. GRB 090510 gives the first evidence for the formation of a Kerr BH or, possibly, a Kerr-Newman BH. Its P-GRB spectrum can be fitted by a convolution of thermal spectra whose origin can be traced back to an axially symmetric dyadotorus. A large value of the angular momentum of the newborn BH is consistent with the large energetics of this S-GRB, which reach in the 1–10000 keV range $E_{\rm iso} = (3.95 \pm 0.21) \times 10^{52}$ erg and in the 0.1–100 GeV range $E_{\rm LAT} = (5.78 \pm 0.60) \times 10^{52}$ erg, the most energetic GeV emission ever observed in S-GRBs. The theoretical redshift $z_{\rm th} = 0.75 \pm 0.17$ that we derive from the fireshell theory is consistent with the spectroscopic measurement $z = 0.903 \pm 0.003$, showing the self-consistency of the theoretical approach. All S-GRBs exhibit GeV emission, when inside the *Fermi*-LAT field of view, unlike S-GRFs, which never evidence it. The GeV emission appears to be the discriminant for the formation of a BH in GRBs, confirmed by their observed overall energetics.

44. Ruffini, R.; Rueda, J. A.; Muccino, M.; Aimuratov, Y.; Becerra, L. M.; Bianco, C. L.; Kovacevic, M.; Moradi, R.; Oliveira, F. G.; Pisani, G. B.; Wang, Y.; On the classification of GRBs and their occurrence rates; The Astrophysical Journal, 832, 136 (2016).

    There is mounting evidence for the binary nature of the progenitors of gamma-ray bursts (GRBs). For a long GRB, the induced gravitational collapse (IGC) paradigm proposes as progenitor, or “in-state”, a tight binary system composed of a carbon-oxygen core ($CO_{\rm core}$) undergoing a supernova (SN) explosion which triggers hypercritical accretion onto a neutron star (NS) companion. For a short GRB, a NS-NS merger is traditionally adopted as the progenitor. We divide long and short GRBs into two sub-classes, depending on whether or not a black hole (BH) is formed in the merger or in the hypercritical accretion process exceeding the NS critical mass. For long bursts, when no BH is formed we have the sub-class of X-ray flashes (XRFs), with isotropic energy $E_{iso} \lesssim 10^{52}$ erg and rest-frame spectral peak energy $E_{p,i} \lesssim 200$ keV. When a BH is formed we have the sub-class of binary-driven hypernovae (BdHNe), with $E_{iso} \gtrsim 10^{52}$ erg and $E_{p,i} \gtrsim 200$ keV. In analogy, short bursts are similarly divided into two sub-classes. When no BH is formed, short gamma-ray flashes (S-GRFs) occur, with $E_{iso} \lesssim 10^{52}$ erg and $E_{p,i} \lesssim 2$ MeV. When a BH is formed, the authentic short GRBs (S-GRBs) occur, with $E_{iso} \gtrsim 10^{52}$ erg and $E_{p,i} \gtrsim 2$ MeV. We give examples and observational signatures of these four sub-classes and their rate of occurrence. From their respective rates it is possible that "in-states" of S-GRFs and S-GRBs originate from the "out-states" of XRFs. We indicate two additional progenitor systems: white dwarf-NS and BH-NS. These systems have hybrid features between long and short bursts. In the case of S-GRBs and BdHNe evidence is given of the coincidence of the onset of the high energy GeV emission with the birth of a Kerr BH.

45. Becerra, L.; Bianco, C. L.; Fryer, C. L.; Rueda, J. A.; Ruffini, R.; On the induced gravitational collapse scenario of gamma-ray bursts associated with supernovae; The Astrophysical Journal, 833, 107 (2016).

    Following the induced gravitational collapse (IGC) paradigm of gamma-ray bursts (GRBs) associated with type Ib/c supernovae, we present numerical simulations of the explosion of a carbon-oxygen (CO) core in a binary system with a neutron-star (NS) companion. The supernova ejecta trigger a *hypercritical* accretion process onto the NS thanks to a copious neutrino emission and the trapping of photons within the accretion flow. We show that temperatures 1–10 MeV develop near the NS surface, hence electron-positron annihilation into neutrinos becomes the main cooling channel leading to accretion rates 10^{-9}–10^{-1} $M_\odot$ s^{-1} and neutrino luminosities 10^{43}–10^{52} erg s^{-1} (the shorter the orbital period the higher the accretion rate). We estimate the maximum orbital period, $P_{\rm max}$, as a function of the NS initial mass, up to which the NS companion can reach by hypercritical accretion the critical mass for gravitational collapse leading to black-hole (BH) formation. We then estimate the effects of the accreting and orbiting NS companion onto a novel geometry of the supernova ejecta density profile. We present the results of a 1.4×10^7 particle simulation which show that the NS induces accentuated asymmetries in the ejecta density around the orbital plane. We elaborate on the observables associated with the above features of the IGC process. We apply this framework to specific GRBs: we find that X-ray flashes (XRFs) and binary-driven hypernovae (BdHNe) are produced in binaries with $P > P_{\rm max}$ and $P < P_{\rm max}$, respectively. We analyze in detail the case of XRF 060218.

46. Pisani, G. B.; Ruffini, R.; Aimuratov, Y.; Bianco, C. L.; Kovacevic, M.;

Moradi, R.; Muccino, M.; Penacchioni, A. V.; Rueda, J. A.; Shakeri, S.; Wang, Y.; On the universal late X-ray emission of binary-driven hypernovae and its possible collimation; The Astrophysical Journal, 833, 159 (2016).

It has been previously discovered a universal power-law behaviour of the late X-ray emission (LXRE) of a "golden sample" (GS) of six long energetic GRBs, when observed in the rest-frame of the source. This remarkable feature, independent on the different isotropic energy (E_{iso}) of each GRB, has been used to estimate the cosmological redshift of some long GRBs. This analysis is here extended to a new class of 161 long GRBs, all with $E_{iso} > 10^{52}$ erg. These GRBs are indicated as binary-driven hypernovae (BdHNe) in view of their progenitors: a tight binary systems composed of a carbon-oxigen core (CO_{core}) and a neutron star (NS) undergoing an induced gravitational collapse (IGC) to a black hole (BH) triggered by the CO_{core} explosion as a supernova (SN). We confirm the universal behaviour of the LXRE for the "enlarged sample" (ES) of 161 BdHNe observed up to the end of 2015, assuming a double-cone emitting region. We obtain a distribution of half-opening angles peaking at $\theta = 17.62°$, with mean value 30.05°, and a standard deviation 19.65°. This, in turn, leads to the possible establishment of a new cosmological candle. Within the IGC model, such universal LXRE behaviour is only indirectly related to the GRB and originates from the SN ejecta, of a standard constant mass, being shocked by the GRB emission. The fulfillment of the universal relation in the LXRE and its independence of the prompt emission, further confirmed in this article, establishes a crucial test for any viable GRB model.

47. Y. Aimuratov, R. Ruffini, M. Muccino, C.L. Bianco, A.V. Penacchioni, G.B. Pisani, D. Primorac, J.A. Rueda, Y. Wang; GRB 081024B and GRB 140402A: Two Additional Short GRBs from Binary Neutron Star Mergers; The Astrophysical Journal, 844, 83 (2017).

    Theoretical and observational evidences have been recently gained for a two-fold classification of short bursts: 1) short gamma-ray flashes (S-GRFs), with isotropic energy $E_{iso} < 10^{52}$ erg and no BH formation, and 2) the authentic short gamma-ray bursts (S-GRBs), with isotropic energy $E_{iso} > 10^{52}$ erg evidencing a BH formation in the binary neutron star merging process. The signature for the BH formation consists in the on-set of the high energy (0.1–100 GeV) emission, coeval to the prompt emission, in all S-GRBs. No GeV emission is expected nor observed in the S-GRFs. In this paper we present two additional S-GRBs, GRB 081024B and GRB 140402A, following the already identified S-GRBs, i.e., GRB 090227B, GRB 090510 and GRB 140619B. We also return on the absence of the GeV emission of the S-GRB 090227B, at an angle of 71° from the *Fermi*-LAT boresight. All the correctly identified S-GRBs correlate to the high energy emission, implying no significant presence of beaming in the GeV emission. The existence of a common power-law behavior in the GeV luminosities, following the BH formation, when measured in the source rest-frame, points to a commonality in the mass and spin of the newly-formed BH in all S-GRBs.

48. J.A. Rueda, Y. Aimuratov, U. Barres de Almeida, L.M. Becerra, C.L. Bianco, C. Cherubini, S. Filippi, M. Karlica, M. Kovacevic, J.D. Melon Fuksman, R. Moradi, M. Muccino, A.V. Penacchioni, G.B. Pisani, D. Primorac, R. Ruffini, N. Sahakyan, S. Shakeri, Y. Wang; The binary systems associated with short and long gamma-ray bursts and their detectability; International Journal of Modern Physics D, 26, 1730016 (2017).

    Short and long-duration gamma-ray bursts (GRBs) have been recently subclassified into seven families according to the binary nature of their progenitors. For short GRBs, mergers of neutron star binaries (NS–NS) or neutron star-black hole binaries (NS-BH) are proposed. For long GRBs, the induced gravitational collapse (IGC) paradigm proposes a tight binary system composed of a carbon–oxygen core (COcore) and a NS companion. The explosion of the COcore as supernova (SN) triggers a hypercritical accretion process onto the NS companion which might reach the critical mass for the gravitational collapse to a BH. Thus, this process can lead either to a NS-BH or to NS–NS depending on whether or not the accretion is sufficient to induce the collapse of the NS into a BH. We shall discuss for the above compact object binaries: (1) the role of the NS structure and the equation-of-state on their final fate; (2) their occurrence rates as inferred from the X and gamma-ray observations; (3) the expected number of detections of their gravitational wave (GW) emission by the Advanced LIGO interferometer.

49. R. Ruffini, Y. Aimuratov, L.M. Becerra, C.L. Bianco, M. Karlica, M. Kovacevic, J.D. Melon Fuksman, R. Moradi, M. Muccino, A.V. Penacchioni, G.B. Pisani, D. Primorac, J.A. Rueda, S. Shakeri, G.V. Vereshchagin, Y. Wang, S.-S. Xue; The cosmic matrix in the 50th anniversary of relativistic astrophysics; International Journal of Modern Physics D, 26, 1730019 (2017).

Our concept of induced gravitational collapse (IGC paradigm) starting from a supernova occurring with a companion neutron star, has unlocked the understanding of seven different families of gamma ray bursts (GRBs), indicating a path for the formation of black holes in the universe. An authentic laboratory of relativistic astrophysics has been unveiled in which new paradigms have been introduced in order to advance knowledge of the most energetic, distant and complex systems in our universe. A novel cosmic matrix paradigm has been introduced at a relativistic cosmic level, which parallels the concept of an S-matrix introduced by Feynmann, Wheeler and Heisenberg in the quantum world of microphysics. Here the "in" states are represented by a neutron star and a supernova, while the "out" states, generated within less than a second, are a new neutron star and a black hole. This novel field of research needs very powerful technological observations in all wavelengths ranging from radio through optical, X-ray and gamma ray radiation all the way up to ultra-high-energy cosmic rays.

50. R. Ruffini, Y. Wang, Y. Aimuratov, U. Barres de Almeida, L.M. Becerra, C.L. Bianco, Y.C. Chen, M. Karlica, M. Kovacevic, L. Li, J.D. Melon Fuksman, R. Moradi, M. Muccino, A.V. Penacchioni, G.B. Pisani, D. Primorac, J.A. Rueda, S. Shakeri, G.V. Vereshchagin, S.-S. Xue; Early X-Ray Flares in GRBs; The Astrophysical Journal, 852, 53 (2018).

    We analyze the early X-ray flares in the GRB "flare-plateau-afterglow" (FPA) phase observed by Swift-XRT. The FPA occurs only in one of the seven GRB subclasses: the binary-driven hypernovae (BdHNe). This subclass consists of long GRBs with a carbon-oxygen core and a neutron star (NS) binary companion as progenitors. The hypercritical accretion of the supernova (SN) ejecta onto the NS can lead to the gravitational collapse of the NS into a black hole. Consequently, one can observe a GRB emission with isotropic energy $E_{iso} \gtrsim 10^{52}$ erg, as well as the associated GeV emission and the FPA phase. Previous work had shown that gamma-ray spikes in the prompt emission occur at $\sim 10^{15}$–10^{17} cm with Lorentz gamma factor $\Gamma \sim 10^2$–10^3. Using a novel data analysis we show that the time of occurrence, duration, luminosity and total energy of the X-ray flares correlate with E_{iso}. A crucial feature is the observation of thermal emission in the X-ray flares that we show occurs at radii $\sim 10^{12}$ cm with $\Gamma \lesssim 4$. These model independent observations cannot be explained by the "fireball" model, which postulates synchrotron and inverse Compton radiation from a single ultra relativistic jetted emission extending from the prompt to the late afterglow and GeV emission phases. We show that in BdHNe a collision between the GRB and the SN ejecta occurs at $\simeq 10^{10}$ cm reaching transparency at $\sim 10^{12}$ cm with $\Gamma \lesssim 4$. The agreement between the thermal emission observations and these theoretically derived values validates our model and opens the possibility of testing each BdHN episode with the corresponding Lorentz gamma factor.

51. R. Ruffini, J. Rodriguez, M. Muccino, J.A. Rueda, Y. Aimuratov, U. Barres de Almeida, L.M. Becerra, C.L. Bianco, C. Cherubini, S. Filippi, D. Gizzi, M. Kovacevic, R. Moradi, F.G. Oliveira, G.B. Pisani, Y. Wang; On the Rate and on the Gravitational Wave Emission of Short and Long GRBs; The Astrophysical Journal, 859, 30 (2018).

    On the ground of the large number of gamma-ray bursts (GRBs) detected with cosmological redshift, we classified GRBs in seven subclasses, all with binary progenitors which emit gravitational waves (GWs). Each binary is composed of combinations of carbon-oxygen cores (COcore), neutron stars (NSs), black holes (BHs), and white dwarfs (WDs). The long bursts, traditionally assumed to originate from a BH with an ultrarelativistic jetted emission, not emitting GWs, have been subclassified as (I) X-ray flashes (XRFs), (II) binary-driven hypernovae (BdHNe), and (III) BH-supernovae (BH-SNe). They are framed within the induced gravitational collapse paradigm with a progenitor COcore-NS/BH binary. The SN explosion of the COcore triggers an accretion process onto the NS/BH. If the accretion does not lead the NS to its critical mass, an XRF occurs, while when the BH is present or formed by accretion, a BdHN occurs. When the binaries are not disrupted, XRFs lead to NS-NS and BdHNe lead to NS-BH. The short bursts, originating in NS-NS, are subclassified as (IV) short gamma-ray flashes (S-GRFs) and (V) short GRBs (S-GRBs), the latter when a BH is formed. There are (VI) ultrashort GRBs (U-GRBs) and (VII) gamma-ray flashes (GRFs) formed in NS-BH and NS-WD, respectively. We use the occurrence rate and GW emission of these subclasses to assess their detectability by Advanced LIGO-Virgo, eLISA, and resonant bars. We discuss the consequences of our results in view of the announcement of the LIGO/Virgo Collaboration of the source GW 170817 as being originated by an NS-NS.

52. J.A. Rueda, R. Ruffini, Y. Wang, Y. Aimuratov, U. Barres de Almeida, C.L. Bianco, Y.-C. Chen, R.V. Lobato, C. Maia, D. Primorac, R. Moradi, J. Rodriguez; GRB 170817A-GW170817-AT 2017gfo and the observations of NS-NS, NS-WD and WD-WD mergers; Journal of Cosmology and Astroparticle Physics, 10, 006 (2018).

The LIGO-Virgo Collaboration has announced the detection of GW170817 and has associated it with GRB 170817A . These signals have been followed after 11 hours by the optical and infrared emission of AT 2017gfo. The origin of this complex phenomenon has been attributed to a neutron star-neutron star (NS-NS) merger. In order to probe this association we confront our current understanding of the gravitational waves and associated electromagnetic radiation with four observed GRBs originating in binaries composed of different combinations NSs and white dwarfs (WDs). We consider 1) GRB 090510 the prototype of NS-NS merger leading to a black hole (BH); 2) GRB 130603B the prototype of a NS-NS merger leading to massive NS (MNS) with an associated kilonova; 3) GRB 060614 the prototype of a NS-WD merger leading to a MNS with an associated kilonova candidate; 4) GRB 170817A the prototype of a WD-WD merger leading to massive WD with an associated AT 2017gfo-like emission. None of these systems support the above mentioned association. The clear association between GRB 170817A and AT 2017gfo has led to introduce a new model based on a new subfamily of GRBs originating from WD-WD mergers. We show how this novel model is in agreement with the exceptional observations in the optical, infrared, X- and gamma-rays of GRB 170817A-AT 2017gfo.

53. R. Ruffini, M. Karlica, N. Sahakyan, J.A. Rueda, Y. Wang, G.W. Mathews, C.L. Bianco, M. Muccino; A GRB Afterglow Model Consistent with Hypernova Observations; The Astrophysical Journal, 869, 101 (2018).

    We describe the afterglows of the long gamma-ray-burst (GRB) 130427A within the context of a binary-driven hypernova. The afterglows originate from the interaction between a newly born neutron star (νNS), created by an Ic supernova (SN), and a mildly relativistic ejecta of a hypernova (HN). Such an HN in turn results from the impact of the GRB on the original SN Ic. The mildly relativistic expansion velocity of the afterglow ($\Gamma \sim 3$) is determined, using our model-independent approach, from the thermal emission between 196 and 461 s. The power law in the optical and X-ray bands of the afterglow is shown to arise from the synchrotron emission of relativistic electrons in the expanding magnetized HN ejecta. Two components contribute to the injected energy: the kinetic energy of the mildly relativistic expanding HN and the rotational energy of the fast-rotating highly magnetized ?NS. We reproduce the afterglow in all wavelengths from the optical (10^{14} Hz) to the X-ray band (10^{19} Hz) over times from 604 s to 5.18×10^6 s relative to the Fermi-GBM trigger. Initially, the emission is dominated by the loss of kinetic energy of the HN component.

After 10^5 s the emission is dominated by the loss of rotational energy of the νNS, for which we adopt an initial rotation period of 2 ms and a dipole plus quadrupole magnetic field of $\lesssim 7 \times 10^{12}$ G or $\sim 10^{14}$ G. This scenario with a progenitor composed of a COcore and an NS companion differs from the traditional ultra-relativistic-jetted treatments of the afterglows originating from a single black hole.

54. R. Ruffini, L.M. Becerra, C.L. Bianco, Y.-C. Chen, M. Karlica, M. Kovacevic, J.D. Melon Fuksman, R. Moradi, M. Muccino, G.B. Pisani, D. Primorac, J.A. Rueda, G.V. Vereshchagin, Y. Wang, S.-S. Xue; On the ultra-relativistic Prompt Emission (UPE), the Hard and Soft X-ray Flares, and the extended thermal emission (ETE) in GRB 151027A; The Astrophysical Journal, 869, 151 (2018).

    We analyze GRB 151027A within the binary-driven hypernova approach, with a progenitor of a carbon–oxygen core on the verge of a supernova (SN) explosion and a binary companion neutron star (NS). The hypercritical accretion of the SN ejecta onto the NS leads to its gravitational collapse into a black hole (BH), to the emission of the gamma-ray burst (GRB), and to a copious e+e- plasma. The impact of this e+e- plasma on the SN ejecta explains the early soft X-ray flare observed in long GRBs. Here, we apply this approach to the ultra-relativistic prompt emission (UPE) and to the hard X-ray flares. We use GRB 151027A as a prototype. From the time-integrated and the time-resolved analysis, we identify a double component in the UPE and confirm its ultra-relativistic nature. We confirm the mildly relativistic nature of the soft X-ray flare, of the hard X-ray flare, and of the extended thermal emission (ETE). We show that the ETE identifies the transition from an SN to a hypernova (HN). We then address the theoretical justification of these observations by integrating the hydrodynamical propagation equations of the e+e- into the SN ejecta, with the latter independently obtained from 3D smoothed particle hydrodynamics simulations. We conclude that the UPE, the hard X-ray flare, and the soft X-ray flare do not form a causally connected sequence. Within our model, they are the manifestation of the same physical process of the BH formation as seen through different viewing angles, implied by the morphology and the ~ 300 s rotation period of the HN ejecta.

55. R. Moradi, R. Ruffini, C.L. Bianco, Y.-C. Chen, M. Karlica, J.D. Melon Fuksman, D. Primorac, J.A. Rueda, S. Shakeri, Y. Wang, S.-S. Xue; Relativistic Behavior and Equitemporal Surfaces in Ultra-Relativistic Prompt

Emission Phase of Gamma-Ray Bursts; Astronomy Reports, 62, 905 (2018).

In this work we study a role of baryon load and interstellar medium density to explain the nature of peaks in the ultra-relativistic prompt emission (UPE) phase of Gamma-ray Bursts (GRBs). We study the behavior of their Γ Lorenz factor fromthe moment of transparency all the way up to interstellar medium. We finally study the characteristic of equitemporal surfaces in the UPE phase.

56. D. Primorac, M. Muccino, R. Moradi, Y. Wang, J.D. Melon Fuksman, R. Ruffini, C.L. Bianco, J.A. Rueda; Structure of the Prompt Emission of GRB 151027A Within the Fireshell Model; Astronomy Reports, 62, 933 (2018).

    Long gamma-ray burst GRB 151027A was observed by all three detectors onboard the Swift spacecraft, and many more, including MAXI, Konus-Wind and Fermi GBM/LAT instruments. This revealed a complex structure of the prompt and afterglow emission, consisting of a double-peak gammaray prompt with a quiescent period and a HRF/SXF within the X-ray afterglow, together with multiple BB components seen within the time-resolved spectral analysis. These features, within the fireshell model, are interpreted as the manifestation of the same physical process viewed at different angles with respect to the HN ejecta. Here we present the time-resolved and time-integrated spectral analysis used to determine the energy of the e-e+ plasma E_{tot} and the baryon load B. These quantities describe the dynamics of the fireshell up to the transparency point. We proceed with the light-curve simulation from which CBM density values and its inhomogeneities are deduced. We also investigate the properties of GRB 140206A, whose prompt emission exhibits a similar structure.

57. Y. Wang, J.A. Rueda, R. Ruffini, C.L. Bianco, L.M. Becerra, L. Li, M. Karlica; Two Predictions of Supernova: GRB 130427A/SN 2013cq and GRB 180728A/SN 2018fip; The Astrophysical Journal, 874, 39 (2019).

    On 2018 July 28, GRB 180728A triggered *Swift* satellites and, soon after the determination of the redshift, we identified this source as a type II binary-driven hypernova (BdHN II) in our model. Consequently, we predicted the appearance time of its associated supernova (SN), which was later confirmed as SN 2018fip. A BdHN II originates in a binary composed of a carbon-oxygen core (CO_{core}) undergoing SN, and the SN ejecta hypercritically accrete onto a companion neutron star (NS). From the time of the SN shock breakout to the time when the hypercritical accretion starts, we infer the binary separation

$\simeq 3 \times 10^{10}$ cm. The accretion explains the prompt emission of isotropic energy $\simeq 3 \times 10^{51}$ erg, lasting ~ 10 s, and the accompanying observed blackbody emission from a thermal convective instability bubble. The new neutron star (νNS) originating from the SN powers the late afterglow from which a νNS initial spin of 2.5 ms is inferred. We compare GRB 180728A with GRB 130427A, a type I binary-driven hypernova (BdHN I) with isotropic energy $> 10^{54}$ erg. For GRB 130427A we have inferred an initially closer binary separation of $\simeq 10^{10}$ cm, implying a higher accretion rate leading to the collapse of the NS companion with consequent black hole formation, and a faster, 1 ms spinning νNS. In both cases, the optical spectra of the SNe are similar, and not correlated to the energy of the gamma-ray burst. We present three-dimensional smoothed-particle-hydrodynamic simulations and visualisations of the BdHNe I and II.

58. J.A. Rueda, R. Ruffini, Y. Wang, C.L. Bianco, J.M. Blanco-Iglesias, M. Karlica, P. Lorén-Aguilar, R. Moradi, N. Sahakyan; Electromagnetic emission of white dwarf binary mergers; Journal of Cosmology and Astroparticle Physics, 03, 044 (2019).

    It has been recently proposed that the ejected matter from white dwarf (WD) binary mergers can produce transient, optical and infrared emission similar to the "kilonovae" of neutron star (NS) binary mergers. To confirm this we calculate the electromagnetic emission from WD-WD mergers and compare with kilonova observations. We simulate WD-WD mergers leading to a massive, fast rotating, highly magnetized WD with an adapted version of the smoothed-particle-hydrodynamics (SPH) code Phantom. We thus obtain initial conditions for the ejecta such as escape velocity, mass and initial position and distribution. The subsequent thermal and dynamical evolution of the ejecta is obtained by integrating the energy-conservation equation accounting for expansion cooling and a heating source given by the fallback accretion onto the newly-formed WD and its magneto-dipole radiation. We show that magnetospheric processes in the merger can lead to a prompt, short gamma-ray emission of up to $\approx 10^{46}$ erg in a timescale of 0.1–1 s. The bulk of the ejecta initially expands non-relativistically with velocity 0.01 c and then it accelerates to 0.1 c due to the injection of fallback accretion energy. The ejecta become transparent at optical wavelengths around ~ 7 days post-merger with a luminosity 10^{41}–10^{42} erg s^{-1}. The X-ray emission from the fallback accretion becomes visible around $\sim$ 150–200 day post-merger with a luminosity of 10^{39} erg s^{-1}. We also predict the post-merger time at which the central WD should appear as a pulsar depending on the value of the magnetic field and rotation period.

59. J.A. Rueda, R. Ruffini, Y. Wang; Induced Gravitational Collapse, Binary-Driven Hypernovae, Long Gramma-ray Bursts and Their Connection with Short Gamma-ray Bursts; Universe, 5, 110 (2019).

There is increasing observational evidence that short and long Gamma-ray bursts (GRBs) originate in different subclasses, each one with specific energy release, spectra, duration, etc, and all of them with binary progenitors. The binary components involve carbon-oxygen cores (CO_{core}), neutron stars (NSs), black holes (BHs), and white dwarfs (WDs). We review here the salient features of the specific class of binary-driven hypernovae (BdHNe) within the induced gravitational collapse (IGC) scenario for the explanation of the long GRBs. The progenitor is a CO_{core}-NS binary. The supernova (SN) explosion of the CO_{core}, producing at its center a new NS (νNS), triggers onto the NS companion a hypercritical, i.e., highly super-Eddington accretion process, accompanied by a copious emission of neutrinos. By accretion the NS can become either a more massive NS or reach the critical mass for gravitational collapse with consequent formation of a BH. We summarize the results on this topic from the first analytic estimates in 2012 all the way up to the most recent three-dimensional (3D) smoothed-particle-hydrodynamics (SPH) numerical simulations in 2018. Thanks to these results it is by now clear that long GRBs are richer and more complex systems than thought before. The SN explosion and its hypercritical accretion onto the NS explain the X-ray precursor. The feedback of the NS accretion, the NS collapse and the BH formation produce asymmetries in the SN ejecta, implying the necessity of a 3D analysis for GRBs. The newborn BH, the surrounding matter and the magnetic field inherited from the NS, comprises the *inner engine* from which the GRB electron-positron (e^+e^-) plasma and the high-energy emission are initiated. The impact of the e^+e^- on the asymmetric ejecta transforms the SN into a hypernova (HN). The dynamics of the plasma in the asymmetric ejecta leads to signatures depending on the viewing angle. This explains the ultrarelativistic prompt emission in the MeV domain and the mildly-relativistic flares in the early afterglow in the X-ray domain. The feedback of the νNS pulsar-like emission on the HN explains the X-ray late afterglow and its power-law regime. All of the above is in contrast with a simple GRB model attempting to explain the entire GRB with the kinetic energy of an ultrarelativistic jet extending through all of the above GRB phases, as traditionally proposed in the "collapsar-fireball" model. In addition, BdHNe in their different flavors lead to νNS-NS or νNS-BH binaries. The gravitational wave emission drives these binaries to merge producing short GRBs. It is thus established a previously unthought interconnection between long and short GRBs and their occurrence rates. This needs to be accounted for in the cosmological evolution of binaries within population synthesis models for the formation of compact-object binaries.

60. R. Ruffini, J.D. Melon Fuksman, G.V. Vereshchagin; On the role of a cavity in the hypernova ejecta of GRB 190114C; The Astrophysical Journal, 883, 191 (2019).

    Within the binary-driven hypernova I (BdHN I) scenario, the gamma-ray burst GRB190114C originates in a binary system composed of a massive carbon-oxygen core (CO_{core}), and a binary neutron star (NS) companion. As the CO_{core} undergoes a supernova explosion with the creation of a new neutron star (νNS), hypercritical accretion occurs onto the companion binary neutron star until it exceeds the critical mass for gravitational collapse. The formation of a black hole (BH) captures 10^{57} baryons by enclosing them within its horizon, and thus a cavity of approximately 10^{11} cm is formed around it with initial density 10^{-7} g/cm^3. A further depletion of baryons in the cavity originates from the expansion of the electron-positron-photon ($e^+e^-\gamma$) plasma formed at the collapse, reaching a density of 10^{-14} g/cm^3 by the end of the interaction. It is demonstrated here using an analytical model complemented by a hydrodynamical numerical simulation that part of the $e^+e^-\gamma$ plasma is reflected off the walls of the cavity. The consequent outflow and its observed properties are shown to coincide with the featureless emission occurring in a time interval of duration t_{rf}, measured in the rest frame of the source, between 11 and 20 s of the GBM observation. Moreover, similar features of the GRB light curve were previously observed in GRB 090926A and GRB 130427A, all belonging to the BdHN I class. This interpretation supports the general conceptual framework presented in R. Ruffini et al. and guarantees that a low baryon density is reached in the cavity, a necessary condition for the operation of the "*inner engine*" of the GRB presented in an accompanying article.

61. R. Ruffini, R. Moradi, J.A. Rueda, L.M. Becerra, C.L. Bianco, C. Cherubini, S. Filippi, Y.C. Chen, M. Karlica, N. Sahakyan, Y. Wang, S.-S. Xue; On the GeV Emission of the Type I BdHN GRB 130427A; The Astrophysical Journal, 886, 82 (2019).

    We propose that the *inner engine* of a type I binary-driven hypernova (BdHN) is composed of a Kerr black hole (BH) in a non-stationary state, embedded in a uniform magnetic field B_0 aligned with the BH rotation axis, and surrounded by an ionized plasma of extremely low density of 10^{-14} g cm^{-3}. Using GRB 130427A as a prototype we show that this *inner engine* acts in a sequence of *elementary impulses*. Electrons are accelerated to ultra-relativistic energy near the BH horizon and, propagating along the polar axis, $\theta = 0$, they can reach energies of $\sim 10^{18}$ eV, and partially contribute to ultra-high energy cosmic rays (UHECRs). When propagating with $\theta \neq 0$ through the magnetic field B_0 they give origin by synchrotron emission to GeV and TeV radiation. The mass of BH, $M = 2.3 M_\odot$, its spin, $\alpha = 0.47$, and the value of magnetic field $B_0 = 3.48 \times 10^{10}$ G, are determined self-consistently in order to fulfill the energetic and the transparency requirement. The repetition time of each elementary impulse of energy $\mathcal{E} \sim 10^{37}$ erg, is $\sim 10^{-14}$ s at the beginning of the process, then slowly increasing with time evolution. In principle, this "*inner engine*" can operate in a GRB for thousands of years. By scaling the BH mass and the magnetic field the same "*inner engine*" can describe active galactic nuclei (AGN).

62. L. Li; Thermal Components in Gamma-ray Bursts. II. Constraining the Hybrid Jet Model; The Astrophysical Journal, 894, 100 (2020).

    In explaining the physical origin of the jet composition of gamma-ray bursts (GRBs), a more general picture, i.e. the hybrid jet model (which introduced another magnetization parameter σ_0 on the basis of the traditional fireball model), has been well studied in Gao & Zhang. However, it still has not yet been applied to a large GRB sample. Here, we first employ the "top-down" approach of Gao & Zhang to diagnose the photosphere properties at the central engine to see how the hybrid model can account for the observed data as well, through applying a *Fermi* GRB sample (eight bursts) with the detected photosphere component, as presented in Li (our Paper I). We infer all physical parameters of a hybrid problem with three typical values of the radius of the jet base (r_0 = 10^7, 10^8, and 10^9 cm). We find that the dimensionless entropy for all the bursts shows $\eta \gg 1$ while the derived (1+σ_0) for five bursts (GRB 081224, GRB 110721A, GRB 090719, GRB 100707, and GRB 100724) is larger than unity, indicating that in addition to a hot fireball component, another cold Poynting-flux component may also play an important role. Our analysis also shows that in a few time bins for all r_0 in GRB 081224 and GRB 110721A, the magnetization parameter at $\sim 10^{15}$cm (1+σ_{r15}) is greater than unity, which implies that internal-collision-induced magnetic reconnection and turbulence may be the mechanism to power the nonthermal emission, rather than internal shocks. We conclude that the majority of bursts (probably all) can be well explained by the hybrid jet problem.

63. J.A. Rueda, R. Ruffini, M. Karlica, R. Moradi, Y. Wang; Magnetic fields and afterglows of bdhne: inferences from grb 130427a, grb 160509a, grb 160625b, grb 180728a, and grb 190114c; The Astrophysical Journal, 893, 148 (2020).

GRB 190114C is the first binary-driven hypernova (BdHN) fully observed from the initial supernova appearance to the final emergence of the optical SN signal. It offers an unprecedented testing ground for the BdHN theory and it is here determined and further extended to additional gamma-ray bursts (GRBs). BdHNe comprise two subclasses of long GRBs with progenitors a binary system composed of a carbon-oxygen star (CO_{core}) and a neutron star (NS) companion. The CO_{core} explodes as a SN leaving at its center a newborn NS (νNS). The SN ejecta hypercritically accretes both on the νNS and the NS companion. BdHNe I are the tightest binaries where the accretion leads the companion NS to gravitational collapse into a black hole (BH). In BdHN II the accretion onto the NS is lower, so there is no BH formation. We observe the same structure of the afterglow for GRB 190114C and other selected examples of BdHNe I (GRB 130427A, GRB 160509A, GRB 160625B) and for BdHN II (GRB 180728A). In all the cases the explanation of the afterglow is reached via the synchrotron emission powered by the νNS: their magnetic fields structures and their spin are determined. For BdHNe I, we discuss the properties of the magnetic field embedding the newborn BH, inherited from the collapsed NS and amplified during the gravitational collapse process, and surrounded by the SN ejecta.

64. J.A. Rueda, R. Ruffini; The blackholic quantum; European Physical Journal C, 80, 300 (2020).

We show that the high-energy emission of GRBs originates in the *inner engine*: a Kerr black hole (BH) surrounded by matter and a magnetic field B_0. It radiates a sequence of discrete events of particle acceleration, each of energy $\mathcal{E} = \hbar\,\Omega_{\rm eff}$, the *blackholic quantum*, where $\Omega_{\rm eff} = 4(m_{\rm Pl}/m_n)^8(c\,a/G\,M)(B_0^2/\rho_{\rm Pl})\Omega_+$. Here M, $a = J/M$, $\Omega_+ = c^2\partial M/\partial J = (c^2/G)\,a/(2Mr_+)$ and r_+ are the BH mass, angular momentum per unit mass, angular velocity and horizon; m_n is the neutron mass, $m_{\rm Pl}$, $\lambda_{\rm Pl} = \hbar/(m_{\rm Pl}c)$ and $\rho_{\rm Pl} = m_{\rm Pl}c^2/\lambda_{\rm Pl}^3$, are the Planck mass, length and energy density. Here and in the following use CGS-Gaussian units. The timescale of each process is $\tau_{\rm el} \sim \Omega_+^{-1}$, along the rotation axis, while it is much shorter off-axis owing to energy losses such as synchrotron radiation. We show an analogy with the Zeeman and Stark effects, properly scaled from microphysics to macrophysics, that allows us to define the *BH magneton*,

$\mu_{\rm BH} = (m_{\rm Pl}/m_n)^4(c\,a/G\,M)e\,\hbar/(Mc)$. We give quantitative estimates for GRB 130427A adopting $M = 2.3\ M_\odot$, $c\,a/(G\,M) = 0.47$ and $B_0 = 3.5 \times 10^{10}$ G. Each emitted *quantum*, $\mathcal{E} \sim 10^{37}$ erg, extracts only 10^{-16} times the BH rotational energy, guaranteeing that the process can be repeated for thousands of years. The *inner engine* can also work in AGN as we here exemplified for the supermassive BH at the center of M87.

65. B. Zhang, Y. Wang, L. Li; Dissecting the Energy Budget of a Gamma-Ray Burst Fireball; The Astrophysical Journal Letters, 909, L3 (2021)

66. L. Li, B. Zhang; Testing the High-latitude Curvature Effect of Gamma-Ray Bursts with Fermi Data: Evidence of Bulk Acceleration in Prompt Emission; The Astrophysical Journal Supplement Series, 253, 43 (2021)

67. L. Li, F. Ryde, A. Pe'er, H.-F. Yu, Z. Acuner; The Astrophysical Journal Supplement Series; 254, 35 (2021)

68. Y. Wang; Do All Long-duration Gamma-Ray Bursts Emit GeV Photons?; The Astrophysical Journal, 913, 86 (2021)

69. L. Li; Searching for Observational Evidence for Binary Star Systems in Gamma-ray Bursts; Astronomy Reports, 65, 973 (2021)

70. Y. Wang; Gamma-Ray Burst from Binary Star: Neutron Star and Carbon–Oxygen Core; Astronomy Reports, 65, 1077 (2021)

71. R. Ruffini; Discovery of the Moment of Formation of the Black Hole in GRB 190114C; Astronomy Reports, 65, 1030 (2021)

72. R. Ruffini, R. Moradi, J.A. Rueda, L. Li, N. Sahakyan, Y.-C. Chen, Y. Wang, Y. Aimuratov, L. Becerra, C.L. Bianco, C. Cherubini, S. Filippi, M. Karlica, G.J. Mathews, M. Muccino, G.B. Pisani, S.-S. Xue; The morphology of the X-ray afterglows and of the jetted GeV emission in long GRBs; Monthly Notices of the Royal Astronomical Society, 504, 5301 (2021)

73. R. Moradi, J.?A. Rueda, R. Ruffini, Liang Li, C.?L. Bianco, S. Campion, C. Cherubini, S. Filippi, Y. Wang, and S.?S. Xue; Nature of the ultrarelativistic prompt emission phase of GRB 190114C; Phys. Rev. D, 104, 063043 (2021)

74. R. Moradi, J.A. Rueda, R. Ruffini and Y. Wang; The newborn black hole in GRB 191014C proves that it is alive; Astronomy & Astrophysics, 649, A75 (2021)

75. Xu, Fan, Geng, Jin-Jun, Wang, Xu, Li, Liang, Huang, Yong-Feng, "Is the birth of PSR J0538+2817 accompanied by a gamma-ray burst?"; Monthly Notices of the Royal Astronomical Society, 509, 4916 (2022)

76. Li, Liang; "Standard GRB Spectral Models "Misused"?"; The Astrophysical Journal, 941, 27 (2022)

77. Marongiu, M.; Guidorzi, C., Stratta, G., Gomboc, A., Jordana-Mitjans, N., Dichiara, S., Kobayashi, S., Kopa?, D., Mundell, C. G.; "Radio data challenge the broadband modelling of GRB 160131A afterglow"; Astronomy & Astrophysics, 658, A11 (2022)

78. Li, Liang; Rueda, J. A. ; Moradi, R.; Wang, Y. ; Xue, S. S. ; Ruffini, R.; "Self-similarities and Power Laws in the Time-resolved Spectra of GRB 190114C, GRB 130427A, GRB 160509A, and GRB 160625B"; The Astrophysical Journal, 945, 10 (2023)

79. Aimuratov, Y.; Becerra, L. M.; Bianco, C. L.; Cherubini, C.; Della Valle, M.; Filippi, S.; Li, Liang; Moradi, R.; Rastegarnia, F. ; Rueda, J. A.; Ruffini, R.; Sahakyan, N.; Wang, Y.; Zhang, S. R.; "GRB-SN Association within the Binary-driven Hypernova Model"; The Astrophysical Journal, 955, 93 (2023)

80. Bianco, C. L. ; Mirtorabi, M. T. ; Moradi, R. ; Rastegarnia, F. ; Rueda, J. A. ; Ruffini, R. ; Wang, Y. ; Della Valle, M.; Li, Liang ; Zhang, S. R.; "Probing electromagnetic-gravitational wave emission coincidence in type I binary-driven hypernova family of long GRBs at very-high redshift"; arXiv:2306.0585 (2023).

4.2 Conference proceedings

1. R. Ruffini, M.G. Bernardini, C.L. Bianco, P. Chardonnet, F. Fraschetti, V. Gurzadyan, L. Vitagliano, S.-S. Xue; "The Blackholic energy: long and short Gamma-Ray Bursts (New perspectives in physics and astrophysics from the theoretical understanding of Gamma-Ray Bursts, II)";

in Proceedings of the XIth Brazilian School on Cosmology and Gravitation, Mangaratiba, Rio de Janeiro (Brazil), July – August 2004, M. Novello, S.E. Perez Bergliaffa, Editors; AIP Conference Proceedings, 782, 42 (2005).

We outline the confluence of three novel theoretical fields in our modeling of Gamma-Ray Bursts (GRBs): 1) the ultrarelativistic regime of a shock front expanding with a Lorentz gamma factor ~ 300; 2) the quantum vacuum polarization process leading to an electron-positron plasma originating the shock front; and 3) the general relativistic process of energy extraction from a black hole originating the vacuum polarization process. There are two different classes of GRBs: the long GRBs and the short GRBs. We here address the issue of the long GRBs. The theoretical understanding of the long GRBs has led to the detailed description of their luminosities in fixed energy bands, of their spectral features and made also possible to probe the astrophysical scenario in which they originate. We are specially interested, in this report, to a subclass of long GRBs which appear to be accompanied by a supernova explosion. We are considering two specific examples: GRB980425/SN1998bw and GRB030329/SN2003dh. While these supernovae appear to have a standard energetics of 10^{49} ergs, the GRBs are highly variable and can have energetics 10^4 – 10^5 times larger than the ones of the supernovae. Moreover, many long GRBs occurs without the presence of a supernova. It is concluded that in no way a GRB can originate from a supernova. The precise theoretical understanding of the GRB luminosity we present evidence, in both these systems, the existence of an independent component in the X-ray emission, usually interpreted in the current literature as part of the GRB afterglow. This component has been observed by Chandra and XMM to have a strong decay on scale of months. We have named here these two sources respectively URCA-1 and URCA-2, in honor of the work that George Gamow and Mario Shoenberg did in 1939 in this town of Urca identifying the basic mechanism, the Urca processes, leading to the process of gravitational collapse and the formation of a neutron star and a supernova. The further hypothesis is considered to relate this X-ray source to a neutron star, newly born in the Supernova. This hypothesis should be submitted to further theoretical and observational investigation. Some theoretical developments to clarify the astrophysical origin of this new scenario are outlined. We turn then to the theoretical developments in the short GRBs: we first report some progress in the understanding the dynamical phase of collapse, the mass-energy formula and the extraction of blackholic energy which have been motivated by the analysis of the short GRBs. In this context progress has also been accomplished on establishing an absolute lower limit to the irreducible mass of the black hole as well as on some critical considerations about the relations of general relativity and the second law of thermodynamics. We recall how this last issue has been one of the most debated in theoretical physics in the past thirty years due to the work of Bekenstein and Hawking. Following these conceptual progresses we analyze the vacuum polarization process around an overcritical collapsing shell. We evidence the existence of a separatrix and a dyadosphere trapping surface in the dynamics of the electron-positron plasma generated during the process of gravitational collapse. We then analyze, using recent progress in the solution of the Vlasov-Boltzmann-Maxwell system, the oscillation regime in the created electron-positron plasma and their rapid convergence to a thermalized spectrum. We conclude by making precise predictions for the spectra, the energy fluxes and characteristic time-scales of the radiation for short-bursts. If the precise luminosity variation and spectral hardening of the radiation we have predicted will be confirmed by observations of short-bursts, these systems will play a major role as standard candles in cosmology. These considerations will also be relevant for the analysis of the long-bursts when the baryonic matter contribution will be taken into account.

2. R. Ruffini, M.G. Bernardini, C.L. Bianco, P. Chardonnet, F. Fraschetti, V. Gurzadyan, L. Vitagliano, S.-S. Xue; "Black hole physics and astrophysics: The GRB-Supernova connection and URCA-1 – URCA-2"; in Proceedings of the Tenth Marcel Grossmann Meeting on General Relativity, Rio de Janeiro, Brazil, July 2003, M. Novello, S.E. Perez-Bergliaffa, Editors; p. 369; World Scientific, (Singapore, 2006).

   We outline the confluence of three novel theoretical fields in our modeling of Gamma-Ray Bursts (GRBs): 1) the ultrarelativistic regime of a shock front expanding with a Lorentz gamma factor ~ 300; 2) the quantum vacuum polarization process leading to an electron-positron plasma originating the shock front; and 3) the general relativistic process of energy extraction from a black hole originating the vacuum polarization process. There are two different classes of GRBs: the long GRBs and the short GRBs. We here address the issue of the long GRBs. The theoretical understanding of the long GRBs has led to the detailed description of their luminosities in fixed energy bands, of their spectral features and made also possible to probe the astrophysical scenario in which they originate. We are specially interested, in this report, to a subclass of long GRBs which appear to be accompanied by a supernova explosion. We are considering two specific examples: GRB980425/SN1998bw and GRB030329/SN2003dh. While these supernovae appear to have a standard energetics of 10^{49} ergs, the GRBs are highly variable and can have energetics 10^4 – 10^5 times larger than the ones of the supernovae. Moreover, many long GRBs occurs without the presence of a supernova. It is concluded that in no way a GRB can originate from a supernova. The precise theoretical understanding of the GRB luminosity we present evidence, in both these systems, the existence of an independent component in the X-ray emission, usually interpreted in the current literature as part of the GRB afterglow. This component has been observed by Chandra and XMM to have a strong decay on scale of months. We have named here these two sources respectively URCA-1 and URCA-2, in honor of the work that George Gamow and Mario Shoenberg did in 1939 in this town of Urca identifying the basic mechanism, the Urca processes, leading to the process of gravitational collapse and the formation of a neutron star and a supernova. The further hypothesis is considered to relate this X-ray source to a neutron star, newly born in the Supernova. This hypothesis should be submitted to further theoretical and observational investigation. Some theoretical developments to clarify the astrophysical origin of this new scenario are outlined.

3. M.G. Bernardini, C.L. Bianco, P. Chardonnet, F. Fraschetti, R. Ruffini, S.-S. Xue; "General features of GRB 030329 in the EMBH model"; in Proceedings of the Tenth Marcel Grossmann Meeting on General Relativity, Rio de Janeiro, Brazil, July 2003, M. Novello, S.E. Perez-Bergliaffa, Editors; p. 2459; World Scientific, (Singapore, 2006).

   GRB 030329 is considered within the EMBH model. We determine the three free parameters and deduce its luminosity in given energy bands comparing it with the observations. The observed substructures are compared with the predictions of the model: by applying the result that substructures observed in the extended afterglow peak emission (E-APE) do indeed originate in the collision of the accelerated baryonic matter (ABM) pulse with the inhomogeneities in the interstellar medium around the black-hole, masks of density inhomogeneities are considered in order to reproduce the observed temporal substructures. The induced supernova concept is applied to this system and the general consequences that we are witnessing are the formation of a cosmological thriptych of a black hole originating the GRB 030329, the supernova SN2003dh and a young neutron star. Analogies to the system GRB 980425–

SN1998bw are outlined.

4. R. Ruffini, M.G. Bernardini, C.L. Bianco, P. Chardonnet, A. Corsi, F. Fraschetti, S.-S. Xue; "GRB 970228 and its associated Supernova in the EMBH model"; in Proceedings of the Tenth Marcel Grossmann Meeting on General Relativity, Rio de Janeiro, Brazil, July 2003, M. Novello, S.E. Perez-Bergliaffa, Editors; p. 2465; World Scientific, (Singapore, 2006).

   The γ-ray burst of 1997 February 28 is analyzed within the Electromagnetic Black Hole model. We first estimate the value of the total energy deposited in the dyadosphere, E_{dya}, and the amount of baryonic matter left over by the EMBH progenitor star, $B = M_B c^2 / E_{dya}$. We then consider the role of the interstellar medium number density n_{ISM} and of the ratio R between the effective emitting area and the total surface area of the γ-ray burst source, in reproducing the prompt emission and the X-ray afterglow of this burst. Some considerations are also done concerning the possibility of explaining, within the theory, the observed evidence for a supernova in the optical afterglow.

5. F. Fraschetti, M.G. Bernardini, C.L. Bianco, P. Chardonnet, R. Ruffini, S.-S. Xue; "Inferences on the ISM structure around GRB980425 and GRB980425-SN1998bw association in the EMBH Model"; in Proceedings of the Tenth Marcel Grossmann Meeting on General Relativity, Rio de Janeiro, Brazil, July 2003, M. Novello, S.E. Perez-Bergliaffa, Editors; p. 2451; World Scientific, (Singapore, 2006).

   We determine the four free parameters within the EMBH model for GRB 980425 and deduce its luminosity in given energy bands, its spectra and its time variability in the prompt radiation. We compute the basic kinematical parameters of GRB 980425. In the extended afterglow peak emission the Lorentz γ factor is lower than the critical value 150 which has been found in Ruffini et al. (2002) to be necessary in order to perform the tomography of the ISM surrounding the GRB as suggested by Dermer & Mitman (1999). The detailed structure of the density inhomogeneities as well as the effects of radial apparent superluminal effects are evaluated within the EMBH model. Under the assumption that the energy distribution of emitted radiation is thermal in the comoving frame, time integrated spectra of EMBH model for prompt emission are computed. The induced supernova concept is applied to this system and general consequences on the astrophysical and cosmological scenario are derived.

6. R. Ruffini, M.G. Bernardini, C.L. Bianco, P. Chardonnet, F. Fraschetti,

R. Guida, S.-S. Xue; "GRB 050315: A step in the proof of the uniqueness of the overall GRB structure"; in "GAMMA-RAY BURSTS IN THE SWIFT ERA: Sixteenth Maryland Astrophysics Conference", Washington, DC, USA, November 29th – December 2nd 2005, Stephen S. Holt, Neil Gehrels, John A. Nousek, Editors; AIP Conference Proceedings, 836, 103 (2006).

Using the Swift data of GRB 050315, we progress in proving the uniqueness of our theoretically predicted Gamma-Ray Burst (GRB) structure as composed by a proper-GRB, emitted at the transparency of an electron-positron plasma with suitable baryon loading, and an afterglow comprising the "prompt radiation" as due to external shocks. Detailed light curves for selected energy bands are theoretically fitted in the entire temporal region of the Swift observations ranging over 10^6 seconds.

7. R. Ruffini, M.G. Bernardini, C.L. Bianco, P. Chardonnet, F. Fraschetti, S.-S. Xue; "Theoretical Interpretation of GRB 031203 and URCA-3"; in "Relativistic Astrophysics and Cosmology - Einstein's Legacy", B. Aschenbach, V. Burwitz, G. Hasinger, B. Leibundgut, Editors; Springer-Verlag (2007).

8. R. Ruffini, M.G. Bernardini, C.L. Bianco, L. Caito, P. Chardonnet, M.G. Dainotti, F. Fraschetti, R. Guida, M. Rotondo, G. Vereshchagin, L. Vitagliano, S.-S. Xue; "The Blackholic energy and the canonical Gamma-Ray Burst"; in Proceedings of the XIIth Brazilian School on Cosmology and Gravitation, Mangaratiba, Rio de Janeiro (Brazil), September 2006, M. Novello, S.E. Perez Bergliaffa, Editors; AIP Conference Proceedings, 910, 55 (2007).

   Gamma-Ray Bursts (GRBs) represent very likely "the" most extensive computational, theoretical and observational effort ever carried out successfully in physics and astrophysics. The extensive campaign of observation from space based X-ray and γ-ray observatory, such as the *Vela*, CGRO, BeppoSAX, HETE-II, INTEGRAL, *Swift*, R-XTE, *Chandra*, XMM satellites, have been matched by complementary observations in the radio wavelength (e.g. by the VLA) and in the optical band (e.g. by VLT, Keck, ROSAT). The net result is unprecedented accuracy in the received data allowing the determination of the energetics, the time variability and the spectral properties of these GRB sources. The very fortunate situation occurs that these data can be confronted with a mature theoretical development. Theoretical interpretation of the above data allows progress in three different frontiers of knowledge: **a)** the ultrarelativistic regimes of a macroscopic source moving at Lorentz gamma factors up to ~ 400; **b)** the occurrence of vacuum polarization process verifying some of the yet untested regimes of ultrarelativistic quantum field theories; and **c)** the first evidence for extracting, during the process of gravitational collapse leading to the formation of a black hole, amounts of energies up to 10^{55} ergs of blackholic energy — a new form of energy in physics and astrophysics. We outline how this progress leads to the confirmation of three interpretation paradigms for GRBs proposed in July 2001. Thanks mainly to the observations by *Swift* and the optical observations by VLT, the outcome of this analysis points to the existence of a "canonical" GRB, originating from a variety of different initial astrophysical scenarios. The communality of these GRBs appears to be that they all are emitted in the process of formation of a black hole with a negligible value of its angular momentum. The following sequence of events appears to be canonical: the vacuum polarization process in the dyadosphere with the creation of the optically thick self accelerating electron-positron plasma; the engulfment of baryonic mass during the plasma expansion; adiabatic expansion of the optically thick "fireshell" of electron-positron-baryon plasma up to the transparency; the interaction of the accelerated baryonic matter with the interstellar medium (ISM). This leads to the canonical GRB composed of a proper GRB (P-GRB), emitted at the moment of transparency, followed by an extended afterglow. The sole parameters in this scenario are the total energy of the dyadosphere E_{dya}, the fireshell baryon loading M_B defined by the dimensionless parameter $B \equiv M_B c^2/E_{dya}$, and the ISM filamentary distribution around the source. In the limit $B \rightarrow 0$ the total energy is radiated in the P-GRB with a vanishing contribution in the afterglow. In this limit, the canonical GRBs explain as well the short GRBs. In these lecture notes we systematically outline the main results of our model comparing and contrasting them with the ones in the current literature. In both cases, we have limited ourselves to review already published results in refereed publications. We emphasize as well the role of GRBs in testing yet unexplored grounds in the foundations of general relativity and relativistic field theories.

9. R. Ruffini, M.G. Bernardini, C.L. Bianco, L. Caito, P. Chardonnet, M.G. Dainotti, F. Fraschetti, R. Guida, G. Vereshchagin, S.-S. Xue; "The role of GRB 031203 in clarifying the astrophysical GRB scenario"; in Proceedings of the 6^{th} Integral Workshop - The Obscured Universe, Moscow, (Russia), July 2006, S. Grebenev, R. Sunyaev, C. Winkler, A. Parmar, L.

Ouwehand, Editors; ESA Special Publication, SP-622, 561 (2007).

The luminosity and the spectral distribution of the afterglow of GRB 031203 have been presented within our theoretical framework, which envisages the GRB structure as composed by a proper-GRB, emitted at the transparency of an electron-positron plasma with suitable baryon loading, and an afterglow comprising the "prompt emission" as due to external shocks. In addition to the GRB emission, there appears to be a prolonged soft X-Ray emission lasting for 10^6–10^7 seconds followed by an exponential decay. This additional source has been called by us URCA-3. It is urgent to establish if this component is related to the GRB or to the Supernova (SN). In this second case, there are two possibilities: either the interaction of the SN ejecta with the interstellar medium or, possibly, the cooling of a young neutron star formed in the SN 2003lw process. The analogies and the differences between this triptych GRB 031203 / SN 2003lw / URCA-3 and the corresponding ones GRB 980425 / SN 1998bw / URCA-1 and GRB 030329 / SN 2003dh / URCA-2, as well as GRB 060218 / SN 2006aj are discussed.

10. M.G. Bernardini, C.L. Bianco, L. Caito, M.G. Dainotti, R. Guida, R. Ruffini; "GRB970228 and the class of GRBs with an initial spikelike emission: do they follow the Amati relation?"; in Relativistic Astrophysics – Proceedings of the 4^{th} Italian-Sino Workshop, Pescara (Italy), July 2007, C.L. Bianco, S.-S. Xue, Editors; AIP Conference Proceedings, 966, 7 (2008).

    On the basis of the recent understanding of GRB050315 and GRB060218, we return to GRB970228, the first Gamma-Ray Burst (GRB) with detected afterglow. We proposed it as the prototype for a new class of GRBs with "an occasional softer extended emission lasting tenths of seconds after an initial spikelike emission". Detailed theoretical computation of the GRB970228 light curves in selected energy bands for the prompt emission are presented and compared with observational *Beppo*SAX data. From our analysis we conclude that GRB970228 and likely the ones of the above mentioned new class of GRBs are "canonical GRBs" have only one peculiarity: they exploded in a galactic environment, possibly the halo, with a very low value of CBM density. Here we investigate how GRB970228 unveils another peculiarity of this class of GRBs: they do not fulfill the "Amati relation". We provide a theoretical explanation within the fireshell model for the apparent absence of such correlation for the GRBs belonging to this new class.

11. C.L. Bianco, M.G. Bernardini, L. Caito, M.G. Dainotti, R. Guida, R. Ruffini;

"The "Fireshell" Model and the "Canonical" GRB Scenario; in Relativistic Astrophysics – Proceedings of the 4^{th} Italian-Sino Workshop, Pescara (Italy), July 2007, C.L. Bianco, S.-S. Xue, Editors; AIP Conference Proceedings, 966, 12 (2008).

In the "fireshell" model we define a "canonical GRB" light curve with two sharply different components: the Proper-GRB (P-GRB), emitted when the optically thick fireshell of electron-positron plasma originating the phenomenon reaches transparency, and the afterglow, emitted due to the collision between the remaining optically thin fireshell and the CircumBurst Medium (CBM). We outline our "canonical GRB" scenario, originating from the gravitational collapse to a black hole, with a special emphasis on the discrimination between "genuine" and "fake" short GRBs.

12. L. Caito, M.G. Bernardini, C.L. Bianco, M.G. Dainotti, R. Guida, R. Ruffini; "GRB 060614: A Progress Report"; in Relativistic Astrophysics – Proceedings of the 4^{th} Italian-Sino Workshop, Pescara (Italy), July 2007, C.L. Bianco, S.-S. Xue, Editors; AIP Conference Proceedings, 966, 16 (2008).

    The explosion of GRB 060614, detected by the Swift satellite, produced a deep break in the GRB scenario opening new horizons of investigation, because it can't be traced back to any traditional scheme of classification. In fact, it manifests peculiarities both of long bursts and of short bursts. Above all, it is the first case of long duration near GRB without any bright Ib/c associated Supernova. We will show that, in our canonical GRB scenario, this "anomalous" situation finds a natural interpretation and allows us to discuss a possible variation to the traditional classification scheme, introducing the distinction between "genuine" and "fake" short bursts.

13. M.G. Dainotti, M.G. Bernardini, C.L. Bianco, L. Caito, R. Guida, R. Ruffini; "GRB 060218 and the Binaries as Progenitors of GRB-SN Systems"; in Relativistic Astrophysics – Proceedings of the 4^{th} Italian-Sino Workshop, Pescara (Italy), July 2007, C.L. Bianco, S.-S. Xue, Editors; AIP Conference Proceedings, 966, 25 (2008).

    We study the Gamma-Ray Burst (GRB) 060218: a particularly close source at $z = 0.033$ with an extremely long duration, namely $T_{90} \sim 2000$ s, related to SN 2006aj. This source appears to be a very soft burst, with a peak in the spectrum at 4.9 keV, therefore interpreted as an X-Ray Flash (XRF). It fullfills the Amati relation. I present the fitting procedure, which is time consuming. In order to show its sensitivity I also present two examples of fits with the same value of B and different value of $E_{e^\pm}^{tot}$. We fit the X- and γ-ray observations by *Swift* of GRB 060218 in the 0.1–150 keV energy band during the entire time of observations from 0 all the way to 10^6 s within a unified theoretical model. The free parameters of our theory are only three, namely the total energy $E_{e\pm}^{tot}$ of the $e^\pm$ plasma, its baryon loading $B \equiv M_B c^2/E_{e\pm}^{tot}$, as well as the CircumBurst Medium (CBM) distribution. We justify the extremely long duration of this GRB by a total energy $E_{e\pm}^{tot} = 2.32 \times 10^{50}$ erg, a very high value of the baryon loading $B = 1.0 \times 10^{-2}$ and the effective CircumBurst Medium (CBM) density which shows a radial dependence $n_{cbm} \propto r^{-\alpha}$ with $1.0 \leq \alpha \leq 1.7$ and monotonically decreases from 1 to 10^{-6} particles/cm^3. We recall that this value of the B parameter is the highest among the sources we have analyzed and it is very close to its absolute upper limit expected. By our fit we show that there is no basic differences between XRFs and more general GRBs. They all originate from the collapse process to a black hole and their difference is due to the variability of the three basic parameters within the range of full applicability of the theory. We also think that the smallest possible black hole, formed by the gravitational collapse of a neutron star in a binary system, is consistent with the especially low energetics of the class of GRBs associated with SNe Ib/c.

14. R. Guida, M.G. Bernardini, C.L. Bianco, L. Caito, M.G. Dainotti, R. Ruffini; "The Amati Relation within the Fireshell Model"; in Relativistic Astrophysics – Proceedings of the 4^{th} Italian-Sino Workshop, Pescara (Italy), July 2007, C.L. Bianco, S.-S. Xue, Editors; AIP Conference Proceedings, 966, 46 (2008).

    In this work we show the existence of a spectral-energy correlation within our "fireshell" model for GRBs. The free parameters of the model are the total energy $E_{tot}^{e\pm}$ of the $e^\pm$ plasma and its baryon loading $B \equiv M_B\, c^2/E_{tot}^{e\pm}$, characterizing the source, and the parameters describing the effective CircumBurst medium (CBM) distribution, namely its particle number density ρ and its effective emitting area R. We build a sample of pseudo-GRBs, i.e. a set of theoretically simulated light curves, varying the total energy of the electron-positron plasma $E_{tot}^{e\pm}$ and keeping the same baryon loading; the parametrization used to describe the distribution of the CircumBurst medium is the same as well for all the pseudo-GRBs. The values of these parameters (B, ρ and R) used in this work are equal to the ones assumed to fit GRB050315, a *Swift* burst representing a good example of what in the literature has been addressed as "canonical light curve". For each GRB of the sample we calculate the νF_ν spectrum integrating the theoretically computed light curve over the total time, namely from our T_0, the end of the Proper-GRB (P-GRB), up to the end of our afterglow phase, when the fireshell Lorentz gamma factor is close to unity; we exclude the P-GRB from this spectral computation because, following our "canonical" GRB scenario, this component of the GRB emission is physically different from the other component, that is our afterglow component, so one should take care in no mixing them. We find that the maximum of this spectrum, that is the observed peak energy $E_{p,tot}$, correlates with the initial electron-positron plasma energy $E^{e\pm}_{tot}$ in a way very similar to the Amati one: $E_{p,tot} \propto (E^{e\pm}_{tot})^{0.5}$.

15. R. Guida, M.G. Bernardini, C.L. Bianco, L. Caito, M.G. Dainotti, R. Ruffini; "Theoretical interpretation of the Amati relation within the fireshell model"; in GAMMA-RAY BURSTS 2007: Proceedings of the Santa Fe Conference, Santa Fe (NM, USA), November 2007, M. Galassi, D. Palmer, E. Fenimore, Editors; AIP Conference Proceedings, 1000, 60 (2008).

    We discuss within our theoretical "fireshell" model for Gamma-Ray Bursts (GRBs) the theoretical interpretation of the phenomenological correlation between the isotropic-equivalent radiated energy of the prompt emission E_{iso} and the cosmological rest-frame νF_ν spectrum peak energy E_p observed by Amati and collaborators. Possible reasons for some of the outliers of this relation are given.

16. L. Caito, M.G. Bernardini, C.L. Bianco, M.G. Dainotti, R. Guida, R. Ruffini; "GRB 060614: a Fake Short Gamma-Ray Burst"; in GAMMA-RAY BURSTS 2007: Proceedings of the Santa Fe Conference, Santa Fe (NM, USA), November 2007, M. Galassi, D. Palmer, E. Fenimore, Editors; AIP Conference Proceedings, 1000, 301 (2008).

    The explosion of GRB 060614 produced a deep break in the GRB scenario and opened new horizons of investigation because it can't be traced back to any traditional scheme of classification. In fact, it manifests peculiarities both of long bursts and of short bursts and, above all, it is the first case of long duration near GRB without any bright Ib/c associated Supernova. We will show that, in our canonical GRB scenario, this "anomalous" situation finds a natural interpretation and allows us to discuss a possible variation to the traditional classification scheme, introducing the distinction between "genuine" and "fake" short bursts.

17. C.L. Bianco, M.G. Bernardini, L. Caito, M.G. Dainotti, R. Guida, R. Ruffini;

"Short and canonical GRBs"; in GAMMA-RAY BURSTS 2007: Proceedings of the Santa Fe Conference, Santa Fe (NM, USA), November 2007, M. Galassi, D. Palmer, E. Fenimore, Editors; AIP Conference Proceedings, 1000, 305 (2008).

Within the "fireshell" model for the Gamma-Ray Bursts (GRBs) we define a "canonical GRB" light curve with two sharply different components: the Proper-GRB (P-GRB), emitted when the optically thick fireshell of electron-positron plasma originating the phenomenon reaches transparency, and the afterglow, emitted due to the collision between the remaining optically thin fireshell and the CircumBurst Medium (CBM). We outline our "canonical GRB" scenario, with a special emphasis on the discrimination between "genuine" and "fake" short GRBs.

18. C.L. Bianco, M.G. Bernardini, L. Caito, M.G. Dainotti, R. Guida, R. Ruffini, G. Vereshchagin, S.-S. Xue; "The Equations of motion of the "fireshell""; in OBSERVATIONAL EVIDENCE FOR BLACK HOLES IN THE UNIVERSE: Proceedings of the 2^{nd} Kolkata Conference, Kolkata (India), February 2008, S.K. Chakrabarti, A.S. Majumdar, Editors; AIP Conference Proceedings, 1053, 259 (2008).

    The Fireshell originating a Gamma-Ray Burst (GRB) encompasses an optically thick regime followed by an optically thin one. In the first one the fireshell self-accelerates from a Lorentz gamma factor equal to 1 all the way to 200-300. The physics of this system is based on the continuous annihilation of electron-positron pairs in an optically thick e^+e^- plasma with a small baryon loading. In the following regime, the optically thin fireshell, composed by the baryons left over after the transparency point, ballistically expands into the CircumBurst Medium (CBM). The dynamics of the fireshell during both regimes will be analyzed. In particular we will re-examine the validity of the constant-index power-law relation between the fireshell Lorentz gamma factor and its radial coordinate, usually adopted in the current literature on the grounds of an "ultrarelativistic" approximation. Such expressions are found to be mathematically correct but only approximately valid in a very limited range of the physical and astrophysical parameters and in an asymptotic regime which is reached only for a very short time, if any.

19. M.G. Bernardini, C.L. Bianco, L. Caito, M.G. Dainotti, R. Guida, R. Ruffini; "The "Canonical" GRBs within the fireshell model"; in OBSERVATIONAL EVIDENCE FOR BLACK HOLES IN THE UNIVERSE: Proceedings of

the 2^{nd} Kolkata Conference, Kolkata (India), February 2008, S.K. Chakrabarti, A.S. Majumdar, Editors; AIP Conference Proceedings, 1053, 267 (2008).

Within the fireshell model we define a “canonical” GRB light curve with two sharply different components: the Proper-GRB (P-GRB), emitted when the optically thick fireshell of electron-positron plasma originating the phenomenon reaches transparency, and the afterglow, emitted due to the collision between the remaining optically thin fireshell and the CircumBurst Medium (CBM). On the basis of the recent understanding of GRB970228 as the prototype for a new class of GRBs with “an occasional softer extended emission lasting tenths of seconds after an initial spikelike emission” we outline our “canonical” GRB scenario, originating from the gravitational collapse to a black hole, with a special emphasis on the discrimination between short GRBs and the ones appearing as such due to their peculiar astrophysical setting.

20. M.G. Dainotti, M.G. Bernardini, C.L. Bianco, L. Caito, R. Guida, R. Ruffini; “GRB 060218: the density mask and its peculiarity compared to the other sources”; in OBSERVATIONAL EVIDENCE FOR BLACK HOLES IN THE UNIVERSE: Proceedings of the 2^{nd} Kolkata Conference, Kolkata (India), February 2008, S.K. Chakrabarti, A.S. Majumdar, Editors; AIP Conference Proceedings, 1053, 283 (2008).

The Swift satellite has given continuous data in the range 0.3–150 keV from 0 s to 106 s for GRB060218 associated with SN2006aj. It has an unusually long duration ($T_{90} \sim 2100$ s). We plan to fit the complete γ- and X-ray light curves of this long duration GRB, including the prompt emission and we give peculiar attention to the afterglow lightcurve in order to better constrain the density mask. We apply our “fireshell” model based on the formation of a black hole, giving the relevant references. The initial total energy of the electron-positron plasma $E^{tot}_{e^\pm} == 2.32 \times 10^{50}$ erg has a particularly low value similarly to the other GRBs associated with SNe. For the first time we observe a baryon loading $B = 10^{-2}$ which coincides with the upper limit for the dynamical stability of the fireshell. The effective CircumBurst Medium (CBM) density shows a radial dependence $n_{cbm} \propto r^{-a}$ with $1.0 \leq a \leq 1.7$ and monotonically decreases from 1 to 10^{-6} particles/cm^3. Such a behavior is interpreted as due to a fragmentation in the fireshell. Such a fragmentation is crucial in explaining both the unusually large T_{90} and the consequently inferred abnormal low value of the CBM effective density. We present the comparison between the density mask of this source and the ones of a normal GRB 050315 and a fake short, GRB

970228, making some assumptions on the CBM behaviour in the surrounding of the Black hole.

21. L. Caito, M.G. Bernardini, C.L. Bianco, M.G. Dainotti, R. Guida, R. Ruffini; "GRB 060614 in the canonical fireshell model"; in OBSERVATIONAL EVIDENCE FOR BLACK HOLES IN THE UNIVERSE: Proceedings of the 2^{nd} Kolkata Conference, Kolkata (India), February 2008, S.K. Chakrabarti, A.S. Majumdar, Editors; AIP Conference Proceedings, 1053, 291 (2008).

    Gamma-Ray Burst (GRB) 060614 is the first nearby long duration GRB clearly not associated to any bright Ib/c Supernova. The explosion of this burst undermines one of the fundamental assumptions of the standard scenario and opens new horizons and hints of investigation. GRB 060614, hardly classifiable as a short GRB, is not either a "typical" long GRB since it occurs in a low star forming region. Moreover, it presents deep similarities with GRB 970228, which is the prototype of the "fake" short bursts, or better canonical GRBs disguised as short ones. Within the "fireshell" model, we test if this "anomalous" source can be a disguised short GRB.

22. L.J. Rangel Lemos, S. Casanova, R. Ruffini, S.S. Xue; "Fermi's approach to the study of pp interactions"; in OBSERVATIONAL EVIDENCE FOR BLACK HOLES IN THE UNIVERSE: Proceedings of the 2^{nd} Kolkata Conference, Kolkata (India), February 2008, S.K. Chakrabarti, A.S. Majumdar, Editors; AIP Conference Proceedings, 1053, 275 (2008).

    The physics of hadronic interactions found much difficulties for explain the experimental data. In this work we study the approach of Fermi (1950) about the multiplicity of pions emitted in pp interactions and in follow we compare with the modern approach

23. R. Ruffini, A.G. Aksenov, M.G. Bernardini, C.L. Bianco, L. Caito, M.G. Dainotti, G. De Barros, R. Guida, G.V. Vereshchagin, S.-S. Xue; "The canonical Gamma-Ray Bursts and their 'precursors"'; in 2008 NANJING GAMMA-RAY BURST CONFERENCE, Proceedings of the 2008 Nanjing Gamma-Ray Burst Conference, Nanjing (China), June 2008, Y.-F. Huang, Z.-G. Dai, B. Zhang, Editors; AIP Conference Proceedings, 1065, 219 (2008).

    The fireshell model for Gamma-Ray Bursts (GRBs) naturally leads to a canonical GRB composed of a proper-GRB (P-GRB) and an afterglow. P-GRBs, introduced by us in 2001, are sometimes considered "precursors" of the main GRB event in the current literature. We show in this paper how the fireshell model leads to the understanding of the structure of GRBs, with precise estimates of the time sequence and intensities of the P-GRB and the of the afterglow. It leads as well to a natural classification of the canonical GRBs which overcomes the traditional one in short and long GRBs.

24. M.G. Bernardini, C.L. Bianco, L. Caito, M.G. Dainotti, R. Guida, R. Ruffini; "Preliminary analysis of GRB060607A within the fireshell model"; in 2008 NANJING GAMMA-RAY BURST CONFERENCE; Proceedings of the 2008 Nanjing Gamma-Ray Burst Conference, Nanjing (China), June 2008, Y.-F. Huang, Z.-G. Dai, B. Zhang, Editors; AIP Conference Proceedings, 1065, 227 (2008).

    GRB060607A is a very distant ($z = 3.082$) and energetic event ($E_{iso} \sim 10^{53}$ erg). Its main peculiarity is that the peak of the near-infrared afterglow has been observed with the REM robotic telescope, allowing to infer the initial Lorentz gamma factor of the emitting system. We present a preliminary analysis of the spectra and light curves of GRB060607A prompt emission within the fireshell model. We show that the N(E) spectrum of the prompt emission, whose behavior is usually described as "simple power-law", can also be fitted in a satisfactory way by a convolution of thermal spectra as predicted by the model we applied. The theoretical time-integrated spectrum of the prompt emission as well as the light curves in the BAT and XRT energy band are in good agreement with the observations, enforcing the plausibility of our approach. Furthermore, the initial value of Lorentz gamma factor we predict is compatible with the one deduced from the REM observations.

25. C.L. Bianco, M.G. Bernardini, L. Caito, M.G. Dainotti, R. Guida, R. Ruffini; "The "fireshell" model and the "canonical GRB" scenario"; in 2008 NANJING GAMMA-RAY BURST CONFERENCE; Proceedings of the 2008 Nanjing Gamma-Ray Burst Conference, Nanjing (China), June 2008, Y.-F. Huang, Z.-G. Dai, B. Zhang, Editors; AIP Conference Proceedings, 1065, 223 (2008).

    The Swift observation of GRB 060614, as well as the catalog analysis by Norris & Bonnell (2006), opened the door "on a new Gamma-Ray Bursts (GRBs) classification scheme that straddles both long and short bursts" (Gehrels et al. 2006). Within the "fireshell" model for the Gamma-Ray Bursts (GRBs) we define a "canonical GRB" light curve with two sharply different components: the

Proper-GRB (P-GRB), emitted when the optically thick fireshell of electron-positron plasma originating the phenomenon reaches transparency, and the afterglow, emitted due to the collision between the remaining optically thin fireshell and the CircumBurst Medium (CBM). We here outline our "canonical GRB" scenario, which implies three different GRB classes: the "genuine" short GRBs, the "fake" or "disguised" short GRBs and the other (so-called "long") GRBs. We also outline some implications for the theoretical interpretation of the Amati relation.

26. G. De Barros, M.G. Bernardini, C.L. Bianco, L. Caito, M.G. Dainotti, R. Guida, R. Ruffini; "Is GRB 050509b a "genuine" short GRB?"; in 2008 NANJING GAMMA-RAY BURST CONFERENCE; Proceedings of the 2008 Nanjing Gamma-Ray Burst Conference, Nanjing (China), June 2008, Y.-F. Huang, Z.-G. Dai, B. Zhang, Editors; AIP Conference Proceedings, 1065, 231 (2008).

    Within our "fireshell" model we introduced a "canonical" GRB scenario which differentiates physically the "proper GRB" (P-GRB) emission when photons decouple, and the afterglow emission due to interaction of the accelerated baryons with the CircumBurst Medium (CBM). The ratio between energetics of the two components is ruled by the baryon loading of the fireshell. We here analyse the possibility that GRB050509b is the first case of a "genuine" short GRB the ones with smaller baryon loading. In such a case, the GRB050509b "prompt emission" would be dominated by the "proper GRB" and, moreover, the P-GRB total energy would be greater than the afterglow one. Our fit of the afterglow data and of the P-GRB energetics indicates that this source present the smallest baryon loading we ever encountered so far, being on the order of 10^{-4}.

27. G. De Barros, A.G. Aksenov, C.L. Bianco, R. Ruffini, G.V. Vereshchagin; "Fireshell versus Fireball scenarios"; in 2008 NANJING GAMMA-RAY BURST CONFERENCE; Proceedings of the 2008 Nanjing Gamma-Ray Burst Conference, Nanjing (China), June 2008, Y.-F. Huang, Z.-G. Dai, B. Zhang, Editors; AIP Conference Proceedings, 1065, 234 (2008).

    We revisit Cavallo and Rees classification based on the analysis of initial conditions in electron-positron-photon plasma which appears suddenly around compact astrophysical objects and gives origin to GRBs. These initial conditions were recently studied in [1,2] by numerical integration of relativistic

Boltzmann equations with collision integrals, including binary and triple interactions between particles. The main conclusion is that the pair plasma in GRB sources quickly reaches thermal equilibrium well before its expansion starts. In light of this work we comment on each of the four scenarios proposed by Cavallo and Rees and discuss their applicability to describe evolution of GRB sources.

28. M.G. Bernardini, C.L. Bianco, L. Caito, M.G. Dainotti, R. Guida, R. Ruffini; "GRB970228 as a prototype for the class of GRBs with an initial spikelike emission"; in Proceedings of the Eleventh Marcel Grossmann Meeting on General Relativity, Berlin, Germany, July 2006, H. Kleinert, R.T. Jantzen, Editors; World Scientific, (Singapore, 2008).

    We interpret GRB970228 prompt emission within our "canonical" GRB scenario, identifying the initial spikelike emission with the Proper-GRB (P-GRB) and the following bumps with the afterglow peak emission. Furthermore, we emphasize the necessity to consider the "canonical" GRB as a whole due to the highly non-linear nature of the model we applied.

29. M.G. Bernardini, C.L. Bianco, L. Caito, M.G. Dainotti, R. Guida, R. Ruffini; "GRB980425 and the puzzling URCA1 emission"; in Proceedings of the Eleventh Marcel Grossmann Meeting on General Relativity, Berlin, Germany, July 2006, H. Kleinert, R.T. Jantzen, Editors; World Scientific, (Singapore, 2008).

    We applied our "fireshell" model to GRB980425 observational data, reproducing very satisfactory its prompt emission. We use the results of our analysis to provide a possible interpretation for the X-ray emission of the source S1. The effect on the GRB analysis of the lack of data in the pre-Swift observations is also outlined.

30. C.L. Bianco, M.G. Bernardini, L. Caito, P. Chardonnet, M.G. Dainotti, F. Fraschetti, R. Guida, R. Ruffini, S.-S. Xue; "Theoretical interpretation of 'long' and 'short' GRBs"; in Proceedings of the Eleventh Marcel Grossmann Meeting on General Relativity, Berlin, Germany, July 2006, H. Kleinert, R.T. Jantzen, Editors; World Scientific, (Singapore, 2008).

    Within the "fireshell" model we define a "canonical GRB" light curve with two sharply different components: the Proper-GRB (P-GRB), emitted when the optically thick fireshell of electron-positron plasma originating the phenomenon reaches transparency, and the afterglow, emitted due to the collision between the remaining optically thin fireshell and the CircumBurst Medium (CBM). We here present the consequences of such a scenario on the theoretical interpretation of the nature of "long" and "short" GRBs.

31. C.L. Bianco, M.G. Bernardini, P. Chardonnet, F. Fraschetti, R. Ruffini, S.-S. Xue; "Theoretical interpretation of luminosity and spectral properties of GRB 031203"; in Proceedings of the Eleventh Marcel Grossmann Meeting on General Relativity, Berlin, Germany, July 2006, H. Kleinert, R.T. Jantzen, Editors; World Scientific, (Singapore, 2008).

    We show how an emission endowed with an instantaneous thermal spectrum in the co-moving frame of the expanding fireshell can reproduce the time-integrated GRB observed non-thermal spectrum. An explicit example in the case of GRB 031203 is presented.

32. C.L. Bianco, R. Ruffini; "The 'Fireshell' model in the Swift era"; in Proceedings of the Eleventh Marcel Grossmann Meeting on General Relativity, Berlin, Germany, July 2006, H. Kleinert, R.T. Jantzen, Editors; World Scientific, (Singapore, 2008).

    We here re-examine the validity of the constant-index power-law relation between the fireshell Lorentz gamma factor and its radial coordinate, usually adopted in the current Gamma-Ray Burst (GRB) literature on the grounds of an "ultrarelativistic" approximation. Such expressions are found to be mathematically correct but only approximately valid in a very limited range of the physical and astrophysical parameters and in an asymptotic regime which is reached only for a very short time, if any.

33. L. Caito, M.G. Bernardini, C.L. Bianco, M.G. Dainotti, R. Guida, R. Ruffini; "Theoretical interpretation of GRB011121"; in Proceedings of the Eleventh Marcel Grossmann Meeting on General Relativity, Berlin, Germany, July 2006, H. Kleinert, R.T. Jantzen, Editors; World Scientific, (Singapore, 2008).

    GRB 011121, detected by the BeppoSAX satellite, is studied as a prototype to understand the presence of flares observed by Swift in the afterglow of many GRB sources. Detailed theoretical analysis of the GRB 011121 light curves in selected energy bands are presented and compared with observational data. An interpretation of the flare of this source is provided by the introduction of the three-dimensional structure of the CircumBurst Medium(CBM).

34. M.G. Dainotti, M.G. Bernardini, C.L. Bianco, L. Caito, R. Guida, R. Ruffini; "On GRB 060218 and the GRBs related to Supernovae Ib/c"; in Proceedings of the Eleventh Marcel Grossmann Meeting on General Relativity, Berlin, Germany, July 2006, H. Kleinert, R.T. Jantzen, Editors; World Scientific, (Singapore, 2008).

    We study the Gamma-Ray Burst (GRB) 060218: a particularly close source at $z = 0.033$ with an extremely long duration, namely $T_{90} \sim 2000$ s, related to SN 2006aj. This source appears to be a very soft burst, with a peak in the spectrum at 4.9 keV, therefore interpreted as an X-Ray Flash (XRF) and it obeys to the Amati relation. We fit the X- and γ-ray observations by Swift of GRB 060218 in the 0.1–150 keV energy band during the entire time of observations from 0 all the way to 106 s within a unified theoretical model. The details of our theoretical analysis have been recently published in a series of articles. The free parameters of the theory are only three, namely the total energy $E^{tot}_{e\pm}$ of the $e^{\pm}$ plasma, its baryon loading $B = M_B c^2/E^{tot}_{e\pm}$, as well as the CircumBurst Medium (CBM) distribution. We fit the entire light curve, including the prompt emission as an essential part of the afterglow. We recall that this value of the B parameter is the highest among the sources we have analyzed and it is very close to its absolute upper limit expected. We successfully make definite predictions about the spectral distribution in the early part of the light curve, exactly we derive the instantaneous photon number spectrum N(E) and we show that although the spectrum in the co-moving frame of the expanding pulse is thermal, the shape of the final spectrum in the laboratory frame is clearly non thermal. In fact each single instantaneous spectrum is the result of an integration of thousands of thermal spectra over the corresponding EQuiTemporal Surfaces (EQTS). By our fit we show that there is no basic differences between XRFs and more general GRBs. They all originate from the collapse process to a black hole and their difference is due to the variability of the three basic parameters within the range of full applicability of the theory.

35. R. Guida, M.G. Bernardini, C.L. Bianco, L. Caito, M.G. Dainotti, R. Ruffini; "Theoretical interpretation of GRB060124"; in Proceedings of the Eleventh Marcel Grossmann Meeting on General Relativity, Berlin, Germany, July 2006, H. Kleinert, R.T. Jantzen, Editors; World Scientific, (Singapore, 2008).

    We show the preliminary results of the application of our "fireshell" model to GRB060124. This source is very peculiar because it is the first event for which both the prompt and the afterglow emission were observed simultaneously by the three Swift instruments: BAT (15 - 350 keV), XRT (0,2 - 10 keV) and UVOT (170 - 650 nm), due to the presence of a precursor $\sim$ 570 s before the main burst. We analyze GRB060124 within our "canonical" GRB scenario, identifying the precursor with the P-GRB and the prompt emission with the afterglow peak emission. In this way we reproduce correctly the energetics of both these two components. We reproduce also the observed time delay between the precursor (P-GRB) and the main burst. The effect of such a time delay in our model will be discussed.

36. R. Ruffini, M.G. Bernardini, C.L. Bianco, L. Caito, P. Chardonnet, C. Cherubini, M.G. Dainotti, F. fraschetti, A. Geralico, R. Guida, B. Patricelli, M. Rotondo, J. Rueda Hernandez, G. Vereshchagin, S.-S. Xue; "Gamma-Ray Bursts"; in Proceedings of the Eleventh Marcel Grossmann Meeting on General Relativity, Berlin, Germany, July 2006, H. Kleinert, R.T. Jantzen, Editors; World Scientific, (Singapore, 2008).

    We show by example how the uncoding of Gamma-Ray Bursts (GRBs) offers unprecedented possibilities to foster new knowledge in fundamental physics and in astrophysics. After recalling some of the classic work on vacuum polarization in uniform electric fields by Klein, Sauter, Heisenberg, Euler and Schwinger, we summarize some of the efforts to observe these effects in heavy ions and high energy ion collisions. We then turn to the theory of vacuum polarization around a Kerr-Newman black hole, leading to the extraction of the blackholic energy, to the concept of dyadosphere and dyadotorus, and to the creation of an electron-positron-photon plasma. We then present a new theoretical approach encompassing the physics of neutron stars and heavy nuclei. It is shown that configurations of nuclear matter in bulk with global charge neutrality can exist on macroscopic scales and with electric fields close to the critical value near their surfaces. These configurations may represent an initial condition for the process of gravitational collapse, leading to the creation of an electron-positron-photon plasma: the basic self-accelerating system explaining both the energetics and the high energy Lorentz factor observed in GRBs. We then turn to recall the two basic interpretational paradigms of our GRB model: 1) the Relative Space-Time Transformation (RSTT) paradigm and 2) the Interpretation of the Burst Structure (IBS) paradigm. These paradigms lead to a "canonical" GRB light curve formed from two different components: a Proper-GRB (P-GRB) and an extended afterglow comprising a raising part, a peak, and a decaying tail. When the P-GRB is energetically predominant we have a “genuine” short GRB, while when the afterglow is energetically predominant we have a so-called long GRB or a “fake” short GRB. We compare and contrast the description of the relativistic expansion of the electron-positron plasma within our approach and within the other ones in the current literature. We then turn to the special role of the baryon loading in discriminating between “genuine” short and long or “fake” short GRBs and to the special role of GRB 991216 to illustrate for the first time the “canonical” GRB bolometric light curve. We then propose a spectral analysis of GRBs, and proceed to some applications: GRB 031203, the first spectral analysis, GRB 050315, the first complete light curve fitting, GRB 060218, the first evidence for a critical value of the baryon loading, GRB 970228, the appearance of “fake” short GRBs. We finally turn to the GRB-Supernova Time Sequence (GSTS) paradigm: the concept of induced gravitational collapse. We illustrate this paradigm by the systems GRB 980425 / SN 1998bw, GRB 030329 / SN 2003dh, GRB 031203 / SN 2003lw, GRB 060218 / SN 2006aj, and we present the enigma of the URCA sources. We then present some general conclusions.

37. R. Ruffini, A.G. Aksenov, M.G. Bernardini, C.L. Bianco, L. Caito, M.G. Dainotti, G. De Barros, R. Guida, G. Vereshchagin, S.-S. Xue; “The canonical Gamma-Ray Bursts: long, ‘fake’-‘disguised’ and ‘genuine’ short bursts; in PROBING STELLAR POPULATIONS OUT TO THE DISTANT UNIVERSE: CEFALU 2008, Proceedings of the International Conference; Cefalù (Italy), September 2008, G. Giobbi, A. Tornambe, G. Raimondo, M. Limongi, L. A. Antonelli, N. Menci, E. Brocato, Editors; AIP Conference Proceedings, 1111, 325 (2009).

    The Gamma-Ray Bursts (GRBs) offer the unprecedented opportunity to observe for the first time the blackholic energy extracted by the vacuum polarization during the process of gravitational collapse to a black hole leading to the formation of an electron-positron plasma. The uniqueness of the Kerr-Newman black hole implies that very different processes originating from the gravitational collapse a) of a single star in a binary system induced by the companion, or b) of two neutron stars, or c) of a neutron star and a white dwarf, do lead to the same structure for the observed GRB. The recent progress of the numerical integration of the relativistic Boltzmann equations with collision integrals including 2-body and 3-body interactions between the particles offer a powerful conceptual tool in order to differentiate the traditional “fireball” picture, an expanding hot cavity considered by Cavallo and Rees, as opposed to the “fireshell” model, composed of an internally cold shell of relativistically expanding electron-positron-baryon plasma. The analysis of the fireshell naturally leads to a canonical GRB composed of a proper-GRB and an extended afterglow. By recalling the three interpretational paradigms for GRBs we show how the fireshell model leads to an understanding of the GRB structure and to an alternative classification of short and long GRBs.

38. M.G. Bernardini, M.G. Dainotti, C.L. Bianco, L. Caito, R. Guida, R. Ruffini; "Prompt emission and X-ray flares: the case of GRB 060607 A"; in PROBING STELLAR POPULATIONS OUT TO THE DISTANT UNIVERSE: CEFALU 2008, Proceedings of the International Conference; Cefalù (Italy), September 2008, G. Giobbi, A. Tornambe, G. Raimondo, M. Limongi, L. A. Antonelli, N. Menci, E. Brocato, Editors; AIP Conference Proceedings, 1111, 383 (2009).

    GRB 060607A is a very distant and energetic event. Its main peculiarity is that the peak of the near-infrared (NIR) afterglow has been observed with the REM robotic telescope, allowing to estimate the initial Lorentz gamma factor within the fireball forward shock model. We analyze GRB 060607A within the fireshell model. The initial Lorentz gamma factor of the fireshell can be obtained adopting the exact solutions of its equations of motion, dealing only with the BAT and XRT observations, that are the basic contribution to the afterglow emission, up to a distance from the progenitor $r \sim 10^{18}$ cm. According to the "canonical GRB" scenario we interpret the whole prompt emission as the peak of the afterglow emission, and we show that the observed temporal variability of the prompt emission can be produced by the interaction of the fireshell with overdense CircumBurst Medium (CBM) clumps. This is indeed the case also of the X-ray flares which are present in the early phases of the afterglow light curve.

39. C.L. Bianco, M.G. Bernardini, L. Caito, M.G. Dainotti, R. Guida, R. Ruffini; "The 'fireshell' model and the 'canonical GRB' scenario. Implications for the Amati relation"; in PROBING STELLAR POPULATIONS OUT TO THE DISTANT UNIVERSE: CEFALU 2008, Proceedings of the International Conference; Cefalù (Italy), September 2008, G. Giobbi, A. Tornambe, G. Raimondo, M. Limongi, L. A. Antonelli, N. Menci, E. Brocato, Editors; AIP Conference Proceedings, 1111, 587 (2009).

    Within the "fireshell" model for GRBs we define a "canonical GRB" light curve with two sharply different components: the Proper-GRB (P-GRB), emitted when the optically thick fireshell reaches transparency, and the extended afterglow, emitted due to the collision between the remaining optically thin fireshell and the CircumBurst Medium (CBM). We here outline our "canonical GRB" scenario, which implies three different GRB classes: the "genuine" short GRBs, the "fake" or "disguised" short GRBs and the other (so-called "long") GRBs. We will also outline the corresponding implications for the Amati relation, which are opening its use for cosmology.

40. R. Ruffini, A.G. Aksenov, M.G. Bernardini, C.L. Bianco, L. Caito, P. Chardonnet, M.G. Dainotti, G. De Barros, R. Guida, L. Izzo, B. Patricelli, L.J. Rangel Lemos, M. Rotondo, J.A. Rueda Hernandez, G. Vereshchagin, S.-S. Xue; "The Blackholic energy and the canonical Gamma-Ray Burst IV: the 'long', 'genuine short' and 'fake – disguised short' GRBs"; in Proceedings of the XIIIth Brazilian School on Cosmology and Gravitation, Mangaratiba, Rio de Janeiro (Brazil), July-August 2008, M. Novello, S.E. Perez Bergliaffa, Editors; AIP Conference Proceedings, 1132, 199 (2009).

    We report some recent developments in the understanding of GRBs based on the theoretical framework of the "fireshell" model, already presented in the last three editions of the "Brazilian School of Cosmology and Gravitation". After recalling the basic features of the "fireshell model", we emphasize the following novel results: 1) the interpretation of the X-ray flares in GRB afterglows as due to the interaction of the optically thin fireshell with isolated clouds in the CircumBurst Medium (CBM); 2) an interpretation as "fake - disguised" short GRBs of the GRBs belonging to the class identified by Norris & Bonnell; we present two prototypes, GRB 970228 and GRB 060614; both these cases are consistent with an origin from the final coalescence of a binary system in the halo of their host galaxies with particularly low CBM density $n_{cbm} \sim 10^{-3}$ particles/cm^3; 3) the first attempt to study a genuine short GRB with the analysis of GRB 050509B, that reveals indeed still an open question; 4) the interpretation of the GRB-SN association in the case of GRB 060218 via the "induced gravitational collapse" process; 5) a first attempt to understand the nature of the "Amati relation", a phenomenological correlation between the isotropic-equivalent radiated energy of the prompt emission E_{iso} with the cosmological rest-frame νF_ν spectrum peak energy $E_{p,i}$. In addition, recent progress on the thermalization of the electron-positron plasma close to their formation phase, as well as the structure of the electrodynamics of Kerr-Newman Black Holes are presented. An outlook for possible explanation of high-energy phenomena in GRBs to be expected from the AGILE and the Fermi satellites are discussed. As an example of high energy process, the work by Enrico Fermi dealing with ultrarelativistic collisions is examined. It is clear that all the GRB physics points to the existence of overcritical electrodynamical fields. In this sense we present some progresses on a unified approach to heavy nuclei and neutron stars cores, which leads to the existence of overcritical fields under the neutron star crust.

41. A.G. Aksenov, M.G. Bernardini, C.L. Bianco, L. Caito, C. Cherubini, G. De Barros, A. Geralico, L. Izzo, F.A. Massucci, B. Patricelli, M. Rotondo, J.A. Rueda Hernandez, R. Ruffini, G. Vereshchagin, S.-S. Xue; "The fireshell model for Gamma-Ray Bursts"; in The Shocking Universe, Proceedings of the conference held in Venice (Italy), September 2009, G. Chincarini, P. D'Avanzo, R. Margutti, R. Salvaterra, Editors; SIF Conference Proceedings, 102, 451 (2010).

    The fireshell model for GRBs is briefly outlined, and the currently ongoing developments are summarized.

42. M.G. Bernardini, C.L. Bianco, L. Caito, L. Izzo, B. Patricelli, R. Ruffini; "The end of the prompt emission within the fireshell model"; in The Shocking Universe, Proceedings of the conference held in Venice (Italy), September 2009, G. Chincarini, P. D'Avanzo, R. Margutti, R. Salvaterra, Editors; SIF Conference Proceedings, 102, 489 (2010)

    The shallow decay emission, revealed by the Swift satellite in the X-ray afterglow of a good sample of bursts, is a puzzle. Within the fireshell model it has been recently proposed an alternative explanation: if we assume that after the prompt phase the system has a range of Lorentz factors, the plateau phase is simply the product of the injection of slower material into the fireshell. This injection produces a modification both in the dynamics of the fireshell and in the spectrum of the emitted radiation. We postulate that this spread in the fireshell Lorentz factor occurs when the fireshell becomes transparent and do not depend on a prolonged activity of the central engine. The aim of this paper is to characterize dynamically the system in order to understand the nature of that material.

43. L. Izzo, M.G. Bernardini, C.L. Bianco, L. Caito, B. Patricelli, R. Ruffini; "GRB 090423 in the fireshell scenario"; in The Shocking Universe, Proceedings of the conference held in Venice (Italy), September 2009, G.

Chincarini, P. D'Avanzo, R. Margutti, R. Salvaterra, Editors; SIF Conference Proceedings, 102, 537 (2010).

44. B. Patricelli, M.G. Bernardini, C.L. Bianco, L. Caito, L. Izzo, R. Ruffini, G. Vereshchagin; "A new spectral energy distribution of photons in the fireshell model of GRBs"; in The Shocking Universe, Proceedings of the conference held in Venice (Italy), September 2009, G. Chincarini, P. D'Avanzo, R. Margutti, R. Salvaterra, Editors; SIF Conference Proceedings, 102, 559 (2010).

    The fireshell model of Gamma Ray Bursts (GRBs) postulates that the emission process is thermal in the comoving frame of the fireshell, but this is just a first approximation. We investigate a different spectrum of photons in the comoving frame in order to better reproduce the observed spectral properties of GRB prompt emission. We introduce a modified thermal spectrum whose low energy slope depends on an index α, left as a free parameter. We test it by comparing the numerical simulations with observed BAT spectra integrated over different intervals of time. We find that the observational data can be correctly reproduced by assuming $\alpha = -1.8$.

45. C.L. Bianco, M.G. Bernardini, L. Caito, G. De Barros, L. Izzo, B. Patricelli, R. Ruffini; "Disguised Short Bursts and the Amati Relation"; in Deciphering the ancient universe with Gamma-Ray Bursts, Proceedings of the conference held in Kyoto (Japan), April 2010, N. Kawai, S. Nagataki, Editors; AIP Conference Proceedings, 1279, 299 (2010).

    The class of "Disguised short" GRBs implied by the fireshell scenario is presented, with special emphasis on the implications for the Amati relation.

46. L. Izzo, M.G. Bernardini, C.L. Bianco, L. Caito, B. Patricelli, L.J. Rangel Lemos, R. Ruffini; "On GRB 080916C and GRB 090902B observed by the Fermi satellite"; in Deciphering the ancient universe with Gamma-Ray Bursts, Proceedings of the conference held in Kyoto (Japan), April 2010, N. Kawai, S. Nagataki, Editors; AIP Conference Proceedings, 1279, 343 (2010).

    We propose a possible explanation, in the context of the Fireshell scenario, for the high-energy emission observed in GRB 080916C and GRB 090902B. The physical process underlying this emission consists mainly in the interaction of the baryon in the Fireshell with some high-density region around the burst site. Moreover we associate the observed delay of the onset of the high-energy emission as due to the P-GRB emission.

47. B. Patricelli, M.G. Bernardini, C.L. Bianco, L. Caito, G. De Barros, L. Izzo, R. Ruffini; "Black Holes in Gamma Ray Bursts"; in Deciphering the ancient universe with Gamma-Ray Bursts, Proceedings of the conference held in Kyoto (Japan), April 2010, N. Kawai, S. Nagataki, Editors; AIP Conference Proceedings, 1279, 406 (2010).

    Within the fireshell model, Gamma Ray Bursts (GRBs) originate from an optically thick $e^{\pm}$ plasma created by vacuum polarization process during the formation of a Black Hole (BH). Here we briefly recall the basic features of this model, then we show how it is possible to interpret GRB observational properties within it. In particular we present, as a specific example, the analysis of GRB 050904 observations of the prompt emission light curve and spectrum in the Swift BAT energy band (15-150 keV).

48. M.G. Bernardini, C.L. Bianco, L. Caito, M.G. Dainotti, R. Guida, R. Ruffini; "The GRB classification within the "fireshell" model: short, long and "fake" short GRBs"; in Proceedings of the 3rd Stueckelberg Workshop on Relativistic Field Theories, Pescara, Italy, July 2008, N. Carlevaro, R. Ruffini, G.V. Vereshchagin, Editors; Cambridge Scientific Publishers, (UK, 2011).

49. C.L. Bianco, M.G. Bernardini, L. Caito, M.G. Dainotti, R. Guida, R. Ruffini, G.V. Vereshchagin, S.-S. Xue; "Equations of motion of the "fireshell""; in Proceedings of the 3rd Stueckelberg Workshop on Relativistic Field Theories, Pescara, Italy, July 2008, N. Carlevaro, R. Ruffini, G.V. Vereshchagin, Editors; Cambridge Scientific Publishers, (UK, 2011).

50. L. Caito, M.G. Bernardini, C.L. Bianco, M.G. Dainotti, R. Guida, R. Ruffini; "GRB 060614: another example of "fake" short burst from a merging binary system"; in Proceedings of the 3rd Stueckelberg Workshop on Relativistic Field Theories, Pescara, Italy, July 2008, N. Carlevaro, R. Ruffini, G.V. Vereshchagin, Editors; Cambridge Scientific Publishers, (UK, 2011).

51. G. De Barros, M.G. Bernardini, C.L. Bianco, L. Caito, R. Guida, R. Ruffini; "Analysis of GRB 050509b"; in Proceedings of the 3rd Stueckelberg Workshop on Relativistic Field Theories, Pescara, Italy, July 2008, N. Carl-

evaro, R. Ruffini, G.V. Vereshchagin, Editors; Cambridge Scientific Publishers, (UK, 2011).

52. R. Ruffini, L. Izzo, A.V. Penacchioni, C.L. Bianco, L. Caito, S.K. Chakrabarti, A. Nandi; "GRB 090618: a possible case of multiple GRB?"; in Proceedings of the 25th Texas Symposium on Relativistic Astrophysics, held in Heidelberg (Germany), December 2010, F.M. Rieger, C. van Eldik, W. Hofmann, Editors; PoS(Texas2010), 101.

53. L.J. Rangel Lemos, C.L. Bianco, H.J. Mosquera Cuesta, J.A. Rueda, R. Ruffini; "Luminosity function of BATSE GRBs dominated by extended afterglow"; in Proceedings of the 25th Texas Symposium on Relativistic Astrophysics, held in Heidelberg (Germany), December 2010, F.M. Rieger, C. van Eldik, W. Hofmann, Editors; PoS(Texas2010), 204.

54. R. Ruffini, A.G. Aksenov, M.G. Bernardini, C.L. Bianco, L. Caito, P. Chardonnet, M.G. Dainotti, G. De Barros, R. Guida, L. Izzo, B. Patricelli, L.J. Rangel Lemos, M. Rotondo, J.A. Rueda Hernandez, G. Vereshchagin, She-Sheng Xue; "Black Holes Energetics and GRBs"; in The Sun, the Stars, the Universe and General Relativity: Proceedings of Sobral 2009; S.E. Perez Bergliaffa, M. Novello , R. Ruffini, Editors; Cambridge Scientific Publishers (UK, 2011).

55. C.L. Bianco, L. Amati, M.G. Bernardini, L. Caito, G. De Barros, L. Izzo, B. Patricelli, R. Ruffini; "The class of 'disguised' short GRBs and its implications for the Amati relation"; in GRBs as probes - from the progenitors environment to the high redshift Universe, Proceedings of the conference held in Como (Italy), May 2011, S. Campana, P. D'Avanzo, A. Melandri, Editors; Mem. S.A.It. Suppl., 21, 139 (2012).

56. A.V. Penacchioni, R. Ruffini, L. Izzo, M. Muccino, C.L. Bianco, L. Caito, B. Patricelli; "Evidences for a double component in the emission of GRB 101023"; in GRBs as probes - from the progenitors environment to the high redshift Universe, Proceedings of the conference held in Como (Italy), May 2011, S. Campana, P. D'Avanzo, A. Melandri, Editors; Mem. S.A.It. Suppl., 21, 230 (2012).

57. M.G. Bernardini, C.L. Bianco, L. Caito, L. Izzo, B. Patricelli, R. Ruffini; "The X-Ray Flares of GRB 060607A within the Fireshell Model"; in Proceedings of the Twelfth Marcel Grossmann Meeting on General Relativ-

ity, Paris, France, July 2009, T. Damour, R.T. Jantzen, R. Ruffini, Editors; World Scientific, (Singapore, 2012).

58. L. Izzo, M.G. Bernardini, C.L. Bianco, L. Caito, B. Patricelli, R. Ruffini; "GRB 090423 in the Fireshell Scenario: A Canonical GRB at Redshift 8.2"; in Proceedings of the Twelfth Marcel Grossmann Meeting on General Relativity, Paris, France, July 2009, T. Damour, R.T. Jantzen, R. Ruffini, Editors; World Scientific, (Singapore, 2012).

59. B. Patricelli, M.G. Bernardini, C.L. Bianco, L. Caito, L. Izzo, R. Ruffini, G.V. Vereshchagin; "A New Spectral Energy Distribution of Photons in the Fireshell Model of GRBs"; in Proceedings of the Twelfth Marcel Grossmann Meeting on General Relativity, Paris, France, July 2009, T. Damour, R.T. Jantzen, R. Ruffini, Editors; World Scientific, (Singapore, 2012).

60. C.L. Bianco, M.G. Bernardini, L. Caito, G. De Barros, L. Izzo, M. Muccino, B. Patricelli, A.V. Penacchioni, G.B. Pisani, R. Ruffini; "Needs for a new GRB classification following the fireshell model: "genuine short", "disguised short" and "long" GRBs"; in Proceedings of the Gamma-Ray Bursts 2012 Conference, held in Munich (Germany), May 2012, A. Rau, J. Greiner, Editors; PoS(GRB 2012), 043.

61. A.V. Penacchioni, G.B. Pisani, R. Ruffini, C.L. Bianco, L. Izzo, M. Muccino; "The proto-black hole concept in GRB 101023 and its possible extension to GRB 110709B"; in Proceedings of the Gamma-Ray Bursts 2012 Conference, held in Munich (Germany), May 2012, A. Rau, J. Greiner, Editors; PoS(GRB 2012), 042.

62. B. Patricelli, M.G. Bernardini, C.L. Bianco, L. Caito, L. Izzo, R. Ruffini; "GRB 050904: The study of a high redshift GRB within the Fireshell Model"; in Proceedings of the Twelfth Marcel Grossmann Meeting on General Relativity, Paris, France, July 2009, T. Damour, R.T. Jantzen, R. Ruffini, Editors; World Scientific, (Singapore, 2012).

63. L. Izzo, G.B. Pisani, M. Muccino, J.A. Rueda, Y.Wang, C.L. Bianco, A.V. Penacchioni, R. Ruffini; "A common behavior in the late X-ray afterglow of energetic GRB-SN systems"; EAS Publications Series, Volume 61, 595-597 (2013).

64. R. Ruffini; “Black Holes, Supernovae and Gamma Ray Bursts”; in Proceedings of the Thirteenth Marcel Grossmann Meeting on General Relativity, Stockholm, Sweden, July 2012, R.T. Jantzen, K. Rosquist, R. Ruffini, Editors; World Scientific, (Singapore, 2015).

65. M. Muccino, R. Ruffini, C.L. Bianco, L. Izzo, A.V. Penacchioni, G.B. Pisani; “GRB 090227B: The missing link between the genuine short and long GRBs”; in Proceedings of the Thirteenth Marcel Grossmann Meeting on General Relativity, Stockholm, Sweden, July 2012, R.T. Jantzen, K. Rosquist, R. Ruffini, Editors; World Scientific, (Singapore, 2015).

66. A.V. Penacchioni, R. Ruffini, C.L. Bianco, L. Izzo, M. Muccino, G.B. Pisani, J.A. Rueda; “The family of the Induced Gravitational Collapse scenario: The case of GRB 110709B”; in Proceedings of the Thirteenth Marcel Grossmann Meeting on General Relativity, Stockholm, Sweden, July 2012, R.T. Jantzen, K. Rosquist, R. Ruffini, Editors; World Scientific, (Singapore, 2015).

67. A.V. Penacchioni, R. Ruffini, C.L. Bianco, L. Izzo, M. Muccino, G.B. Pisani; “GRB 111228, analysis within the Induced Gravitational Collapse scenario and association with a supernova”; in Proceedings of the Thirteenth Marcel Grossmann Meeting on General Relativity, Stockholm, Sweden, July 2012, R.T. Jantzen, K. Rosquist, R. Ruffini, Editors; World Scientific, (Singapore, 2015).

68. G.B. Pisani, L. Izzo, R. Ruffini, C.L. Bianco, M. Muccino, A.V. Penacchioni, J.A. Rueda, Y. Wang; “On a novel distance indicator for Gamma-Ray Bursts associated with supernovae”; in Proceedings of the Thirteenth Marcel Grossmann Meeting on General Relativity, Stockholm, Sweden, July 2012, R.T. Jantzen, K. Rosquist, R. Ruffini, Editors; World Scientific, (Singapore, 2015).

69. M. Muccino, R. Ruffini, C.L. Bianco, L. Izzo, A.V. Penacchioni, G.B. Pisani; “GRB 090510, explosion of a GRB in the highest circumburst medium even inferred: a disguised short GRB”; in Proceedings of the Thirteenth Marcel Grossmann Meeting on General Relativity, Stockholm, Sweden, July 2012, R.T. Jantzen, K. Rosquist, R. Ruffini, Editors; World Scientific, (Singapore, 2015).

70. L. Izzo, G.B. Pisani, M. Muccino, R. Ruffini, C.L. Bianco, M. Enderli, Y. Wang; "Hints for a physically based GRB distance indicator"; in Proceedings of the Thirteenth Marcel Grossmann Meeting on General Relativity, Stockholm, Sweden, July 2012, R.T. Jantzen, K. Rosquist, R. Ruffini, Editors; World Scientific, (Singapore, 2015).

71. R. Ruffini, Y. Aimuratov, V. Belinski, C.L. Bianco, M. Enderli, L. Izzo, M. Kovacevic, G.J. Mathews, R. Moradi, M. Muccino, A.V. Penacchioni, G.B. Pisani, J.A. Rueda, G.V. Vereshchagin, Y. Wang, S.-S. Xue; Cosmic matrix in the jubilee of relativistic astrophysics; in THE SECOND ICRANET CÉSAR LATTES MEETING: Supernovae, Neutron Stars and Black Holes, Proceedings of the conference held in Rio de Janeiro – Niterói – João Pessoa – Recife – Fortaleza (Brazil), 13-22 April 2015, U. Barres de Almeida, P. Chardonnet, R. Picanco Negreiros, J. Rueda, R. Ruffini, G. Vereshchagin, C. Zen Vasconcellos, Editors; AIP Conference Proceedings, 1693, 020001 (2015).

72. L. Becerra, C.L. Bianco, F. Cipolletta, M. Enderli, C.L. Fryer, L. Izzo, M. Kovacevic, R. Camargo Rodrigues de Lima, M. Muccino, F.G. de Oliveira, A.V. Penacchioni, G.B. Pisani, J.A. Rueda, R. Ruffini, Y. Wang, E. Zaninoni; Black holes, neutron stars and supernovae within the induced gravitational collapse paradigm for GRBs; in THE SECOND ICRANET CÉSAR LATTES MEETING: Supernovae, Neutron Stars and Black Holes, Proceedings of the conference held in Rio de Janeiro – Niterói – João Pessoa – Recife – Fortaleza (Brazil), 13-22 April 2015, U. Barres de Almeida, P. Chardonnet, R. Picanco Negreiros, J. Rueda, R. Ruffini, G. Vereshchagin, C. Zen Vasconcellos, Editors; AIP Conference Proceedings, 1693, 020002 (2015).

73. L.J. Rangel Lemos, C.L. Bianco, R. Ruffini; Applying the luminosity function statistics in the fireshell model; in THE SECOND ICRANET CÉSAR LATTES MEETING: Supernovae, Neutron Stars and Black Holes, Proceedings of the conference held in Rio de Janeiro – Niterói – João Pessoa – Recife – Fortaleza (Brazil), 13-22 April 2015, U. Barres de Almeida, P. Chardonnet, R. Picanco Negreiros, J. Rueda, R. Ruffini, G. Vereshchagin, C. Zen Vasconcellos, Editors; AIP Conference Proceedings, 1693, 070004 (2015).

74. J.A. Rueda, R. Ruffini, J.F. Rodriguez, M. Muccino, Y. Aimuratov, U.

Barres de Almeida, L.M. Becerra, C.L. Bianco, C. Cherubini, S. Filippi, M. Kovacevic, R. Moradi, G.B. Pisani, Y. Wang; The binary progenitors of short and long GRBs and their gravitational-wave emission; EPJ Web of Conferences, 168, 01006 (2018).

75. M. Muccino, R. Ruffini, Y. Aimuratov, L.M. Becerra, C.L. Bianco, M. Karlika, M. Kovacevic, J.D. Melon Fuksman, R. Moradi, A.V. Penacchioni, G.B. Pisani, D. Primorac, J.A. Rueda, S. Shakeri, G.V. Vereshchagin, S.-S. Xue, Y. Wang; What can we learn from GRBs?; EPJ Web of Conferences, 168, 01015 (2018).

76. L.M. Becerra, C.L. Bianco, C. Fryer, J.A. Rueda, R. Ruffini; On the Induced Gravitational Collapse; EPJ Web of Conferences, 168, 02005 (2018).

77. G.B. Pisani, R. Ruffini, Y. Aimuratov, C.L. Bianco, M. Karlika, M. Kovacevic, R. Moradi, M. Muccino, A.V. Penacchioni, D. Primorac, J.A. Rueda, Y. Wang; The first ICRANet catalog of Binary-Driven Hypernovae; EPJ Web of Conferences, 168, 04002 (2018).

78. D. Primorac, R. Ruffini, G.B. Pisani, Y. Aimuratov, C.L. Bianco, M. Karlika, J.D. Melon Fuksman, R. Moradi, M. Muccino, A.V. Penacchioni, J.A. Rueda, Y. Wang; GRB 110731A within the IGC paradgm; EPJ Web of Conferences, 168, 04008 (2018).

79. J.D. Melon Fuksman, L.M. Becerra, C.L. Bianco, M. Karlika, M. Kovacevic, R. Moradi, M. Muccino, G.B. Pisani, D. Primorac, J.A. Rueda, R. Ruffini, G.V. Vereshchagin, Y. Wang; Evolution of an electron-positron plasma produced by induced gravitational collapse in binary-driven hypernovae; EPJ Web of Conferences, 168, 04009 (2018).

THE ASTROPHYSICAL JOURNAL, 945:10 (23pp), 2023 March 1 https://doi.org/10.3847/1538-4357/acb20b

Self-similarities and Power Laws in the Time-resolved Spectra of GRB 190114C, GRB 130427A, GRB 160509A, and GRB 160625B

Liang Li[1,2,3], J. A. Rueda[4,5,6,7], R. Moradi[2,4,8], Y. Wang[2,4,8], S. S. Xue[4,8], and R. Ruffini[2,5,6,7,8,9]
[1] ICRANet, Piazza della Repubblica 10, I-65122 Pescara, Italy; liang.li@icranet.org
[2] INAF—Osservatorio Astronomico d'Abruzzo, Via M. Maggini snc, I-64100, Teramo, Italy; rahim.moradi@inaf.it, yu.wang@icranet.org, ruffini@icra.it
[3] Dip. di Fisica and ICRA, Sapienza Universita di Roma, Piazzale Aldo Moro 5, I-00185 Rome, Italy
[4] International Center for Relativistic Astrophysics Network, Piazza della Repubblica 10, I-65122 Pescara, Italy; jorge.rueda@icra.it, xue@icra.it
[5] ICRANet-Ferrara, Dipartimento di Fisica e Scienze della Terra, Università degli Studi di Ferrara, Via Saragat 1, I-44122 Ferrara, Italy
[6] Dipartimento di Fisica e Scienze della Terra, Università degli Studi di Ferrara, Via Saragat 1, I-44122 Ferrara, Italy
[7] INAF, Viale del Parco Mellini 84, I-00136 Rome, Italy
[8] ICRA, Università di Roma "La Sapienza," Piazzale Aldo Moro 5, I-00185 Roma, Italy
[9] ICRANet-Rio, Centro Brasileiro de Pesquisas Físicas, Rua Dr. Xavier Sigaud 150, 22290–180 Rio de Janeiro, Brazil
Received 2022 November 19; revised 2023 January 8; accepted 2023 January 9; published 2023 March 1

Abstract

Binary-driven hypernova (BdHN) models have been adopted to explain the observed properties of long gamma-ray bursts (GRBs). Here, we perform a comprehensive data analysis (temporal and spectral analysis, GeV emission, and afterglow) on GRB 130427A, GRB 160509A, and GRB 160625B. We identify three specific episodes characterized by different observational signatures and show that these episodes can be explained and predicted to occur within the framework of the BdHNe I model, as first observed in GRB 190114C and reported in an accompanying paper. Episode 1 includes the "SN-rise" with the characteristic cutoff power-law spectrum; Episode 2 is initiated by the moment of formation of the black hole, coincident with the onset of the GeV emission and the ultrarelativistic prompt emission phase, and is characterized by a cutoff power law and blackbody spectra; Episode 3 is the "cavity," with its characteristic featureless spectrum.

Unified Astronomy Thesaurus concepts: Gamma-ray bursts (629)

1. Introduction

It has been proposed that binary-driven hypernova (BdHN) models (e.g., Rueda et al. 2021, for a review) can explain the observed properties of long gamma-ray bursts (GRBs). This scheme (see Figure 1) starts at the second SN explosion in the evolutionary path of a massive binary leading to a BdHN progenitor (see, e.g., Fryer et al. 2015), namely a carbon–oxygen star (CO_{core}) forming a tight (orbital period $\sim$5 minutes) binary with a neutron star (NS) companion. The CO_{core} of mass $\lesssim$9–10 $M_\odot$ undergoes core collapse, forming at its center a newborn NS (hereafter νNS) and, at the same time, ejecting the outermost layers in a type Ic supernova (SN) explosion. The ejecta expand, and their first observational appearance is what we call the "SN-rise." The ejecta reach the NS companion, triggering a hypercritical accretion process onto it also thanks to copious neutrino–antineutrino emission (Fryer et al. 2014; Becerra et al. 2018). Numerical simulations have shown that the NS companion, by accretion, reaches the critical mass for gravitational collapse, hence forming a black hole (BH). This was first shown by two-dimensional simulations in Becerra et al. (2015) and by three-dimensional ones, first in Becerra et al. (2016) and more recently in improved smoothed-particle-hydrodynamics simulations in Becerra et al. (2019), from which the simulated images shown in Figure 1 have been taken. The fundamental contribution of these simulations has been to provide a visualization of the SN morphology that is modified from its original sphericity. A low-density region, a "cavity," is carved by the NS companion and, once that collapses, the region is further depleted to a density as low as $\sim 10^{-14}$ g cm^{-3} by the BH formation process (see Ruffini et al. 2019b). The newborn Kerr BH, embedded in the magnetic field inherited from the collapsed NS, aligned with the BH rotation axis, and surrounded by the low-density ionized plasma of the cavity, is what forms the "inner engine" of the GRB; see Ruffini et al. (2019d) and Rueda & Ruffini (2020). The "inner engine" leads to MeV emission due to the e^+e^- plasma created by vacuum polarization in the ultra-relativistic prompt emission (UPE) and to GeV emission by the synchrotron emission of accelerated electrons moving in the magnetic field. Details of these quantum and classical electrodynamics processes driven by the "inner engine" are given in companion papers (Moradi et al. 2021; Ruffini et al. 2021). The portion of the e^+e^- plasma that enters the high-density region of the ejecta produces X-ray flares observed in the early afterglow (Ruffini et al. 2018d). The synchrotron emission by relativistic particles injected from the νNS into the expanding ejecta in the νNS magnetic field explains the X-ray afterglow and its power-law luminosity (Ruffini et al. 2018c; Wang et al. 2019b). Finally, the optical emission from the ejecta due to the traditional nickel decay is observed in the optical bands a few days after the GRB trigger.

On 2019 January 15, we indicated that GRB 190114C, discovered by the Fermi Gamma-ray Burst Monitor (GBM) on 2019 January 14 (Hamburg et al. 2019), with a redshift $z = 0.424$ observed by the Nordic Optical Telescope (Selsing et al. 2019), had to be identified as a BdHN I due to its high isotropic total energy (Ruffini et al. 2019c). As a BdHN, we indicated that, within 18.8 ± 3.7 days, an SN should be expected to appear in the same location as the GRB. After an extended campaign involving tens of observatories worldwide, the expected optical SN signal was confirmed (Melandri et al. 2019). This success and the

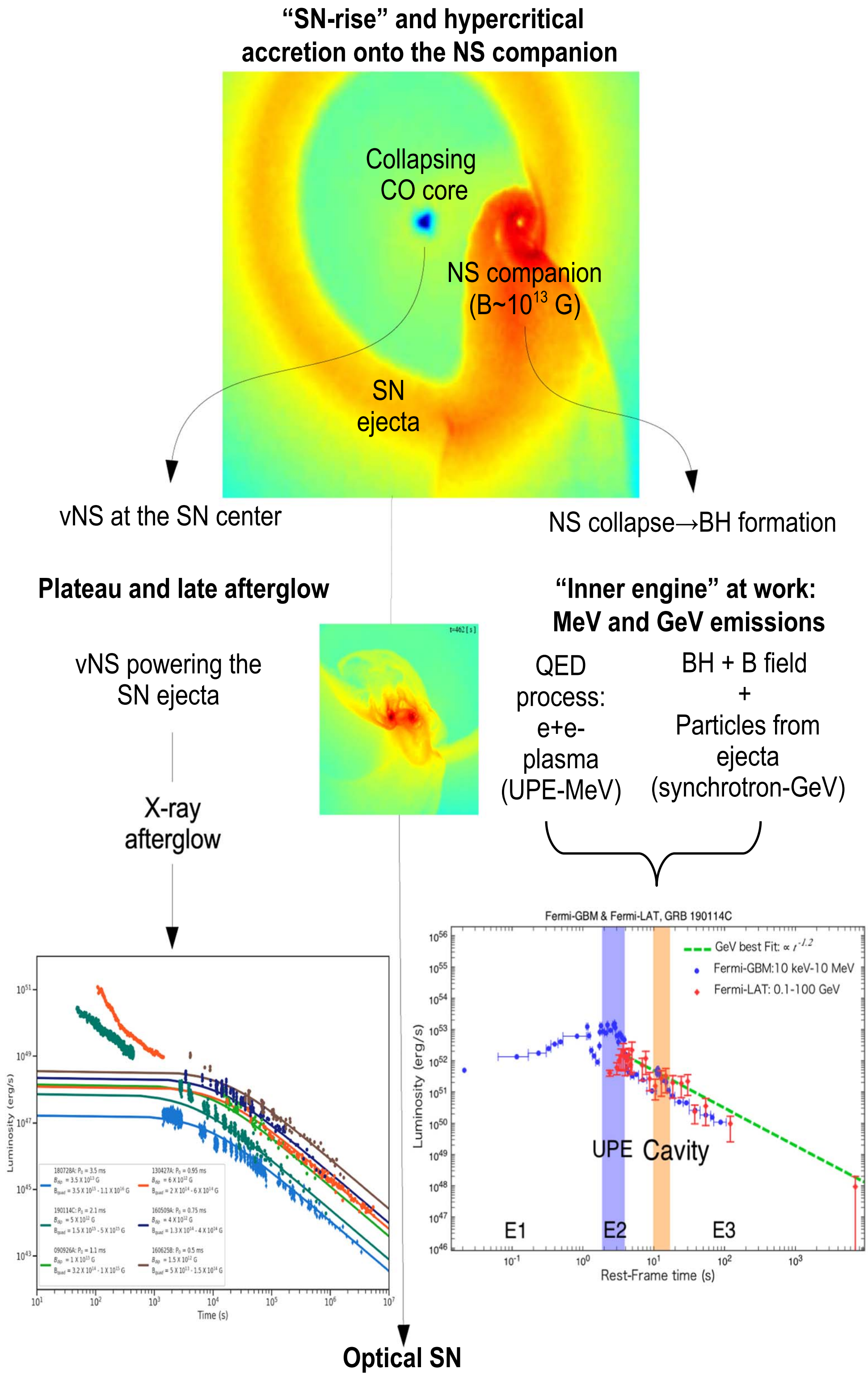

Figure 1. A diagram showing a BdHN's evolutionary history, including binary evolution, SN explosion, NS accretion, BH formation, GRB prompt and afterglow emissions, and SN appearance (see also Rueda et al. 2020).

detection of TeV radiation by MAGIC (Mirzoyan et al. 2019) make GRB 190114C one of the best examples of multi-wavelength astronomy. GRB 190114C is central for the understanding of BdHNe. For the first time all the BdHN phases are fully observable (Ruffini et al. 2019a) in a source with well determined redshift: starting from the GBM trigger, progressing to the first appearance of the SN (the SN-rise), to the accretion of the SN ejecta in the companion neutron star (NS), to the moment of formation of the BH and the concomitant onset of the GeV emission, the discovery of self-similarities in the GBM emission (the UPE phase), the X-ray emission from the cavity (Ruffini et al. 2019b), the emission of the afterglow (Rueda et al. 2020), the late emission of the GeV and TeV radiation and the determination of the BH mass (Ruffini et al. 2019d), finally reaching the optical SN observations mentioned above (Melandri et al. 2019; Wang et al. 2019b). The premises have been set to reach an understanding of the nature of the TeV radiation as soon as they are published. GRB 190114C signals a profound change of paradigm in the traditional understanding of GRBs from both an observational and a theoretical point of view.

It has been well established that all GRBs can be subdivided into nine subclasses of binary systems, each composed of a different combination of white dwarfs (WDs), carbon–oxygen cores (CO_{core}), NSs, and BHs (see, e.g., Wang et al. 2019a, and references therein). The most numerous subclass are BdHNe with progenitor binary systems composed of a CO_{core}, undergoing an SN explosion in the presence of an NS or BH companion (Ruffini et al. 2018d). A subclass of BdHN is represented by BdHNe I, sources with a binary period as short as ∼4–5 minutes, where the hypercritical accretion of the SN onto the companion NS leads it to reach the critical mass for gravitational collapse, and so to form a BH. GRB 190114C is the first complete example of a BdHN I. A second subclass is represented by BdHNe II, sources with a longer binary period/larger separation, where the hypercritical accretion of the SN onto the NS companion is not sufficient to reach the critical mass. In both BdHNe I and II the trigger of the GRB is signaled by the SN event, which leads to the formation of a new NS (νNS), to the appearance of the SN-rise, and to the consequent hypercritical accretion on both the companion NS and the νNS. By proceeding with an unprecedented spectral analysis in ever decreasing time steps, we have discovered self-similarities in the GBM emission of the UPE phase; see Ruffini et al. (2019a). There, we have addressed the nature of the "inner engine" of BdHNe creating the structure of self-similarity: a Kerr BH embedded in a magnetic field aligned with its rotation axis and surrounded a very low-density electron–ion plasma (Ruffini et al. 2019b). We have shown that the extraction of energy from the BH leads to the discrete and quantized MeV and GeV radiation, as presented in the companion papers (Ruffini et al. 2019a, 2019d; Rueda & Ruffini 2020).

The main purpose of this article is to verity that the results obtained in GRB 190114C are not an isolated case; on the contrary, they are verified to exist to an equal level of confidence in the other BdHNe I: GRB 130427A, GRB 160509A, and GRB 160625B. In all these sources, starting from the GBM trigger and a well determined redshift, we have progressed to identify: in Episode 1, the precursor including the first appearance of the SN (the "SN-rise") and the accretion of the SN ejecta onto the companion NS; in Episode 2, the moment of formation of the BH, the simultaneous onset of the GeV emission, and the onset of of the UPE phase with its characteristic cutoff power law plus blackbody spectra observed by Fermi; in Episode 3, the X-ray emission from the "cavity" recently modeled in Ruffini et al. (2019b). GRB 130427A is characterized by its extremely high fluence in MeV and GeV emission (Maselli et al. 2014; Ruffini et al. 2015). GRB 160509A is found to have a significant GeV evolution (Tam et al. 2017). GRB 160625B is famous for the confident detection of polarization (Troja et al. 2017). The data analysis in these papers confirms the existence of three light-curve structures in the initial tens of seconds, and in this paper we perform a more detailed analysis and give the astrophysical interpretations, categorizing the three light-curve structures as (1) SN-rise (Ruffini et al. 2019a), (2) UPE phase (Ruffini et al. 2019a), and (3) transition from SN to hypernova (Ruffini et al. 2018b). Particular attention is given to the accuracy of the spectral analysis to identify the above three episodes, as well as the much more complex iterative statistical analysis on the UPE to identify the self-similarities and the associated power laws. The fact that in all these cases the results have been successful implies that we have made great progress in ascertaining the taxonomy of a standard BdHN I. We are also going to show an example of BdHN II to compare and contrast the results. It is by now clear that the research is open in two different directions: in deepening the nature of each single component of a BdHN I, by inserting it into a population synthesis analysis (see, e.g., discussion in Fryer et al. 2015), and in studying the microphysical and physical origin of the self-similarities and the associated power laws.

As pointed out in the well documented book by Zhang (2018), the traditional approach in the spectroscopic data analysis of BATSE on board the Compton Gamma-Ray Observatory (Preece et al. 2000) has typically addressed a time-integrated spectral analysis over the entire duration of T_{90} and the finding of commonalities in all GRBs. This approach has been continued all the way to the current Fermi-GBM observations and the observations of the BAT instrument on board the Neil Gehrels Swift Observatory (see, e.g., Abdo et al. 2009; Hamburg et al. 2019, by the Fermi team). The time-integrated spectrum has been traditionally fitted by a smoothly connected, broken power-law function, named the "Band" function (Band et al. 1993). The Band function is based on four parameters (A, α, β, and E_p) whose values vary from source to source without reaching universal values. A complementary spectral analysis limited to the brightest time bin has been addressed by fitting with power laws, smoothly broken power laws, and Comptonized and Band models (Gruber et al. 2014). On the other hand, GRBs are known to have strong spectral evolution (e.g., Lu et al. 2012; Guiriec et al. 2013, 2015b; Li 2019a; Yu et al. 2019; Li et al. 2021). Therefore, in order to study their potential radiation mechanism in great detail, a time-resolved spectral analysis approach is required. The time-resolved spectral analysis has been performed for some bright bursts by some authors, e.g., GRB 090618, GRB 130427A, GRB 190114C, and many others (e.g., Ryde 2004, 2005; Izzo et al. 2012; Ruffini et al. 2014, 2015, 2019a).

The Fermi satellite, launched in 2008, provides a wider observational window in energy (Fermi-GBM: 8 keV–40 MeV, Fermi-LAT: 100 MeV–100 GeV), as well as a higher time resolution (as low as 2 μs for time-tagged event data; see, e.g., Meegan et al. 2009; von Kienlin et al. 2014). Gruber et al. (2014) presented the catalog of spectral analyses of GRBs by Fermi-GBM during its first four years of operation. Their aim was to generalize the statistical properties from the observations, not to differentiate the processes occurring in different episodes. They studied two types of spectra: the time-integrated spectrum and the spectrum of the brightest time bin. The software of RMfit (version 4.0rcl) was employed, which applies a modified, forward-folding Levenberg–Marquardt algorithm for spectral fitting. Four different spectral models were adopted: Band, Comptonized cutoff power law (CPL), power law (PL), and smoothly broken power law (SBPL). For the fitting results of the time-integrated spectra, they found the fractions of the best model from the statistical results are 29.9%, 6.6%, 8.6%, and 54.7% for PL, SBPL, Band, and CPL, respectively. For the fitting results of the brightest time bin, they found the fractions of the best model from the statistical results are 54.4%, 1.9%, 2.6%, and 39.7% for PL, SBPL, Band, and CPL, respectively. The Band and SBPL models are not preferred for most GRBs. The PL and CPL models are preferred for most GRBs; the popularity of the simple PL model was interpreted as an observational effect. In our approach since 2018, we have used the data from the Neil Gehrels Swift and Fermi satellites; our priority of having bright GRBs has already been stated in the introduction. The reason why these four different models are adopted is that the measurable spectrum of GRBs is dependent on intensity, and less intense bursts provide fewer data to support a large number of parameters. This may appear obvious, but it allows us to determine why in many situations a particular empirical function provides a poor fit, while in other cases it provides an accurate fit. For example, the energy spectra of GRBs are normally well fit by two smoothly joined power laws. For particularly bright GRBs, the Band and SBPL functions are typically an accurate description of the spectrum, while for weaker bursts the Comptonized function is most appropriate. Bursts that have signal significance of the order of the background fluctuations do not have a detectable distinctive break in their spectrum and so the power law is the most appropriate function. These facts reflect that in order to affirm the reliable physical interpretation from the spectra, both the quality and quantity of the observed data are important. In other words, capable satellites and bright GRBs are required. In this article, our sample consists of bright GRBs, which are well observed by both Fermi-GBM and Fermi-LAT. For these GRBs, Fermi is able to distinguish, for a small time interval (e.g., 0.1 s), the best model from two or more given models; therefore, a time-resolved spectral analysis can confidently be performed. In practice, we consider that an entire GRB phenomenon is composed of many episodes. We analyze the time-resolved spectral evolution and check that the goodness of the data is able to differentiate the episodes occurring at different times, including precursor, SN-rise, UPE, cavity, afterglow, and GeV emission. Consequently, from the composition of different episodes in each GRB, the taxonomy of nine subclasses of GRBs is obtained.

Therefore, we have correspondingly defined our priorities: (1) to address only the brightest GRBs observed by Fermi-GBM, Fermi-LAT, and the Neil Gehrels Swift Observatory, so addressing a limited number of sources with high significance S and in a wider range of spectral energies; (2) in view of the strongest significance S, to identify episodes that present specific spectral structures and determine the duration ΔT of each episode in the source rest frame; (3) to perform a detailed time-resolved spectral analysis on ever decreasing time intervals, within the total duration ΔT, which has led to identification of the presence of self-similar structures and associated power laws. We have determined new statistically significant spectral distributions and evaluated the corresponding luminosity in the cosmological rest frame.

The structure of this article is as follows. Section 2 presents the detailed time-resolved data analysis procedure. We have fully considered the spectral contribution from thermal components. Our approach to the spectral analysis is based on fitting Bayesian models by using the Markov Chain Monte Carlo (MCMC) technique. In Section 3, we derive our complete spectral analysis for all the episodes of GRB 160625B. In Section 4, we derive the complete spectral analysis for GRB 160509A. In Section 5, we present the corresponding analysis for GRB 130427A, which is the only case in which the UPE analysis is hampered by the pileup problem. In Section 6, we recall the result of the BdHNe II GRB 180728A. In Section 7, we summarize the results on the analysis of the SN-rise of BdHNe I and II, and present the implications of these results in the physical and astrophysical scenario of BdHNe. In Section 8, we draw the general conclusions of this work.

2. Data Analysis

2.1. Spectral Analysis

The temporal and spectral analysis of Fermi-GBM data is performed using the Bayesian approach package, namely, the Multi-Mission Maximum Likelihood Framework (3ML, Vianello et al. 2015). The GBM (Meegan et al. 2009) carries 14 detectors: 12 sodium iodide (NaI, 8 keV–1 MeV) and two bismuth germinate (BGO, 200 keV–40 MeV) scintillation detectors. We select up to three NaI detectors and one BGO detector, the incident angles of which are less than 60° (Bhat et al. 2016). The time-tagged event and spectral response files are used for the sets of detectors selected. The pre-source and the post-source data are used to fit the background with a 0–4 order polynomial function. The time interval of the source is selected to be longer than the duration of bursts (T_{90}), in order to cover the entire background-subtracted emission. During the fitting procedure, the likelihood-based statistics, the so-called Pgstat, is used, given by a Poisson (observation, Cash 1979)–Gaussian (background) profile likelihood. We replace the Band model by the CPL model to perform the spectral fitting throughout the paper, since thermal components are generally observed in the left shoulder of the Band spectrum (low-energy region, below $E_{\rm p}$); its existence does not affect the high-energy β index (above $E_{\rm p}$). The spectral analysis is performed by employing an MCMC technique to fit Bayesian models, and the model parameters in the Monte Carlo iteration vary in the following ranges: PL model, index: $[-5, 1]$; blackbody (BB) model, kT (keV): $[1, 10^3]$; CPL model, α: $[-5, 1]$, $E_{\rm c}$ (keV): $[1, 10^4]$. We use the typical spectral parameters from the Fermi-GBM catalog (Gruber et al. 2014) as the informative priors: $\alpha \sim \mathcal{N}(\mu = -1, \sigma = 0.5)$; $E_{\rm c} \sim \mathcal{N}(\mu = 200, \sigma = 300)$; $\beta \sim \mathcal{N}(\mu = -2.2, \sigma = 0.5)$. Each time we perform 20 chains and each chain includes 10,000 time iterations. The final value and its uncertainty (68% (1σ) Bayesian credible level) are calculated from the last 80% of the iterations. In this paper, we adopt the deviance information criterion (DIC) to select the better of two different models, defined as DIC $= -2\log[p(\text{data}|\hat{\theta})] + 2p_{\rm DIC}$, where $\hat{\theta}$ is the posterior mean of the parameters and $p_{\rm DIC}$ is the effective number of parameters. The preferred model is the model with the lowest DIC score. We define ΔDIC = DIC(CPL + BB) − DIC (CPL); for instance, if ΔDIC is negative it indicates that the CPL + BB is better than CPL. These methods have been applied in each episode.

2.2. Spectral Models

Several basic spectral components have been proposal previously (Kaneko et al. 2006; Guiriec et al. 2010, 2011, 2015a; Zhang et al. 2011; Yu et al. 2016, 2019; Li 2019a, 2019b, 2020, 2022a, 2022b; Li et al. 2019, 2021;

Ravasio et al. 2019; Li & Zhang 2021). The observed GRB spectrum in the keV–MeV band can usually be fitted by a nonthermal component, namely, the Band (or CPL) function (Band et al. 1993). The Band function defined as

$$f_{\rm BAND}(E) = A\begin{cases}\left(\frac{E}{E_{\rm piv}}\right)^{\alpha}\exp(-\frac{E}{E_0}), & E \leqslant (\alpha-\beta)E_0\\ \left[\frac{(\alpha-\beta)E_0}{E_{\rm piv}}\right]^{(\alpha-\beta)}\exp(\beta-\alpha)\left(\frac{E}{E_{\rm piv}}\right)^{\beta}, & E \geqslant (\alpha-\beta)E_0\end{cases} \tag{1}$$

where

$$E_{\rm p} = (2+\alpha)E_0, \tag{2}$$

has two power-law photon indices: the low-energy power-law photon spectral index α (typically ~-1.0), and the high-energy power-law photon spectral index β (typically ~-2.2), which are connected at the peak energy $E_{\rm p}$ (typically $\sim$220 keV) in the νF_ν space (e.g., Preece et al. 2000; Kaneko et al. 2006; Li et al. 2021; Li 2022a). A is the normalization factor at 100 keV in units of photons $\rm cm^{-2}\,keV^{-1}\,s^{-1}$, $E_{\rm piv}$ is the pivot energy fixed at 100 keV, and E_0 is the break energy in units of keV.

For the UPE phase, we mainly adopt the CPL model, or the so-called Comptonized model, which is given by

$$f_{\rm COMP}(E) = A\left(\frac{E}{E_{\rm piv}}\right)^{\alpha} e^{-E/E_0} \tag{3}$$

where A, $E_{\rm piv}$, α, and E_0 are as defined above.

Some bursts have an additional thermal component and are generally fitted with a Planck BB function. The Planck function is given by

$$f_{\rm BB}(E, t) = A(t)\frac{E^2}{\exp[E/kT(t)]-1}, \tag{4}$$

where $A(t)$ is the normalization, k is the Boltzmann constant, and $kT(t)$ is the blackbody temperature.

For the high-energy Fermi-LAT emission, the best-fit spectral model is usually a power-law model (e.g., Abdo et al. 2010; Zhang et al. 2011; Ajello et al. 2019; Tak et al. 2019) in the 0.1–100 GeV energy band, i.e.,

$$f_{\rm PL}(E) = A\left(\frac{E}{E_{\rm piv}}\right)^{\Gamma}, \tag{5}$$

where A is the normalization and Γ is the power-law index.

In the spectral fitting for the MeV UPE phase, we adopt a Bayesian analysis and model comparison using the ΔDIC value (e.g., Spiegelhalter et al. 2002; Moreno et al. 2013). For the GeV emission, a maximum likelihood estimate analysis is used to obtain the best fitting (e.g., Goldstein et al. 2012; Ackermann et al. 2013; Gruber et al. 2014; Bhat et al. 2016; Ajello et al. 2019; Li et al. 2019).

2.3. Calculation of Luminosity and Energetics

In addition to reporting the flux and fluence of each GRB, for the subset of GRBs with measured redshift z we also calculate their total radiated energy ($E_{\rm iso}$).

The observed flux, $\Phi(E_1, E_2, z)$, integrated between the minimum energy E_1 and the maximum energy E_2 is defined as

$$\Phi(E_1, E_2, z) = \int_{E_1/(1+z)}^{E_2/(1+z)} E\, f_{\rm obs}(E)\,dE. \tag{6}$$

In principle, for different models and different energy bands the values of E_1, E_2, and $f_{\rm obs}$ would be different. For instance, for GeV radiation $E_1 = 0.1$ GeV, $E_2 = 100$ GeV, and $f_{\rm obs} = f_{\rm PL}$ is obtained from Equation (5) with a typical value of $\Gamma \approx -2.5$ (Ajello et al. 2019).

We adopt a flat FLRW universe model with $\Omega_\Lambda = 0.714$, $\Omega_M = 0.286$, and $H_0 = 69.6$ $\rm km\,s^{-1}\,Mpc^{-1}$ (Bennett et al. 2014; Planck Collaboration et al. 2016), and then the luminosity distance is given by (Weinberg 1972)

$$d_L(z, \Omega_\Lambda, \Omega_M) = (1+z)\frac{c}{H_0}\int_0^z \frac{dz'}{\sqrt{\Omega_M(1+z')^3+\Omega_\Lambda}}. \tag{7}$$

The isotropic radiated luminosity is

$$L_{\rm iso} = \frac{4\pi\, d_L^2}{1+z}\Phi(E_1, E_2, z), \tag{8}$$

where d_L is the luminosity distance and z is the redshift. The observed fluence S is given by

$$S(E_1, E_2, z) = \Delta T_{\rm i}\Phi(E_1, E_2, z), \tag{9}$$

where $\Delta T_{\rm i}$ is the duration of the time interval in which the analysis is made; see Ajello et al. (2019) for details.

The radiated energy, which is assumed to be radiated isotropically, is defined as

$$E_{\rm iso} = \frac{4\pi\, d_L^2}{1+z} S(E_1, E_2, z). \tag{10}$$

The isotropic luminosity ($L_{\rm X}$) for the X-ray afterglow data (Swift/XRT) can be derived as

$$L_{\rm X,iso} = 4\pi k d_L^2 F_{\rm X,b}, \tag{11}$$

where $F_{\rm X}$ is the flux, $k = (1+z)^{\beta-1}$, and β is the spectral index, which were computed from the Swift BA + XRT repository: http://www.swift.ac.uk/burst_analyser/.

3. GRB 160625B

On 2016 June 25 at 22:40:16.28 UT, GRB 160625B triggered GBM on board the NASA Fermi Gamma-ray Space Telescope (Burns 2016). Fermi-LAT began observation 188.54 s after the trigger (Dirirsa et al. 2016), and detected more than 300 photons with energy >100 MeV; the highest photon energy was about 15 GeV (Lü et al. 2017). Swift-XRT began observation at a later time ($>10^4$ s) and found a power-law behavior with decaying index ~-1.25 (Melandri et al. 2016). GRB 160625B is one of the most energetic GRBs with an isotropic energy $\approx 3\times10^{54}$ erg (Troja et al. 2017; Zhang et al. 2018). The redshift $z = 1.406$ is reported in Xu et al. (2016). GRB 160625B is a luminous GRB with clearly detected polarization (Troja 2017). There is no supernova confirmation due to its high redshift, $z > 1$ (Woosley & Bloom 2006). The early emission can be defined as three episodes as suggested by several independent studies in the literature (Troja et al. 2017; Zhang et al. 2018): a short precursor (G_1), a main burst (G_2), and a long-lasting tail (G_3). Troja et al. (2017) detected a significant and variable linear optical polarization in G_2, and they inferred, from the degree of polarization of 8.3% ± 0.8%, that the GRB outflows might be dominated by Poynting flux, of which the magnetic energy is dissipated rapidly before the magnetic reconnection, producing bright gamma rays. Zhang et al. (2018) performed a meticulous time-resolved analysis and found an evolution of the thermal component in G_1. The bright G_2 episode was divided into 71 slices, each having at least 2500 net counts, to conduct a fine time-resolved spectral analysis. All the slices can be successfully fitted by a Band function; no thermal component was determined. G_3 is faint, and its time-resolved spectra were fitted by a single power law or a cutoff power law. From the spectral evolution from thermal to nonthermal, they suggest a transition of the outflow from fireball to Poynting-flux-dominated.

Based on the temporal and spectral analysis, we confirm that the gamma-ray light curve of GRB 160625B has three different episodes, shown in Figure 2 (see also Table 1). Three different physical episodes have been identified in the keV–MeV energy range (see Figures 2, 3, and Table 1): (1) SN-rise, the time interval from $t_{\rm rf} = 0.00$ s to $t_{\rm rf} = 0.83$ s; (2) UPE phase, the time interval from $t_{\rm rf} = 77.72$ s to $t_{\rm rf} = 87.70$ s; (3) cavity, the time interval from $t_{\rm rf} = 87.70$ s to $t_{\rm rf} = 92.27$ s.

In a BdHN I, the "inner engine" starts at the moment of formation of the BH, accelerating charged particles that radiate photons in a wide energy band, thus generating the UPE phase and the GeV photons. The onset of the UPE phase is indicated by the appearance of the thermal component since the plasma is originally optically thick. Since the count rate of GeV photons observed in the onset phase is a few per second, it is necessary to have a discrepancy of at most a fraction of a second between the observed starting time of the UPE and the GeV. Indeed, for GRB 160625B, the starting time of its thermal emission is just 0.38 s ahead of the time of observation of the first GeV photon, which for the above reasons can be considered temporally coincident. This time coincidence is also observed in the other BdHNe I studied in this article.

1. *SN-rise*. Figure 3 (upper left panel) shows the fit of the SN-rise spectrum during its rest-frame time interval of occurrence, i.e., from 0 to $t_{\rm rf} \simeq 0.83$ s. It is best fitted by a PL + BB model with temperature 17.5 keV and power-law index −2.0.
2. *UPE phase*. Similarly to GRB 190114C, we also find a self-similarity in the UPE phase for GRB 160625B after carrying out the detailed time-resolved spectral analysis, with a cutoff power law + blackbody (CPL + BB) model, for five successive iteration processes on shorter and shorter timescales[10] (expressed in the laboratory and in the rest frame). For the first iteration, Figure 4 (first layer) shows the best fit of the spectrum of the entire duration of the UPE from $t_{\rm rf} = 77.72$ s to $t_{\rm rf} = 87.70$ s. We then divide the rest-frame time interval in half and again perform the same spectral analysis for the two intervals, each of 4.99 s, i.e., [77.72–82.71 s] and [82.71–87.70 s], obtaining the results shown in Figure 4 (second layer). In the third iteration, we divide each of these half intervals in half again. We continue this procedure up to five iterations, i.e., up to dividing the UPE into 16 time subintervals. For each iterative step, we give the duration and the spectral parameters of the CPL + BB model, including the low-energy photon index α, the peak energy $E_{\rm c}$, the BB temperature kT (k is the Boltzmann constant), the model comparison parameter (DIC), the BB flux, the total flux, the ratio of BB to total flux, and the total energy. The results are summarized in Figure 4 and the properties of the iterations are listed in Table 2. They confirm the validity, also in GRB 160625B, of the self-similar structure first discovered in GRB 190114C. Figure 5 shows the luminosity of the Fermi-GBM as a function of the rest-frame time, derived from the fifth iteration (see Table 2). We also show the corresponding evolution of the rest-frame temperature (Figure 5). The best-fit parameters for each spectrum (α, $E_{\rm c}$), along with its time interval, ΔDIC, blackbody temperature kT, blackbody flux ($F_{\rm BB}$), total flux ($F_{\rm total}$), ratio of thermal to total flux, and the total energy are summarized in Table 2.
3. *Cavity*. Figure 3 (upper right panel) shows the spectrum of the cavity for GRB 160625B, from $t_{\rm rf} = 87.70$ s to $t_{\rm rf} = 92.27$ s. It can be well fitted by a featureless CPL model with photon index $\alpha = 0.95$ and cutoff energy of 239 keV.
4. *GeV emission*. Figure 3 (lower left panel) shows the luminosity of the GeV emission in the rest frame as a function of the rest-frame time.
5. *Afterglow*. Figure 3 (lower right panel) shows the (k-corrected) afterglow luminosity (Swift/XRT data) in the rest-frame as a function of rest-frame time. The best-fit parameters were obtained with a power-law index of 1.319 ± 0.021.

4. GRB 160509A

GRB 160509A was observed by the Fermi satellite on 2016 May 9 at 08:59:04.36 UT (Longo et al. 2016). It was a strong source of GeV photons detected by Fermi-LAT, including a photon of 52 GeV that arrived at 77 s, and another one of 29 GeV at ∼70 ks (Laskar et al. 2016). Swift has a late-time follow-up, with a total exposure time of 1700 s starting from 7278 s (Kangas et al. 2020). The redshift of 1.17 is measured by the Gemini North telescope (Tanvir et al. 2016), implying a high isotropic energy of 1.06×10^{54} erg (Tam et al. 2017). Pak-Hin Thomas Tam and collaborators (Tam et al. 2017) analyzed in great detail the bright multipeaked pulse from −10 to 30 s, and a weaker emission period from 280 to 420 s. They divided these two episodes into six time slices, of which the Fermi-GBM and Fermi-LAT data are together fitted by a Band function or a Band function with an exponential high-energy cutoff. In Figure 6, we show the result of our highly time-resolved analysis applied to GRB 160509A, which further extends the results of Tam et al. (2017).

Based on the temporal and spectral analysis, three different physical processes are identified in the keV–MeV energy range (see Figures 6, 7, and Table 3). (1) SN-rise, the time interval from $t_{\rm rf} = 0.92$ s to $t_{\rm rf} = 1.84$ s. (2). UPE phase, the time interval from $t_{\rm rf} = 4.84$ s to $t_{\rm rf} = 8.53$ s. (3). Cavity, the time interval from $t_{\rm rf} = 10.14$ s to $t_{\rm rf} = 13.82$ s.

1. *SN-rise*. Figure 7 (upper left panel) shows the SN-rise and the spectral fitting of the cavity emission during its rest-frame time interval of occurrence. The spectrum of the

[10] The "inner engine" of the BdHN extracts the rotational energy from a Kerr BH through a Wald–Papapetrou solution, located in the cavity, and a discrete emission of quanta of 10^{37} erg in a time sequence as short as 10^{-4} s, which is expected within the framework of the BdHN models. To verify this, an in-depth time-resolved spectral analysis is required; for details see Ruffini et al. (2019a).

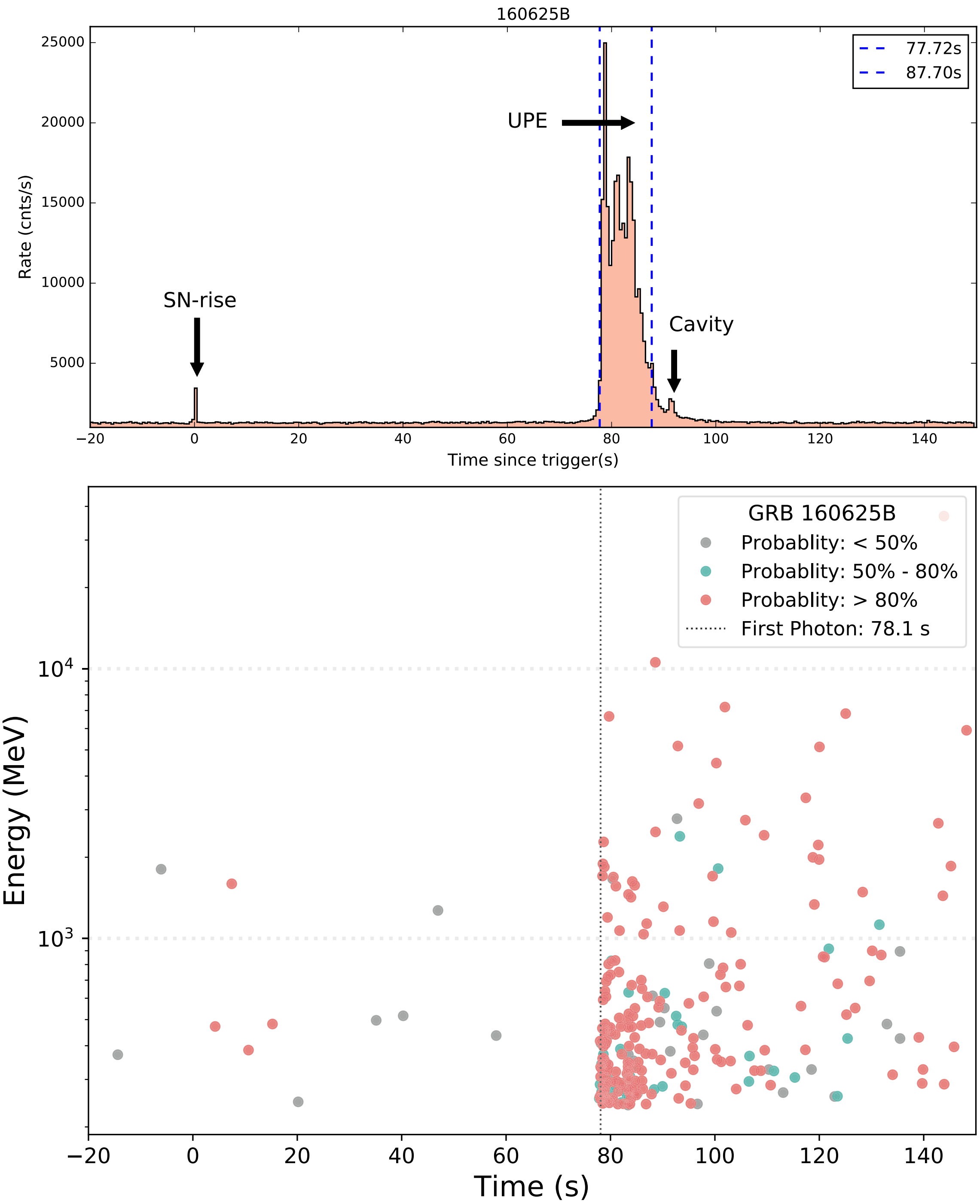

Figure 2. Upper panel: the proposed three new episodes of GRB 160625B as a function of the rest-frame time. Episode 1 occurs from $t_{rf} = 0$ s to $t_{rf} = 0.83$ s. The initial weak pulse represents the SN-rise. Episode 2 occurs from $t_{rf} = 77.72$ s to $t_{rf} = 87.70$ s, and includes the UPE emission. Episode 3 occurs from $t_{rf} = 87.70$ s to $t_{rf} = 92.27$ s. The redshift for GRB 160625B is 1.406 (Xu et al. 2016). The light curve consists of two clear spikes; the isotropic energy in the first one is $(1.09 \pm 0.20) \times 10^{52}$ erg. The total energy is $\approx 3 \times 10^{54}$ erg. Lower panel: the rest-frame time and the energy of Fermi-LAT photons in the energy band 0.1–100 GeV. The first photon of the GeV emission occurs at $t_{rf} = 78.1$ s. The onset of the GeV radiation coincides with the onset of the UPE. Detailed information for each episode (SN-rise, UPE phase, cavity, GeV, and afterglow emission) is given in Section 3 and Table 1, which includes the typical starting time, the ending time, the isotropic energy, and the preferred model.

SN-rise of GRB 160509A is best fitted by a CPL + BB model, from $t_{rf} \simeq 0.92$s to $t_{rf} \simeq 1.84$ s. The spectrum contains a BB component of temperature 25.61 keV and a photon index α of -1.22, with $E_c = 1769.76$ keV.

2. *UPE phase*. We perform the corresponding time-resolved spectral analysis from which we can see that the self-similarity first discovered in GRB 190114C is confirmed in the case of GRB 160509A. For the first iteration, we present the best fit of the spectrum of the entire duration of the UPE from $t_{rf} = 4.84$ s to $t_{rf} = 8.53$ s (see Figure 8, first layer). We then divide the rest-frame time interval in half and again perform the same spectral analysis for the

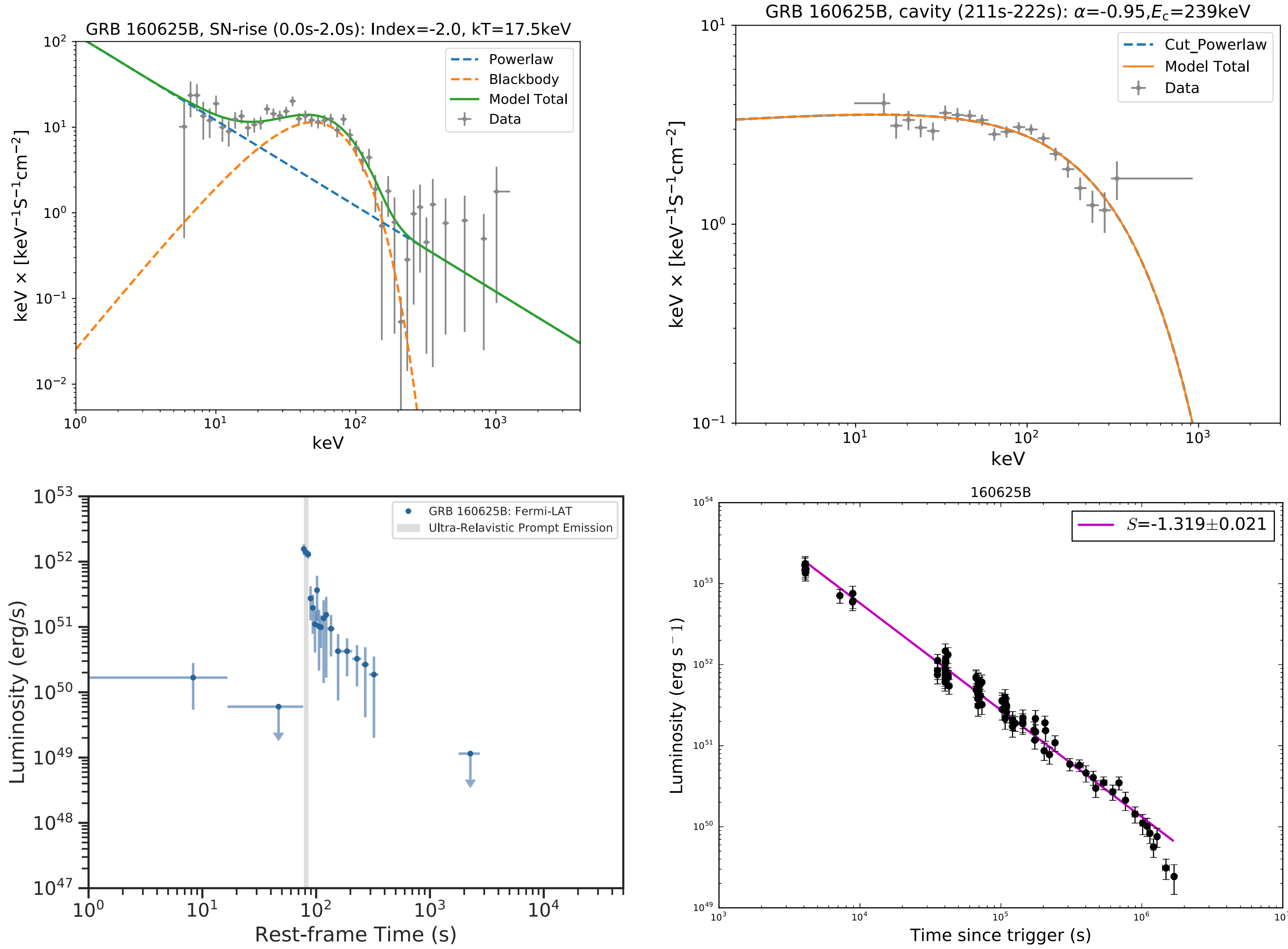

Figure 3. SN-rise, cavity, GeV, and afterglow of GRB 160625B; see also Table 1, which includes, for each episode, the starting time, the ending time, the isotropic energy, and the model that best fits the spectrum. Upper left: the spectrum of the SN-rise from 0 s to ≈2.0 s ($t_{\rm rf} \approx 0.83$ s). The spectrum is fitted by a blackbody of temperature 17.5 keV (in the observer's frame) plus a power law of index −2.0. Upper right: the cavity spectrum, from ≈211 s ($t_{\rm rf} = 87.70$ s) to ≈222 s ($t_{\rm rf} = 92.27$ s), is well fitted by a CPL, where the photon index α is −1.67 and the cutoff energy is 251 keV in the observer's frame. Lower left: Fermi-LAT rest-frame luminosity in the 100 MeV–100 GeV energy band (the UPE region is shaded gray). Lower right: k-corrected X-ray afterglow luminosity observed by Swift-XRT in the 0.3–10 keV band, as a function of the rest-frame time. It is best fitted by a power law with index 1.319 ± 0.021.

Table 1
Episodes of GRB 160625B, Including the Starting Time, the Ending Time, the Energy (Isotropic), the Preferred Spectral Model, and the References

Episode	Starting Time Rest-frame (s)	Ending Time Rest-frame (s)	Energy (erg)	Spectrum	References
SN-rise	0	0.83	1.09×10^{52}	CPL + BB	this paper
UPE	77.72	87.70	4.53×10^{54}	CPL + BB	this paper
Cavity	87.70	92.27	2.79×10^{52}	CPL	this paper
GeV	78.1	>300	2.99×10^{53}	PL	this paper
Afterglow	4082	>10 days	1.08×10^{53}	PL	this paper

Note. For the starting time of GeV emission, we take the time of the first GeV photon from the BH. The GeV emission may last for a very long time, but the observational time is limited because Fermi-LAT is not capable of resolving the late-time low-flux emission; therefore the ending time of GeV observation in the table is a lower limit. The starting time of X-ray afterglow in the table is taken from the starting time of Swift-XRT. The energy in the afterglow is integrated from 10^2 to 10^6 s. All times are given in the rest frame.

two 1.85 s intervals, i.e., [4.84–6.68 s] and [6.68–8.53 s], obtaining the results shown in Figure 8. Iteration 3: we then divide each of these half intervals in half again, i.e., $\Delta t_{\rm rf} = 0.92$ s corresponding to [4.84–5.76 s], [5.76–6.68 s], [6.68–7.60 s], and [7.60–8.53 s], and redo the previous spectral analysis, obtaining the results still in Figure 8. In a fourth iteration we divide the UPE into eight subintervals of $\Delta t_{\rm rf} = 0.46$ s corresponding to the time intervals [4.84–5.30

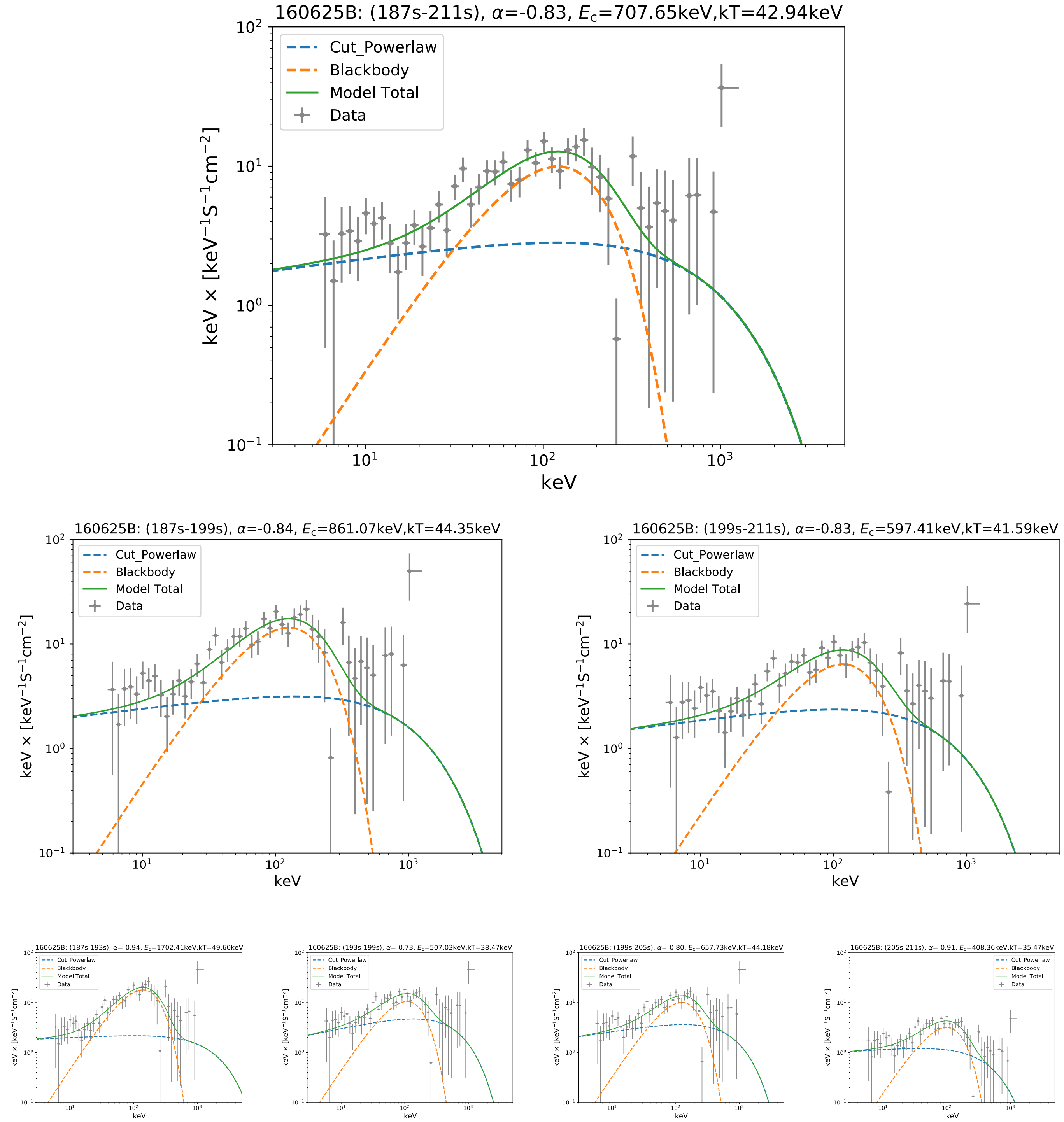

Figure 4. Time-resolved spectral analysis of GRB 160625B. All the layers have the same time coverage, from ≈187 s ($t_{\rm rf}$ = 77.72 s) to ≈211 s ($t_{\rm rf}$ = 87.70 s), but with different time divisions: one interval (top layer), two equal parts (second layer), four equal parts (third layer), eight equal parts (fourth and fifth layers), and sixteen equal parts (sixth, seventh, eighth, and ninth layers), respectively. The results of spectral analysis including duration, temperature, and cutoff energy are obtained in the observed frame, as shown in this figure. We have converted them to get their corresponding values in the rest frame: Table 2 shows the rest-frame time in column 2 and the rest-frame temperature in column 6.

s], [5.30–5.76 s], [5.76–6.22 s], [6.22–6.68 s], [6.68–7.14 s], [7.14–7.60 s], [7.60–8.06 s], and [8.06–8.53 s], and redo the spectral analysis (see Figure 8). In the fifth and final iteration of this process we divide the UPE into 16 subintervals of $\Delta t_{\rm rf} = 0.23$ s and we perform the corresponding spectral analysis and find the self-similar CPL + BB emission in the time intervals [4.84–5.07 s], [5.07–5.30 s], [5.30–5.53 s], [5.53–5.76 s], [5.76–5.99 s], [5.99–6.22 s], [6.22–6.45 s], [6.45–6.68 s], [6.68–6.91 s], [6.91–7.14 s], [7.14–7.37 s], [7.37–7.60 s], [7.60–7.83 s], [7.83–8.06 s], [8.06–8.29 s], and [8.29–8.53 s]; see Figure 8. Figure 9 shows the luminosity of the Fermi-GBM as a function of

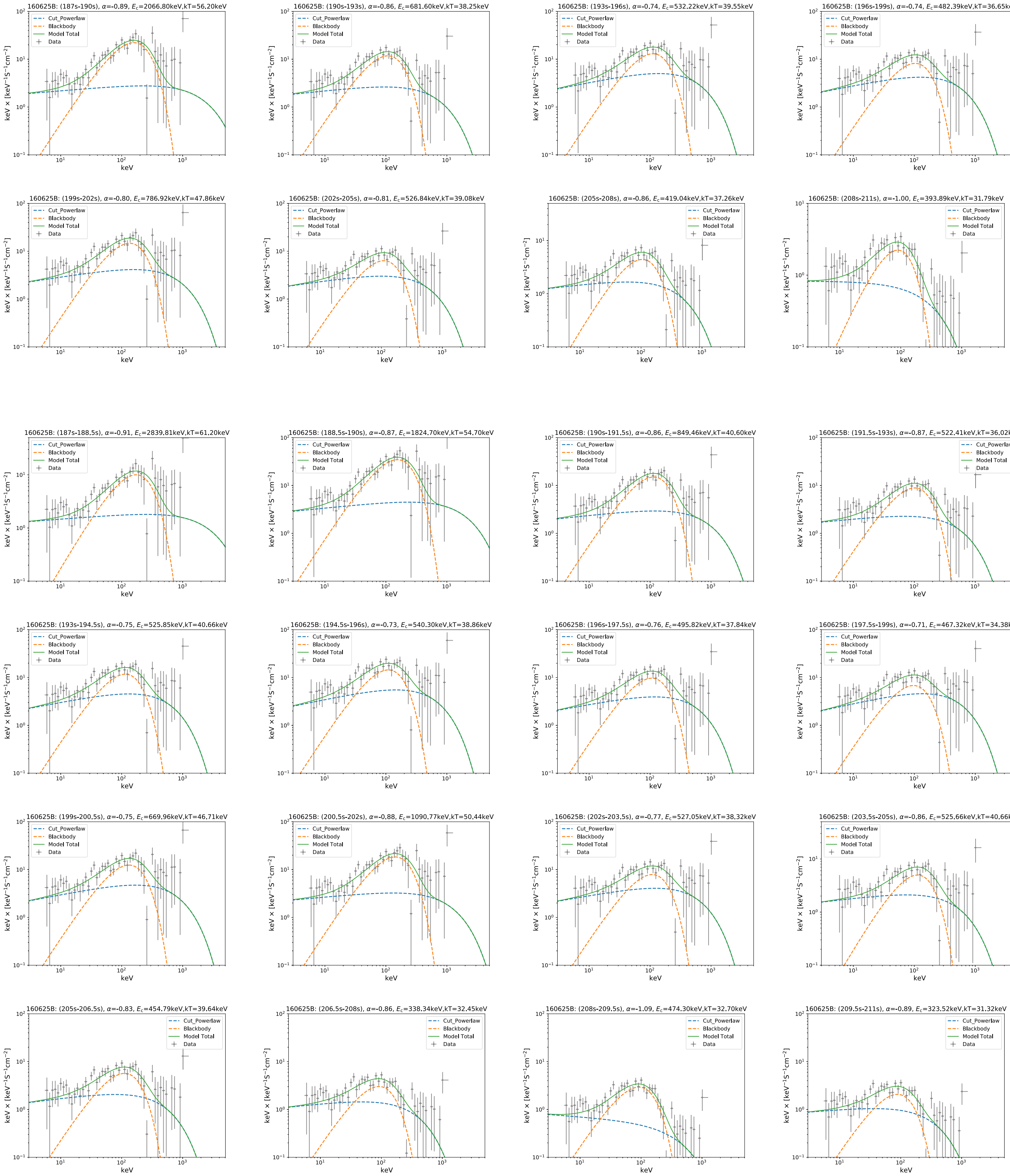

Figure 4. (Continued.)

the rest-frame time, derived from the fifth iteration (see Table 4). We also show the corresponding evolution of the rest-frame temperature (Figure 9). The best-fit parameters for each spectrum (α, E_c), along with its time interval, ΔDIC, blackbody temperature kT, blackbody flux (F_{BB}), total flux (F_{total}), ratio of thermal to total flux, and the total energy are summarized in Table 4.

3. *Cavity*. Figure 7 (upper right panel) shows the spectral fitting of the cavity emission during the rest-frame time interval of its occurrence, i.e., from $t_{rf} = 10.14$ to 13.82 s.

Table 2
Results of the Time-resolved Spectral Fits of GRB 160625B (CPL + BB Model) from $t_{rf} = 77.72$ s to $t_{rf} = 87.70$ s

$t_1 \sim t_2$ (s) Obs.	$t_{rf,1} \sim t_{rf,2}$ (s) Rest-frame	S	α	E_c (keV)	kT (keV) Rest-frame	ΔDIC	F_{BB} (10^{-6}) (erg cm^{-2} s^{-1})	F_{tot} (10^{-6}) (erg cm^{-2} s^{-1})	F_{ratio}	E_{tot} (erg)
187.00 ~ 211.00	77.72 ~ 87.70	649.12	$-0.83^{+0.01}_{-0.01}$	$707.6^{+13.0}_{-12.9}$	$42.9^{+0.4}_{-0.4}$	−2840.2	$3.13^{+0.16}_{-0.15}$	$35.50^{+0.81}_{-0.87}$	$0.09^{+0.0}_{-0.0}$	4.53e+54
187.00 ~ 199.00	77.72 ~ 82.71	566.19	$-0.84^{+0.01}_{-0.01}$	$861.1^{+20.8}_{-20.9}$	$44.4^{+0.5}_{-0.5}$	−2789.1	$4.67^{+0.23}_{-0.24}$	$48.44^{+1.41}_{-1.40}$	$0.10^{+0.01}_{-0.01}$	3.09e+54
199.00 ~ 211.00	82.71 ~ 87.70	421.10	$-0.83^{+0.01}_{-0.01}$	$597.4^{+15.8}_{-15.9}$	$41.6^{+0.8}_{-0.8}$	−716.6	$1.95^{+0.18}_{-0.18}$	$24.53^{+0.83}_{-0.87}$	$0.08^{+0.01}_{-0.01}$	1.57e+54
187.00 ~ 193.00	77.72 ~ 80.22	426.56	$-0.94^{+0.01}_{-0.01}$	$1702.4^{+42.5}_{-42.7}$	$49.6^{+0.5}_{-0.5}$	−2935.0	$6.51^{+0.35}_{-0.32}$	$69.51^{+1.80}_{-1.92}$	$0.09^{+0.01}_{-0.01}$	2.22e+54
193.00 ~ 199.00	80.22 ~ 82.71	421.75	$-0.73^{+0.01}_{-0.01}$	$507.0^{+12.2}_{-12.4}$	$38.5^{+0.8}_{-0.8}$	−784.9	$2.95^{+0.30}_{-0.28}$	$37.46^{+1.33}_{-1.31}$	$0.08^{+0.01}_{-0.01}$	1.19e+54
199.00 ~ 205.00	82.71 ~ 85.20	409.24	$-0.80^{+0.01}_{-0.01}$	$657.7^{+18.1}_{-18.6}$	$44.2^{+0.9}_{-0.9}$	−729.7	$3.25^{+0.35}_{-0.28}$	$40.93^{+1.57}_{-1.59}$	$0.08^{+0.01}_{-0.01}$	1.31e+54
205.00 ~ 211.00	85.20 ~ 87.70	205.28	$-0.91^{+0.02}_{-0.02}$	$408.4^{+25.3}_{-25.8}$	$35.5^{+1.4}_{-1.4}$	−105.6	$0.82^{+0.17}_{-0.15}$	$9.08^{+0.75}_{-0.68}$	$0.09^{+0.02}_{-0.02}$	2.90e+53
187.00 ~ 190.00	77.72 ~ 78.97	344.58	$-0.89^{+0.01}_{-0.01}$	$2066.8^{+50.1}_{-50.0}$	$56.2^{+0.7}_{-0.7}$	−2860.2	$9.08^{+0.63}_{-0.55}$	$105.00^{+3.03}_{-3.29}$	$0.09^{+0.01}_{-0.01}$	1.67e+54
190.00 ~ 193.00	78.97 ~ 80.22	282.28	$-0.86^{+0.01}_{-0.01}$	$681.6^{+31.2}_{-31.7}$	$38.2^{+0.8}_{-0.8}$	−603.9	$3.30^{+0.37}_{-0.35}$	$32.41^{+1.93}_{-1.63}$	$0.10^{+0.01}_{-0.01}$	5.17e+53
193.00 ~ 196.00	80.22 ~ 81.46	333.07	$-0.74^{+0.01}_{-0.01}$	$532.2^{+17.1}_{-17.0}$	$39.5^{+0.9}_{-1.0}$	−546.1	$3.76^{+0.51}_{-0.42}$	$43.09^{+2.07}_{-1.84}$	$0.09^{+0.01}_{-0.01}$	6.87e+53
196.00 ~ 199.00	81.46 ~ 82.71	287.45	$-0.74^{+0.01}_{-0.01}$	$482.4^{+16.9}_{-16.5}$	$36.6^{+1.3}_{-1.3}$	−287.5	$2.17^{+0.45}_{-0.34}$	$32.03^{+1.67}_{-1.50}$	$0.07^{+0.01}_{-0.01}$	5.11e+53
199.00 ~ 202.00	82.71 ~ 83.96	341.22	$-0.80^{+0.01}_{-0.01}$	$786.9^{+29.1}_{-29.2}$	$47.9^{+1.0}_{-1.0}$	−661.0	$5.16^{+0.56}_{-0.50}$	$56.34^{+3.11}_{-2.55}$	$0.09^{+0.01}_{-0.01}$	8.99e+53
202.00 ~ 205.00	83.96 ~ 85.20	258.65	$-0.81^{+0.02}_{-0.02}$	$526.8^{+21.7}_{-21.7}$	$39.1^{+1.5}_{-1.5}$	−181.9	$1.79^{+0.34}_{-0.31}$	$26.95^{+1.52}_{-1.45}$	$0.07^{+0.01}_{-0.01}$	4.30e+53
205.00 ~ 208.00	85.20 ~ 86.45	182.22	$-0.86^{+0.03}_{-0.03}$	$419.0^{+28.9}_{-28.9}$	$37.3^{+1.7}_{-1.6}$	−90.1	$1.20^{+0.27}_{-0.27}$	$12.55^{+1.16}_{-1.06}$	$0.10^{+0.02}_{-0.02}$	2.00e+53
208.00 ~ 211.00	86.45 ~ 87.70	116.10	$-1.00^{+0.04}_{-0.04}$	$393.9^{+46.2}_{-47.4}$	$31.8^{+2.1}_{-2.1}$	−37.9	$0.51^{+0.19}_{-0.15}$	$5.63^{+0.84}_{-0.67}$	$0.09^{+0.04}_{-0.03}$	8.97e+52
187.00 ~ 188.50	77.72 ~ 78.35	147.15	$-0.91^{+0.01}_{-0.01}$	$2839.8^{+140.7}_{-141.4}$	$61.2^{+1.8}_{-1.8}$	−706.0	$4.47^{+0.74}_{-0.59}$	$63.65^{+3.89}_{-3.71}$	$0.07^{+0.01}_{-0.01}$	5.08e+53
188.50 ~ 190.00	78.35 ~ 78.97	354.91	$-0.87^{+0.01}_{-0.01}$	$1824.7^{+49.3}_{-49.4}$	$54.7^{+0.8}_{-0.8}$	−2291.1	$13.77^{+1.02}_{-0.93}$	$147.60^{+4.86}_{-5.17}$	$0.09^{+0.01}_{-0.01}$	1.18e+54
190.00 ~ 191.50	78.97 ~ 79.59	227.35	$-0.86^{+0.02}_{-0.02}$	$849.5^{+52.9}_{-53.5}$	$40.6^{+1.1}_{-1.1}$	−465.8	$4.46^{+0.63}_{-0.58}$	$45.19^{+3.19}_{-3.25}$	$0.10^{+0.02}_{-0.01}$	3.60e+53
191.50 ~ 193.00	79.59 ~ 80.22	181.28	$-0.87^{+0.03}_{-0.03}$	$522.4^{+37.1}_{-37.6}$	$36.0^{+1.4}_{-1.4}$	−178.9	$2.34^{+0.48}_{-0.42}$	$21.81^{+2.08}_{-1.89}$	$0.11^{+0.02}_{-0.02}$	1.74e+53
193.00 ~ 194.50	80.22 ~ 80.84	229.41	$-0.75^{+0.02}_{-0.02}$	$525.9^{+25.5}_{-25.2}$	$40.7^{+1.5}_{-1.5}$	−223.5	$3.48^{+0.69}_{-0.62}$	$38.84^{+2.72}_{-2.41}$	$0.09^{+0.02}_{-0.02}$	3.10e+53
194.50 ~ 196.00	80.84 ~ 81.46	254.52	$-0.73^{+0.02}_{-0.02}$	$540.3^{+23.0}_{-23.0}$	$38.9^{+1.2}_{-1.2}$	−338.7	$4.12^{+0.67}_{-0.58}$	$47.26^{+3.01}_{-2.65}$	$0.09^{+0.02}_{-0.01}$	3.77e+53
196.00 ~ 197.50	81.46 ~ 82.09	212.08	$-0.76^{+0.02}_{-0.02}$	$495.8^{+24.6}_{-24.4}$	$37.8^{+1.6}_{-1.6}$	−188.9	$2.65^{+0.55}_{-0.49}$	$31.87^{+2.17}_{-2.17}$	$0.08^{+0.02}_{-0.02}$	2.54e+53
197.50 ~ 199.00	82.09 ~ 82.71	205.41	$-0.71^{+0.02}_{-0.02}$	$467.3^{+22.3}_{-22.4}$	$34.4^{+2.2}_{-2.2}$	−114.0	$1.72^{+0.60}_{-0.51}$	$32.16^{+2.31}_{-2.18}$	$0.05^{+0.02}_{-0.02}$	2.56e+53
199.00 ~ 200.50	82.71 ~ 83.33	239.62	$-0.75^{+0.02}_{-0.02}$	$670.0^{+31.7}_{-31.3}$	$46.7^{+1.6}_{-1.6}$	−256.6	$4.24^{+0.73}_{-0.65}$	$50.78^{+3.52}_{-3.33}$	$0.08^{+0.02}_{-0.01}$	4.05e+53
200.50 ~ 202.00	83.33 ~ 83.96	256.45	$-0.88^{+0.02}_{-0.02}$	$1090.8^{+73.8}_{-74.6}$	$50.4^{+1.3}_{-1.2}$	−458.5	$6.88^{+0.91}_{-0.81}$	$66.21^{+5.27}_{-4.91}$	$0.10^{+0.02}_{-0.01}$	5.28e+53
202.00 ~ 203.50	83.96 ~ 84.58	215.38	$-0.77^{+0.02}_{-0.02}$	$527.0^{+25.3}_{-25.2}$	$38.3^{+1.8}_{-1.8}$	−132.1	$2.18^{+0.54}_{-0.44}$	$34.45^{+2.53}_{-2.25}$	$0.06^{+0.02}_{-0.01}$	2.75e+53
203.50 ~ 205.00	84.58 ~ 85.20	157.84	$-0.86^{+0.03}_{-0.03}$	$525.7^{+39.3}_{-39.2}$	$40.1^{+2.4}_{-2.4}$	−63.6	$1.43^{+0.46}_{-0.37}$	$19.61^{+2.12}_{-1.73}$	$0.07^{+0.02}_{-0.02}$	1.56e+53
205.00 ~ 206.50	85.20 ~ 85.83	150.18	$-0.83^{+0.03}_{-0.03}$	$454.8^{+37.1}_{-37.9}$	$39.6^{+2.0}_{-2.0}$	−71.7	$1.63^{+0.47}_{-0.39}$	$16.59^{+1.96}_{-1.59}$	$0.10^{+0.03}_{-0.03}$	1.32e+53
206.50 ~ 208.00	85.83 ~ 86.45	112.49	$-0.86^{+0.05}_{-0.05}$	$338.3^{+41.3}_{-40.5}$	$32.5^{+2.9}_{-2.9}$	−29.1	$0.70^{+0.39}_{-0.27}$	$8.59^{+1.40}_{-1.15}$	$0.08^{+0.05}_{-0.03}$	6.85e+52
208.00 ~ 209.50	86.45 ~ 87.07	84.98	$-1.09^{+0.06}_{-0.06}$	$474.3^{+88.9}_{-88.7}$	$32.7^{+2.2}_{-2.2}$	−34.0	$0.70^{+0.28}_{-0.21}$	$5.46^{+1.27}_{-0.84}$	$0.13^{+0.06}_{-0.04}$	4.35e+52
209.50 ~ 211.00	87.07 ~ 87.70	82.67	$-0.89^{+0.06}_{-0.06}$	$323.5^{+52.4}_{-51.0}$	$31.3^{+3.4}_{-8.4}$	−58.7	$0.26^{+0.56}_{-0.19}$	$6.03^{+1.91}_{-1.15}$	$0.04^{+0.09}_{-0.03}$	4.81e+52

Note. This table reports: the time intervals in both rest frame and observer's frame, the significance (S) for each time interval, the power-law index, cutoff energy, temperature, ΔDIC, BB flux, total flux, ratio of BB to total flux F_{BB}/F_{tot}, and finally the isotropic energy. To select the best model from two different given models, we adopt the deviance information criterion, defined as DIC $= -2\log[p(\text{data}\,|\hat{\theta})] + 2p_{DIC}$, where $\hat{\theta}$ is the posterior mean of the parameters and p_{DIC} is the effective number of parameters. The preferred model is the model with the lowest DIC score. Here we define ΔDIC = (CPL + BB) − CPL; if ΔDIC is negative it indicates that the CPL + BB is better. After comparing the DICs, we find the CPL + BB model is preferred to the CPL and other models. The ΔDIC scores are reported in column 7.

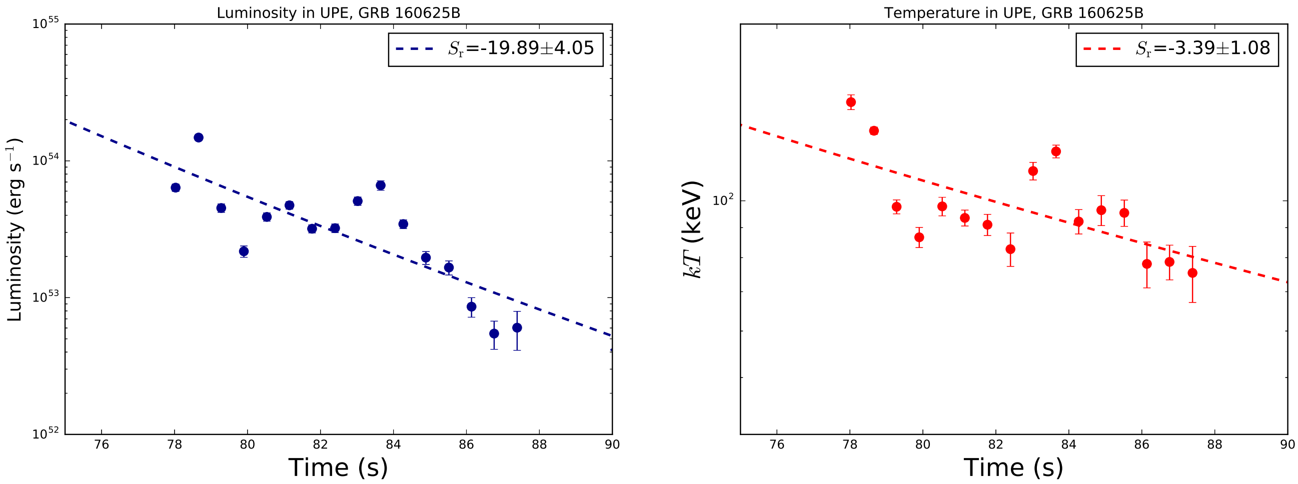

Figure 5. Left: light curve of the UPE of GRB 160625B derived from the fifth iteration with 16 subintervals. The values of the best-fit parameters from Table 2 are used to apply the k-correction and plot the rest-frame luminosity as a function of rest-frame time. The power-law index of the luminosity is -19.89 ± 4.05. For more information about GeV luminosity behavior see Wang et al. (2019a). Right: corresponding rest-frame temperature of the UPE as a function of the rest-frame time.

The best fit of the spectrum is a CPL model with a photon index α of -1.20 and a cutoff energy of 314 keV.

4. *GeV emission*. Figure 7 (lower left panel) shows the luminosity of the GeV emission and the luminosity in the afterglow as a function of the rest-frame time.
5. *Afterglow*. Figure 7 (lower right panel) shows the (k-corrected) rest-frame afterglow luminosity (Swift/XRT data) as a function of rest-frame time. The best-fit parameters were obtained with a power-law index of -1.259 ± 0.025.

5. GRB 130427A

A very bright burst, GRB 130427A, was announced by Fermi-GBM at 07:47:06.42 UT on 2013 April 27 (von Kienlin 2013). Swift-BAT was triggered 51.1 s later. Swift-UVOT and Swift-XRT began to observe at 181 and 195 s after the trigger (Maselli et al. 2013). Its redshift of $z = 0.34$ was detected and confirmed by the Gemini North telescope (Levan et al. 2013), Nordic Optical Telescope (Xu et al. 2013b), and VLT/X-shooter (Flores et al. 2013). The isotropic energy is 1.4×10^{54} erg, as detailed in Levan et al. (2013), von Kienlin (2013), Xu et al. (2013b), Flores et al. (2013), and Ruffini et al. (2015). A well observed fluence was recorded for GRB 130427A in the optical, X-ray, gamma-ray, and GeV bands. The Fermi-GBM count rate of GRB 130427A is shown in Figure 10. During the UPE phase the event count rate of n9 and n10 of Fermi-GBM surpasses $\sim 8 \times 10^4$ counts per second in the prompt radiation between rest-frame times $T_0 + 3.4$ s and $T_0 + 8.6$ s. The GRB is there affected by pileup,[11] which significantly deforms the spectrum; details can be found in Ackermann et al. (2014) and Ruffini et al. (2015). Only the data between $t_{rf} = 0.0$ and $t_{rf} = 1.49$ s can be used for a spectral analysis in the prompt phase. As shown in Figure 10 (see also Table 5) clearly identified parts are:

1. *SN-rise*. Figure 11 (upper left panel) shows the clear identification of the SN-rise, as also reported in Figure 10. The spectrum of the SN-rise of GRB 130427A is best fitted by a CPL + BB model, from 0.0 s ($t_{rf} \simeq 0.0$ s) to 0.65 s ($t_{rf} \simeq 0.49$ s). The spectrum contains a BB component of temperature 42.63 keV and photon index $\alpha = -0.58$, and $E_c = 547.59$ keV.
2. *Cavity*. Figure 11 (upper right panel) shows the featureless spectrum of the cavity emission of GRB 130427A from $\approx$15 s ($t_{rf} = 11.19$ s) to $\approx$25.5 s ($t_{rf} = 19.03$ s); it is fitted by a CPL model with photon index $\alpha = -1.52$ and cutoff energy 496.13 keV.
3. *GeV emission*. Figure 11 (lower left panel) shows the rest-frame luminosity of the GeV emission as a function of the rest-frame time.
4. *Afterglow*. Figure 11 (lower right panel) shows the (k-corrected) luminosity of the afterglow (Swift/XRT data) as a function of the rest-frame time, We apply the k-correction and measure the afterglow luminosity (Swift/XRT data) as a function of time; we obtain as best fit a power-law index of -1.276 ± 0.002.

6. BdHN II: GRB 180728A

GRB 180728A triggered Swift-BAT at 17:29:00 UT on 2018 July 28 (Starling et al. 2018). Due to the Earth's limb, Swift-XRT began the observation 1730.8 s after the trigger (Perri et al. 2018). Fermi was triggered at 17:29:02.28 UT; no GeV photon was detected though the initial Fermi-LAT boresight angle was only 35° (Veres et al. 2018). This burst occurred at a close distance of redshift $z = 0.117$ and was detected by VLT/X-shooter (Rossi et al. 2018). On July 28, we made a prediction of the SN appearance in $\sim$15 days (Ruffini et al. 2018a; Wang et al. 2019b), and indeed the SN optical peak was confirmed then (Izzo et al. 2018; Selsing et al. 2018). This GRB is composed of two pulses, see Figure 12 and Table 6.

1. *First pulse as SN-rise*. The first spike, the precursor, shows a power-law spectrum with a power-law index of -2.31 ± 0.08 in its 2.75 s duration. The averaged luminosity is $3.24^{+0.78}_{-0.55} \times 10^{49}$ erg s^{-1}, and the integrated energy gives $7.98^{+1.92}_{-1.34} \times 10^{49}$ erg in the range from 1 keV to 10 MeV. This energy emitted is in agreement

[11] Note that due to the pileup effect, the total energy of GRB 130427A has not been obtained.

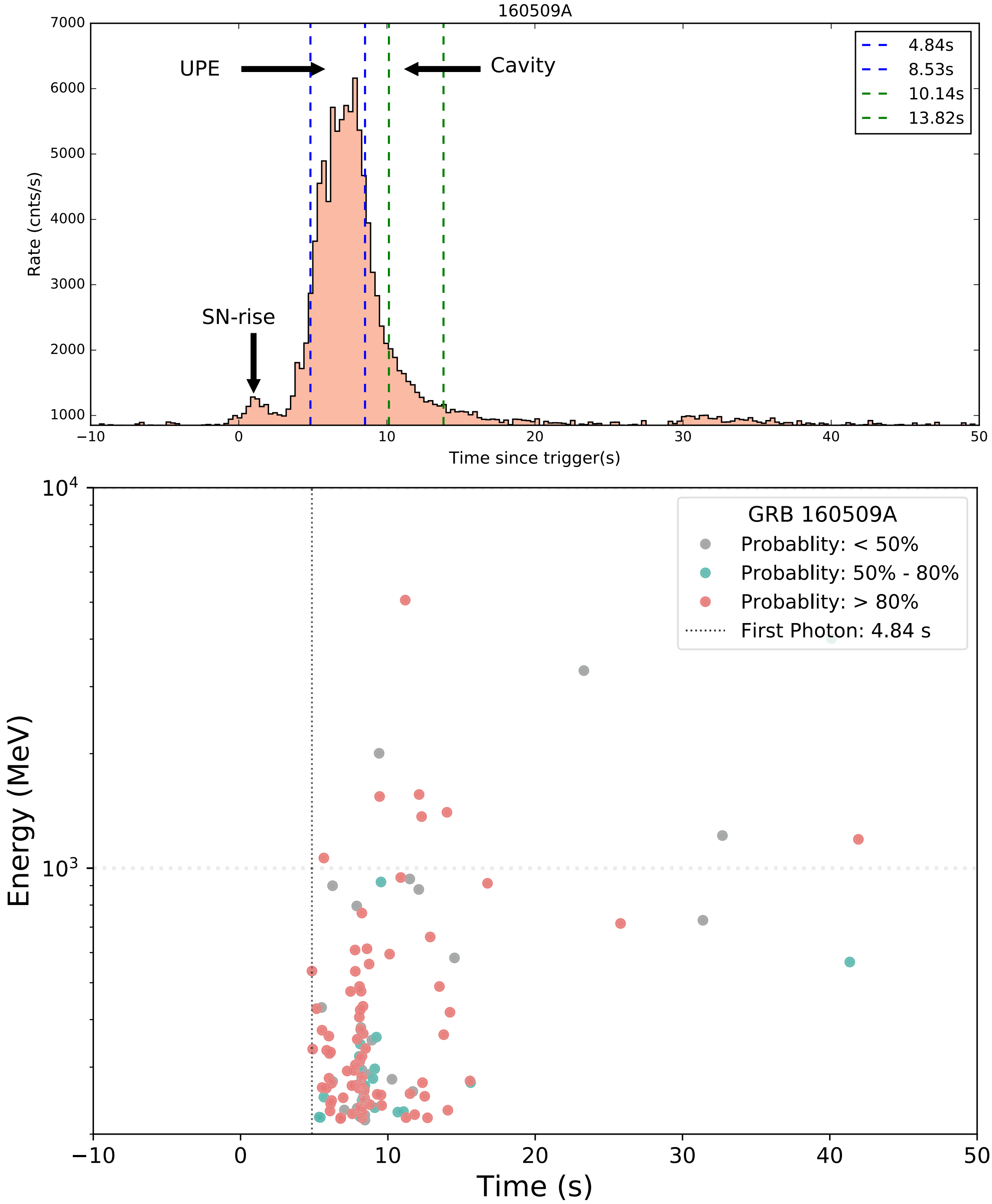

Figure 6. Upper panel: the proposed three new episodes of GRB 160509A as a function of the rest-frame time. Episode 1 occurs from $t_{\rm rf} = 0.92$ s to $t_{\rm rf} = 1.84$ s. Episode 2 including the UPE phase starts from $t_{\rm rf} = 4.84$ s and ends at $t_{\rm rf} = 8.53$ s in the rest frame. Episode 3 starts at $t_{\rm rf} = 10.14$ s and ends at $t_{\rm rf} = 13.82$ s. The redshift for GRB 160509A is 1.17 (Tanvir et al. 2016). The light curve consists of two spikes; the isotropic energy in the first small one is $\sim 1.47 \times 10^{52}$ erg. The total energy is 1.06×10^{54} erg (Tam et al. 2017). Lower panel: the energy and time of each Fermi-LAT photon of energy >100 MeV. The first GeV photon occurs at 4.84 s in the rest frame. The onset of the GeV radiation exactly coincides with the onset of the UPE. For detailed information on each episode (SN-rise, UPE phase, cavity, GeV, and Afterglow) see Section 4 and Table 3, which includes the starting time, the duration, the isotropic energy, and the preferred model.

with the conversion of the kinetic energy of SN-rise into electromagnetic emission.

2. *Second pulse as the hypercritical accretion of the SN ejecta onto the companion NS*. This pulse starts from 8.72 s, lasts 13.82 s, and contains 2.73×10^{51} erg isotropic energy. The best fit, which is a CPL + BB model of temperature $\approx$7 keV in the observer's frame, is shown in Figure 12. The BB component is interpreted as a matter outflow driven by the Rayleigh–Taylor convective instability developed in the accretion process (see, e.g., Izzo et al. 2012). From the time between observation of the SN-rise and the starting time of the hypercritical accretion, $\Delta t \approx 10$ s, a binary separation of $\approx 3 \times 10^{10}$ cm has been inferred. The binary separation determines, by

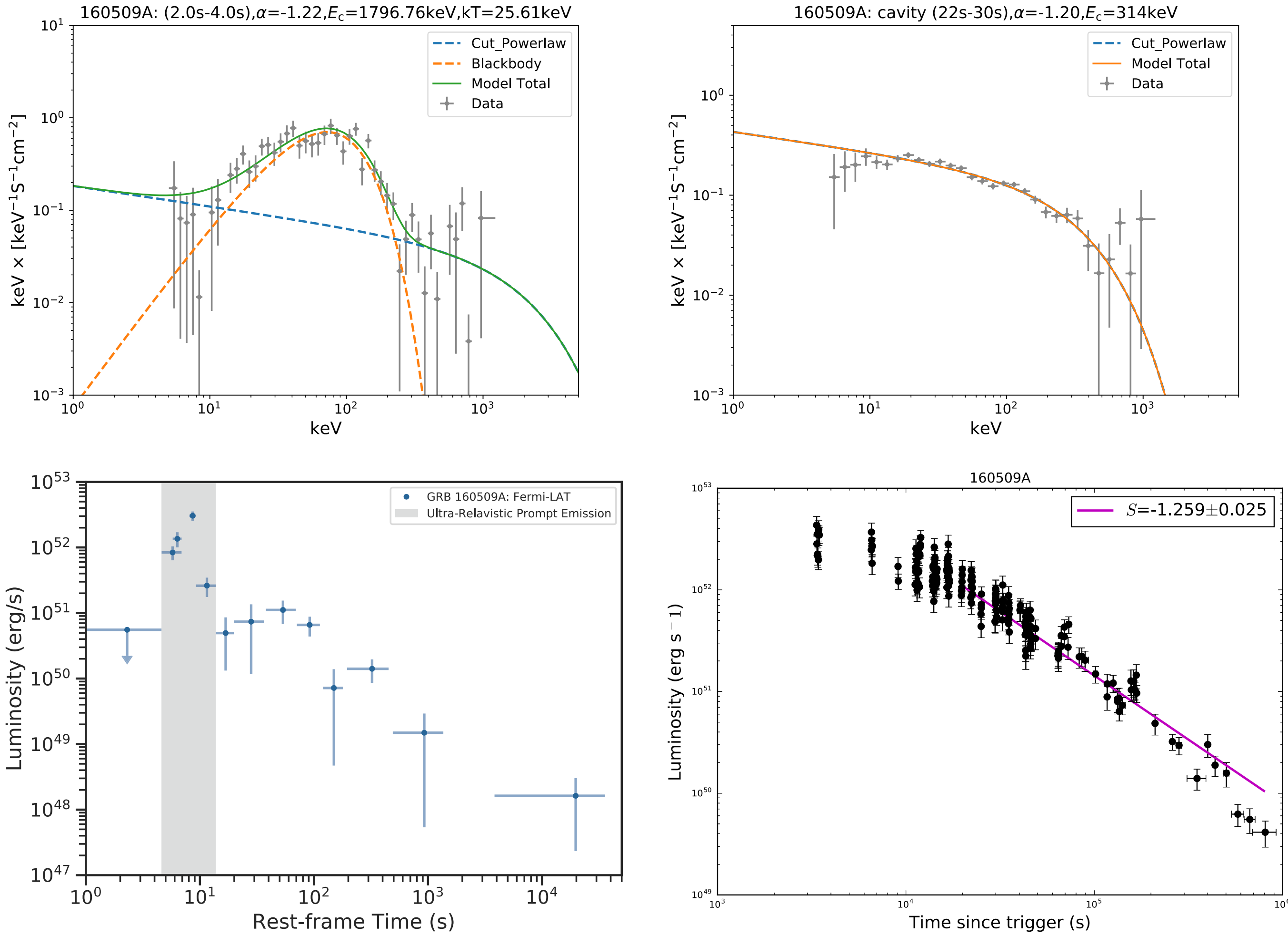

Figure 7. SN-rise, cavity, GeV, and afterglow of GRB 160509A; see also Table 3, which includes, for each episode, the starting time, the duration, the isotropic energy, and the model that best fits the spectrum. Upper left: The CPL + BB spectrum of the SN-rise, for the time interval from $t = 2.0$ s ($t_{\rm rf} = 0.92$ s) to $t = 4.0$ s ($t_{\rm rf} = 1.84$ s), spectral index $\alpha = -1.22$, cutoff energy $E_c = 1769.76$ keV, and temperature 25.61 keV in the observer's frame. Upper right: featureless spectrum of the cavity emission, fitted by a CPL model, from 22 s ($t_{\rm rf} = 10.14$ s) to 30 s ($t_{\rm rf} = 13.82$ s), where the photon index α is -1.20 and the cutoff energy is $E_c = 314$ keV in the observer's frame. Lower left: rest-frame Fermi-LAT light curve in the 100 MeV–100 GeV energy range. The UPE region is shaded gray. Lower right: k-corrected soft X-ray afterglow in the energy band 0.3–10 keV, observed by the Swift-XRT satellite, as a function of rest-frame time. It is best fitted by a power law with index 1.259 ± 0.025.

Table 3
Episodes of GRB 160509A with the Parameters Defined as in Table 1

Episode	Starting Time Rest-frame	Ending Time Rest-frame	Energy (erg)	Spectrum	References
SN-rise	0.92 s	1.84 s	1.47×10^{52}	CPL + BB	New in this paper
UPE	4.84 s	8.53 s	1.06×10^{54}	CPL + BB	New in this paper
Cavity	10.14 s	13.82 s	3.66×10^{52}	CPL	New in this paper
GeV	4.84 s	$>2 \times 10^4$ s	3.59×10^{53}	PL	New in this paper
Afterglow	7287s	~20 days	1.36×10^{52}	PL	New in this paper

angular momentum conservation, the spin period of ≈2.5 ms of the νNS left from the collapse of $CO_{\rm core}$. This νNS powers the afterglow by dissipating its rotational energy (Wang et al. 2019b).

7. Discussion

In Table 7, we compare and contrast the duration, the fluxes, the energy, and the temperature of the BB component associated with the SN-rise of the above BdHNe I and II; we also give, for each GRB, the corresponding redshift and $E_{\rm iso}$. In the case of BdHNe I, all of them have a similar SN-rise duration of nearly a second, consistent with the radius of the $CO_{\rm core}$ of 10^{10} cm, and energies of the order of 10^{52} erg. These energies are much larger than the one we have found here in the SN-rise of BdHNe II, $\sim 10^{50}$ erg, which is comparable to that of isolated SNe (see, e.g., Arnett 1982; Bethe 1990; Waxman & Katz 2017). As listed in Table 7, the SN-rise energy $E_{\rm sh}$ for BdHNe I is of the order of 10^{52} erg, and for BdHNe II it is close to 10^{50} erg; both values are greater than the SN-rise energy of a

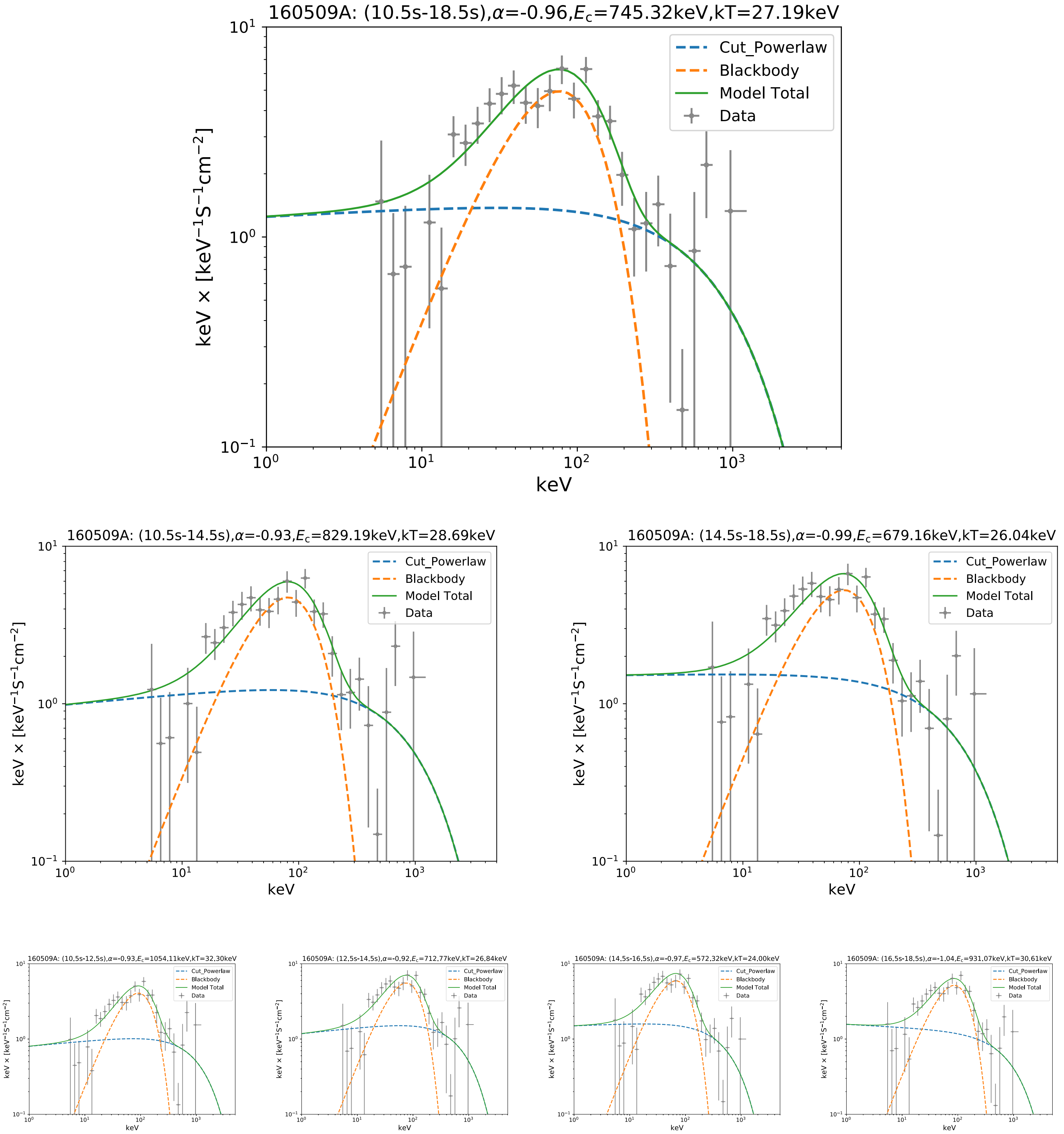

Figure 8. Time-resolved spectral analysis of GRB 160509A. All the layers have the same time coverage, from 10.5 s ($t_{\rm rf} = 4.84$ s) to 18.5 s ($t_{\rm rf} = 8.53$ s), but with different time divisions: one part (top layer), two equal parts (second layer), four equal parts (third layer), eight equal parts (fourth and fifth layers), and sixteen equal parts (sixth, seventh, eighth, and ninth layers), respectively. Two dashed lines represent CPL (blue) and BB (orange) components, while the solid line represents the total model (green). The results of spectral analysis including duration, temperature, and cutoff energy are obtained in the observed frame, as shown in this figure. We have converted them to get their corresponding values in the rest frame; Table 4 shows the rest-frame time in column 2, rest-frame cutoff energy in column 5, and rest-frame temperature in column 6.

normal SN (Bethe 1990; Waxman & Katz 2017). As we shall see below, such a difference can in principle be explained by a difference stemming from the configuration of the progenitors, such that the BdHN originated from a binary system, while a normal supernova originates from an isolated single star.

7.1. The SN-rise Energetics of BdHNe I

The larger energies of the SN-rise associated with BdHNe I discovered here can also be ascribed to a more energetic, rapidly rotating $CO_{\rm core}$. This can be the result of the binary

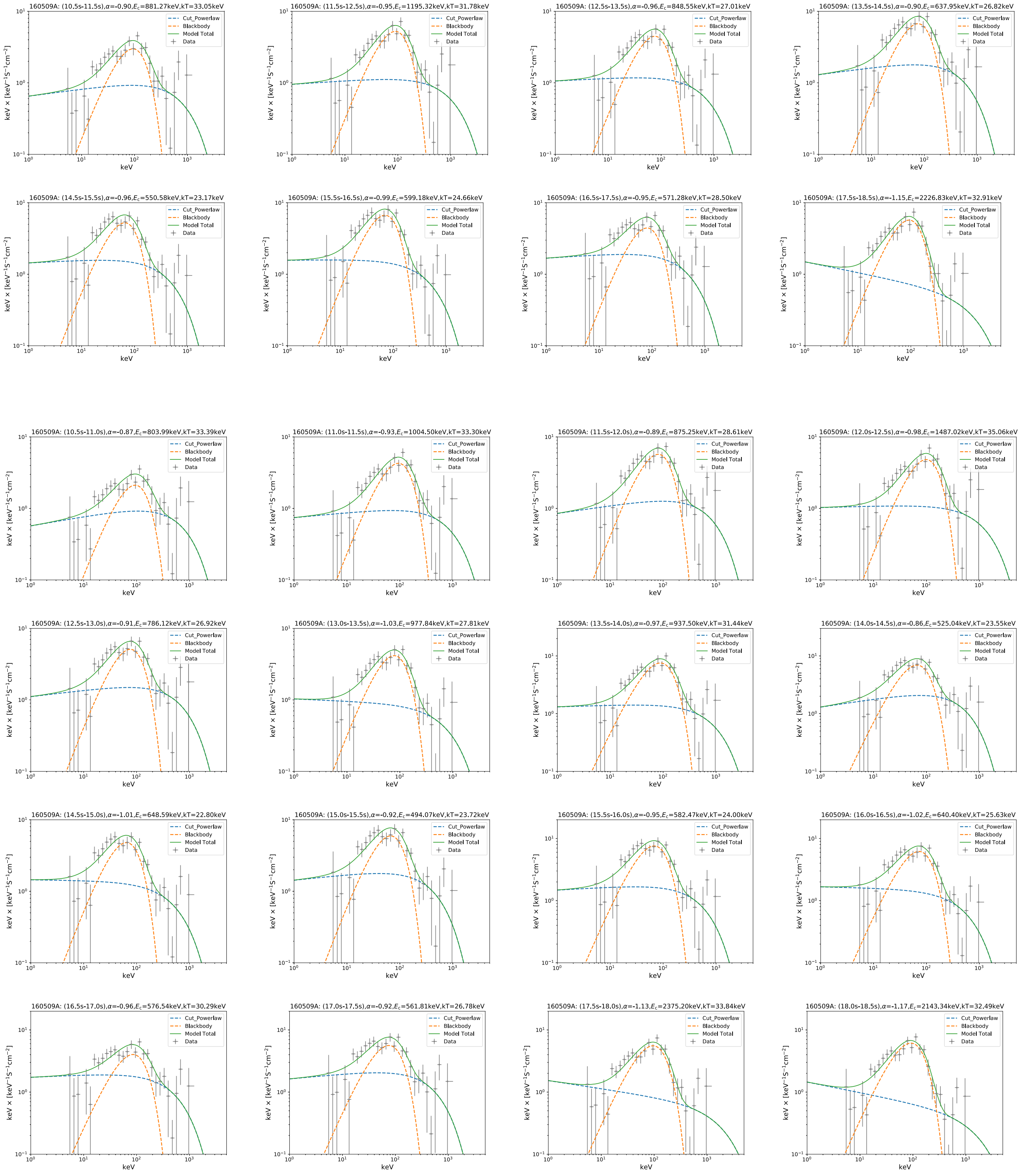

Figure 8. (Continued.)

nature of the progenitor with a short orbital period of the order of 4–5 minutes, in which angular momentum transfer by tidal effects during the previous evolutionary stages has been at work very efficiently.

Let us estimate the rotational energy of the CO_{core} assuming that the binary is tidally locked. In this case the rotation period of the CO_{core}, P_{CO}, equals the binary orbital period, P_{orb} (see, e.g., Hurley et al. 2002), i.e.,

$$P_{CO} = P_{orb} = 2\pi\sqrt{\frac{a_{orb}^3}{GM_{tot}}}, \tag{12}$$

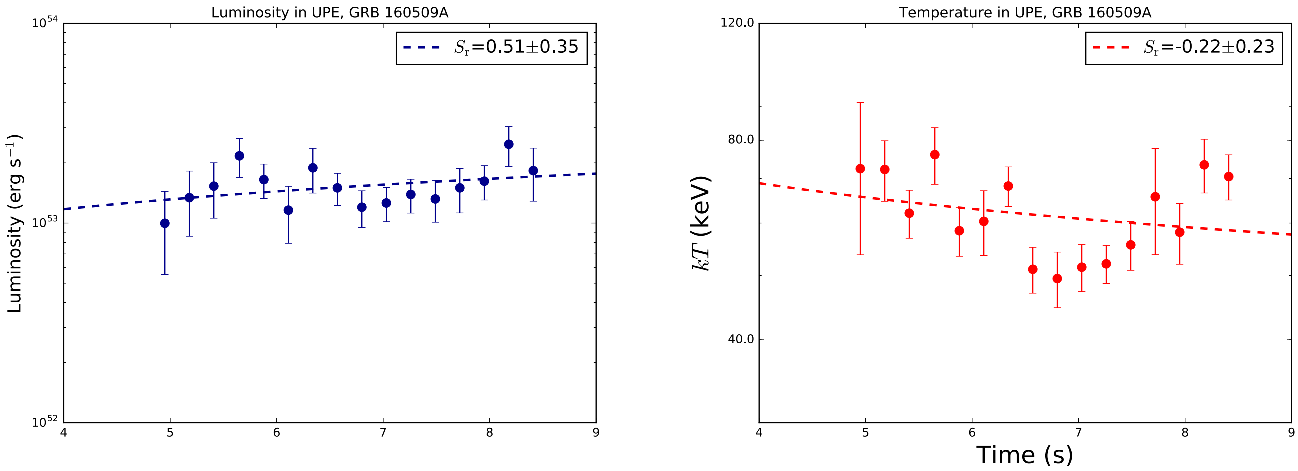

Figure 9. Left: luminosity light curve of the UPE of GRB 160509A as derived from the fifth iteration with 16 subintervals. The values of the best fit parameters from Table 4 are used to apply the k-correction and measure the luminosity as a function of time. The power-law index of 0.51 ± 0.35 for the luminosity is similar to the one obtained in the GeV emission luminosity after the UPE phase with index of -0.22 ± 0.23. For more information about GeV luminosity behavior see Wang et al. (2019a). Right: evolution of the rest-frame temperature of the UPE as derived from the fifth iteration with 16 subintervals, as reported in Table 4.

which is related to the binary separation $a_{\rm orb}$ and the total mass of the system $M_{\rm tot}$; G is the gravitational constant. Let us adopt a typical progenitor of a BdHN from Becerra et al. (2019): a $\rm CO_{core}$ obtained from the evolution of a $30\,M_\odot$ zero-age main-sequence (ZAMS) progenitor star, which has a total mass of $M_{\rm CO} = 8.9\,M_\odot$ and radius $R_{\rm CO} = 7.83 \times 10^9$ cm, and forms a binary with an NS companion of $M_{\rm NS} = 2\,M_\odot$. As for the orbital period/separation, we constrain our systems by the condition that there is no Roche-lobe overflow at the moment of the supernova explosion of the $\rm CO_{core}$. The Roche-lobe radius of the $\rm CO_{core}$ can be estimated as (Eggleton 1983)

$$\frac{R_{\rm RL}}{a_{\rm orb}} = \frac{0.49q^{2/3}}{0.6q^{2/3} + \ln(1 + q^{1/3})}, \tag{13}$$

where $q = M_{\rm CO}/M_{\rm NS}$. Therefore, the minimum orbital period of the binary, $a_{\rm orb,min}$, is obtained when $R_{\rm CO} = R_{\rm RL}$. For the above parameters, $a_{\rm orb,min} \approx 1.53 \times 10^{10}$ cm and correspondingly the minimum orbital period is $P_{\rm orb,min} \approx 5.23$ minutes.

The rotational energy for a $\rm CO_{core}$ is

$$E_{\rm rot,CO} = \frac{1}{2} I_{\rm CO}\omega_{\rm CO}^2 = \frac{1}{2} I_{\rm CO}\left(\frac{2\pi}{P_{\rm CO}}\right)^2, \tag{14}$$

where $I_{\rm CO}$ is the moment of inertia of the $\rm CO_{core}$. So, adopting $P_{\rm CO} = P_{\rm orb,min}$ ($\omega_{\rm CO} \approx 0.03$ rad s^{-1}) and $I_{\rm CO} \approx (2/5) M_{\rm CO} R_{\rm CO}^2$, we obtain $E_{\rm rot,CO} \approx 8.7 \times 10^{49}$ erg. This is of course lower than the gravitational binding energy $|W| \approx (3/5) G M_{\rm CO}^2/R_{\rm CO} \approx 1.6 \times 10^{51}$ erg and lower than the internal thermal energy as from the virial theorem. If we adopt the $\rm CO_{core}$ from the $25\,M_\odot$ ZAMS progenitor (see Table 1 in Becerra et al. 2019), characterized by $M_{\rm CO} = 6.85\,M_\odot$ and $R_{\rm CO} = 5.86 \times 10^9$ cm, and for the corresponding minimum orbital period $P_{\rm orb,min} \approx 4$ minutes ($\omega_{\rm CO} \approx 0.02$ rad s^{-1}), we obtain $E_{\rm rot,CO} \approx 6.3 \times 10^{49}$ erg.

Therefore, a much more energetic SN-rise can be the result of an exploding $\rm CO_{core}$ that rotates much faster than the rate set by tidal synchronization. In the above two examples, the ratio of rotational to gravitational energy is $E_{\rm rot}/|W| \approx 0.05$. However, from the stability point of view, it is known from the theory of Newtonian ellipsoids that secular axisymmetric instability sets in at $E_{\rm rot}/|W| \approx 0.14$ and dynamical instability at $E_{\rm rot}/|W| \approx 0.25$ (Chandrasekhar 1969).

Indeed, three-dimensional simulations of SN explosions confirm these stability limits and so explore SN explosions from pre-SN cores with high rotation rates of the order of 1 rad s^{-1} (see, e.g., Nakamura et al. 2014; Gilkis 2018; Fujisawa et al. 2019). These angular velocities are a factor 30–50 faster than the ones we have considered above. This implies that the rotational energy of the pre-SN core can be up to a factor 10^3 higher, namely $E_{\rm rot} \sim$ few $\times\, 10^{52}$ erg.

7.2. The SN-rise Energetics of BdHNe II

In the case of BdHNe II, the SN-rise has been shown to have a much smaller energy, 10^{49}–10^{50} erg. A similar case in the literature is represented by SN 2006aj, associated with GRB 060218 (Campana et al. 2006; Ferrero et al. 2006; Mirabal et al. 2006; Pian et al. 2006; Sollerman et al. 2006). The GRB 060218/SN 2006aj association was indeed interpreted in Becerra et al. (2016) as a BdHN II (at that time called "X-ray flash"). As we have mentioned, the energetics of these SN-rises are closer to the typical ones encountered in isolated SNe (see, e.g., Arnett 1982; Bethe 1990; Waxman & Katz 2017). This is consistent with the longer orbital periods of BdHNe II (Becerra et al. 2016) since, being farther apart, in the prior evolutionary stages binary interactions have been less effective in transferring angular momentum to the $\rm CO_{core}$. This explains why the SNe associated with BdHNe II, even if they occur in a binary, are more similar to isolated SNe.

As a final remark, we recall that the occurrence of the SN is deduced from direct optical observations for GRB sources at $z < 1$, and for all cases the SN occurrence is also inferred, indirectly, from the observation of the afterglows. Indeed, the afterglow originates from the feedback of the emission of the νNS, created in the SN event, into the expanding SN ejecta, given the proof of the SN occurrence (see Ruffini et al. 2018c; Rueda et al. 2020; Wang et al. 2019b, for details).

Table 4
Results of the Time-resolved Spectral Fits of GRB 160509A (CPL + BB Model) from $t_{rf} = 4.84$ s to $t_{rf} = 8.53$ s

$t_1 \sim t_2$ (s) Obs.	$t_{rf,1} \sim t_{rf,2}$ (s) Rest-frame	S	α	E_c (keV)	kT (keV)	ΔDIC	F_{BB} (10^{-6} erg cm^{-2} s^{-1})	F_{tot} (10^{-6} erg cm^{-2} s^{-1})	F_{ratio}	E_{tot} (erg)
10.50 ~ 18.50	4.84 ~ 8.53	292.18	$-0.96^{+0.01}_{-0.01}$	$745.3^{+27.6}_{-26.9}$	$27.2^{+0.6}_{-0.6}$	−633.8	$0.98^{+0.13}_{-0.11}$	$18.01^{+1.10}_{-1.00}$	$0.05^{+0.01}_{-0.01}$	5.40e+53
10.50 ~ 14.50	4.84 ~ 6.68	199.13	$-0.93^{+0.02}_{-0.02}$	$829.2^{+47.6}_{-47.0}$	$28.7^{+0.9}_{-0.9}$	−335.4	$1.00^{+0.19}_{-0.15}$	$18.50^{+1.70}_{-1.57}$	$0.05^{+0.01}_{-0.01}$	2.77e+53
14.50 ~ 18.50	6.68 ~ 8.53	232.97	$-0.99^{+0.01}_{-0.01}$	$679.2^{+31.9}_{-32.3}$	$26.0^{+0.8}_{-0.8}$	−324.2	$0.99^{+0.19}_{-0.15}$	$18.00^{+1.28}_{-1.27}$	$0.05^{+0.01}_{-0.01}$	2.70e+53
10.50 ~ 12.50	4.84 ~ 5.76	127.55	$-0.93^{+0.02}_{-0.02}$	$1054.1^{+97.5}_{-97.1}$	$32.3^{+1.7}_{-1.7}$	−145.5	$0.94^{+0.30}_{-0.22}$	$18.83^{+2.62}_{-2.40}$	$0.05^{+0.02}_{-0.01}$	1.41e+53
12.50 ~ 14.50	5.76 ~ 6.68	161.51	$-0.92^{+0.02}_{-0.02}$	$712.8^{+47.1}_{-47.4}$	$26.8^{+1.1}_{-1.1}$	−205.1	$1.08^{+0.26}_{-0.20}$	$18.81^{+1.96}_{-1.82}$	$0.06^{+0.01}_{-0.01}$	1.41e+53
14.50 ~ 16.50	6.68 ~ 7.60	169.80	$-0.97^{+0.02}_{-0.02}$	$572.3^{+32.9}_{-33.2}$	$24.0^{+1.0}_{-1.0}$	−203.4	$1.02^{+0.27}_{-0.20}$	$16.14^{+1.53}_{-1.39}$	$0.06^{+0.02}_{-0.01}$	1.21e+53
16.50 ~ 18.50	7.60 ~ 8.53	169.78	$-1.04^{+0.02}_{-0.02}$	$931.1^{+87.8}_{-86.6}$	$30.6^{+1.6}_{-1.6}$	−147.6	$1.15^{+0.31}_{-0.27}$	$20.87^{+2.83}_{-2.24}$	$0.06^{+0.02}_{-0.01}$	1.56e+53
10.50 ~ 11.50	4.84 ~ 5.30	77.67	$-0.90^{+0.04}_{-0.04}$	$881.3^{+135.4}_{-141.4}$	$33.0^{+3.3}_{-3.3}$	−43.8	$0.69^{+0.45}_{-0.27}$	$14.27^{+3.75}_{-2.93}$	$0.05^{+0.03}_{-0.02}$	5.35e+52
11.50 ~ 12.50	5.30 ~ 5.76	104.90	$-0.95^{+0.02}_{-0.02}$	$1195.3^{+126.1}_{-124.3}$	$31.8^{+1.9}_{-1.9}$	−117.1	$1.21^{+0.45}_{-0.33}$	$23.14^{+3.53}_{-3.11}$	$0.05^{+0.02}_{-0.02}$	8.67e+52
12.50 ~ 13.50	5.76 ~ 6.22	102.77	$-0.96^{+0.03}_{-0.03}$	$848.5^{+91.0}_{-89.5}$	$27.0^{+1.8}_{-1.8}$	−81.4	$0.86^{+0.37}_{-0.25}$	$17.63^{+2.89}_{-2.59}$	$0.05^{+0.02}_{-0.02}$	6.61e+52
13.50 ~ 14.50	6.22 ~ 6.68	129.10	$-0.90^{+0.03}_{-0.03}$	$638.0^{+53.1}_{-52.7}$	$26.8^{+1.4}_{-1.4}$	−128.1	$1.30^{+0.38}_{-0.31}$	$20.50^{+3.12}_{-2.65}$	$0.06^{+0.02}_{-0.02}$	7.68e+52
14.50 ~ 15.50	6.68 ~ 7.14	117.25	$-0.96^{+0.03}_{-0.03}$	$550.6^{+44.3}_{-44.5}$	$23.2^{+1.5}_{-1.5}$	−85.7	$0.86^{+0.32}_{-0.26}$	$15.20^{+2.37}_{-1.68}$	$0.06^{+0.02}_{-0.02}$	5.69e+52
15.50 ~ 16.50	7.14 ~ 7.60	127.21	$-0.99^{+0.03}_{-0.03}$	$599.2^{+52.7}_{-52.5}$	$24.7^{+1.3}_{-1.3}$	−124.5	$1.17^{+0.40}_{-0.28}$	$17.14^{+2.23}_{-2.19}$	$0.07^{+0.03}_{-0.02}$	6.42e+52
16.50 ~ 17.50	7.60 ~ 8.06	131.95	$-0.95^{+0.03}_{-0.03}$	$571.3^{+47.4}_{-46.6}$	$28.5^{+2.3}_{-2.4}$	−49.8	$0.90^{+0.46}_{-0.34}$	$19.51^{+2.69}_{-2.19}$	$0.05^{+0.02}_{-0.02}$	7.31e+52
17.50 ~ 18.50	8.06 ~ 8.53	112.19	$-1.15^{+0.02}_{-0.02}$	$2226.8^{+325.2}_{-326.2}$	$32.9^{+1.9}_{-1.9}$	−133.0	$1.33^{+0.47}_{-0.34}$	$27.25^{+4.66}_{-3.82}$	$0.05^{+0.02}_{-0.01}$	1.02e+53
10.50 ~ 11.00	4.84 ~ 5.07	48.87	$-0.87^{+0.06}_{-0.06}$	$804.0^{+189.6}_{-191.8}$	$33.4^{+8.6}_{-8.3}$	−23.1	$0.33^{+0.86}_{-0.24}$	$12.55^{+5.59}_{-3.97}$	$0.03^{+0.07}_{-0.02}$	2.35e+52
11.00 ~ 11.50	5.07 ~ 5.30	61.64	$-0.93^{+0.05}_{-0.05}$	$1004.5^{+202.6}_{-211.2}$	$33.3^{+3.5}_{-3.5}$	−40.8	$1.00^{+0.67}_{-0.42}$	$16.82^{+6.06}_{-4.34}$	$0.06^{+0.05}_{-0.03}$	3.15e+52
11.50 ~ 12.00	5.30 ~ 5.53	74.34	$-0.89^{+0.05}_{-0.05}$	$875.2^{+145.3}_{-147.8}$	$28.6^{+2.4}_{-2.4}$	−64.6	$1.13^{+0.55}_{-0.37}$	$19.22^{+5.94}_{-4.13}$	$0.06^{+0.03}_{-0.02}$	3.60e+52
12.00 ~ 12.50	5.53 ~ 5.76	75.45	$-0.98^{+0.03}_{-0.03}$	$1487.0^{+208.8}_{-205.9}$	$35.1^{+3.4}_{-3.4}$	−57.0	$1.16^{+0.74}_{-0.44}$	$27.26^{+6.00}_{-4.46}$	$0.04^{+0.03}_{-0.02}$	5.11e+52
12.50 ~ 13.00	5.76 ~ 5.99	81.26	$-0.91^{+0.03}_{-0.03}$	$786.1^{+96.3}_{-96.7}$	$26.9^{+2.3}_{-2.3}$	−49.0	$0.94^{+0.54}_{-0.34}$	$20.82^{+4.08}_{-3.74}$	$0.05^{+0.03}_{-0.02}$	3.90e+52
13.00 ~ 13.50	5.99 ~ 6.22	65.10	$-1.03^{+0.05}_{-0.05}$	$977.8^{+201.9}_{-199.4}$	$27.8^{+3.1}_{-3.1}$	−39.8	$0.77^{+0.62}_{-0.34}$	$14.55^{+4.63}_{-3.02}$	$0.05^{+0.05}_{-0.03}$	2.73e+52
13.50 ~ 14.00	6.22 ~ 6.45	90.78	$-0.97^{+0.04}_{-0.04}$	$937.5^{+151.2}_{-151.4}$	$31.4^{+2.1}_{-2.1}$	−77.7	$1.62^{+0.68}_{-0.42}$	$23.85^{+6.01}_{-4.95}$	$0.07^{+0.03}_{-0.02}$	4.47e+52
14.00 ~ 14.50	6.45 ~ 6.68	93.73	$-0.86^{+0.04}_{-0.04}$	$525.0^{+50.2}_{-49.4}$	$23.6^{+1.9}_{-1.9}$	−65.2	$1.13^{+0.61}_{-0.37}$	$18.94^{+3.46}_{-3.06}$	$0.06^{+0.03}_{-0.02}$	3.55e+52
14.50 ~ 15.00	6.68 ~ 6.91	80.00	$-1.01^{+0.04}_{-0.04}$	$648.6^{+79.1}_{-80.5}$	$22.8^{+2.2}_{-2.2}$	−41.5	$0.75^{+0.51}_{-0.30}$	$15.08^{+3.14}_{-2.32}$	$0.05^{+0.04}_{-0.02}$	2.82e+52
15.00 ~ 15.50	6.91 ~ 7.14	87.43	$-0.92^{+0.04}_{-0.04}$	$494.1^{+51.9}_{-50.7}$	$23.7^{+1.9}_{-1.9}$	−50.0	$0.96^{+0.54}_{-0.33}$	$15.80^{+3.08}_{-2.56}$	$0.06^{+0.04}_{-0.02}$	2.96e+52
15.50 ~ 16.00	7.14 ~ 7.37	91.73	$-0.95^{+0.04}_{-0.04}$	$582.5^{+63.7}_{-65.1}$	$24.0^{+1.6}_{-1.6}$	−80.8	$1.30^{+0.56}_{-0.39}$	$17.48^{+3.38}_{-2.64}$	$0.07^{+0.03}_{-0.02}$	3.27e+52
16.00 ~ 16.50	7.37 ~ 7.60	90.06	$-1.02^{+0.04}_{-0.04}$	$640.4^{+91.4}_{-92.2}$	$25.6^{+2.2}_{-2.2}$	−51.2	$1.10^{+0.58}_{-0.41}$	$16.62^{+3.91}_{-2.84}$	$0.07^{+0.04}_{-0.03}$	3.11e+52
16.50 ~ 17.00	7.60 ~ 7.83	90.67	$-0.96^{+0.04}_{-0.04}$	$576.5^{+78.4}_{-77.9}$	$30.3^{+5.5}_{-5.2}$	−25.1	$0.71^{+0.87}_{-0.48}$	$18.83^{+4.75}_{-3.42}$	$0.04^{+0.05}_{-0.03}$	3.53e+52
17.00 ~ 17.50	7.83 ~ 8.06	97.88	$-0.92^{+0.04}_{-0.04}$	$561.8^{+62.8}_{-63.6}$	$26.8^{+2.8}_{-2.8}$	−40.2	$1.03^{+0.72}_{-0.42}$	$20.40^{+3.97}_{-3.30}$	$0.05^{+0.04}_{-0.02}$	3.82e+52
17.50 ~ 18.00	8.06 ~ 8.29	82.94	$-1.13^{+0.03}_{-0.03}$	$2375.2^{+440.5}_{-440.1}$	$33.8^{+3.1}_{-3.2}$	−68.8	$1.35^{+0.83}_{-0.55}$	$31.18^{+7.03}_{-5.27}$	$0.04^{+0.03}_{-0.02}$	5.84e+52
18.00 ~ 18.50	8.29 ~ 8.53	77.25	$-1.17^{+0.04}_{-0.04}$	$2143.3^{+521.4}_{-532.9}$	$32.5^{+2.5}_{-2.5}$	−65.0	$1.37^{+0.74}_{-0.45}$	$23.06^{+6.84}_{-4.79}$	$0.06^{+0.04}_{-0.02}$	4.32e+52

Note. The definitions of parameters are the same as in Table 2.

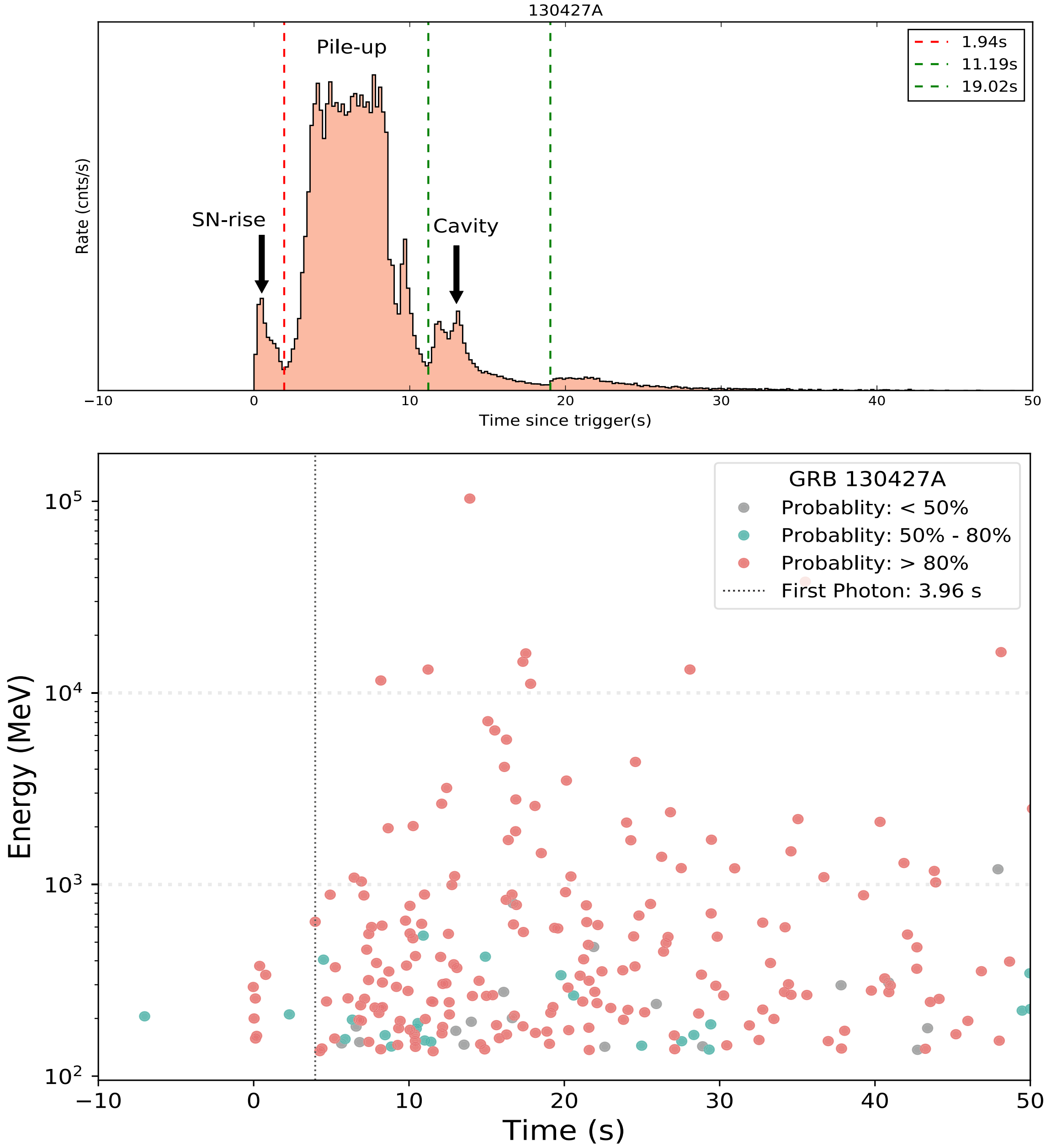

Figure 10. Upper panel: time structure of the prompt emission phase of GRB 130427A presented in the rest frame. The Fermi-GBM observation is strongly piled up due to the high fluence, hence the detection of each episode, especially the starting time of the UPE phase, cannot be determined accurately. Lower panel: the energy and time of each Fermi-LAT photon in the rest-frame; the first photon of GeV energy occurs at $t_{rf} = 3.96$ s. The onset of the GeV radiation coincides with the onset of the UPE. For detailed information for each episode (SN-rise, cavity, GeV, and afterglow), see Section 5 and Table 5, which includes the starting time, the duration, the isotropic energy, and the preferred model.

Table 5
Episodes of GRB 130427A with the Parameters Defined as in Table 1

Episode	Starting Time Rest-frame	Ending Time Rest-frame	Energy (erg)	Spectrum	References
SN-rise	0 s	0.49 s	6.5×10^{51}	CPL + BB	New in this paper
UPE	1.94 s	11.19 s	$\sim 1.4 \times 10^{54}$	CPL + BB	New in this paper
Cavity	11.19 s	19.03 s	1.97×10^{52}	CPL	New in this paper
GeV	3.96 s	$>2 \times 10^4$ s	5.69×10^{52}	PL	Ruffini et al. (2015)
Afterglow	107 s	>10 days	2.65×10^{52}	PL	Ruffini et al. (2015)

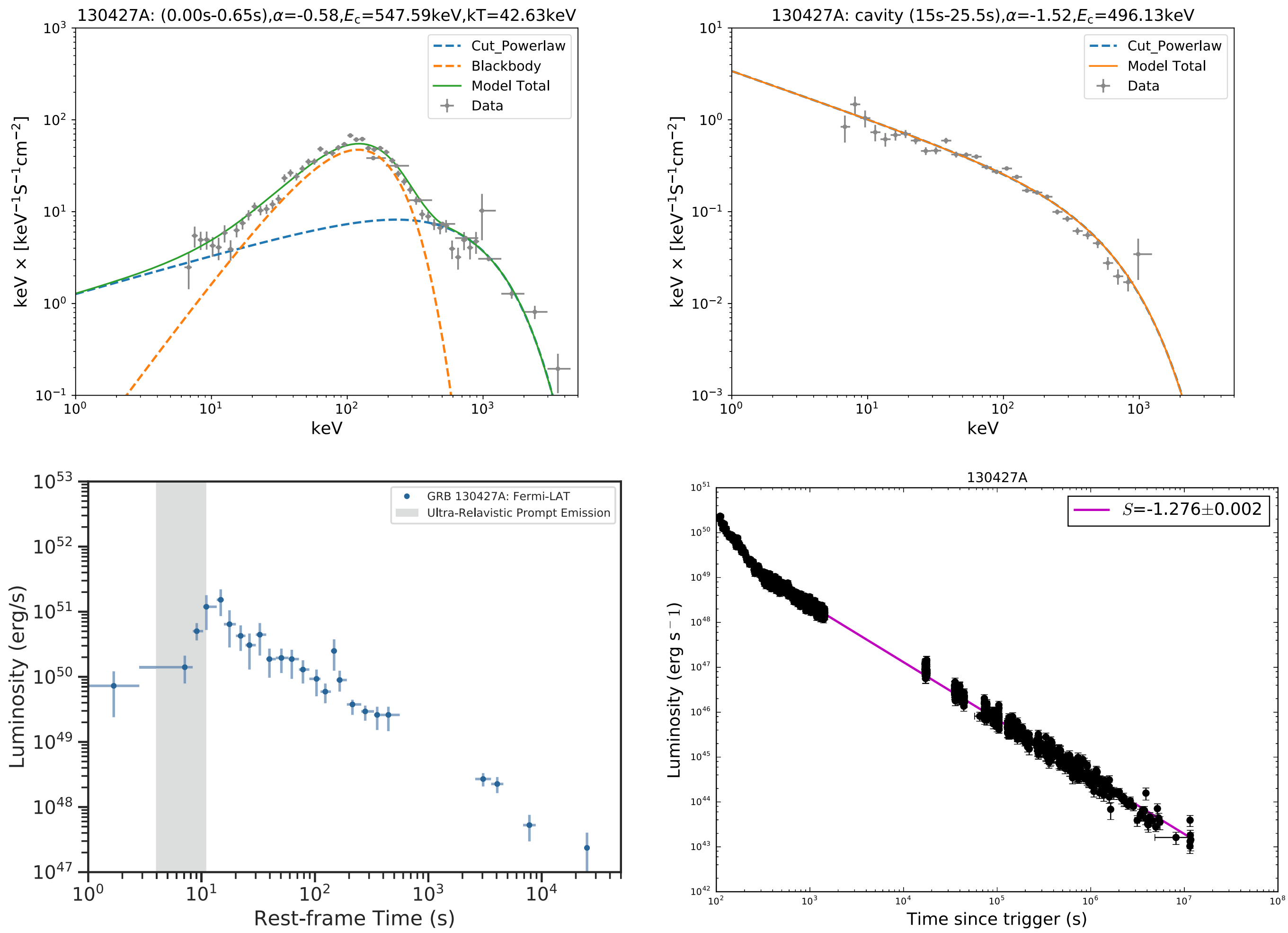

Figure 11. SN-rise, cavity, GeV, and afterglow of GRB 130427A; see also Table 5, which includes, for each episode, the starting time, the duration, the isotropic energy, and the model that best fits the spectrum. Upper left: SN-rise spectrum, well fitted by a CPL + BB model, from 0 to 0.65 s ($t_{rf} \simeq 0.49$ s); the spectral index α is -0.58, cutoff energy E_c is 547.59 keV, and the BB temperature is 42.63 keV in the observer's frame. The detailed information of the properties of the SN-rise in BdHNe I for the case can be found in Section 5 and in Table 7, which includes the duration in both the rest frame and observer's frame, the energy flux, the energy of SN-rise, the total energy, the blackbody temperature, and the redshift. Upper right: featureless spectrum of the cavity emission from ≈15 s ($t_{rf} = 11.19$ s) to ≈25.5 s ($t_{rf} = 19.03$ s) fitted by a CPL, where the photon index α is -1.52 and the cutoff energy is 496.13 keV in the observer's frame. For detailed information on each episode (SN-rise, cavity, GeV, and afterglow), see Section 5 and Table 5, which includes the starting time, the duration, the isotropic energy, and the preferred model. Lower left: Fermi-LAT rest-frame light curve in the 100 MeV–100 GeV energy range. The UPE region is shaded gray. Lower right: k-corrected X-ray afterglow luminosity observed by Swift-XRT in the 0.3–10 keV energy range, as a function of the rest-frame time. It is best fitted by a power law with index 1.276 ± 0.002.

8. Conclusions

In this paper, we have selected for this extended analysis three BdHNe I, GRB 160625B, GRB 160509A, and GRB 130427A, as well as BdHN II GRB 180728A, aiming to identify and verify the BdHNe I properties in these three additional sources, and compare and contrast the results with those of the BdHN II (Wang et al. 2019b). In GRB 160509A and GRB 160625B, we have first identified the aforementioned three BdHN I episodes. In the UPE phase, we have performed a time-resolved spectral analysis following the iterative process in a sequence of ever decreasing time intervals. We have also examined both the GeV radiation and the afterglow following the UPE phase. The same procedure has been repeated in the case of GRB 130427A with the exception of the UPE phase in view of a pileup problem. The case of GRB 180728A, a BdHN II, has been used as a counterexample. For GRB 160509A and GRB 160625B, we have also performed a time-resolved analysis on an iterative process in a sequence of ever decreasing time intervals: this has allowed us to find the self-similar structures and identify as well the associated power laws in the UPE phase. We have also identified in all four sources, following the analysis of GRB 130427A in the companion paper (Ruffini et al. 2019d), the GeV radiation during and following the UPE phase as well as in the afterglow emission. Also in all the four sources, we describe the spectral properties of their afterglow emission, including the mass estimate of the νNS, following the results presented in the companion paper (Rueda et al. 2020).

The unprecedented vast spectral analysis, iterative in ever decreasing time steps, has successfully led to confirmation of the self-similarities and power laws, discovered initially in GRB 190114C, as a common feature of the UPE of BdHNe I. The results of the spectral analysis of GRB 190114C have been confirmed and have validated the common properties in all BdHNe I: the three episodes as well as the self-similar structures and the associated power laws in the UPE phase. The profound similarities of the results have made a significant step

Table 6
Episodes of GRB 180728A with the Parameters Defined as in Table 1 Except This GRB as a BdHN II has no GeV Emission

Episode	Starting Time Rest-frame	Ending Time Rest-frame	Energy (erg)	Spectrum	References
SN-rise	0 s	2.46 s	7.98×10^{49}	PL	Wang et al. (2019b)
Prompt emission	7.81 s	11.82 s	2.73×10^{51}	CPL + BB	Wang et al. (2019b)
Cavity	…	…	…	…	Wang et al. (2019b)
GeV	…	…	…	…	Wang et al. (2019b)
Afterglow	1556 s	>10 days	5.81×10^{50}	PL	Wang et al. (2019b)

Note. Prompt emission is without self-similarity.

Table 7
Properties of the SN-rise in BdHNe I: GRB 190114C, GRB 130427A, GRB 160509A, and GRB 160625B; and in a BdHN II: GRB 180728A

GRB	$t_1 \sim t_2$ (s) (Observation)	Duration (s) (Rest)	Flux (erg cm^{-2} s^{-1})	E_{sh} (erg) (SN-rise)	E_{iso} (erg) (Total)	Temperature (keV) (Rest)	Redshift	References (For SN-rise)
190114C	$1.12 \sim 1.68$	0.39	$1.06^{+0.20}_{-0.20} \times 10^{-4}$	$2.82^{+0.13}_{-0.13} \times 10^{52}$	$(2.48 \pm 0.20) \times 10^{53}$	$27.4^{+45.4}_{-25.6}$	0.424	Melandri et al. (2019)
130427A	$0.0 \sim 0.65$	0.49	$2.14^{+0.28}_{-0.26} \times 10^{-5}$	$650^{+1.70}_{-1.70} \times 10^{51}$	$\sim 1.40 \times 10^{54}$	$44.9^{+1.5}_{-1.5}$	0.3399	Xu et al. (2013a)
160509A	$2.0 \sim 4.0$	0.92	$1.82^{+1.23}_{-0.76} \times 10^{-6}$	$1.47^{+0.60}_{-0.60} \times 10^{52}$	$\sim 1.06 \times 10^{54}$	$25.6^{+4.8}_{-4.7}$	1.17	Tam et al. (2017)
160625B	$0 \sim 2.0$	0.83	$6.8^{+1.6}_{-1.6} \times 10^{-7}$	$1.09^{+0.20}_{-0.20} \times 10^{52}$	$\sim 3.00 \times 10^{54}$	$36.8^{+1.9}_{-1.9}$	1.406	This paper
180728A	$-1.57 \sim 1.18$	0.83	$4.82^{+1.16}_{-0.82} \times 10^{-8}$	$7.98^{+1.92}_{-1.34} \times 10^{-3}$	$2.76^{+0.11}_{-0.10} \times 10^{51}$	…	0.117	Izzo et al. (2018)

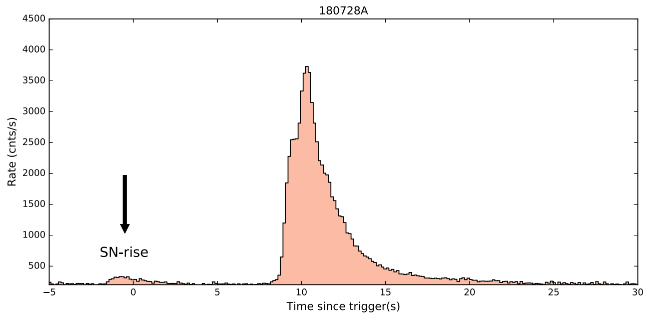

Figure 12. We identify the SN-rise from the CO_{core} of a BdHN II in GRB 180728A (Wang et al. 2019b). This GRB is composed of two spikes. The first spike, the precursor, shows a power-law spectrum with a power-law index of -2.31 ± 0.08 in its 2.75 s duration. The averaged luminosity is $3.24^{+0.78}_{-0.55} \times 10^{49}$ erg s^{-1}, and the integrated energy gives $7.98^{+1.92}_{-1.34} \times 10^{49}$ erg in the range from 1 keV to 10 MeV. This energy emitted is in agreement with the conversion of the kinetic energy of the SN-rise into electromagnetic emission. We consider the second pulse (prompt emission without self-similarity) as due to the hypercritical accretion of the SN ejecta onto the companion NS, starting from 8.72 s and lasting 13.82 s. This pulse contains 2.73×10^{51} erg isotropic energy. The best fit is a CPL + BB model of temperature ≈7 keV in the observer's frame. The BB component is interpreted as a matter outflow driven by the Rayleigh–Taylor convective instability developed in the accretion process. From the time between observation of the SN-rise and the starting time of the hypercritical accretion, $\Delta t \approx 10$ s, a binary separation of $\approx 3 \times 10^{10}$ cm has been inferred. From the binary separation, by angular momentum conservation, it has been inferred that the spin period of the νNS left from the collapse of the CO_{core} is ≈2.5 ms (Wang et al. 2019b). This νNS powers the afterglow by dissipating its rotational energy.

forward in the taxonomy of GRBs and in evidencing a standard composition of BdHNe I. This opens the opportunity of a wider inquiry into the astrophysical nature of their components in the population synthesis approach: e.g., the BH formation in all BdHNe I occurs due to accretion of the SN ejecta in a tight binary system with a neutron star companion that reaches its critical mass, leading to the formation of the BH. The SN-rises in all five BdHNe are compared and contrasted. The most far-reaching discovery of self-similarities and power laws (see also Ruffini et al. 2019a, 2019d), confirmed extensively here, leads to the existence of a discrete quantized repetitive polarized emission, in both the GeV and MeV energies observed by Fermi-GBM and Fermi-LAT, on a timescale as short as 10^{-14} s. These results open new paths in the discovery of fundamental physical laws.

In Ruffini et al. (2019a), we have introduced a novel time-resolved spectral analysis technique, adopting ever decreasing time steps, in the analysis of GRB 190114C. This has led to the discovery of the three episodes and the self-similarity and power laws in BdHNe I. In this paper, we have made a major effort in applying such a time-resolved spectral analysis to BdHNe I: GRB 130427A, GRB 160509A, and GRB 160625B. We have proved that, indeed, all the results obtained in GRB 190114C, far from making it an exception, do characterize the physics of BdHNe I. This opens as well a new direction of research, that is to insert in population synthesis analyses the nature of every single component of a BdHN. At the same time, there is the urgency of understanding the physical origin of the self-similarity and power laws, which has been addressed for the first time in the companion paper (Ruffini et al. 2019d).

These results open new perspective of research: (1) to study the new physical process characterizing each single episode of a BdHN in the context of previously unexplored regimes: e.g., the analysis of the SN not following the traditional description as an isolated system and identifying their properties within a BdHN I, and alternatively in a BdHN II; (2) to insert the BdHN evolution in the framework of a population synthesis analysis; (3) to address the new physical process underlying the existence of the observed self-similarities and power laws, which reveals a discrete sequence of quantized events with quanta of 10^{37} erg on new timescales of 10^{-14} s (see Ruffini et al. 2019d; Rueda & Ruffini 2020), and to explore the new directions open to the identification of fundamental new laws of our universe.

In the BdHN model, the BH inner engine starts to act once it forms: it accelerates charged particles, which meanwhile radiate photons in a wide energy band, generating the UPE phase and the GeV light curve. The UPE phase is signified by the thermal components since the original plasma is optically thick. As we have observed in the above BdHNe I, the starting time of thermal emission is very close to the observational time of the first GeV photon, with a discrepancy of at most a fraction of a second. Considering that the initial count rate of GeV photons reaches only a few photons per second, it is reasonable to assume that the thermal emission coincides with the GeV emission from the observation.

Since we have now shown that BdHNe I are standard, we compare and contrast their SN-rise with one example of a BdHN II and with the case of SN shockwave breakout in GRB 060218 as an example of how it is not possible to speak of a SN out of context of its evolution as one example of this new astrophysics.

We thank the anonymous referee for his/her valuable comments and suggestions. Some important points of this work were performed during the authors' visit to University of Science and Technology of China, Hefei.

ORCID iDs

Liang Li https://orcid.org/0000-0002-1343-3089
R. Moradi https://orcid.org/0000-0002-2516-5894
R. Ruffini https://orcid.org/0000-0003-0829-8318

References

Abdo, A. A., Ackermann, M., Ajello, M., et al. 2010, ApJ, 712, 558
Abdo, A. A., Ackermann, M., Arimoto, M., et al. 2009, Sci, 323, 1688
Ackermann, M., Ajello, M., Asano, K., et al. 2013, ApJS, 209, 11
Ackermann, M., Ajello, M., Asano, K., et al. 2014, Sci, 343, 42
Ajello, M., Arimoto, M., Axelsson, M., et al. 2019, ApJ, 878, 52
Arnett, W. D. 1982, ApJ, 253, 785
Band, D., Matteson, J., Ford, L., et al. 1993, ApJ, 413, 281
Becerra, L., Bianco, C. L., Fryer, C. L., Rueda, J. A., & Ruffini, R. 2016, ApJ, 833, 107
Becerra, L., Cipolletta, F., Fryer, C. L., Rueda, J. A., & Ruffini, R. 2015, ApJ, 812, 100
Becerra, L., Ellinger, C. L., Fryer, C. L., Rueda, J. A., & Ruffini, R. 2019, ApJ, 871, 14
Becerra, L., Guzzo, M. M., Rossi-Torres, F., et al. 2018, ApJ, 852, 120
Bennett, C. L., Larson, D., Weiland, J. L., & Hinshaw, G. 2014, ApJ, 794, 135
Bethe, H. A. 1990, RvMP, 62, 801
Bhat, P. N., Meegan, C. A., von Kienlin, A., et al. 2016, ApJS, 223, 28
Burns, E. 2016, GCN, 19581, 1
Campana, S., Mangano, V., Blustin, A. J., et al. 2006, Natur, 442, 1008
Cash, W. 1979, ApJ, 228, 939
Chandrasekhar, S. 1969, Ellipsoidal Figures of Equilibrium (New Haven, CT: Yale Univ. Press)
Dirirsa, F., Vianello, G., Racusin, J., & Axelsson, M. 2016, GCN, 19586, 1
Eggleton, P. P. 1983, ApJ, 268, 368
Ferrero, P., Kann, D. A., Zeh, A., et al. 2006, A&A, 457, 857
Flores, H., Covino, S., Xu, D., et al. 2013, GCN, 14491, 1
Fryer, C. L., Oliveira, F. G., Rueda, J. A., & Ruffini, R. 2015, PhRvL, 115, 231102
Fryer, C. L., Rueda, J. A., & Ruffini, R. 2014, ApJL, 793, L36
Fujisawa, K., Okawa, H., Yamamoto, Y., & Yamada, S. 2019, ApJ, 872, 155
Gilkis, A. 2018, MNRAS, 474, 2419
Goldstein, A., Burgess, J. M., Preece, R. D., et al. 2012, ApJS, 199, 19
Gruber, D., Goldstein, A., von Ahlefeld, V. W., et al. 2014, ApJS, 211, 12
Guiriec, S., Briggs, M. S., Connaugthon, V., et al. 2010, ApJ, 725, 225
Guiriec, S., Connaughton, V., Briggs, M. S., et al. 2011, ApJL, 727, L33
Guiriec, S., Daigne, F., Hascoët, R., et al. 2013, ApJ, 770, 32
Guiriec, S., Kouveliotou, C., Daigne, F., et al. 2015a, ApJ, 807, 148
Guiriec, S., Mochkovitch, R., Piran, T., et al. 2015b, ApJ, 814, 10
Hamburg, R., Veres, P., Meegan, C., et al. 2019, GCN, 23707, 1
Hurley, J. R., Tout, C. A., & Pols, O. R. 2002, MNRAS, 329, 897
Izzo, L., Rossi, A., Malesani, D. B., et al. 2018, GCN, 23142, 1
Izzo, L., Rueda, J. A., & Ruffini, R. 2012, A&A, 548, L5
Kaneko, Y., Preece, R. D., Briggs, M. S., et al. 2006, ApJS, 166, 298
Kangas, T., Fruchter, A. S., Cenko, S. B., et al. 2020, ApJ, 894, 43
Laskar, T., Alexander, K. D., Berger, E., et al. 2016, ApJ, 833, 88
Levan, A. J., Cenko, S. B., Perley, D. A., & Tanvir, N. R. 2013, GCN, 14455, 1
Li, L. 2019a, ApJS, 242, 16
Li, L. 2019b, ApJS, 245, 7
Li, L. 2020, ApJ, 894, 100
Li, L. 2022a, ApJ, 941, 27
Li, L. 2022b, arXiv:2211.12187
Li, L., Geng, J.-J., Meng, Y.-Z., et al. 2019, ApJ, 884, 109
Li, L., Ryde, F., Pe'er, A., Yu, H.-F., & Acuner, Z. 2021, ApJS, 254, 35
Li, L., & Zhang, B. 2021, ApJS, 253, 43
Longo, F., Bissaldi, E., Bregeon, J., et al. 2016, GCN, 19403, 1
Lü, H.-J., Lü, J., Zhong, S.-Q., et al. 2017, ApJ, 849, 71
Lu, R.-J., Wei, J.-J., Liang, E.-W., et al. 2012, ApJ, 756, 112
Maselli, A., Beardmore, A. P., Lien, A. Y., et al. 2013, GCN, 14448, 1
Maselli, A., Melandri, A., Nava, L., et al. 2014, Sci, 343, 48
Meegan, C., Lichti, G., Bhat, P. N., et al. 2009, ApJ, 702, 791
Melandri, A., D'Avanzo, P., D'Elia, V., et al. 2016, GCN, 19585, 1
Melandri, A., Izzo, L., D'Avanzo, P., et al. 2019, GCN, 23983, 1
Mirabal, N., Halpern, J. P., An, D., Thorstensen, J. R., & Terndrup, D. M. 2006, ApJL, 643, L99
Mirzoyan, R., Noda, K., Moretti, E., et al. 2019, GCN, 23701, 1
Moradi, R., Rueda, J. A., Ruffini, R., et al. 2021, PhRvD, 104, 063043
Moreno, E., Vazquez-Polo, F. J., & Robert, C. P. 2013, arXiv:1310.2905
Nakamura, K., Kuroda, T., Takiwaki, T., & Kotake, K. 2014, ApJ, 793, 45
Perri, M., Evans, P. A., Osborne, J. P., et al. 2018, GCN, 23049, 1
Pian, E., Mazzali, P. A., Masetti, N., et al. 2006, Natur, 442, 1011
Planck Collaboration, Ade, P. A. R., Aghanim, N., et al. 2016, A&A, 594, A13
Preece, R. D., Briggs, M. S., Mallozzi, R. S., et al. 2000, ApJS, 126, 19
Ravasio, M. E., Ghirlanda, G., Nava, L., & Ghisellini, G. 2019, A&A, 625, A60
Rossi, R., Izzo, L., Milvang-Jensen, B., et al. 2018, GCN, 23055, 1
Rueda, J. A., & Ruffini, R. 2020, EPJC, 80, 300
Rueda, J. A., Ruffini, R., Karlica, M., Moradi, R., & Wang, Y. 2020, ApJ, 893, 148
Rueda, J. A., Ruffini, R., Moradi, R., & Wang, Y. 2021, IJMPD, 30, 2130007
Ruffini, R., Aimuratov, Y., Bianco, C. L., et al. 2018a, GCN, 23066, 1
Ruffini, R., Becerra, L., Bianco, C. L., et al. 2018b, ApJ, 869, 151
Ruffini, R., Karlica, M., Sahakyan, N., et al. 2018c, ApJ, 869, 101
Ruffini, R., Li, L., Moradi, R., et al. 2019a, arXiv:1904.04162
Ruffini, R., Melon Fuksman, J. D., & Vereshchagin, G. V. 2019b, ApJ, 883, 191
Ruffini, R., Moradi, R., Aimuratov, Y., et al. 2019c, GCN, 23715, 1
Ruffini, R., Moradi, R., Rueda, J. A., et al. 2019d, ApJ, 886, 82
Ruffini, R., Moradi, R., Rueda, J. A., et al. 2021, MNRAS, 504, 5301
Ruffini, R., Muccino, M., Bianco, C. L., et al. 2014, A&A, 565, L10
Ruffini, R., Wang, Y., Aimuratov, Y., et al. 2018d, ApJ, 852, 53
Ruffini, R., Wang, Y., Enderli, M., et al. 2015, ApJ, 798, 10
Ryde, F. 2004, ApJ, 614, 827
Ryde, F. 2005, ApJL, 625, L95
Selsing, J., Izzo, L., Rossi, A., et al. 2018, GCN, 23181, 1
Selsing, J., Fynbo, J. P. U., Heintz, K. E., & Watson, D. 2019, GCN, 23695, 1
Sollerman, J., Jaunsen, A. O., Fynbo, J. P. U., et al. 2006, A&A, 454, 503
Spiegelhalter, D. J., Best, N. G., Carlin, B. P., & van der Linde, A. 2002, J. R. Stat. Soc.: Ser. B, 64, 583
Starling, R. L. C., Barthelmy, S. D., Lien, A. Y., et al. 2018, GCN, 23046, 1
Tak, D., Guiriec, S., Uhm, Z. L., et al. 2019, ApJ, 876, 76
Tam, P.-H.-T., He, X.-B., Tang, Q.-W., & Wang, X.-Y. 2017, ApJL, 844, L7
Tanvir, N. R., Levan, A. J., Cenko, S. B., et al. 2016, GCN, 19419, 1
Troja, E. 2017, AAS/HEAD, 16, 305.05
Troja, E., Lipunov, V. M., Mundell, C. G., et al. 2017, Natur, 547, 425
Veres, P., Meegan, C., & Mailyan, B. 2018, GCN, 23053, 1
Vianello, G., Lauer, R. J., Younk, P., et al. 2015, arXiv:1507.08343
von Kienlin, A. 2013, GCN, 14473, 1
von Kienlin, A., Meegan, C. A., Paciesas, W. S., et al. 2014, ApJS, 211, 13
Wang, Y., Li, L., Moradi, R., & Ruffini, R. 2019a, arXiv:1901.07505
Wang, Y., Rueda, J. A., Ruffini, R., et al. 2019b, ApJ, 874, 39
Waxman, E., & Katz, B. 2017, in Handbook of Supernovae, ed. A. W. Alsabti & P. Murdin (Cham: Springer), 967

Weinberg, S. 1972, Gravitation and Cosmology: Principles and Applications of the General Theory of Relativity (New York: Wiley-VCH), 688
Woosley, S. E., & Bloom, J. S. 2006, ARA&A, 44, 507
Xu, D., de Ugarte Postigo, A., Leloudas, G., et al. 2013a, ApJ, 776, 98
Xu, D., de Ugarte Postigo, A., Schulze, S., et al. 2013b, GCN, 14478, 1
Xu, D., Malesani, D., Fynbo, J. P. U., et al. 2016, GCN, 19600, 1
Yu, H.-F., Dereli-Bégué, H., & Ryde, F. 2019, ApJ, 886, 20
Yu, H.-F., Preece, R. D., Greiner, J., et al. 2016, A&A, 588, A135
Zhang, B. 2018, The Physics of Gamma-Ray Bursts (Cambridge: Cambridge Univ. Press)
Zhang, B.-B., Zhang, B., Castro-Tirado, A. J., et al. 2018, NatAs, 2, 69
Zhang, B.-B., Zhang, B., Liang, E.-W., et al. 2011, ApJ, 730, 141

The Astrophysical Journal, 955:93 (29pp), 2023 October 1 https://doi.org/10.3847/1538-4357/ace721

GRB-SN Association within the Binary-driven Hypernova Model

Y. Aimuratov[1,2], L. M. Becerra[2,3], C. L. Bianco[2,4,5,6], C. Cherubini[2,7,8], M. Della Valle[2,9], S. Filippi[2,7,10], Liang Li (李亮)[2,4,11], R. Moradi[2,4,11], F. Rastegarnia[2,12], J. A. Rueda[2,4,6,13,14], R. Ruffini[2,4,5,15], N. Sahakyan[2,16], Y. Wang (王瑜)[2,4,11], and S. R. Zhang (张书瑞)[2,13,17,18]

[1] Fesenkov Astrophysical Institute, Observatory 23, 050020 Almaty, Kazakhstan
[2] ICRANet, Piazza della Repubblica 10, I-65122 Pescara, Italy; rahim.moradi@icranet.org, jorge.rueda@icra.it, ruffini@icra.it
[3] Escuela de Física, Universidad Industrial de Santander, A.A.678, Bucaramanga, 680002, Colombia
[4] ICRA, Dipartamento di Fisica, Sapienza Università di Roma, Piazzale Aldo Moro 5, I-00185 Rome, Italy
[5] Université de Nice Sophia-Antipolis, Grand Château Parc Valrose, Nice, CEDEX 2, France
[6] INAF, Istituto di Astrofisica e Planetologia Spaziali, Via Fosso del Cavaliere 100, I-00133 Rome, Italy
[7] ICRA, University Campus Bio-Medico of Rome, Via Alvaro del Portillo 21, I-00128 Rome, Italy
[8] Department of Science and Technology for Sustainable Development and One Health, Università Campus Bio-Medico di Roma, Via Alvaro del Portillo, 21–I-00128 Rome, Italy
[9] INAF—Osservatorio Astronomico di Capodimonte, Salita Moiariello 16, I-80131, Napoli, Italy
[10] Department of Engineering, Università Campus Bio-Medico di Roma, Via Alvaro del Portillo, 21–I-00128 Rome, Italy
[11] INAF, Osservatorio Astronomico d'Abruzzo, Via M. Maggini snc, I-64100, Teramo, Italy
[12] Department of Physics, Faculty of Physics and Chemistry, Alzahra University, Tehran, Iran
[13] ICRANet-Ferrara, Dip. di Fisica e Scienze della Terra, Università degli Studi di Ferrara, Via Saragat 1, I-44122 Ferrara, Italy
[14] Dipartamento di Fisica e Scienze della Terra, Università degli Studi di Ferrara, Via Saragat 1, I-44122 Ferrara, Italy
[15] INAF, Viale del Parco Mellini 84, I-00136 Rome, Italy
[16] ICRANet-Armenia, Marshall Baghramian Avenue 24a, Yerevan 0019, Armenia
[17] School of Astronomy and Space Science, University of Science and Technology of China, Hefei 230026, People's Republic of China
[18] CAS Key Laboratory for Research in Galaxies and Cosmology, Department of Astronomy, University of Science and Technology of China, Hefei 230026, People's Republic of China

Received 2023 January 17; revised 2023 June 23; accepted 2023 July 11; published 2023 September 22

Abstract

Observations of supernovae (SNe) Ic occurring after the prompt emission of long gamma-ray bursts (GRBs) are addressed within the binary-driven hypernova (BdHN) model where GRBs originate from a binary composed of a $\sim 10 M_\odot$ carbon–oxygen (CO) star and a neutron star (NS). The CO core collapse gives the trigger, leading to a hypernova with a fast-spinning newborn NS (νNS) at its center. The evolution depends strongly on the binary period, $P_{\rm bin}$. For $P_{\rm bin} \sim 5$ min, BdHNe I occur with energies 10^{52}–10^{54} erg. The accretion of SN ejecta onto the NS leads to its collapse, forming a black hole (BH) originating the MeV/GeV radiation. For $P_{\rm bin} \sim 10$ min, BdHNe II occur with energies 10^{50}–10^{52} erg and for $P_{\rm bin} \sim$ hours, BdHNe III occur with energies below 10^{50} erg. In BdHNe II and III, no BH is formed. The 1–1000 ms νNS originates, in all BdHNe, the X-ray-optical-radio afterglows by synchrotron emission. The hypernova follows an independent evolution, becoming an SN Ic, powered by nickel decay, observable after the GRB prompt emission. We report 24 SNe Ic associated with BdHNe. Their optical peak luminosity and time of occurrence are similar and independent of the associated GRBs. From previously identified 380 BdHN I comprising redshifts up to $z = 8.2$, we analyze four examples with their associated hypernovae. By multiwavelength extragalactic observations, we identify seven new episodes, theoretically explained, fortunately not yet detected in Galactic sources, opening new research areas. Refinement of population synthesis simulations is needed to map the progenitors of such short-lived binary systems inside our galaxy.

Unified Astronomy Thesaurus concepts: Gamma-ray bursts (629)

1. Introduction

The pioneering work of the BeppoSAX telescope, linking for the first time the success of gamma-ray astronomy with the discovery of gamma-ray bursts (GRBs; Klebesadel et al. 1973) and the CGRO/BATSE era (Fishman et al. 1982) to the X-ray astronomy of binary X-ray sources (Giacconi & Ruffini 1978), led to the discovery of the GRB X-ray afterglow (Costa et al. 1997) and the determination of the GRB cosmological nature (Metzger et al. 1997). Following these successes, we have returned to address the fundamental issue of the observational coincidence of GRBs with Ic supernovae (SNe):

(1) Our theoretical framework started with the induced gravitational collapse (IGC) scenario (Rueda & Ruffini 2012) introduced to originate stellar-mass black holes (BHs) powering long GRBs associated with type Ic SNe. It was soon followed by the binary-driven hypernovae (BdHNe) model (Ruffini et al. 2014a), which assumes a binary system composed of a carbon–oxygen (CO) star of $\lesssim 10 M_\odot$ and a companion neutron star (NS) as the GRB progenitor. The GRB trigger occurs when the CO core collapses, originating a newborn NS (νNS) and an SN Ic. The SN ejecta accretes onto the NS companion and the νNS because of matter fallback (Becerra et al. 2019, 2022).

(2) The first evidence for such BdHN was presented by analyzing two sources: GRB 090618 at $z = 0.54$ (Izzo et al. 2012a, 2012b) and GRB 090423 (Salvaterra et al. 2009; Tanvir et al. 2009; Ruffini et al. 2014b). The extraordinary result of GRB 090423 was that it was observed at $z = 8.2$, which was

and still is the farthest GRB in our Universe with a spectroscopic confirmation. We are currently examining GRB 090429B, with a photometric redshift $z = 9.4$ (Cucchiara et al. 2011), within the BdHN model (R. Ruffini et al. 2023, in preparation). In the meantime, the existence of 380 BdHNe has been presented (Ruffini et al. 2021). Their distribution ranges from above $z = 8.2$ to close extragalactic GRBs in the local Universe. Their enormous energies range between 10^{49} erg and nearly 10^{55} erg of GRB 220101A (Atteia 2022) and of GRB 221009A (Burns et al. 2023). A crucial point is that the compact CO-NS systems of the BdHN model are the final stage of a peculiar binary evolution, short-lived and rare, as GRBs are. The probability of their occurrence in our Galaxy is extremely low. Since the progenitors are short-lived, their frequency of occurrence essentially mimics the evolution of the cosmic star formation rate with redshift, peaking at $z \sim 2$–2.5 (e.g., Madau & Dickinson 2014; see also Yüksel et al. 2008; Grieco et al. 2012; Graham & Schady 2016; Graham & Fruchter 2017). Based on the low rate of long-duration GRBs in the current cosmic epoch in our Galaxy (Guetta & Della Valle 2007), which is ∼3 orders of magnitude lower than the observed core-collapse SN rate (Shivvers et al. 2017), the potential GRB progenitors currently *ready to explode* in the Milky Way are, in the most optimistic view, a handful of objects. The observed density rate of BdHN I is ~ 1 Gpc^{-3} yr^{-1} (Ruffini et al. 2016a, 2018b). Therefore, it is not surprising that we can acknowledge the existence of such compact binary progenitors only through their cataclysmic fate leading to GRBs thanks to their extragalactic, cosmological nature. Interestingly, the above feature could not be fortuitous since an energetic GRB inside our Galaxy might represent a catastrophe for life on Earth (see, e.g., Chen & Ruffini 2015).

(3) The crucial topic of extreme interest has been the byproducts of the GRB observations: (a) the discovery of SNe of characteristic energy of 10^{49} erg associated with all different classes of BdHN (this article is dedicated to this topic); (b) the discovery of seven different episodes characterizing the most general GRB and presenting new physical processes in ultrarelativistic regimes impossible to discover within our Galaxy; (c) the fundamental knowledge developed in decades of observations in Earth-based accelerators pointing to vacuum polarization processes (see Ruffini et al. 2010, and references therein) are here discovered in ultrarelativistic regimes and overcritical quantum electrodynamical processes. These processes, when occurring outside our Galaxy, give the unique opportunity to extend the knowledge reached on our planet, but, at the same time, they indicate the danger of the occurrence of these events for the survival of life if they should occur in our Galaxy. An unexpected additional result has been the possibility to apply, in the comprehension of BdHNe, the still untested configuration of rapidly rotating self-gravitating systems that have attracted the attention of the greatest scientists in world history: from Isaac Newton (*Principia*, Book III, Propositions XVIII–XX; Newton 1687) to Colin Maclaurin (MacLaurin 1742), Carl Gustav Jacob Jacobi (Jacobi 1834), George Darwin (Darwin 1886), James Hopwood Jeans (Jeans 1928), and more recently Subrahmanyan Chandrasekhar (Chandrasekhar 1969); see Section 10 for details.

A new era for relativistic astrophysics started, grounded on the classical results obtained on compact stellar X-ray sources originating from binary massive systems derived on Galactic observations (Tauris & van den Heuvel 2006), as well as on the concepts of BHs expressed by the mathematical equations of Roy Kerr (Kerr 1963) and by the mass-energy formula of Christodoulou–Ruffini (Christodoulou 1970; Christodoulou & Ruffini 1971) and Hawking (Hawking 1971) finally here reaching confirmations in extragalactic sources. It opens to the fundamental issues of understanding the role of GRBs and their intriguing possible interaction with the birth and the end of life in the Universe.

Since their discovery, the enormous energetics led to the idea that GRBs are associated with massive stars' gravitational collapse, leading to NSs or BHs. The community widely accepts the seminal proposal that mergers of NS-NS or NS-BH binaries are the progenitors of short GRBs (Goodman 1986; Paczynski 1986; Eichler et al. 1989; Narayan et al. 1991). For long GRBs, our sources of interest here, the traditional model is based on a *collapsar*, the core collapse of a single massive star leading to a BH (or a magnetar) surrounded by an accretion disk (Woosley 1993). We refer the reader to Mészáros (2002) and Piran (2004), for comprehensive reviews.

In the GRB traditional model, the prompt emission originates in the dynamics, expansion, and transparency of a *fireball*, an optically thick electron–positron (e^-e^+)-photon plasma in equilibrium with baryons (Cavallo & Rees 1978; Goodman 1986; Paczynski 1986; Narayan et al. 1991, 1992). The fireball expands in a collimated relativistic jet with Lorentz factor $\Gamma \sim 10^2$–10^3 (Shemi & Piran 1990; Rees & Meszaros 1992; Meszaros et al. 1993; Piran et al. 1993; Mao & Yi 1994). In this picture, the interaction of internal and external shocks with the surrounding and interstellar medium is responsible for the prompt emission and the afterglow, including the very-high-energy (VHE) emission by synchrotron self-Compton radiation (Mészáros 2002; Piran 2004; MAGIC Collaboration et al. 2019; Zhang 2019). We refer to Zhang (2018) for the latest developments of the GRB traditional model.

From the energetics, dynamics, and radiation efficiency, two difficulties arise in the traditional model. (1) Only a small fraction of the energy of the ultrarelativistic jet is radiated by the synchrotron emission, so much of the kinetic energy remains in the jet. (2) The radiation from the jet implies the absence of afterglow in some long GRBs, while it is clear that the afterglow is present in all GRBs.

We now turn to one of this article's main topics, the GRB-SN connection. The follow-up of the optical afterglow, extended by the Neil Gehrels Swift Observatory (Barthelmy et al. 2005; Burrows et al. 2005; Roming et al. 2005), led to the discovery of the association of long GRBs with type Ic SNe, first marked with the temporal and spatial coincidence of GRB 980425 and SN 1998bw (Galama et al. 1998). Since then, further observations have confirmed the GRB-SN connection (Woosley & Bloom 2006; Della Valle 2011; Hjorth & Bloom 2012; Cano et al. 2017). The association of GRBs with SNe Ic is possibly one of the most relevant observational clues for theoretical models. Several theoretical and observational consequences from the GRB-SN connection constrain models of GRBs and the associated SNe Ic:

(i) Long GRBs and SNe have different energetics. SNe radiate energies $\sim 10^{49}$–10^{52} erg, while GRBs show energies in the much wider range $\sim 10^{49}$–10^{55} erg. The energy release of energetic GRBs is associated with the gravitational collapse to a BH, while SNe originate in the core collapse of a massive star to an NS.

(ii) Most (if not all) long-duration GRBs originate from binary stars. (a) In recent decades, growing evidence has shown that long-duration GRBs are associated with the explosions of massive stars. This fact has been well established both on a statistical basis (e.g., Fruchter et al. 2006; Kelly et al. 2008; Raskin et al. 2008) and from stellar evolution, which, even if constraining the zero-age main-sequence (ZAMS) mass of the SN progenitor is highly model-dependent, points undoubtedly to massive stellar progenitors from modeling the photometric and spectroscopic follow-up of SNe-Ibc associated with GRBs, e.g., SN 1998bw, 25–40$M_{\odot}$ (Maeda et al. 2006; Woosley & Bloom 2006); SN 2003dh 35–40$M_{\odot}$ (Mazzali et al. 2003; Nomoto et al. 2003); SN 2003lw 25$M_{\odot}$ (Mazzali et al. 2006); 2008D 30$M_{\odot}$ (Tanaka et al. 2009); 2010bh 25$M_{\odot}$ (Bufano et al. 2012); and 2016jca 35$M_{\odot}$ (Ashall et al. 2019). (b) It is well known that a significant fraction of massive stars is in binaries (about 70%; e.g., Kobulnicky & Fryer 2007; Sana et al. 2012). (c) In addition, although stellar evolution models predict the direct formation of a BH from the gravitational collapse for progenitor stars $\gtrsim 25 M_{\odot}$ (Heger et al. 2003), two observational facts pose serious challenges to GRB-SN models in which both a BH and SN originate from a single star: (1) the direct gravitational collapse of a massive star to a BH should occur without SN emission; (2) observed pre-SN progenitors have masses $\lesssim 18\, M_{\odot}$ (see Smartt 2009, 2015, for details). Therefore, it is unlikely that the GRB and the SN can originate from the very same single star. Indeed, it is an extreme request for the gravitational collapse of a massive star to form a collapsar, a jetted fireball, and an SN explosion. Some models attempt to supply (partial) solutions to these issues, like an efficient neutrino emission from the accretion disk (e.g., MacFadyen & Woosley 1999) or the presence of an outflow/wind where the nucleosynthesis of the nickel for the optical SN can occur (see, e.g., Kohri et al. 2005; Lindner et al. 2012; Milosavljević et al. 2012). The direct conclusion from the abovementioned points is that most long-duration GRBs occur in binaries. Indeed, Cantiello et al. (2007) tested the idea of producing rapidly rotating Wolf–Rayet (WR) stars in massive close binaries as possible progenitors of collapsars. The above facts also motivated our development of a model for long-duration GRBs that fully exploit the binary nature of progenitors.

(iii) The SNe associated with GRBs are of type Ic. The lack of hydrogen (H) and helium (He) in the spectra of type Ic SNe has the leading explanation that they originate in bare He, CO, or WR stars that lose the outermost hydrogen and helium layers during their evolution (see, e.g., Smith et al. 2011; Teffs et al. 2020). Numerical simulations indicate that the most natural mechanism for He/CO/WR stars to get rid of their H/He envelope is from interactions with a compact-star companion (e.g., NS) through multiple mass-transfer and common-envelope phases (see, e.g., Nomoto & Hashimoto 1988; Iwamoto et al. 1994; Fryer et al. 2007; Yoon et al. 2010; Smith et al. 2011; Kim et al. 2015; Yoon 2015).

Although the above is not a complete list of possible drawbacks of the single-star scenario, it is already clear that considering alternatives is natural. In their pioneering work, Fryer et al. (1999) showed that various binary stellar evolution channels can lead to diverse GRB events. This alternative binary approach has contributed, as mentioned above, in the study of short GRBs (see, e.g., Ruffini et al. 2016b; Aimuratov et al. 2017), as well as an enigmatic long-lasting GRB 060614 without SN (Della Valle et al. 2006a) interpreted as a white dwarf (WD)-NS merger (Caito et al. 2009; Rueda et al. 2018) and the weakest GRBs from WD-WD mergers (see, e.g., Rueda et al. 2019b, 2022b).

We specialize in the BdHN model of long GRBs based on the IGC scenario (Rueda & Ruffini 2012). Following the evolution of stripped-envelope binaries, the BdHN model proposes as a GRB progenitor a CO-NS binary at the end of the thermonuclear life of the CO star, i.e., the second core-collapse SN event in the binary lifetime. The first SN formed the NS companion of the CO star. The CO nature of the exploding star explains why the SNe associated with GRBs are type Ic. This SN explosion in the CO-NS binary triggers the physical processes that explain the seven episodes observed in the GRB (Izzo et al. 2012a; Rueda & Ruffini 2012; Fryer et al. 2014; Becerra et al. 2015; Fryer et al. 2015; Becerra et al. 2016, 2019). Figure 1 shows an example of numerical simulation performed by Becerra et al. (2019) of the explosion of a CO star leading to a newborn NS (νNS) and the SN Ic, in the presence of an NS companion. These simulations, which include hydrodynamics, neutrino emission, and general relativistic effects, show a variety of outcomes of the system, leading to a variety of GRB events, a BdHN classification, which we discuss below. One of the most relevant results is that, among the possible fates, the NS companion can reach the point of gravitational collapse, forming a rotating, newborn Kerr BH. As recalled, the BdHN progenitors have not been simulated in population synthesis or binary stellar evolution models. Thus, in our numerical simulations, we have to use pre-SN stars resulting from the stellar evolution of single stars and assume the presence of the NS companion. Therefore, the binary evolution leading to the compact BdHN system could start with a different ZAMS mass than the one we are currently considering. Namely, single and binary evolutionary paths can lead to different ZAMS masses starting from a given pre-SN star mass. The latter scenario can lead to a less-massive ZAMS progenitor than the former (see, e.g., Zapartas et al. 2019, for the case of binary progenitors of type II SNe). For the early phases of the BdHN model, we have scrutinized the simulations derived by Tauris & van den Heuvel (2006; e.g., their Figures 16.12 and 16.15). Such simulations are based on X-ray observations of stellar evolution in our Galaxy. We generally confirm the applicability of these models up to the common-envelope phase. Following that phase, the explanation of the multiwavelength observations (from X-rays to GeV and ultrahigh energy) of long GRBs within the BdHN model predicts the existence of CO-NS binaries with orbital periods from hours to days (BdHN II and III) to minutes (BdHN I), taking into due account the relevant role of the angular momentum (see Section 2, and references therein). In view of the low occurrence rate of GRBs in a single galaxy, the necessity of forming CO–NS binaries has been evidenced only by extragalactic observations, whose comprehension has been made possible under the complementary information gained from galactic systems (e.g., Tauris & van den Heuvel 2006).

In Section 2, we recall the basics of the BdHN model and address how the interplay between the SN, νNS, and NS companion leads to the variety of long GRBs.

Section 3 recalls a relativistic formulation's framework in the source's cosmological rest frame, including the k-correction.

In Section 4, we analyze 24 SNe associated with GRBs. We show that the SN bolometric peak luminosity and its time of occurrence in the source cosmological rest frame are nearly the same for all sources (see Figures 2 and 3). We also present the

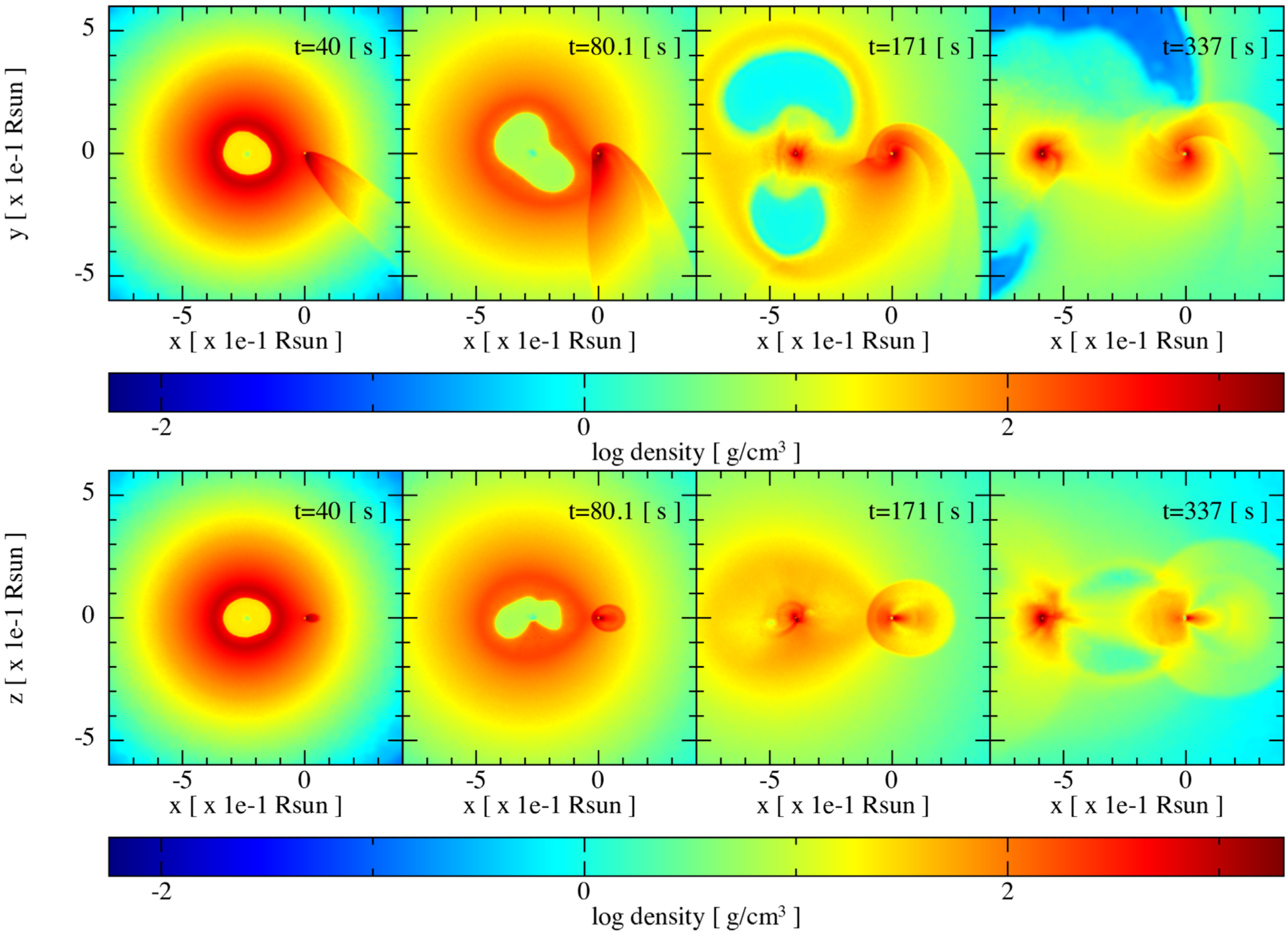

Figure 1. SPH simulation of a BdHN I: model "30m1p1eb" of Table 2 in Becerra et al. (2019). The binary progenitor comprises a CO star of $\approx 9M_{\odot}$ (produced by a ZAMS star of $30M_{\odot}$) and a $2M_{\odot}$ NS companion. The orbital period is $\approx$6 min. From left to right, each snapshot corresponds to selected increasing times where $t = 0$ s refers to the SN shock breakout. The upper and lower panel shows the mass density on the equatorial plane and the plane orthogonal to the latter. The reference system is rotated and translated to align the x-axis with the line joining the binary components. The origin of the reference system is located at the NS companion position. In the first snapshot at $t = 40$ s, particles in the NS gravitational capture region form a tail behind the NS companion. These particles then circularize around the NS, forming a thick disk visible in the second snapshot at $t = 80$ s. Part of the ejecta produces a fallback accretion process onto the νNS visible in the third snapshot at $t = 171$ s. At $t = 337$ s (about one orbital period), a disk structure is visible around the νNS and the NS companion. This figure has been produced with the SNsplash visualization program (Price 2011). The figure highlights that the νNS is coeval with the SN explosion and remains at the SN center while the ejecta expands. It also shows that the timescale of the physical phenomena leading to the transient activity of the GRB (e.g., the hypercritical accretion and its consequences) is shorter than the timescale of changes in the orbital properties, e.g., an orbital widening or eventual binary disruption owing to mass loss (Blaauw 1961; van den Heuvel & Heise 1972; Fryer et al. 2015).

prompt gamma-ray energy ($E_{\rm iso}$) of the associated GRB. We show that $E_{\rm iso}$ spans over 6 orders of magnitude, while the SN bolometric peak luminosity and the time of occurrence of the peak remain relatively constant; see Figures 4 and 5. These results constrain GRB models and will be explained within the BdHN model in the following sections.

Section 5 describes the physical phenomena in the different BdHN types and relates them to specific GRB observables, namely the seven episodes of BdHNe; see Table 2 for details.

In Section 6, after recalling the observations that made possible the identification of GRB 180720B as BdHN I (Ruffini et al. 2018c), we address the seven episodes characterizing the source as a BdHN I.

Section 7 investigates the second BdHN I fully understood in the BdHN model: GRB 190114C (Moradi et al. 2021c; Ruffini et al. 2021). We recall the observations that identified this source as BdHN I (Ruffini et al. 2019b) and discuss its corresponding seven episodes, following an analogous presentation for GRB 180720B in Section 6.

In Section 8, we turn to the case of a BdHN II, GRB 190829A.

Since in BdHN II, the BH is not formed, the number of episodes in this GRB reduces from seven to three, which we address in detail.

In Section 9, we analyze the only example analyzed to date of a BdHN III: GRB 1711205A. Similar to BdHN II, in BdHN III, the BH is not formed.

The number of episodes in this GRB reduces from seven to two, which we present in detail.

Section 10 summarizes new physical phenomena triggered by the SN occurrence in BdHNe, not previously studied in the GRB physics literature.

Finally, we outline conclusions in Section 11.

2. BdHN Classification

The BdHN model assumes that some long GRB progenitors are binaries composed of a CO star of mass of $\sim 10M_{\odot}$ and a

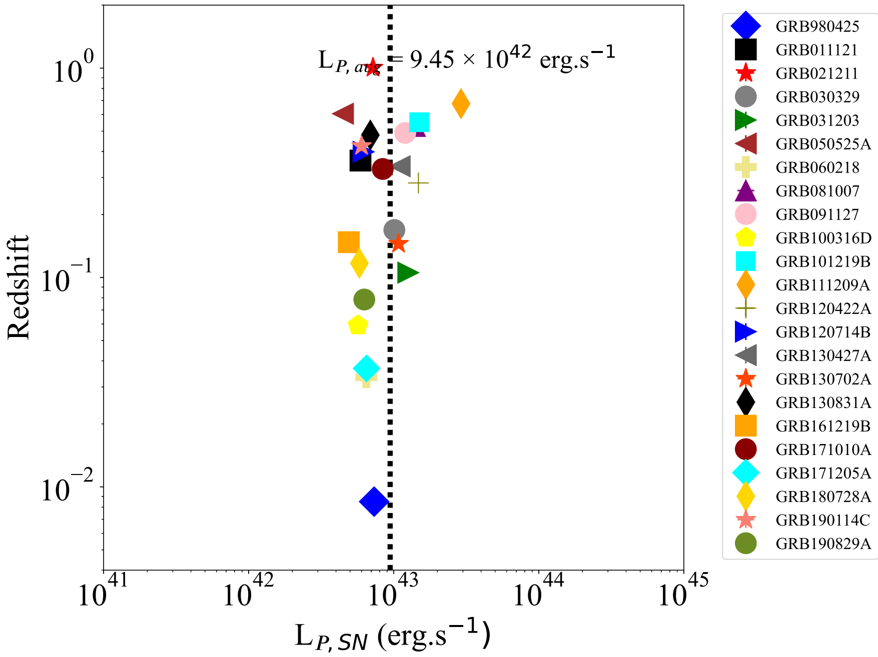

Figure 2. GRB redshifts (z) vs. the values of peak luminosity of the bolometric light curve of the associated SN ($L_{\rm P,SN}$). The plot shows the spread in data points and the lack of correlation between these two quantities.

companion NS of $\sim 2.0 M_\odot$. It also assumes that the gravitational collapse of the CO star generates an SN explosion and creates a newborn NS (νNS) at its center. The νNS with a mass of $1.5 M_\odot$ is assumed to spin with a period of $\sim$1–100 ms. It further assumes that $\sim$7–$8 M_\odot$ are ejected during the SN explosion. The theoretical motivations and the observation constraints leading to these assumptions are given in Sections 5–10, and implications are presented in Section 11. The SN ejecta drive an accretion process onto the NS companion and a fallback accretion onto the νNS. The accretion rates proceed at hypercritical rates (i.e., highly super-Eddington) due to the efficient neutrino emission (Fryer et al. 2014; Becerra et al. 2016, 2018). We differentiate three types of BdHN: I, II, and III, as a function of their overall energetics. A dependence of these energetics from the total initial angular momentum of the Co star-NS binary is evidenced. The shorter the binary period, the higher the BdHN total radiated energy.

2.1. BdHN I

We indicate by BdHN I the most energetic class of long GRBs with energies in the range of 10^{52} erg $\lesssim E_{\rm iso} \lesssim 10^{54}$ erg. Their orbital period is of the order of $\gtrsim$5 min, which implies an orbital separation of $\sim 10^{10}$ cm, just bigger than the CO star radii (see, e.g., Fryer et al. 2014; Becerra et al. 2016, 2019). The hypercritical accretion of the SN ejecta onto the companion NS leads it to reach the critical mass, consequently forming a Kerr BH. Simulations show that the peak accretion rate onto the NS companion can reach $\dot{M}_{\rm peak} \sim 10^{-3}$–$10^{-2} M_\odot$ s^{-1}, which implies accreting 0.5–$1 M_\odot$ in about one orbital period time (Becerra et al. 2016, 2019). The NS gains a large angular momentum, $\Delta J \sim G M_{\rm NS} \Delta M_{\rm acc}/c \sim 10^{49}$ g cm^2 s^{-1}; hence, it reaches the critical mass at millisecond rotation rates. The accretion energy gain when bringing the NS to the critical mass and the energy involved in the BH formation process set a lower edge of $\sim 10^{52}$ erg of energy released in a BdHN I. Therefore, BdHNe I explain the long GRBs with energies $E_{\rm iso} \gtrsim 10^{52}$ erg (see Ruffini et al. 2018b, for details). The fallback accretion onto the νNS also proceeds at hypercritical rates, and the presence of the NS companion generates a double-peak accretion (Becerra et al. 2019; see also Becerra et al. 2022 for recent simulations and implications). The first peak of accretion is of a few $10^{-3} M_\odot$ s^{-1} and lasts for about one-tenth of the orbit (Becerra et al. 2019). The νNS reaches a high rotation period of 0.5 ms, near the mass-shedding limit (Cipolletta et al. 2015). The fast-spinning νNS gives origin to the GRB afterglow as explained in Section 5. Examples of BdHNe I are GRB 180720B (see Section 6) , GRB 190114C (Section 7), and GRB 130427A (Ruffini et al. 2019c, 2021).

In Rueda & Ruffini (2012), Fryer et al. (2015), and Ruffini et al. (2016a), we have advanced that the CO-NS compact binaries leading to BdHN I could form in an evolutionary path similar to that leading to the so-called ultrastripped binaries (see, e.g., Tauris et al. 2015, 2017, as well as, e.g., Dewi et al. 2006; Dessart et al. 2020, for alternative stellar evolution scenarios). However, population synthesis simulations of those systems lead to binaries with orbital periods longer than those of the BdHN systems (see, e.g., Figure 16.15 in Tauris & van den Heuvel 2006). We currently consider with great interest scrutinizing the possibility that the evolution following the common-envelope phases (the last evolutionary stages of the binary) can have a relevant role of the angular momentum of the stellar components, as suggested by the BdHN modeling of long GRBs, branching off a formation channel of BdHN systems. Certainly, BdHN progenitors can form in our own Galaxy, and likely some currently observed binary X-ray sources could, in due time, lead to a BdHN. However, it is observationally established that the probability of occurrence of a GRB in a single galaxy is extremely low, e.g., for the Milky Way, the observed GRB rate suggests one source every million years or so (see, e.g., Podsiadlowski et al. 2004). The GRB

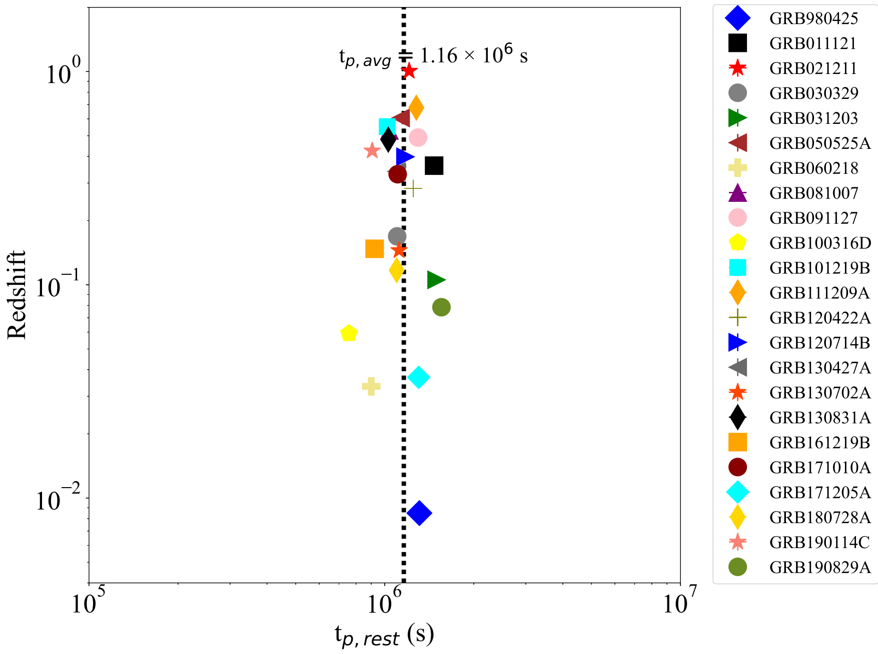

Figure 3. GRB redshifts (z) vs. the peak time of luminosity of the bolometric light curve of the associated SN ($t_{\mathrm{P,SN}}$). The plot shows the lack of correlation between these two quantities.

detection rate on Earth originates from extragalactic sources, which, given the GRB's enormous energetics, allow us to sample an enormous volume containing billions of galaxies, leading to nearly daily detections. We recall that the observed density rate of BdHN I is $\sim$1 Gpc^{-3} yr^{-1} (Ruffini et al. 2016a, 2018b), so a small subpopulation of $\approx$0.01%–0.1% of ultrastripped binaries following such a particular evolution branch might be sufficient to explain the BdHN I population (see Fryer et al. 2015; Ruffini et al. 2016a, for details), given that ultrastripped binaries compose 0.1%–1% of the total SNe (Tauris et al. 2015); see also Section 11.

2.2. BdHN II

These binaries are characterized by longer orbital periods of $\sim$20–40 minutes, so binary separations of a few 10^{10} cm. Numerical simulations show that in these binaries, the accretion rate onto the NS companion occurs at lower rates, $\dot{M}_{\mathrm{peak}} \sim 10^{-5}$–$10^{-4} M_{\odot}$ s^{-1}. The NS does not reach the critical mass in these systems, so it does not form a BH. The above range of accretion rates implies that the BdHN II subclass can explain long GRBs with energies $E_{\mathrm{iso}} \sim 10^{50}$–$10^{52}$ erg (see, e.g., Ruffini et al. 2016a, 2018b).

Regarding the νNS, although the first peak of fallback accretion is similar to that of BdHN I, the second peak is considerably lower, so in the end, the fallback accretion leads the νNS to a slower rotation than its BdHN I counterpart. Still, the νNS in BdHN II reaches rotation periods of $\sim$10 ms, sufficient to explain the afterglow by the associated synchrotron radiation; see Section 5. Examples of BdHN II are GRB 180728A (Wang et al. 2019) and GRB 190829A; see Section 8.

2.3. BdHN III

There are CO-NS binaries with orbital periods that can be even hours, corresponding to a binary separation of the order of a few 10^{11} cm. The accretion rate onto the NS companion is negligible, and the SN explosion likely disrupts the binary. In these cases, the fallback accretion onto the νNS and its interaction with the SN ejecta are the only ones responsible for the long GRB emission. This BdHN III system explains low-luminous GRBs with an energy release of $E_{\mathrm{iso}} \sim 10^{49}$–$10^{50}$ erg, and the νNS reaches a period of $\sim$50–100 ms, which are sufficient to explain the afterglow by the associated synchrotron emission; see Section 5. An example of BdHN III is GRB 171205A, for which we refer the reader to the recent and detailed analysis and simulations presented in Wang et al. (2022) and Section 9.

From all of the above, all BdHNe types are endowed with an X-ray afterglow that can be explained by synchrotron radiation powered by the fast-spinning νNS.

If the binary is not disrupted by the mass loss in the SN explosion (see Fryer et al. 2015 for details), BdHNe I produce NS-BH binaries and BdHN II NS-NS binaries. In BdHN III, the SN is expected to disrupt the system. For a few minutes binary, the merger time is of the order of 10^4 yr, when they will lead to short GRBs. Given the short time to merge, the surviving newborn compact-object binaries will not travel far from the long GRB site, which implies a direct link between long and short GRBs (Fryer et al. 2015; Ruffini et al. 2018b). Interestingly, the recent analysis of the population of long and short GRBs by Bianco et al. (2023) supports the above long-short GRB connection, which is a unique prediction of the BdHN model.

We now turn to the observational data of 24 long GRBs and associated Ic SNe and proceed to a selected sample of two BdHN I, one BdHN II, and one BdHN III and their associated HNe.

3. Cosmological Rest-frame Time and *k*-correction

We here introduce the conversion factor adopted in deriving a luminosity and time both in the cosmological rest frame of the source (see Ruffini et al. 2018e). This conversion, known as

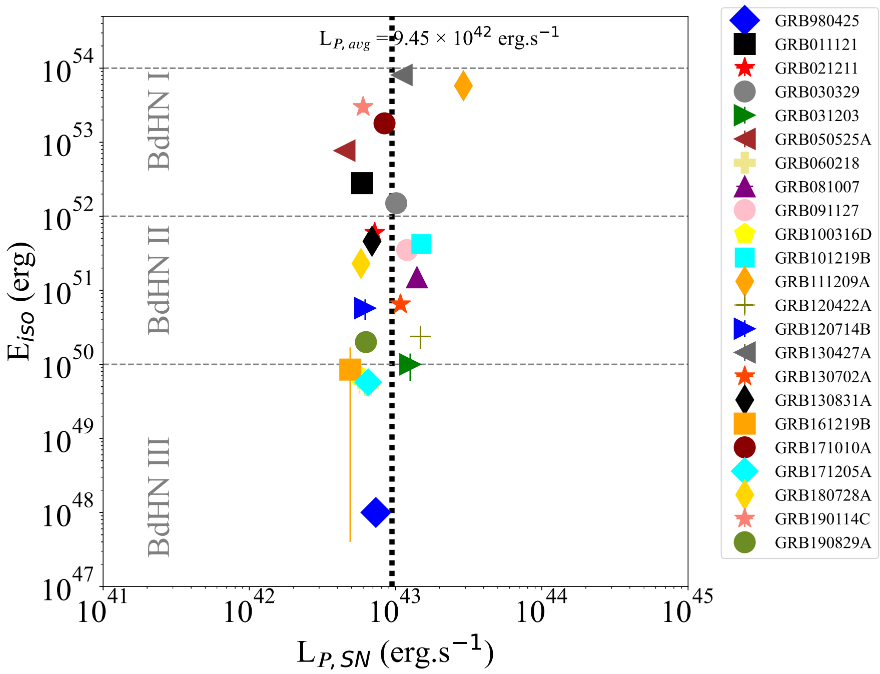

Figure 4. Isotropic-equivalent energy ($E_{\gamma,\mathrm{iso}}$) of GRB vs. the peak luminosity of the bolometric light curve of the associated SN ($L_{\mathrm{P,SN}}$). The plot shows the lack of correlation: the SN luminosities stay within an order of magnitude spread, while the GRB energy spans ∼6 orders of magnitude.

k-correction, has been often neglected in the literature (Chincarini et al. 2007; Falcone et al. 2007; Margutti et al. 2010).

The observation time (t_{obs}) of the source is related to the time measured in the cosmological rest frame (t_{rf}) on the Earth by $t_{\mathrm{obs}} = (1 + z)t_{\mathrm{rf}}$. The observed flux f_{obs}, namely the energy per unit area and time in a fixed detector energy bandwidth $[\epsilon_{\mathrm{obs},1}; \epsilon_{\mathrm{obs},2}]$, is

$$f_{\mathrm{obs},[\epsilon_{\mathrm{obs},1};\epsilon_{\mathrm{obs},2}]} = \int_{\epsilon_{\mathrm{obs},1}}^{\epsilon_{\mathrm{obs},2}} \epsilon\ n_{\mathrm{obs}}(\epsilon) d\epsilon, \tag{1}$$

where n_{obs} is the photon spectrum, i.e., the number of observed photons per unit energy, area, and time.

The total energy emitted in the $[\epsilon_{\mathrm{obs},1}; \epsilon_{\mathrm{obs},2}]$ bandwidth per unit time, which by definition is in the source cosmological rest frame, is

$$L_{[\epsilon_{\mathrm{obs},1}(1+z);\epsilon_{\mathrm{obs},2}(1+z)]} = 4\pi D_L^2(z) f_{\mathrm{obs},[\epsilon_{\mathrm{obs},1};\epsilon_{\mathrm{obs},2}]}, \tag{2}$$

where $D_L(z)$ is the source luminosity distance.

To express the luminosity L in the cosmological rest-frame energy band, $[E_1; E_2]$, common to all sources, we rewrite Equation (2) as

$$L_{[E_1;E_2]} = 4\pi D_L^2 f_{\mathrm{obs},\left[\frac{E_1}{1+z};\frac{E_2}{1+z}\right]} \tag{3}$$

$$= 4\pi D_L^2 k[\epsilon_{\mathrm{obs},1};\ \epsilon_{\mathrm{obs},2};\ E_1;\ E_2;\ z] f_{\mathrm{obs},[\epsilon_{\mathrm{obs},1};\epsilon_{\mathrm{obs},2}]} \tag{4}$$

where the k-correction factor is defined as

$$k[\epsilon_{\mathrm{obs},1};\ \epsilon_{\mathrm{obs},2};\ E_1;\ E_2;\ z] = \frac{f_{\mathrm{obs},\left[\frac{E_1}{1+z};\frac{E_2}{1+z}\right]}}{f_{\mathrm{obs},[\epsilon_{\mathrm{obs},1};\epsilon_{\mathrm{obs},2}]}} \tag{5}$$

$$= \frac{\int_{E_1/(1+z)}^{E_2/(1+z)} \epsilon\ n_{\mathrm{obs}}(\epsilon) d\epsilon}{\int_{\epsilon_{\mathrm{obs},1}}^{\epsilon_{\mathrm{obs},2}} \epsilon\ n_{\mathrm{obs}}(\epsilon) d\epsilon}. \tag{6}$$

Throughout this article, we use a ΛCDM cosmology with $H_0 = 69.6\ \mathrm{km s^{-1}\ Mpc^{-1}}$, $\Omega_{\mathrm{M}} = 0.286$, and $\Omega_\Lambda = 0.714$ for performing the k-correction related to the cosmological rest frame of sources.

4. Type Ic SNe Associated with BdHN I, BdHN II, and BdHN III

We address the observations of a sample of 24 spectroscopically well-identified SNe associated with long GRBs (GRB-SN). In Table 1, we give the name of the SN, the SN type, the cosmological redshift, our best estimate of E_{iso} of the associated long GRB, the peak luminosity of the SN ($L_{p,\mathrm{SN}}$), and the time of occurrence of the peak ($t_{p,\mathrm{SN}}$). We also give the analogous information from the literature.

The optical observations are performed during the long-lived multiwavelength afterglow of each GRB. As pointed out by Cano et al. (2017, and references therein), the spectroscopic analysis of the light curve close to their maxima, through the identified presence of strong absorption/emission lines (Cappellaro 2022), allows us to classify the type of the SN, e.g., Ib/c or Ic-BL. The photometric observation also indicates evidence for an emerging SN by a characteristic rise in the optical afterglow at around 7–20 days after the main GRB trigger. The rise in apparent magnitude points to the energy deposited in the expanding outflow by the decay of radioactive nickel mass synthesized during the SN explosion (see Section 5).

Since the first evidence of the GRB-SN association, GRB 980425-SN 1998bw in 2018 (Galama et al. 1998), to the end of 2019, about 60 GRB-SN events have been detected. We collected data from literature and catalogs (Lien et al. 2016;

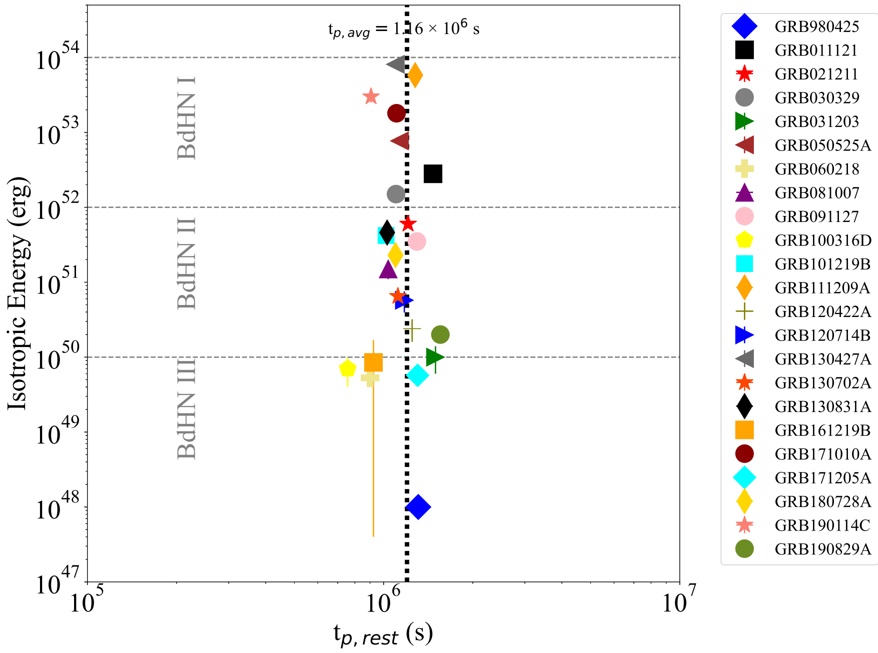

Figure 5. Isotropic-equivalent energy ($E_{\gamma,\rm iso}$) of GRB vs. the peak time of luminosity of the bolometric light curve of the associated SN ($t_{\rm P,SN}$). The plot shows the lack of correlation: the SN peaking times (in the rest frame) stay within an order of magnitude spread, while the GRB energy spans ∼6 orders of magnitude.

Poolakkil et al. 2021), Gamma-ray Coordinates Network (GCN),[19] tables[20,21] and databases.[22,23] Among these associations, there are 24 SNe identified spectroscopically and 26 SNe showing only a prominent "bump" in the late optical afterglow and any obtained spectra.[24] Interestingly, half of the sample occurred within Fermi space observatory operational era, thus extending information to the high-energy counterpart of the accompanying GRBs (Ajello et al. 2019); see Table 1.

Due to incomplete data in some of the observed GRB-SN, we cannot use the entire population. Therefore, we further focus on the 24 spectroscopically confirmed SNe associated with GRBs to the end of 2019.

The peak luminosity integrated over the optical bands is similar in all observed SNe associated with GRBs independent of their redshift; see Figure 2. The same applies to the time of occurrence of the peak measured since the GRB trigger and is independent of the redshift of the SN; see Figure 3. As we will point out in Section 5, the determination of the trigger time strongly depends on the luminosity of the GRB and the instrument with the indeterminacy of $\sim 10^4$ s. The average peak bolometric luminosity is $L_{\rm p,avg} = (9.45 \pm 3.8) \times 10^{42}$ erg s^{-1} and the average peaking time in the rest frame is $t_{\rm p,avg} = (1.16 \pm 0.24) \times 10^6$ s.

Quite apart from this universality, it follows from Figures 4 and 5 that the peak luminosity of the associated SN Ic and its time of occurrence are not correlated to the $E_{\rm iso}$ of the BdHN I, II, and III.

[19] https://gcn.gsfc.nasa.gov
[20] https://www.mpe.mpg.de/~jcg/grbgen.html
[21] https://user-web.icecube.wisc.edu/~grbweb_public/index.html
[22] https://www.wis-tns.org
[23] http://simbad.cds.unistra.fr/simbad/
[24] It was noted by Cappellaro (2022) that due to the recent emergence of transient surveys, the current SN discovery rate is counting to about 1000 events per year. Thus, only a small fraction of them receives a spectroscopic confirmation.

As is recalled in Section 1, we assume that the progenitors of the SN Ic associated with long GRBs are composed of a $\sim 10 M_\odot$ CO star and a $\sim 2 M_\odot$ companion NS. As is recalled in Section 2, the same progenitors also characterize the BdHNe. In both cases, the trigger is marked by the collapse of the CO core. From the results presented above, a new problem arises: how can the thermonuclear evolution of the SN Ic, characterized by a standard energy of $\sim 10^{49}$ erg, be unaffected by the presence of BdHN I, II, and III with energies in the range of $\sim 10^{49}$–10^{54} erg. To answer this fundamental question and the above energetic difference, we proceed in Section 5 to illustrate the physical processes in the seven fundamental episodes characterizing a most general BdHN and their spectral properties. In Sections 6–9, we provide BdHN I, II, and III examples.

5. BdHN Emission Episodes

The advantage of introducing the BdHN model may be to bring a certain amount of clarity in a field in which a great deal of confusion exists even in interpreting the specific spectral data (see, e.g., Li 2023).

As is recalled in Section 1, the differences in addressing the fundamental question of what is considered a long GRB are as follows: in the traditional literature, the long GRB is described by a single event originating from a "collapsar" and manifesting itself by an ultrarelativistic jetted emission. A much more scientifically complex and vaster picture starts from a binary progenitor.

We have also recalled how the large observational support and the equally profound theoretical comprehension following the breakthrough of the BeppoSAX promoted the unification of traditional gamma-ray astronomy to X-ray astronomy. This led to an expansion to additional multiwavelength observations. The leading conceptual progress has emerged from explaining the spatial and temporal coincidence of two very different

Table 1
GRB-SN Spectroscopically Confirmed Sample

GRB	SN	SN	z	This Study			Literature			Data Source
				$E_{\mathrm{iso},\gamma}$	$L_{\mathrm{p,SN}}$ ($\times 10^{42}$	$t_{\mathrm{p,SN}}$	$E_{\mathrm{iso},\gamma}$	$L_{\mathrm{p,SN}}$ ($\times 10^{42}$	$t_{\mathrm{p,SN}}$	
Name	Name	Type	Redshift	(erg)	erg s^{-1})	(days)	($\times 10^{52}$ erg)	erg s^{-1})	($\times 10^6$ s)	References
980425	1998bw	Ic-BL	0.0085	$(8.6 \pm 0.2) \times 10^{47}$	7.33	15.16	0.000086	14.5	1.30464	(1)-(5)
011121	2001ke	Ic	0.362	$(7.8 \pm 2.1) \times 10^{52}$	5.90	17	7.8	$\sim$5.9, 13.7	1.4688	(3), (6)
021211	2002lt	Ic	1.006	$(1.12 \pm 0.13) \times 10^{52}$	7.20	14.00	0.828	⋯	2.16	(3), (7)–(11)
030329	2003dh	Ic	0.1687	$(1.5 \pm 0.3) \times 10^{52}$	10.1	12.75	1,515	10.1	1.1016	(3), (7)
031203	2003lw	Ic	0.1055	$(8.6 \pm 4.0) \times 10^{49}$	12.6	17.33	0.0098	12.6	1.497312	(3), (7)
050525	2005nc	Ic	0.606	$(2.5 \pm 0.43) \times 10^{52}$	4.47	13.10	2.945	⋯	⋯	(3), (12)
060218	2006aj	Ic-BL	0.0334	$(5.3 \pm 0.3) \times 10^{49}$	6.47	10.42	0.0053	6.47	0.90029	(3)
081007A	2008hw	Ic	0.5295	$(1.5 \pm 0.4) \times 10^{51}$	14.0	12.00	0.15	$\sim$14	$\sim$1.0368	(3)
091127	2009nz	Ic	0.4904	$(1.5 \pm 0.2) \times 10^{52}$	12.0	15.00	1.5	$\sim$12	$\sim$1.296	(3)
100316D	2010bh	Ic-BL	0.0592	$>5.9 \times 10^{49}$	5.67	8.76	>0.0059	5.67	0.756864	(3)
101219B	2010ma	Ic	0.5519	$(4.2 \pm 0.5) \times 10^{51}$	15.0	11.80	0.42	15	1.01952	(3)
111209A	2011kl	SLSN-I	0.677	$(5.82 \pm 0.73) \times 10^{53}$	29.1	14.80	58.2	29.1	1.27872	(3)
120422A	2012bz	Ib/c	0.2825	$(2.4 \pm 0.8) \times 10^{50}$	14.8	14.45	0.024	14.8	1.24848	(3)
120714B	2012eb	Ib/c	0.3984	$(5.94 \pm 1.95) \times 10^{50}$	6.20	13.60	0.3174195	⋯	13.6 ± 0.7	(3), (13)
130215A	2013ez	Ic	0.597				3.1	⋯	⋯	(3)
130427A	2013cq	Ic	0.3399	$(8.1 \pm 0.8) \times 10^{53}$	9.12	12.68	89	⋯	⋯	(3), (14)–(17)
130702A	2013dx	Ic-BL	0.145	$(6.4 \pm 1.3) \times 10^{50}$	10.8	12.94	0.064	10.8, 19.2	1.118016	(3), (6)
130831A	2013fu	Ib/c	0.4791	$(4.6 \pm 0.2) \times 10^{51}$	6.90	11.90	0.59221795	⋯	1.60704 ± 0.05789	(3), (13), (18)
161219B	2016jca	Ic-BL	0.1475	$(8.50 \pm 8.46) \times 10^{49}$	4.90	10.70	0.0858	10.4	0.92448	(6), (19), (20)
171010A	2017htp	Ic-BL	0.33	$(1.80 \pm 0.30) \times 10^{53}$	8.4	12.80	18, 22	21 ± 9	⋯	(21)–(23)
171205A	2017iuk	Ic-BL	0.0368	$(5.72 \pm 0.80) \times 10^{49}$	6.5	15.08	0.00218	⋯	1.09728	(24)
180728A	2018fip	Ic-BL	0.117	$(2.30 \pm 0.10) \times 10^{51}$	5.8	12.70	0.2545	⋯	1.27008 ± 0.25056	(25)–(27)
190114C	2019jrj	Ic	0.4245	$(3.0 \pm 0.5) \times 10^{53}$	6.0	10.50	30	⋯	1.62432 ± 0.31968	(28)–(30)
190829A	2019oyw	Ic-BL	0.0785	$(2.0 \pm 0.3) \times 10^{50}$	6.27	18.00	0.018	⋯	0.794016 ± 0.0216	(31)–(32)

Note. Information on SN type is retrieved from Transient Name Server (www.wis-tns.org) and SIMBAD Astronomical Database (http://simbad.cds.unistra.fr/simbad/), except for the following events: SN 2001ke: Bloom et al. (2002); SN 2009nz: Berger et al. (2011); SN 2011kl: Greiner et al. (2015); SN 2019jrj: Melandri et al. (2022); SN 2019oyw: Hu et al. (2021). **References for *z* by GRB name**: 980425: Galama et al. (1998); 011121: Infante et al. (2001); 021211: Vreeswijk et al. (2003); 030329: Thöne et al. (2007); 031203: Prochaska et al. (2003); 050525: Della Valle et al. (2006b); 060218: Pian et al. (2006); 081007A: Berger et al. (2008); 091127: Vergani et al. (2011); 100316D: Bufano et al. (2012); 101219B: Sparre et al. (2011); 111209A: Vreeswijk et al. (2011); 120422A: Schulze et al. (2014); 120714B: Fynbo et al. (2012); 130215A: Cucchiara & Fumagalli (2013); 130427A: Flores et al. (2013); 130702A: Mulchaey et al. (2013); 130831A: Cucchiara & Perley (2013); 161219B: Tanvir et al. (2016); 171010A: Kankare et al. (2017); 171205A: Izzo et al. (2017); 180728A: Rossi et al. (2018); 190114C: Selsing et al. (2019); 190829A: Valeev et al. (2019). **References for data sources**: (1) Hoeflich et al. (1998), (2) Iwamoto et al. (1999), (3) Cano et al. (2017), (4) Yamazaki et al. (2003), (5) Lyman et al. (2016), (6) Lian et al. (2022), (7) Ulanov et al. (2005), (8) Ghirlanda et al. (2004), (9) Fox et al. (2003), (10) Pandey et al. (2003), (11) Della Valle et al. (2004), (12) Amati (2006), (13) Klose et al. (2019), (14) Golenetskii et al. (2013), (15) Ruffini et al. (2019c), (16) Levan et al. (2014), (17) Vurm et al. (2014), (18) Cano et al. (2014), (19) Minaev & Pozanenko (2019), (20) Frederiks et al. (2016), (21) Frederiks et al. (2017), (22) Kumar et al. (2022), (23) Bright et al. (2019), (24) D'Elia et al. (2018), (25) Frederiks et al. (2018a), (26) Ruffini et al. (2021), (27) Ruffini et al. (2018d), (28) Hamburg et al. (2019), (29) Ruffini et al. (2019b), (30) Jordana-Mitjans et al. (2020), (31) Tsvetkova et al. (2019), (32) Hu et al. (2021).

astrophysical events: the occurrence of SN Ic and the occurrence of long GRBs.

The BdHN model is rooted in the explanation of this coincidence, as explained in this article: we soon realized that both systems have a common origin in a progenitor composed of a CO core and a binary NS companion (see Section 1). Their evolution leads to an SN explosion, which, in addition to a large amount (7–8$M_{\odot}$) of ejecta, gives origin to a millisecond pulsar at its center. We have indicated in Section 2 the crucial role of the initial large angular momentum of the CO-NS binary systems due to the short initial binary period P_{bin}. Three different BdHN types originate from very different energies: BdHN I with P_{bin} of $\sim$4–5 minutes and energies ranging in 10^{52}–10^{54} erg, BdHN II with $P_{\mathrm{bin}} \sim 20$ minutes and energies ranging 10^{50}–10^{52} erg, and BdHN III with P_{bin} up to a few hours and energies below 10^{50} erg. Equally remarkable is the fact that the same progenitors, as shown in Table 2 and Figures 2–5, lead to SNe Ic of a standard energy of 10^{49} erg and an HN with the kinetic energy of $\sim 10^{52}$ erg. This result points to a thermonuclear evolution of the SN Ic largely independent of the associated GRB.

The present effort is dedicated to addressing the physics and evolution of GRBs and SN Ic with quantum and classical field theories, which are currently full of conceptual holes. Within the BdHN model, we address the explanation of the above observational facts and justify the assumptions we have made. We have identified seven basic episodes in the most general BdHN. Each episode has been characterized through a specific new physical process, partly an extension to new extreme regimes of previously known processes or new processes introduced here for the first time. This has been made possible by extragalactic observations of phenomena never observed in our local Universe. Each episode has been duly scrutinized, and the new physical laws introduced for their explanation have been validated by a time-resolved spectral analysis. The importance of these episodes can hardly be overestimated since they offer the most reliable guide we have in classifying and interpreting the rapidly growing and already very complex

Table 2
Physical Phenomena Occurring in BdHN I, II, and III, and Their Associated Observations in the GRB Data

Physical Phenomenon	BdHN Type	GRB Episodes											
		0	I	II	III	IV	V			VI			VII
		(SN-rise)	(νNS-rise)	(NS-rise)	(BH-rise Overcritical)	(BH-rise Undercritical)	(BH Echoes)			(Afterglows)			(SN Ic and HN)
		SN-rise (X-γ)	νNS-rise (X-γ)	NS-rise (X-γ)	UPE (X-γ)	Jetted Emission (GeV)	Cavity (X-γ)	HXF (X-γ)	SXF (X)	X	Opt.	Rad.	Opt. SN and HN
CO core collapse[a]	I,II,III	$\otimes$											
νNS accretion[b]	I,II,III		$\otimes$										
NS accretion[b]	I,II			$\otimes$									
BH QED[d]	I				$\otimes$								
BH CED[e]	I					$\otimes$							
BH disk accretion[f]	I						$\otimes$	$\otimes$	$\otimes$				
νNS synchr. +pulsar emission[g]	I,II,III									$\otimes$	$\otimes$	$\otimes$	
Nickel decay + ejecta kinetic energy[h]	I,II,II												$\otimes$
		Section 5.1	Section 5.2	Section 5.2	Section 5.3	Section 5.4	Section 5.5			Section 5.6			Section 5.7

Note. References in the table: [a]Wang et al. (2019, 2022); Rueda et al. (2022). [b]Fryer et al. (2014); Becerra et al. (2016); Wang et al. (2022); Becerra et al. (2022); Rueda et al. (2022). [c]Ruffini et al. (2019c); Moradi et al. (2021b, 2021c). [d]Bianco et al. (2001); Moradi et al. (2021c); Rastegarnia et al. (2022). [e]Ruffini et al. (2019c); Rueda & Ruffini (2020); Moradi et al. (2021b); Rueda et al. (2022b). [f]Ruffini et al. (2018e). [g]Ruffini et al. (2018a); Wang et al. (2019); Rueda et al. (2020). [h] Cano et al. (2017) and this paper. UPE stands for ultrarelativistic prompt emission, SXFs for soft X-ray flares, HXFs for hard X-ray flares, CED for classical electrodynamics, QED for quantum electrodynamics, SN for supernova, and HN for hypernova.

observational picture. After some general considerations, we refer in the following sections to the seven specific episodes, the related observable, and the BdHN type in which they are present. We then proceed in the following sections to providing specific examples; two BdHNe I in Section 6 on GRB 180720B (in Table 2 we identify the physical phenomena), on GRB 190114C in Section 7, GRB 190829A as a BdHN II in Section 8, and GRB 171205A as BdHN III in Section 9.

In the following, "MeV" emission refers to the radiation in the 100 keV–10 MeV energy range typical, e.g., of Fermi-GBM; "GeV" emission refers to the radiation in the 100 MeV–10 GeV energy range, typical of Fermi-LAT; and "TeV" emission refers to the radiation at higher energies, above 100 GeV, e.g., typical of the High Energy Stereoscopic System (H.E.S.S.) and MAGIC.

5.1. The SN-rise

As mentioned in Section 4, the BdHN process, which includes the formation of an SN Ic and the associated GRB, is triggered by the gravitational collapse of the CO core. The early detection of this event, namely the first appearance of the SN related to the CO core collapse (SN-rise), is quite rare. It depends on various factors, including the GRB energy, the distance of the source, and especially the operation of the multiwavelength detectors at the unpredictable moment of the occurrence of the gravitational collapse. The possible examples in BdHN I are GRB 160625B (Ruffini et al. 2021), GRB 221009A, and GRB 220101A (R. Ruffini et al. 2023, in preparation). We are progressing in determining this episode's spectral signature, which is essential to identifying the underlying physical processes originating the SN explosion. These observational features constrain SN explosion models, which still need theoretical developments to provide successful explosions in the presence of a CO core with substantial rotation and match the GRB-SN features. Although we have mentioned the difficulties in the observational identification of this episode, we have recently identified it in a handful of GRBs (R. Ruffini et al. 2023, in preparation).

Subsequently to the SN-rise, the hypercritical accretion of the 7–8$M_\odot$ onto the νNS and the NS companion shows up as episodes of the GRB prompt emission (Becerra et al. 2016; Wang et al. 2019, 2022; Becerra et al. 2022).

5.2. The νNS-rise

The prompt GRB emission starts with the transfer of energy and angular momentum due to the accretion of the SN ejecta both on a very rapidly spinning νNS and the slower rotating companion NS. The period of the νNS ranges from 1 ms in the case of a BdHN I to $\sim$100 ms periods in the case of a BdHN III. We have indicated as νNS-rise this first BdHN episode. This process occurs in all three BdHNe types, with a characteristic CPL spectrum (see, e.g., Rueda et al. 2022a). In parallel to the νNS emission, the SN ejecta accretion that occurs on the companion NS is energetically much weaker. However, in the case of BdHN I, the hypercritical accretion onto the NS companion, a few seconds after the trigger given by the νNS-rise, leads to the formation of the BH and the new episode of the ultrarelativistic prompt emission (UPE) occurs, with a clear CPL + thermal emission (see Section 5.3). Initially, the UPE and the νNS-rise emissions have comparable luminosities. In the case of GRB 180720B, a first νNS-rise I episode, lasting 4.84 s, is followed by a prominent UPE I episode lasting 1.21 s, both identifiable by their different spectral properties. Soon after, the νNS-rise II episode starts, lasting for 3.02 s, followed by the UPE II episode for 1.82 s; see details in Table. 3. What is fascinating and identifiable is the noninterference of the emission process from the νNS-rise and the UPE. A similar behavior is present in GRB 190114C; see details in Table 4.

In both cases of GRB 180720B and GRB 190114C, the millisecond rotation of νNS has given the possibility of examining the equilibrium configurations of a triaxial Jacobi ellipsoid soon evolving into a Maclaurin spheroid with possible emission of gravitational waves (Rueda et al. 2022a). Such possibility, theoretically indicated as necessary in the early evolution of the Crab Nebula pulsar (Ferrari & Ruffini 1969), can now be submitted to direct observations in BdHN I.

Following the νNS-rise, which again we recall exists in all BdHN types, the synchrotron radiation emitted by the rapidly spinning νNS, in the wavelengths ranging from X-rays to optical to radio, gives origin to the afterglows. It is satisfactory that the afterglows are identically present in all BdHN types; see Section 5.6.

Numerical simulations show that the accretion process can be observed as a double-peak emission, where the relative time and intensity of the peaks depend on the orbital period and the angular momentum of the NS at the beginning of the accretion process (see Becerra et al. 2019, 2022, for details). The NS companion can reach the critical mass for BH formation before the second peak of fallback accretion onto the νNS (see Becerra et al. 2019, 2022, for recent simulations). Since the accretion process and associated νNS-rise is not exclusively for binaries forming a BH, the above double-peak emission from the accretion can appear as the prompt emission in a BdHN II, as in the case of GRB 190829A (Wang et al. 2022). The prompt emission appears without a double-peak structure in BdHN III, like in GRB 171205A (Wang et al. 2023); see Section 9.

We refer to Section 6 for details on the νNS-rise in GRB 180720B, Section 7 for GRB 190114C, Section 8 for GRB 190829A, and Section 9 for GRB 171205A.

5.3. The UPE Phase

The UPE phase is the first new process that has made possible the extrapolation of the well-known quantum electrodynamics (QED) process of vacuum polarization, which, for a long time, approached in Earth-bound experiments without reaching observational support, and now observing the new regime of overcritical fields in extragalactic astrophysics sources (see Ruffini et al. 2010, and references therein).

These processes were pioneered by decades of theoretical works in the 1930s by Paul Dirac (Dirac 1930), Gregory Breit and John Archibald Wheeler (Breit & Wheeler 1934), and by Fritz Sauter (Sauter 1931a, 1931b), Werner Heisenberg, and Hans Euler (Euler 1936; Heisenberg & Euler 1936), and later in the 1940s by Julian Schwinger (Schwinger 1948, 1949a, 1949b) and Richard Feynmann (Feynman 1948, 1949a, 1949b); see e.g., Cherubini et al. (2009) and Ruffini et al. (2010). Despite many efforts, the inverse of the Breit–Wheeler process, namely pair creation by two photons, was never observed in Earth-bound experiments, neither in the past at DESY and SLAC, nor in the present in Brookhaven and Darmstadt, nor at ELI[25] nor XFEL.[26] It is clear today that these processes are routinely observed in

[25] https://eli-laser.eu/
[26] https://www.xfel.eu

Table 3
Episodes and Afterglows of GRB 180720B

Episode	Event	Duration (s)	Spectrum	$E_{\rm iso}$ (erg)	Physical Phenomena
0	SN-rise	⋯	⋯	⋯	$\rm CO_{core}$ collapse
I	νNS-rise				νNS accretion
	νNS-rise I	4.84	Band	$(1.53 \pm 0.09) \times 10^{53}$	
	νNS-rise II	3.02	CPL	$(1.13 \pm 0.04) \times 10^{53}$	
II	NS-rise	Not observable	Not observable	Not observable	Companion NS accretion
III	BH-rise (overcritical)				BH QED
	UPE I	1.21	CPL+BB	$(6.37 \pm 0.48) \times 10^{52}$	
	UPE II	1.82	CPL+BB	$(1.60 \pm 0.10) \times 10^{53}$	
IV	BH-rise (undercritical)				BH CED
	Jetted GeV emission	600	PL	$(2.2 \pm 0.2) \times 10^{52}$	
IV	BH-echoes				BH disk accretion
	Cavity	3.02	CPL	$(4.32 \pm 0.19) \times 10^{52}$	
	HXF	6.03	CPL+BB	$(3.93 \pm 0.33) \times 10^{52}$	
	SXF	15.12	PL	$(2.89 \pm 042) \times 10^{52}$	
VI	The Afterglows				νNS synchrotron+pulsar emission
	X-ray	10^7	PL	$(2.61 \pm 1.01) \times 10^{52}$	
	TeV	$\sim 3 \times 10^3$	PL	$(2.40 \pm 1.80) \times 10^{50}$	
	Optical	$\sim 3 \times 10^5$	PL	$(6.10 \pm 1.00) \times 10^{50}$	
	Radio	$\sim 2.21 \times 10^6$	PL	$(2.21 \pm 0.24) \times 10^{46}$	
VII	SN Ic and HN	No data	No data	No data	Nickel decay

Note. This table reports the name, the underlying astrophysical process, the duration (seconds), the best-fit spectrum, and the isotropic energy (ergs) for each event in GRB 180720B. GRB 180720B has a redshift $z = 0.654$ and $T_{90}^{\rm total} = 29.56$ s (corrected in the rest frame). The NS-rise in GRB 180720B is not observable because of the formation of the BH.

GRBs on the vastest possible energy scales up to 10^{54} erg s^{-1}, on the shortest time intervals up to 10^{-9} s, and highest energies up to $\sim 10^{18}$ eV.

A novel *hierarchical* (*self-similar*) structure has been evidenced in the UPE spectra of GRB 190114C and GRB 180720B, composed of a blackbody (BB) plus a cutoff power-law (CPL) model; see Sections 6 and 7. Namely, the spectra of the UPE, rebinned in time intervals up to a fraction of a second, are all fitted by analogous BB+CPL models. This feature implies a microscopic phenomenon at work on ever shorter timescales. The explanation of the UPE phase of these BdHN I requires the interplay of general relativity, QED, and plasma physics in an overcritical regime, which has been observed for the first time.

In BdHN I, ionized matter and the magnetic field inherited from the collapsed NS surround the newborn Kerr BH. These three components comprise the *inner engine* that drives the GRB radiation above MeV energies, i.e., the prompt and the GeV emission (Ruffini et al. 2019c; Rueda & Ruffini 2020; Moradi et al. 2021b, 2021c; Ruffini et al. 2021).

The QED process at work in the UPE originates in the vacuum polarization of the BH vicinity by the electric field, E, induced by the gravitomagnetic interaction of the Kerr BH and the magnetic field, B_0. At the BH horizon, $r = r_H = (1 + \sqrt{1 - \alpha^2})GM/c^2$, the electric field is approximately given by (see, e.g., Ruffini et al. 2019c; Rueda & Ruffini 2020)

$$E(r_H) \sim \frac{v_H}{c} B_0 \sim \frac{\Omega_H r_H}{c} B_0 = \frac{\alpha\, B_0}{2} \approx \frac{Q_{\rm eff}}{r_H^2}, \tag{7}$$

where M, J, $\alpha = cJ/(GM^2)$, and $\Omega_H = c\,\alpha/(2\,r_H)$ are, respectively, the BH mass, angular momentum, dimensionless spin parameter, and angular velocity. The last expression introduces the *effective charge* (the BH has zero net charge), defined by $Q_{\rm eff} = (G/c^3)2B_0 J$ (see Ruffini et al. 2019c; Rueda & Ruffini 2020; Moradi et al. 2021b, for details).

For a magnetic field strength $B_0 > 2B_c/\alpha_0$, or conversely, for an initial BH spin parameter $\alpha_0 \geqslant 2B_c/B_0$, the induced electric field is initially overcritical, i.e., $E(r_H) \geqslant E_c = m_e^2 c^3/(e\hbar) \approx 1.32 \times 10^{16}$ V cm^{-1}. Therefore, on a short timescale of the order of the Compton time, $\sim \hbar/(m_e c^2) \approx 10^{-21}$ s, the approximate vacuum around the BH is rapidly filled with electron–positron pairs (e^+e^-), forming an optically thick plasma. The e^+e^- pairs self-accelerate and engulf baryons from the low-density medium around the BH. The plasma reaches transparency at large distances from the BH (e.g., $R_{\rm tr} \sim 10^9$ cm), with large Lorentz factor (e.g., $\Gamma \sim 10^2$; see Moradi et al. 2021c). There is no single transparency event but a train of transparencies that continues when the electric field reaches the critical value. This occurs when the spin parameter has been reduced from its initial value, α_0, to $\alpha \sim 2B_c/B_0$.

The e^+e^- plasma energy comes from the electric energy stored in the electric field induced by the interaction of the external magnetic field and the gravitomagnetic field of the Kerr BH. Thus, the ultimate energy reservoir is the BH extractable energy, $E_{\rm ext} = (M - M_{\rm irr})c^2$, where $M_{\rm irr}$ is the BH irreducible mass. The latter is related to the other BH parameters by the mass-energy formula (Christodoulou 1970;

Table 4
Episodes and Afterglows of GRB 190114C

Episode	Event	Duration (s)	Spectrum	E_{iso} (erg)	Physical Phenomena
0	SN-rise	…	…	…	CO_{core} collapse
I	νNS-rise				νNS accretion
	νNS-rise I	0.79	CPL	$(3.52 \pm 0.15) \times 10^{52}$	
	νNS-rise II	0.84	CPL	$(3.75 \pm 0.11) \times 10^{52}$	
II	NS-rise	Not observable	Not observable	Not observable	Companion NS accretion
III	BH-rise (overcritical)				BH QED
	UPE I	0.39	CPL+BB	$(1.00 \pm 0.11) \times 10^{53}$	
	UPE II	2.09	CPL+BB	$(1.47 \pm 0.20) \times 10^{53}$	
IV	BH-rise (undercritical)				BH CED
	Jetted GeV emission	600	PL	$(1.8 \pm 1.3) \times 10^{53}$	
IV	BH-echoes				BH disk accretion
	Cavity	13.1	CPL	$(2.49 \pm 0.12) \times 10^{52}$	
	HXF	…	…	…	
	SXF	…	…	…	
VI	The Afterglows				νNS synchrotron+pulsar–like emission
	X-ray	$\sim 10^7$	PL	$(3.20 \pm 1.28) \times 10^{52}$	
	TeV	$\sim 3 \times 10^3$	PL	$(4.00 \pm 1.80) \times 10^{51}$	
	Optical	$\sim 3 \times 10^5$	PL	$(7.10 \pm 1.20) \times 10^{50}$	
	Radio	$\sim 2 \times 10^6$	PL	$(3.31 \pm 0.34) \times 10^{46}$	
VII	SN Ic and HN	$\sim 10^7$	BB	3×10^{49}	Nickel decay
	$M_{\mathrm{ej}} = (6.0 \pm 4.0) M_\odot$				
	$M_{\mathrm{Ni}} = (0.4 \pm 0.2) M_\odot$				
	$E_K = (2.5 \pm 1.8) \times 10^{52}$ erg				

Note. This table reports the name, the underlying astrophysical process, the duration (seconds), the best-fit spectrum, and the isotropic energy (ergs) for each event in GRB 190114C. GRB 190114C has a redshift $z = 0.424$ and $T_{90}^{\mathrm{total}} = 81.4$ s (corrected in the rest frame).

Christodoulou & Ruffini 1971; Hawking 1971)

$$M^2 = \frac{c^2 J^2}{4G^2 M_{\mathrm{irr}}^2} + M_{\mathrm{irr}}^2. \tag{8}$$

As shown in Moradi et al. (2021c) and Rastegarnia et al. (2022), each transparency process reduces the BH angular momentum by a small fractional amount $\Delta J/J \sim 10^{-9}$, leading to a slightly smaller angular momentum $J^* = J - \Delta J$. The BH mass changes by $\Delta M \approx \Omega_H \Delta J/c^2$ (keeping the BH irreducible mass approximately constant in the process), so $\Delta M/M \sim \Delta J/J$. Therefore, the system starts a new process with the same magnetic field B_0, kept constant, and a new effective charge of $Q_{\mathrm{eff}}^* = Q_{\mathrm{eff}} - \Delta Q_{\mathrm{eff}}$, with $\Delta Q_{\mathrm{eff}}/Q_{\mathrm{eff}} = \Delta J/J$.

We refer the reader to Section 6 (and Rastegarnia et al. 2022) for details on the UPE phase in GRB 180720B, and to Section 7 (and Moradi et al. 2021c) for GRB 190114C.

The UPE structure has been found as well in GRB 160625B (z = 1.406), extending from $t_{\mathrm{rf}} = 77.72$ s to $t_{\mathrm{rf}} = 87.70$ s, and GBR 160509A (z = 1.17), spanning from $t_{\mathrm{rf}} = 4.84$ s to $t_{\mathrm{rf}} = 8.53$ s (see Li et al. 2023, for more details). A detailed time-resolved spectral analysis of the UPE phase of GRB 160625B is given in Table 2 and Figure 4 of Li et al. (2023), and the luminosity and temperature of the thermal components are given as a function of the rest-frame time in Figure 5 of Li et al. (2023). The same analysis has been carried out for the UPE phase of GRB 160509A, it is presented in Table 4, Figure 8, and Figure 9 of Li et al. (2023). Although the UPE has been successfully analyzed in both sources, we are verifying the remaining six episodes.

Thus, the UPE is expected to be present only in the prompt emission of BdHN I. The ν NS-rise instead dominates the prompt emission of BdHN II. We advance the possibility that a UPE-like emission could also occur under some conditions around a highly magnetic, fast-rotating NS, and the differences between the two cases could be checked through the prompt emission of BdHNe I and II.

5.4. High-energy Jetted (GeV) Emission

The UPE ends when the strength of the induced electric field becomes lower than the critical field's. Hence, the vacuum polarization's QED process is no longer active. Yet, the induced electric field is sufficiently large to power the GeV emission by the following classical electrodynamics (CED) process. The electric field accelerates charged particles that move along and spiral around the magnetic field lines given the magnetic dominance, i.e., $\boldsymbol{B}^2 - \boldsymbol{E}^2 > 0$, leading to radiation by acceleration, e.g., synchrotron emission. In particular, for a magnetic field aligned and parallel to the BH spin, electrons move outward in the polar region around the BH rotation axis ($\theta = 0$) at angles $-60° \lesssim \theta \lesssim 60°$ in the northern hemisphere, and the analogous region in the southern hemisphere because of the reflection symmetry of the Kerr BH spacetime. For the involved pitch angles (see, e.g., Moradi et al. 2021b, for details), those electrons emit most of the synchrotron radiation at GeV energies with a luminosity that explains the observed GeV radiation in (some, see below) long GRBs (Ruffini et al. 2019c; Rueda & Ruffini 2020; Moradi et al. 2021b). We refer the reader to Rueda et al. (2022b) for a fully general relativistic treatment of the above process. As for the UPE phase, the BH extractable energy powers the GeV emission, which decreases with time following a power law with an index of $\alpha_{\mathrm{GeV}} = -1.19 \pm 0.04$. Thus, the mass and angular momentum of the BH keeps decreasing with time. In this case, each process of emission extracts a fraction of the BH mass-energy $\Delta M/M \sim 10^{-18}$ and angular momentum $\Delta J/J \sim 10^{-16}$ (see, e.g., Moradi et al. 2021b; Rueda et al. 2022b).

Unlike the isotropic afterglow emission, which originates from the νNS and is present in *all* types of BdHN, the GeV radiation occurs only in BdHN I since the Kerr BH powers it and is anisotropic, occurring in a double-cone of semiaperture angle $\approx 60^{\circ}$, centered on the BH rotation axis. Therefore, it is not observable in every BdHN I, which explains the absence of observed GeV emission in a fraction of them (see Ruffini et al. 2021, for details).

We refer to Section 6 for details on the GeV emission in GRB 180720B (see also Ruffini et al. 2019c), and Section 7 for GRB 190114C (see also Rueda & Ruffini 2020; Moradi et al. 2021b).

5.5. The BH Echoes

The hypercritical accretion onto the NS companion and the consequent BH formation in BdHN I decrease the matter density around the BH (Becerra et al. 2019). Numerical simulations show that the expanding e^+e^- plasma causes a further decrease of the density from 10^{-7} g cm^{-3} to a value as low as 10^{-14} g cm^{-3}. The collision and partial reflection of the expanding e^+e^- plasma with the cavity walls generates emission, known as *cavity*, characterized by a spectrum similar to a Comptonized blackbody with a peak energy of a few hundred keV (Ruffini et al. 2019a).

The density of the matter surrounding the newborn BH site is highly asymmetric (see Figure 1). Consequently, the baryons that the e^+e^- plasma loads during its expansion have an angular dependence. The transparency of the plasma in regions with $\mathcal{B} \lesssim 10^{-2}$ explains the radiation of the UPE phase, where $\mathcal{B}$ is the baryon load parameter. The transparency in regions with $\mathcal{B} \sim 50$ and Lorentz factors of $\Gamma \lesssim 5$ explain the soft X-ray flares (SXFs) and hard X-ray flares (HXFs; see Ruffini et al. 2018e, for numerical simulations). The emission is visible at intermediate angles between the binary plane and the rotation axis (see, e.g., Ruffini et al. 2021). We notice that low Lorentz factors $\Gamma \lesssim 5$ are indeed inferred from the time-resolved analysis of the X-ray data, which rule out any ultrarelativistic bulk motion (e.g., massive jets) of the emitter (see Ruffini et al. 2018e, for details).

We expect SXFs and/or HXFs to appear only in BdHN I since they are related to the transparency in the high-density regions of the e^+e^- plasma, which originated in the formation of the newborn Kerr BH (explained above in the UPE). However, the emission is not observable in every BdHN I because of the angular dependence of the emission, which becomes visible only for lines of sight close to the binary plane (Ruffini et al. 2018e).

5.6. Multiwavelength (X, Optical, Radio) Afterglow

In the BdHN scenario, the synchrotron radiation generated by relativistic electrons in the ejecta expanding in the magnetized medium provided by the νNS magnetic field, and powered by the νNS rotational energy, explains the afterglow emission in the X-rays, optical, and radio wavelengths (Ruffini et al. 2018a; Wang et al. 2019; Rueda et al. 2020, 2022a).

Because the afterglow emission depends only on the existence of the νNS, the SN ejecta, and the synchrotron radiation from an isotropic distribution of pitch angles is isotropic, the afterglow synchrotron emission must be present in *all* BdHNe. Indeed, the X-ray afterglow is observed in all 380 BdHN I identified in Ruffini et al. (2021), and in all observed BdHN II and III, as shown in this article, which proves that the afterglow emission is spherically symmetric with excellent approximation. A further implication comes from the nature of the BdHN progenitor. Every gravitational collapse of a CO star with a sufficient short orbital period must necessarily lead to a νNS (see Section 11).

A semianalytic theoretical treatment of the above synchrotron emission in BdHN can be found in Rueda et al. (2022a) and Wang et al. (2022). The synchrotron luminosity follows a power-law behavior with the same power-law index in all energy bands. The fit of the multiwavelength afterglow data with the above model gives information on the SN ejecta expansion velocity, the νNS magnetic field, the energy and distribution of electrons in the ejecta, and the power injected by the νNS into the SN ejecta. This description of the GRB afterglow within the BdHN scenario differs from that of traditional GRB models, which consider that an ultrarelativistic jet with Lorentz factor >100 produces the prompt emission and then continues to expand, leading to the afterglow by synchrotron emission from the accelerated electrons swept in.

In general, the X-ray emission has the contribution of the synchrotron emission and the νNS pulsar. The νNS pulsar luminosity is characterized by a plateau, followed by a power-law decay at times longer than the characteristic spin-down timescale. Thus, in the X-rays, the sum of the synchrotron and the pulsar emission can result in a power-law luminosity that is shallower than the power-law luminosity of pure synchrotron radiation. Therefore, from the energetics of the afterglow, and the fit of the X-ray light curve, it is possible to infer the evolution of the νNS rotation period and magnetic field strength (see, e.g., Ruffini et al. 2018a; Wang et al. 2019; Rueda et al. 2020; Ruffini et al. 2021; Rueda et al. 2022a; Wang et al. 2022).

5.7. The Classic SN Emission Powered by Nickel Decay

Finally, the emission is observed in the optical band powered by the energy release of nickel decay (into cobalt) in the SN ejecta. We refer the reader to Rueda et al. (2019a, 2021) and Rueda (2021) for recent reviews on the BdHN scenario of long GRBs and the related physical phenomena.

The nuclear energy released by the decay of nickel into cobalt within the SN ejecta powers the observed energy of the SN Ic emission. The SNe associated with GRBs are similar to each other irrespectively on the GRB energetics (see, e.g., Cano et al. 2017). The GRB-SN connection is one of the most relevant observational properties constraining GRB models. We introduce in this article additional observational features of the GRB-associated SNe and discuss how they constrain GRB models.

Therefore, within the BdHN model, the SN optical emission is always present and observable for $z < 1$ with current telescopes or $z > 1$ for future missions. Using the BdHN model, we have successfully predicted the time of occurrence and luminosity of the SN optical emission for the BdHN I, GRB 130427A (Ruffini et al. 2013), GRB 190114C (Ruffini et al. 2019b), GRB 211023A (Aimuratov et al. 2021), and GRB 221009A (Aimuratov et al. 2022a); for the BdHN II, GRB 180728A (Ruffini et al. 2018d), and GRB 190829A (Wang et al. 2022); for the BdHN III, GRB 171205A (Wang et al. 2022).

Having given the details of the physical origin of each episode and the information about the time-resolved spectral analysis, we now turn to specific examples of two BdHNe I (GRB 180720B in Section 6, and GRB 190114C in Section 7), one BdHN II (GRB 190829A in Section 8), and one BdHN III (GRB 171205A in Section 9).

6. GRB 180720B as an Example of BdHN I

GRB 180720B was detected by Fermi-GBM (Roberts & Meegan 2018), CALET Gamma-ray Burst Monitor (Cherry et al. 2018), Swift-BAT (Siegel et al. 2018), Fermi-LAT (Bissaldi & Racusin 2018), and Konus-Wind (Frederiks et al. 2018b), in gamma-ray radiation. H.E.S.S. also observed this source in 100–440 GeV bandwidth (Abdalla et al. 2019). In X-ray radiation, the Swift-XRT started to observe the GRB afterglow from 91 s after the Fermi-GBM trigger (Siegel et al. 2018), MAXI/GSC at 296 s (Negoro et al. 2018) and NuStar from 243–318 ks (Bellm & Cenko 2018). In the optical and near-infrared, the 1.5 m Kanata telescope observed the source at 78 s from the GRB trigger time (Sasada et al. 2018). Complementary observations in optical, infrared, and radio telescopes were also reported in Covino & Fugazza (2018), Crouzet & Malesani (2018), Itoh et al. (2018), Izzo et al. (2018), Jelinek et al. (2018), Kann et al. (2018), Lipunov et al. (2018), Martone et al. (2018), Sasada et al. (2018), Schmalz et al. (2018), Sfaradi et al. (2018), Watson et al. (2018), Zheng & Filippenko (2018), and Abdalla et al. (2019). With the redshift, $z = 0.654$, identified by the Fe II and Ni II lines in the optical observations by the VLT/X-shooter telescope (Vreeswijk et al. 2018), the GRB 180720B isotropic energy is $E_{\rm iso} = 5.92 \times 10^{53}$ erg (Ruffini et al. 2018f; Abdalla et al. 2019; Fraija et al. 2019).

GRB 180720B possesses different episodes relating to specific astrophysical processes identified in the time-resolved spectral analysis of GRB 180720B (see Moradi et al. 2021a; Rueda et al. 2022a; Rastegarnia et al. 2022; see also Table 3 and Figure 6).

We summarize in Table 3 the name of each episode, their physical event, the duration, the spectrum, $E_{\rm iso}$, and the physical phenomena originating each event. Similarly, in Figure 6, we represent the luminosity in wavelengths ranging from radio to TeV and show the spectra corresponding to each physical process.

The νNS-rise I. The radiation originating from the fallback of the SN ejecta onto the νNS (Becerra et al. 2019, 2022). The first evidence of this episode in GRB 180720B, referred to as the *νNS-rise*, extends from $t_{\rm rf} = 0$ s to $t_{\rm rf} = 4.84$ s time interval, with an isotropic energy of $E_{\rm iso} = (1.53 \pm 0.09) \times 10^{53}$ erg. A Band model best fits its spectrum with $E_p = 1064$ keV, $\alpha = -0.99$, and $\beta = -2.00$.

The UPE I. This episode pinpoints the first emission originating from the BH (BH-rise). The UPE I of GRB 180720B occurs from $t_{\rm rf} = 4.84$ s to $t_{\rm rf} = 6.05$ s. Its measured isotropic energy is $E^{\rm MeV}_{\rm UPE\,I} = (6.37 \pm 0.48) \times 10^{52}$ erg, and its spectrum is best fitted by a CPL+BB model (index $\alpha = -1.13$, cutoff energy $E_c = 2220.569$ keV, and BB temperature $kT = 50.31$ keV in the observer frame).

The νNS-rise II. It spans from $t_{\rm rf} = 6.05$ s to $t_{\rm rf} = 9.07$ s. The isotropic energy of this phase is $E^{\rm MeV}_{\nu\rm NS} = (1.13 \pm 0.04) \times 10^{53}$ erg, and its spectrum is best fitted by a CPL model ($\alpha = -0.98$, and $E_c = 737$ keV, in the observer frame).

The UPE II . It is evidenced by the first significant observed GeV photon at $t_{\rm rf} = 7.06$ s. The UPE phase is also continued during this phase (UPE II), which lasts from $t_{\rm rf} = 9.07$ to $t_{\rm rf} = 10.89$ s, with isotropic energy of $E^{\rm MeV}_{\rm UPE\,II} = (1.6 \pm 0.95) \times 10^{53}$ erg. A CPL+BB model with model parameters of $\alpha = -1.06^{+0.01}_{-0.01}$, $E_c = 1502.5^{+88.6}_{-87.5}$ keV, and $kT = 39.8^{+1.6}_{-1.6}$ keV best fits the spectrum.

The Cavity. This emission extends from $t_{\rm rf} = 16.94$ s to $t_{\rm rf} = 19.96$ s, with an isotropic energy of $E^{\rm MeV}_{\rm CV} = (4.32 \pm 0.19) \times 10^{52}$ erg, characterized by a CPL spectrum ($\alpha = -1.16$, $E_c = 607.96$ keV) with an energy of $\sim 10^{52}$ erg and a luminosity of $\sim 10^{51}$ erg s^{-1}.

The HXF and SXF. The HXF of GRB 180720B extends from $t_{\rm rf} = 28.95$ s to $t_{\rm rf} = 34.98$ s, with $L^{\rm MeV}_{\rm HXF,iso} = (7.8 \pm 0.07) \times 10^{51}$ erg s^{-1}. Its spectrum is best fitted by a CPL model with $E_c = (5.5^{+0.8}_{-0.7}) \times 10^2$ keV, $\alpha = -1.198 \pm 0.031$. The SXF occurs from $t_{\rm rf} = 55$ s to $t_{\rm rf} = 75$ s, with $L^{\rm X}_{\rm SXF,iso} = 1.45 \times 10^{50}$ erg s^{-1}. Its spectrum is best fitted by a PL+BB model with $\alpha = -1.79 \pm 0.23$, and $kT = 0.99 \pm 0.13$ keV; see Table 3. Because the interaction of expanding e^+e^- with the SN ejecta produces the cavity, the HXF, and the SXF, their energetics are similar to the UPE phase (see Ruffini et al. 2021, and references therein).

The GeV emission. The 0.1–10 GeV emission of GRB 180720B observed by Fermi-LAT starts at $t_{\rm rf} = 7.01$ s. The highest photon energy corresponding to this GRB is 4.9 GeV, which was detected 137 s after the Fermi-GBM trigger (Ronchi et al. 2020). The luminosity rises up to $t_{\rm rf} \sim 40$ s. After $t_{\rm rf} \sim 40$ s, the GeV luminosity follows a temporal decaying luminosity of $L_{\rm GeV} = 4.6 \times 10^{53}\, t^{-1.94 \pm 0.0.13}$ erg s^{-1}. It has a total isotropic energy of $E_{\rm iso,GeV} = (2.2 \pm 0.2) \times 10^{52}$ erg.

The radio, optical, and X-ray afterglows. The X-ray afterglow luminosity observed by Swift-XRT starts at $t_{\rm rf} = 52$ s with a time decaying luminosity of $L_{\rm X} = 2.5 \times 10^{53} t^{-1.44 \pm 0.01}$ erg s^{-1}, and its isotropic energy is $E_{\rm iso,X} = 2.61 \times 10^{52}$ erg. The X-ray afterglow is accompanied by the radio, optical, and TeV afterglows with isotropic energies of $E_{\rm iso,radio} = 2.21 \times 10^{46}$ erg, $E_{\rm iso,opt} = 6.1 \times 10^{50}$ erg, and $E_{\rm iso,TeV} = 2.4 \times 10^{50}$ erg, respectively.

In Rueda et al. (2022a), the above afterglows of GRB 180720B have been explained within the synchrotron scenario described in Section 5.6. The X-ray afterglow of GRB 180720B exhibits two distinct power laws, the first at times 10^2–10^3 s and the second at times $>10^4$ s (there is a data gap at 10^3–10^4 s). The X-ray luminosity in the time interval 10^2–10^3 s exhibits a shallower power-law than the pure synchrotron luminosity, as evidenced by comparing it with the power laws of the optical and radio synchrotron at times $>10^4$ s. The above is explained by the contribution of the νNS magnetic-braking radiation (see Section 5.6). Around 10^2 s, the critical synchrotron radiation energy falls below the keV range, so the X-rays synchrotron luminosity decays exponentially afterward. At lower energies, the power-law behavior remains. The subsequent dominance of the pulsar emission in the observed X-ray emission has allowed us to infer the strength of the magnetic field dipole and quadrupole and the rotation period of

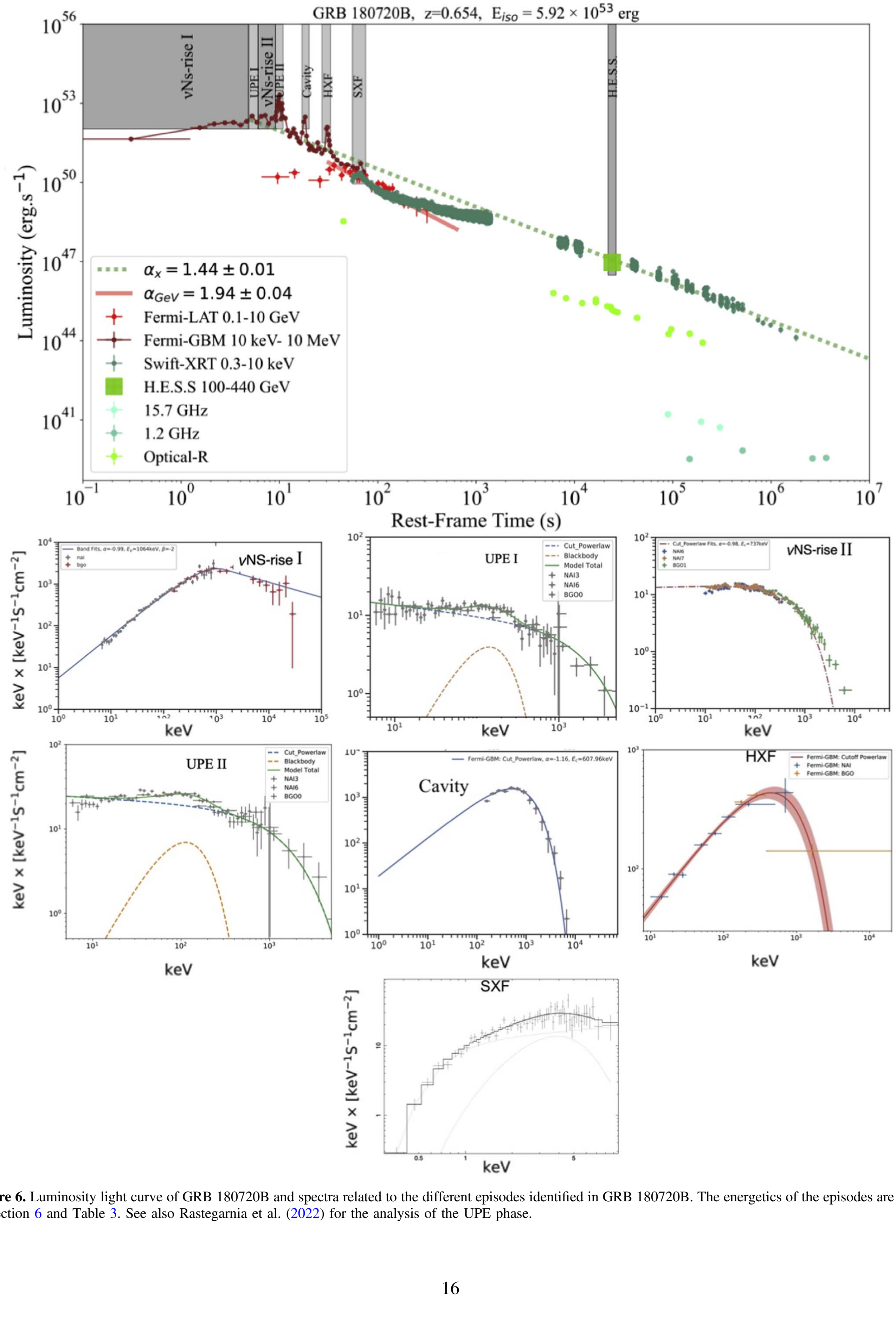

Figure 6. Luminosity light curve of GRB 180720B and spectra related to the different episodes identified in GRB 180720B. The energetics of the episodes are given in Section 6 and Table 3. See also Rastegarnia et al. (2022) for the analysis of the UPE phase.

the νNS. We refer the reader to Rueda et al. (2022a) for more details. There is a technical difficulty in detecting the early (from the GRB trigger up to a few tens of seconds) X-ray afterglow by Swift-XRT. Only recently, thanks to the cosmological time dilation effect, has it been possible to pinpoint this νNS emission in its early phase using high-z sources (Bianco et al. 2023). The extrapolation of the X-ray afterglow power-law behavior, backward in time from 10^4 s, indicates our theoretical prediction at early times, confirmed in the few cases where observations have allowed us to do it.

The optical SN. As a BdHN I source, GRB 180720B was expected to have an associated SN emission, with an optical peak at 21.8 ± 4.3 days after the trigger (Ruffini et al. 2018f). Unfortunately, no telescope observed the source at those times to confirm the SN appearance.

In conclusion, the total energy released by the GRB 180720B is $E_{\rm tot} = 6.5 \times 10^{53}$ erg of which 3.57×10^{53} erg is due to the BH with mass with a lower limit of $M = 2.4 M_\odot$ and initial spin with an upper limit of $\alpha = 0.6$. The remaining 2.93×10^{53} erg is due to the accreting νNS with a period of 1 ms.

7. GRB 190114C as an Example of BdHN I

GRB 190114C was first detected by the Fermi-GBM (Hamburg et al. 2019), and the Neil Gehrels Swift Burst Alert Telescope (BAT; Gropp et al. 2019). The highest-energy GeV photon detected by Fermi-LAT (with a boresight angle of 68°) is a 22.9 GeV event, which was observed 15 s after the GBM trigger (Kocevski et al. 2019). The Nordic Optical Telescope (NOT) announced a redshift of $z = 0.424$ (Selsing et al. 2019), which leads to an isotropic energy of $E_{\rm iso} = (2.48 \pm 0.22) \times 10^{53}$ erg. The late-time 0.3–10 keV light curve observed by Swift X-ray Telescope (XRT) revealed a temporal power-law decay (D'Elia et al. 2019). Given the above observations, at 15:29:54 GMT on 2019 January 15, we identified (Ruffini et al. 2019b) this GRB as a BdHN I and predicted that an optical SN should appear in the same location of the GRB within 18.8 ± 3.7 days, which indeed was confirmed by Melandri et al. (2019). This successful prediction and the following detection of TeV radiation by MAGIC (Mirzoyan et al. 2019) have made GRB 190114C a prototype in which all of the BdHN phases have been observed (Ruffini et al. 2019d).

The GRB 190114C reveals different episodes of specific astrophysical processes identified in the time-resolved spectral analysis; see Table 4 and Figure 7.

We summarize in Table 4 the name of each episode, their physical event, the duration, the spectrum, $E_{\rm iso}$, and the physical phenomena originating in each event. Similarly, in Figure 7, we represent the luminosity in wavelengths ranging from radio to TeVs and show the spectra corresponding to each physical process.

The νNS-rise I. With an isotropic energy of $E_{\rm iso} = (3.52 \pm 0.15) \times 10^{52}$ erg, it extends from $t_{\rm rf} = 0$ s to $t_{\rm rf} = 0.79$ s time interval. Its spectrum is best fitted by a CPL model with $E_c = 710^{+21.3}_{-26.1}$.

The UPE I. It starts from $t_{\rm rf} = 0.79$ s and ends at $t_{\rm rf} = 1.18$ s. Its spectrum is best fitted by a cutoff power law plus blackbody (CPL+BB) with parameters having a power-law index $\alpha = -0.62^{+0.03}_{-0.03}$, cutoff energy $E_c = 524.7^{+20.1}_{-20.1}$, temperature, $kT = 18.4^{+0.5}_{-0.5}$ keV, with an isotropic energy of $E_{\rm iso} = (1.00 \pm 0.11) \times 10^{53}$ erg.

The νNS-rise II . With an isotropic energy of $E_{\rm iso} = (3.75 \pm 0.11) \times 10^{52}$ erg, it spans from $t_{\rm rf} = 1.18$ s to $t_{\rm rf} = 1.9$ s time interval. Its spectrum is best fitted by a CPL model with $E_c = 770^{+22.4}_{-21.8}$.

The UPE II. It is signed by a CPL+BB spectrum with power-law index $\alpha = -0.71^{+0.02}_{-0.02}$, cutoff energy $E_c = 717.6^{+25.4}_{-25.4}$, temperature, $kT = 111.64^{+2.5}_{-2.5}$ keV, and a self-similar structure deduced from an appropriate time-resolved analysis (Moradi et al. 2021c); see Figure 8. With an isotropic energy of $E_{\rm iso} = (1.47 \pm 0.20) \times 10^{53}$ erg, it starts from $t_{\rm rf} = 1.9$ s, and ends at $t_{\rm rf} = 3.99$ s. The following mass and spin parameter of the newborn BH have been inferred, $M = 4.5 M_\odot$, and $\alpha = 0.54$, respectively (see, e.g., Moradi et al. 2021c, for details).

The Cavity. It extends from $t_{\rm rf} = 11$ to $t_{\rm rf} = 17$ s. Its spectrum is best fitted by a CPL model with a photon index $\alpha = -1.67$ and cutoff energy $E_c = 251$ keV. The enclosure of the companion NS and the accreted material (i.e., $\approx 10^{57}$ baryons) inside the BH horizon creates a large cavity of $\approx 10^{11}$ cm around it. The density distribution around the newborn BH has been inferred in Ruffini et al. (2019a), and the data have confirmed the spatial extension of the cavity (see Table 4 and Figure 7).

The HXF and SXF. It was demonstrated in Ruffini et al. (2018g) and Ruffini et al. (2021) that the HXF and SXF are observable when the BdHNe viewing angle is closed to the equatorial plane of the binary progenitors. GRB 190114C is a BdHNI observed with a viewing angle orthogonal to the orbital plane of the GRB binary (Ruffini et al. 2021). Therefore, the HXF and SXF of GRB 190114C are not observable from the polar axis.

The GeV emission. The onset of GeV radiation is also signed by the first GeV photon in the range 0.1–100 GeV observed by Fermi-LAT. The total energy emitted by this source in the above GeV range is $E_{\rm GeV} = (1.8 \pm 0.9) \times 10^{53}$ erg (Ruffini et al. 2021), comparable to the energy observed by the GBM.

The radio, optical, and X-ray afterglows. The X-ray afterglow luminosity observed by Swift-XRT starts at $t_{\rm rf} = 52$ s with a temporal decaying luminosity of $L_X = 5.14 \times 10^{52} t^{-1.37 \pm 0.05}$ erg s^{-1}, and its equivalent isotropic energy is $E_{\rm iso,X} = 3.2 \times 10^{52}$ erg. The X-ray afterglow of GRB 190114C is accompanied by the radio, optical, and TeV afterglows with isotropic energies of $E_{\rm iso,radio} = 3.31 \times 10^{46}$ erg, $E_{\rm iso,opt} = 7.1 \times 10^{50}$ erg, and $E_{\rm iso,TeV} = 4.0 \times 10^{51}$ erg, respectively. These afterglows originated from synchrotron radiation powered by the interaction of the νNS, with an initial period of $P_0 = 1$ ms, and SN ejecta Rueda et al. (2022a; see also Table 4 and Figure 7).

The optical SN. The optical signal of SN 2019jrj, a typical GRB-associated SN Ic (see Figures 5 and 2), peaks at $\sim 10^6$ s (see also Figure 7). Deducing certain physical properties of SN 2019jrj is difficult due to the relatively low quality of the light curve and spectra (see, e.g., Melandri et al. 2022). Therefore, we use the average values reported in Cano et al. (2017) obtained using the nickel radioactive-heating model for the bolometric SN light curve (Arnett 1982). The corresponding total SN ejected mass, nickel mass, and SN kinetic energy are, respectively, $M_{\rm ej} = 6.0 \pm 4.0\, M_\odot$, $M_{\rm Ni} = 0.4 \pm 0.2\, M_\odot$, and $E_K = (2.5 \pm 1.8) \times 10^{52}$ erg (Cano et al. 2017).

In conclusion, the total energy released by the GRB 180720 is $E_{\rm tot} = 3.8 \times 10^{53}$ erg of which (i) 2.7×10^{53} erg is due to the BH with mass with a lower limit of $M = 4.53 M_\odot$ and initial spin with an upper limit of $\alpha = 0.54$, (ii) 1.1×10^{53} erg is due to the accreting νNS with a period of 1 ms, and (iii) 3×10^{49} erg is due to the optical SN emission corresponding to the HN ejecta with a kinetic energy of 2.5×10^{52} erg.

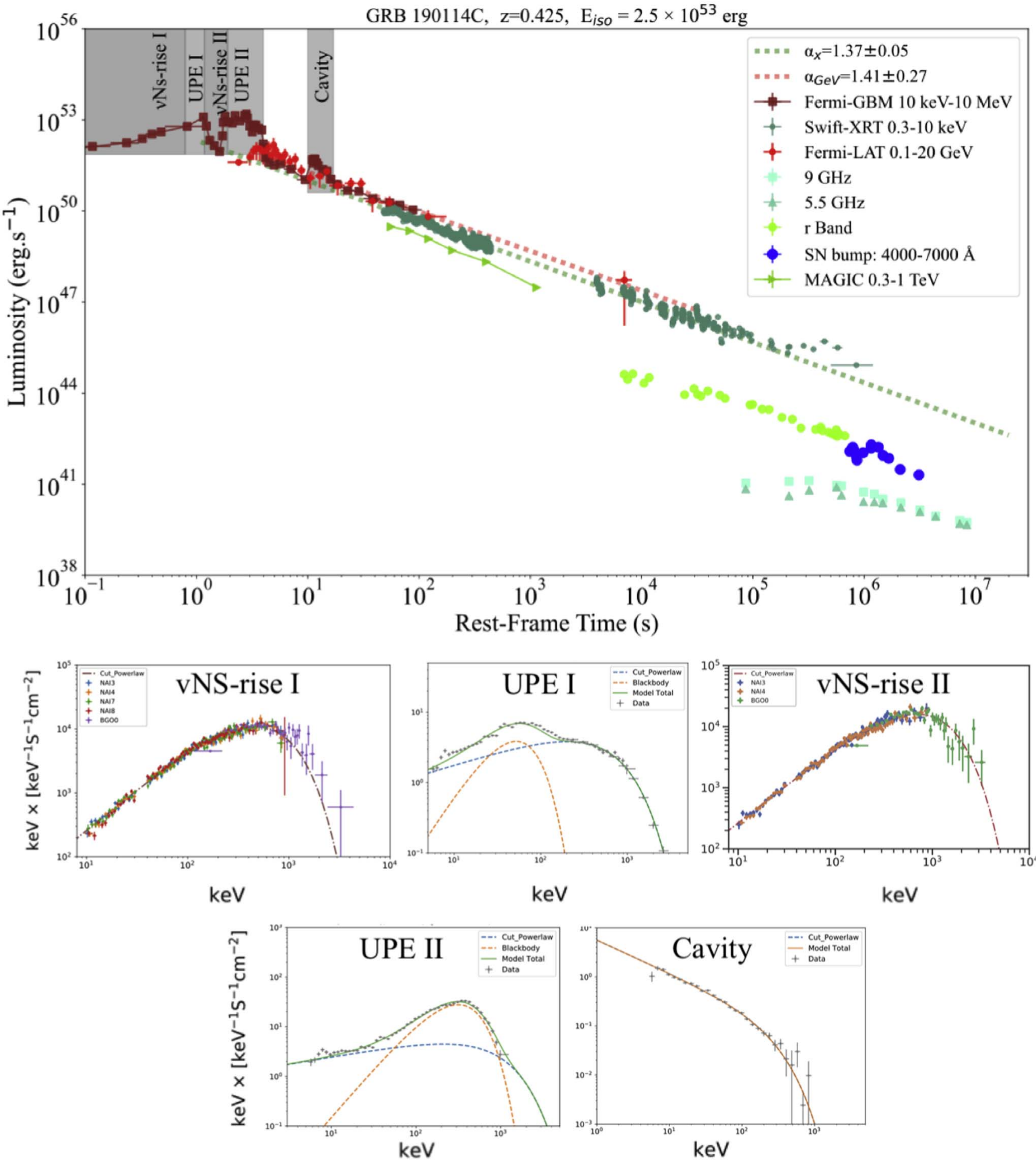

Figure 7. BdHNe I: GRB 190114C. Luminosity light curves obtained from Fermi-GBM, in 10 keV–10 MeV, Fermi-LAT in 0.1 GeV–10 GeV, Swift-BAT in 15 keV–50 keV, Swift-XRT in 3 keV–10 keV and optical *R* band. The late X-ray afterglow luminosity of BdHN I GRB 190114C observed by Swift-XRT is best fit by a temporal decaying power law of $L_X = (2.5 \pm 0.4) \times 10^{53}\, t^{1.44\pm0.01}$ erg s^{-1}. The light curve of Fermi-LAT in is fitted by temporal decaying power law of $L_{\rm GeV} = (4.6 \pm 2.9) \times 10^{53}\, t^{-1.94\pm0.04}$ erg. The prediction of the associated SN by Ruffini et al. (2019b) has been successfully observed by Melandri et al. (2019) and has made GRB 190114C as a prototype of BdHN I (Moradi et al. 2021c) to study the properties of GRB-SN sources. The rest-frame visual absolute magnitude of the SN associated with GRB 190114C is ~ -18 mag Melandri et al. (2019), which is $\sim$1 mag less than the famous SN 1998bw (Patat et al. 2001). This fainter brightness could be due to the extinction of this event (Kann et al. 2019). The energies of the episodes are given in Section 7 and Table 4.

8. GRB 190829A as an Example of BdHN II

GRB 190829A triggered the Fermi-GBM at 19:55:53 UT on 2019 August 29 (Fermi GBM Team 2019). Swift-BAT was triggered 51 s later. The Swift-XRT started observing 148.3 s later after the Fermi trigger (Dichiara et al. 2019). Swift-UVOT (Dichiara et al. 2019), Half Meter Telescope (Xu et al. 2019), NOT (Heintz et al. 2019) and Gran Telescopio Canarias (GTC; Hu et al. 2021) detected a redshift of $z = 0.0785 \pm 0.005$, as one of the

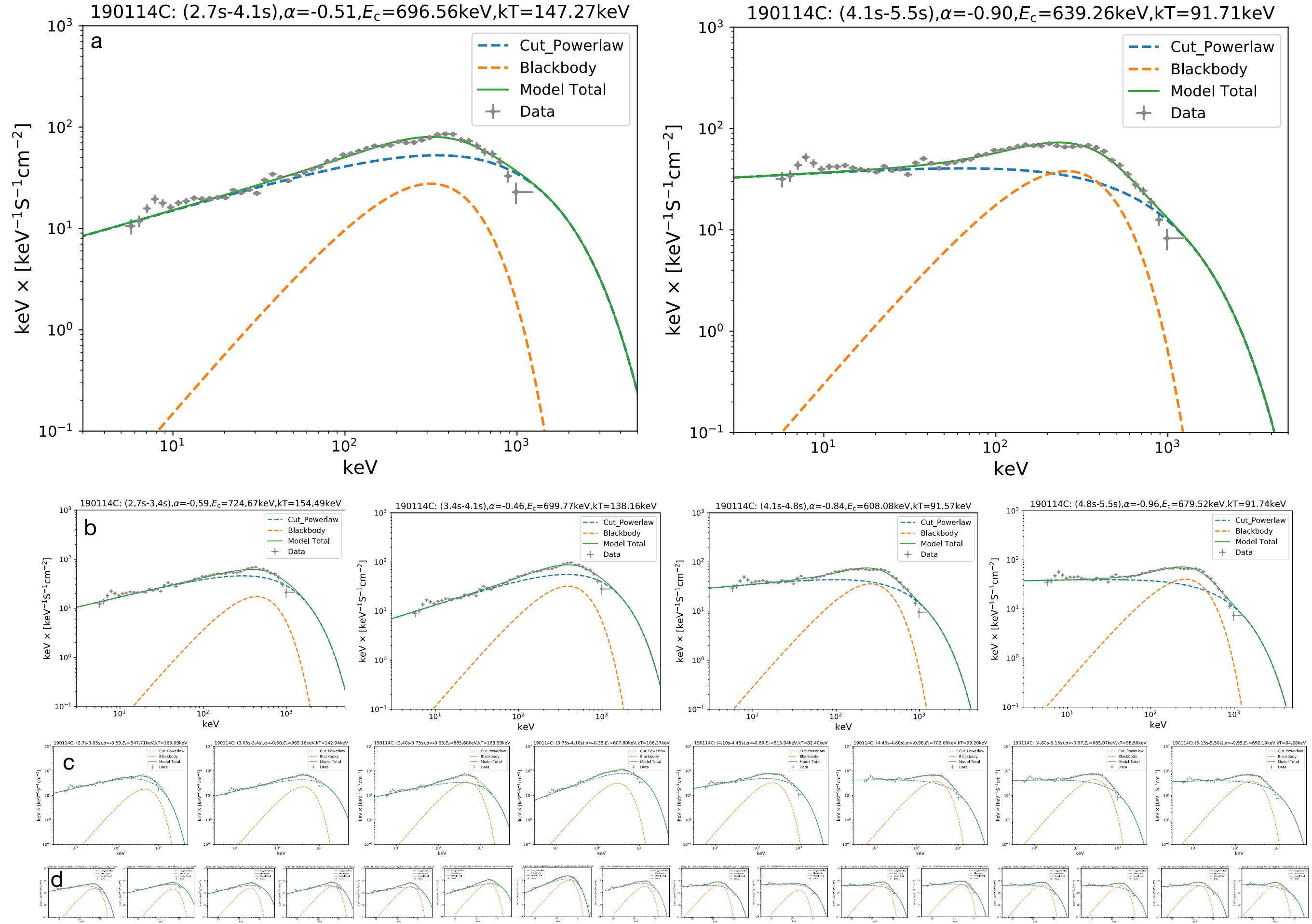

Figure 8. Time-resolved spectral analysis of UPE II phase of GRB 190114C from $t = 2.7$ s ($t_{rf} = 1.9$ s) to $t = 5.5$ s ($t_{rf} = 3.9$ s). The self-similar spectral structure is present when (a) the time interval is divided into two parts, (b) four parts, (c) eight parts, and (d) 16 parts, respectively. The plot is adapted from Ruffini et al. (2019d) with the authors' permission.

nearest GRBs. The flattening of the optical light-curve observed by Perley & Cockeram (2019a, 2019b) and Bolmer et al. (2019) provided the initial evidence for the optical SN emergence. Finally, the confirmation of an associated Type Ic-BL SN named SN 2019oyw came from the spectroscopic observation performed by de Ugarte Postigo et al. (2019).

The SN-rise is not observed for this source. Two pulses are observed in the Fermi-GBM and The Neil Gehrels Swift–BAT light curves (Wang et al. 2022). The initial pulse rises at time −0.70 s, peaks at 1.02 s, and declines at time 7.46 s. After a time delay of 35.65 s, the second, more luminous pulse begins at 43.11 s, peaks at 47.89 s, and declines at 59.34 s. All of the times are indicated in the rest frame. A cutoff power-law function best fits the first pulse. It has an isotropic energy $4.25 \pm 1.02 \times 10^{49}$ erg s^{-1} and average luminosity $4.84 \pm 1.16 \times 10^{48}$ erg s^{-1}. The second pulse shows a Band function spectrum. It is nearly 1 order of magnitude more energetic than the first pulse, with isotropic energy $3.56 \pm 0.50 \times 10^{50}$ erg, and its average luminosity is $(2.05 \pm 0.29) \times 10^{49}$ erg s^{-1}; see Table 5 for a summary of the GRB 190829A episodes.

The accretion onto the NS companion and the enhanced fallback accretion onto the νNS are responsible for the above two pulses. Comparison of GRB 190829A, especially the time separation between two pulses (∼50 s), with several CO-NS binaries simulated in Becerra et al. (2019) and Becerra et al. (2022), indicates as the possible progenitor of this GRB a binary comprising a CO star and an NS with an orbital period in the range 20–40 minutes.

Figure 9 shows the visualization of the three-dimensional numerical simulation that shows the νNS and the NS companion surrounded by high-density material and undergoing their corresponding accretion processes.

The first peak corresponds to the SN ejecta accretion onto the companion NS; see details in Wang et al. (2022). A part of the ejecta is altered by the companion NS and flows back to the νNS, leading to a second fallback accretion episode onto the νNS, leading to the second peak.

At a time >100 s, the afterglow started and was observed by Swift-XRT for the soft X-ray band, GTC for the optical band, and AMI-LA for the radio band, as shown in Figure 10. The X-ray afterglow from ∼1000 s follows a power-law decay with an index of ∼ −1.1. A single power-law function best fits its spectrum with a photon index ∼ −2.15. The optical and radio light curves share similar power-law behavior. The total energy released until 10^7 s is $\sim 4 \times 10^{50}$ erg. We attribute this energy to the rotational energy of the νNS, which leads to an initial period of 8 ms (Wang et al. 2022).

Table 5
Episodes of GRB 190829A

Episode	Event	Duration (s)	Spectrum	E_{iso} (erg)	Physical Phenomena
0	SN-rise	⋯	⋯	⋯	CO_{core} collapse
I	νNS-rise	16.23	Band	$(3.5 \pm 0.5) \times 10^{50}$	νNS accretion
II	NS-rise	8.16	CPL	$(4.2 \pm 1.0) \times 10^{49}$	Companion NS accretion
III	BH-rise (overcritical)	⋯	⋯	⋯	BH QED
IV	BH-rise (undercritical)	⋯	⋯	⋯	BH CED
IV	BH-echoes	⋯	⋯	⋯	BH disk accretion
VI	The Afterglows				νNS synchrotron+pulsar–like emission
	X-ray	$>10^7$	PL	$>4 \times 10^{50}$	
	TeV	$\sim 2 \times 10^5$	PL	$>3 \times 10^{49}$	
	Optical	$>10^7$	PL	$>4 \times 10^{48}$	
	Radio	$>10^7$	PL	$>10^{44}$	
VII	SN Ic and HN $M_{ej} = 5.67 \pm 0.72\, M_\odot$ $M_{Ni} = 0.5 \pm 0.1\, M_\odot$ $E_K = (1.35 \pm 0.51) \times 10^{52}$ erg	$\sim 10^7$	BB	$>3 \times 10^{49}$	Nickel decay

Note. The episodes of accretion onto the companion star and the νNS are triggered by SN explosion. According to the BdHN terminology, they can be classified as subepisodes of SN-rise. Times are measured in the source rest frame.

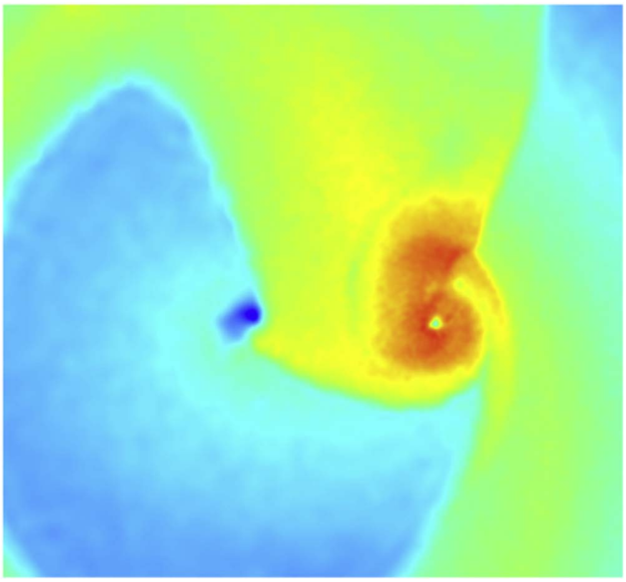

Figure 9. Ongoing accretion process of SN ejecta onto the νNS and the NS companion, simulated in Becerra et al. (2019). The νNS is located at the center of the dark-blue spot accumulating material around it. And at the center of the green spot, the NS companion is also accreting SN ejecta. Also, we notice that a portion of the SN ejecta is flowing back toward νNS due to the distortion of SN ejecta caused by the companion NS.

In addition, the ejected mass by the CO core collapse, $M_{ej} = 5.67 \pm 0.72 M_\odot$, contributes in three different ways: (1) in spinning up the νNS, which then releases dipole and/or multipole radiation; (2) in the accretion on the NS; and (3) in the kinetic energy, $E_K = (1.35 \pm 0.51) \times 10^{52}$ erg, of the remaining SN ejecta moving with mildly relativistic velocities. All three components contribute to the overall energetics, which reaches its peak emission within the first 100 s.

The optical emission of the SN Ic 2019oyw, due to a nickel mass of $M_{Ni} = (0.5 \pm 0.1)\, M_\odot$, commonly occurs around $\sim 10^6$ s with the emission of 10^{49} erg; see Figures 2–5, (see Cano et al. 2017 and Hu et al. 2021, for an in-depth discussion of the SN observation and calculations).

The remaining kinetic energy of expansion of the ejecta leads to establishing the HN associated with GRB 190829A with the total energy of 1.35×10^{52} erg (kinetic energy plus all of the radiation energy).

In addition to being a very close GRB at $z = 0.0785$, which has allowed for an especially significant data analysis of GRB 190829A, one of the remarkable peculiarities of this source, has been the discovery of the TeV emission very similar to the case of GRB 180720B and GRB 190114C. In all of these systems, the TeV emission behavior closely follows the $\sim$10% level of the X-ray afterglow power-law emission. This is the most significant since being a BdHN II, no BH is present in this source, which suggests linking the TeV radiation to the νNS activity. However, the explanation of the TeV emission within the BdHN model still needs further research, which we are currently pursuing (see Section 10.4). We can now conclude that the total energy of BdHN 190829A, observed in the keV, subMeV, TeV, optical, and radio bands, is $E_{tot} > 8.5610^{50}$ erg.

9. GRB 171205A as an Example of BdHN III

At 07:20:43 UT, GRB 171205A (Swift trigger 794972) with T_{90} of 189.4 ± 35.0 s and $z = 0.0368$ (Izzo et al. 2017), was triggered and located by the Swift BAT (Barthelmy et al. 2017; D'Elia et al. 2017). The Swift–XRT (Kennea et al. 2017) and Swift–UVOT (GCN22181) started the observation after 134 s and 154 s, respectively, from the BAT trigger.

The prompt emission maintains its luminosity of 10^{46}–10^{47} erg s^{-1} for $\sim$100 s then drops following a power law; see Figure 11. Its spectrum is best fitted by a cutoff power-law function with peak energy 148.55 ± 121.97 keV and low-energy power-law index -1.10 ± 0.35. The total isotropic energy within the T_{90} of BAT gives $E_{iso} = (1.71 \pm 0.35) \times 10^{49}$ erg; see Wang et al. (2022) and Table 6 for details.

As we discussed in the previous section for BdHN II, there are three episodes of accretion, and the last two are unique features of BdHNe. In the case of GRB 171205A, the progenitor system is a single CO star or a CO-NS binary with negligible interaction between the binary components because of a large orbital separation. Hence, only the first fallback

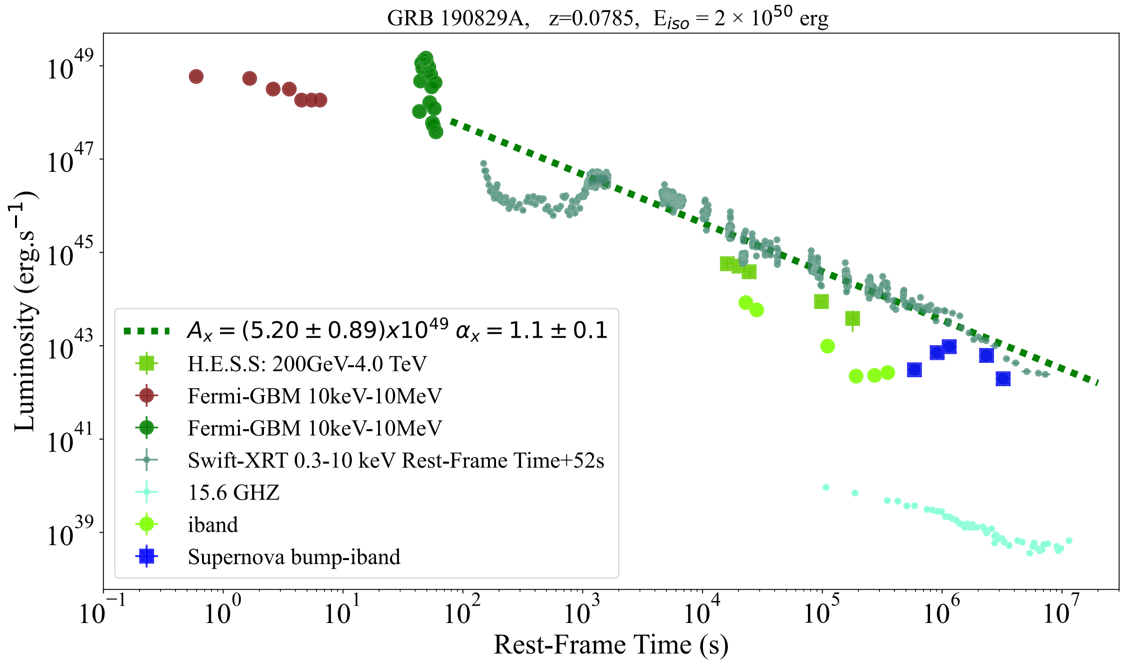

Figure 10. BdHN II: GRB 190829A. Luminosity light curves obtained from H.E.S.S. in 200 GeV–4 TeV, Fermi-GBM in 10 keV–10 MeV, Swift-BAT in 15–50 keV, Swift-XRT in 3–10 keV and i band and radio band. An SN component at $\sim 10^6$ is indicated as the blue color. The power-law fitting of the X-ray, shown as a green dotted line, gives a power-law index of -1.1. The T_0 is taken from the trigger of Fermi-GBM to which the initial time of other telescopes is aligned.

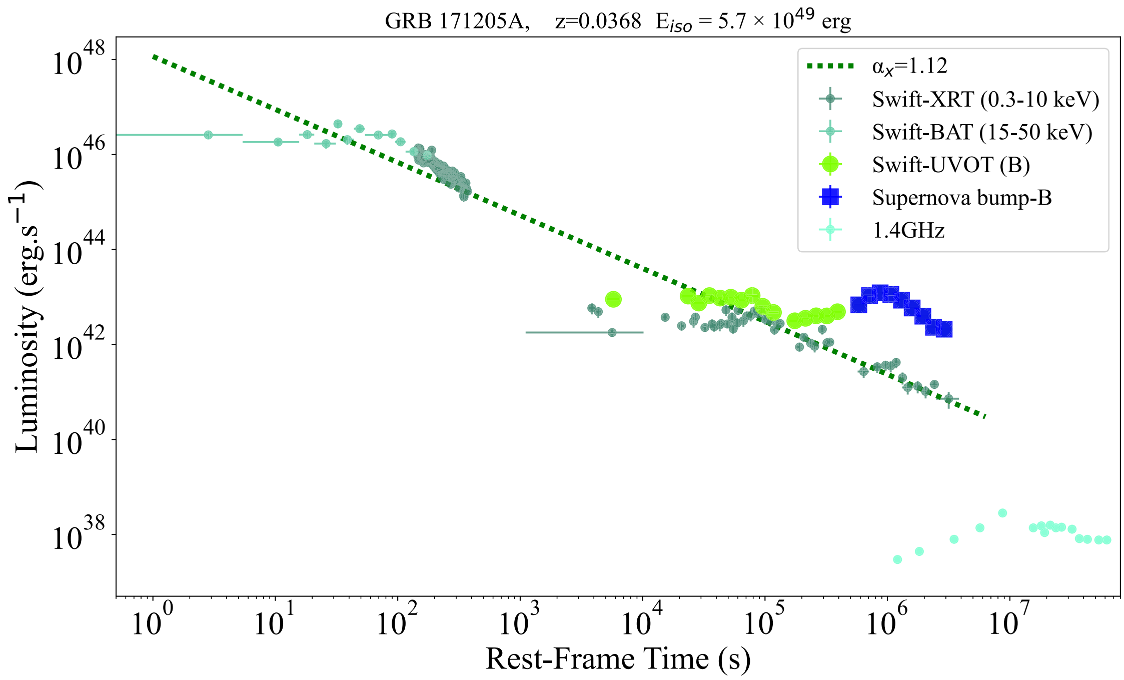

Figure 11. BdHN III: GRB 171205A. Luminosity light curves obtained from Swift-BAT in 15–50 keV, Swift-XRT in 3–10 keV and Swift-UVOT in the V and B bands. After $t_{rf} \sim 10^5$ s, it follows a decaying power law with index $\alpha_X = 1.12 \pm 0.08$ and amplitude of $A_X = (1.1 \pm 0.8) \times 10^{48}$ erg s^{-1}. The optical and radio data were taken from D'Elia et al. (2018) and Maity & Chandra (2021), and the X-ray data were retrieved from the Swift-XRT repository. The blue color indicates an SN bump.

accretion onto the νNS is expected. We also discussed that a large part of the energy from the accretion propagates inside the SN ejecta and accelerates its outermost layer, which has a steep density gradient, to a mild relativistic speed of Lorentz factor <10. The fast-moving material produces a luminosity of $<10^{47}$ erg s^{-1} for some minutes, which is often missed by Fermi-GBM or Swift-BAT. But for GRB 171205A, one of the nearest GRBs at redshift $z = 0.0368$, this weak signal is resolvable and detected by Swift-BAT, shown as the initial hundreds of seconds of prompt emission. This physical picture is similar to the hot cocoon, which is produced by a narrow jet passing through the shells of the progenitor (see, e.g., Mészáros & Rees 2001; Ramirez-Ruiz et al. 2002; Zhang et al. 2004; Nakar & Piran 2017). The difference comes from the outflow in

Table 6
Episodes of GRB 171205A

Episode	Event	Duration (s)	Spectrum	E_{iso} (erg)	Physical Phenomena
0	SN-rise	...	...	...	CO_{core} collapse
I	νNS-rise	182.5	CPL	$(1.7 \pm 0.4) \times 10^{49}$	νNS accretion
II	NS-rise	...	...	...	Companion NS accretion
III	BH-rise (overcritical)	...	...	...	BH QED
IV	BH-rise (undercritical)	...	...	...	BH CED
IV	BH-echoes	...	...	...	BH disk accretion
VI	The Afterglows				νNS synchrotron+pulsar emission
	X-ray	$>10^8$	PL	$>1 \times 10^{48}$	
	Optical	$>10^8$	PL	$>2 \times 10^{47}$	
	Radio	$>10^8$	PL	$>10^{44}$	
VII	SN Ic and HN $M_{ej} = 4.9 \pm 0.9\, M_\odot$ $M_{Ni} = 0.18 \pm 0.01\, M_\odot$ $E_K = (2.4 \pm 0.9) \times 10^{52}$ erg	$\sim 10^7$	BB	$>3 \times 10^{49}$	Nickel decay

Note. The first episode of prompt emission contains energy from the fallback accretion onto the νNS and the emission from the heated SN ejecta; the latter contributes the most energy. The optical afterglow emission is dominated by the cooling of fast-moving ejecta and the SN nickel radioactive decay. The synchrotron emission mainly contributes to the X-ray and radio bands.

our picture having a clear accretion origin onto the νNS, which emits radiation at a wider opening angle. The heated SN ejecta emits thermal emissions, a temperature of $\sim$80 eV is observed by Swift-XRT in the initial $\sim$400 s (see Figure 2 in Wang et al. 2022), then cools to optical bands observed by Swift-UVOT, VLT/X-shooter, and GTC/OSIRIS.

Different from more luminous GRBs, the emission from the accelerated fast-moving material has an obvious impact on the observation of the weak GRB 171205A. Before the transparency time $\sim 10^5$ s of the fast-moving material of mass $\sim 10^{-2} M_\odot$, the X-ray and optical light curves form a long plateau phase (see Figure 11). The growing transparent part of the fast-moving material dominates the X-ray flux through the synchrotron mechanism, and the thermal radiation from the rest opaque part dominates the optical flux. After $\sim 10^5$ s, the X-ray light curve decays as a typical power law with power-law index ~ -1, and optical emission starts to be taken over by the emission from the radioactive decay of SN ejecta. The 1000 day radio observation by uGMRT (Maity & Chandra 2021) shows the radio flux rises until $\sim 10^7$ then decays as a power law, and no jet break signature was observed, indicating the outflow has a wide opening angle. Like GRB 190829A, the same synchrotron simulation for the fast-moving material was applied on GRB 171205A (Wang et al. 2022). To fit the power-law decay behavior of the X-ray and radio afterglow, an νNS with an initial magnetic field of $\sim 3 \times 10^{13}$ G and a spin period of 58 ms is required (see Figure 5 in Wang et al. 2022).

The optical signal of SN 2017iuk, a typical GRB-associated Ic SN (see Figures 2, 5, and 11), peaks at $\sim 10^6$ s. Using the nickel radioactive-heating model for the bolometric SN light curve, the estimated total SN ejected mass, nickel mass, and total SN kinetic energy are $M_{ej} = 4.9 \pm 0.9\, M_\odot$, and $M_{Ni} = 0.18 \pm 0.01\, M_\odot$, $E_K = (2.4 \pm 0.9) \times 10^{52}$ erg, respectively, comparable to the average value deduced for the GRB-SN sample (Arnett 1982; Cano et al. 2017; Izzo et al. 2019).

10. New Physics Regimes in Hypernovae and GRBs Physics

The above description of the richness of physical phenomena triggered by the SN in the BdHN brings us to new physics in the explanation of long GRBs, which deserves to be highlighted. Below, we summarize new physics regimes made possible by understanding long GRBs and HNe.

10.1. Evidence from Triaxiality in the νNS Early Evolution

The νNS-rise and the afterglow emission are powered by the rotational energy of the νNS. Recent analysis of the νNS parameters and energetics in GRB 180720B and GRB 190114C (Rueda et al. 2022a) has shown that the νNS at the beginning of the νNS-rise is characterized by a rotation period at the verge of the bifurcation point of the Maclaurin sequence of equilibrium spheroids into the Jacobi ellipsoidal sequence. The presence of the highly spinning νNS deserves deeper attention in the core collapse of the CO star.

Therefore, the νNS might have evolved from a triaxial Jacobi-like ellipsoid into the axially symmetric Maclaurin spheroid by emission of gravitational waves, as anticipated in early models of pulsars (Ferrari & Ruffini 1969; Ostriker & Gunn 1969; Ruffini & Wheeler 1971), and theoretically verified by Chandrasekhar (1970) and Miller (1974). The triaxial configuration lives for a short time, i.e., approximately less than a second, due to the copious emission of gravitational waves, before the GRB emission. The gravitational-wave emission could be, in principle, detected for sources located at distances closer than 100 Mpc (see Rueda et al. 2022a, for details). This appears to be the only emission of gravitational waves associated with the long GRB in the BdHN scenario: the core collapse leading to the νNS radiates poor gravitational waves ($\sim 10^{-7} M_\odot c^2 \sim 10^{47}$ erg; see Dimmelmeier et al. 2002; Fryer & New 2011). In addition, given the stringent limits on the ultrarelativistic jetted emission, both in the GeV radiation and in the X-ray afterglow, previous gravitational-wave estimates (e.g., Leiderschneider & Piran 2021) do not apply (Rueda et al. 2022b).

10.2. QED Radiation Process in the UPE

At every expansion and transparency of the e^+e^- plasma, the energy radiated by the plasma is paid by the Kerr BH that reduces its mass and angular momentum by amounts ΔM and

ΔJ, respectively (see Section 5 for details). The lower value of the BH spin leads to a lower value of the induced electric field, which implies that a new self-expansion and transparency can occur with a lower e^+e^- plasma energy (Moradi et al. 2021c; Rastegarnia et al. 2022). The QED process and the approach to transparency are analogous. Still, the plasma parameters are different, which explains the hierarchical structure and similarity of the spectra in the time-resolved analysis of the UPE.

10.3. Classic Electrodynamics Radiation in the GeV Emission

At the end of the UPE phase, the induced electric field is still sufficiently high to power the GeV emission of the GRB, which is emitted in the polar regions above and below the BH within an angle $\approx 60^\circ$ from the polar axis. The radiation power, timescale, and the energy stored in the electric field to accelerate the electrons confabulate to power luminosities of the order of 10^{51} erg s^{-1} in the GeV domain for magnetic fields $B_0 \sim 10^{11}$ G (Ruffini et al. 2019c; Moradi et al. 2021b; Rueda et al. 2022b). The acceleration and radiation process occurs thanks to the magnetic dominance, $B^2 - E^2 > 0$, and the existence of regions where the component of the electric field parallel to the magnetic field is nonzero, i.e., $\boldsymbol{E} \cdot \boldsymbol{B} \neq 0$. As for the UPE, the rotational energy of the BH, the reservoir, powers this radiation process, the extension of this approach to AGNs (e.g., M87*; see Moradi et al. 2021b).

10.4. Additional Knowledge from the Physics Frontier: The TeV Emission

As we have shown in the above sections, the SN has triggered not only the path to the new physical processes and understandings of phenomena in the BdHN, but there is also a focus on the part of GRB radiation that is not yet theoretically understood and has only recently begun in Earth band experiments: TeV radiation. In particular, what is most impressive is the presence of the TeV radiation in the prompt phase of BdHN I GRB 190114C (Ruffini et al. 2021) as well as in the afterglow of a BdHN I, GRB 180720B (Rueda et al. 2022a; Rastegarnia et al. 2022), and in the afterglow of a BdHN II, GRB 190829A (Wang et al. 2022).

The first crucial information possibly contributing to the understanding of these processes is the fact that the energy flux of TeVs is 10%–60% of the energy flux of the afterglow. The second essential information is that TeV emission has been observed in the case of the BdHN II, GRB 190829A, hence, without a BH (Wang et al. 2022). These two observations lead to an energy emission of the TeV radiation linked to the rapidly spinning νNS emission. For all of these reasons, we predicted the TeV luminosity of GRB 221009A (Aimuratov et al. 2022b).

Finally, new perspectives have emerged from the knowledge on the seven episodes of BdHNe presented in this article for long GRBs, for the analysis of short GRBs previously studied, e.g., GRB 140619B (Ruffini et al. 2015), GRB 090510 (Ruffini et al. 2016b), GRB 081024B and GRB 140402A (Aimuratov et al. 2017).

11. Conclusions

A new era in physics and astrophysics started in 1996 when the BeppoSAX satellite promoted the extension of the observational techniques from gamma rays, the domain where GRBs were initially discovered, to X-rays, optical, and radio observations. Further extensions to GeV, TeV, and VHE emissions observations were soon implemented. Three main discoveries were made possible at the time as follows: (i) the presence in long GRBs of an afterglow with long-lasting X-ray emission (Costa et al. 1997). As we showed, these afterglows have contributed significantly to our understanding of long GRBs; (ii) the cosmological nature of the GRBs, implying energies up to 10^{54} erg (Metzger et al. 1997); and (iii) the outstanding spatial and temporal coincidence between the Type Ic SN 1998bw, with optical emission of 10^{49} erg (Galama et al. 1998), and long GRB 980425 of 10^{48} erg (Ruffini et al. 2007). This article is rooted in explaining this outstanding coincidence and additionally illustrates the exponential growth of knowledge in physics and astrophysics made possible by an equally impressive growth of new technologies.

We have recalled in Section 1 the earlier description of long GRBs as originating from a single BH and an ultrarelativistic jet: the "collapsar" model. The lengthy and gradual evolution to a binary progenitor follows the pioneering work of Fryer et al. (1999). A further change of perspective happened with the introduction of the concept of IGC (Rueda & Ruffini 2012). The idea was there advanced that BHs in long GRBs were not primordial but could be created by reaching the critical mass of an already existing accreting NS during the evolution of the binary progenitor. We also recalled how, motivated by a multiyear inquiry of long GRBs, we finally proposed the BdHN model with a $\sim 10 M_\odot$ CO core and $\sim 2 M_\odot$ NS binary companion as progenitors for long GRBs. The CO core collapse triggers the GRB event.

We also recalled how the BdHN approach has gained relevance because of the observed spatial and temporal coincidences of long GRBs with type Ic SNe. Most SN Ic progenitors assume ultrastripped binaries based on a multiyear effort evolution analysis. This fact has been a guiding factor in further developing our BdHN model, which naturally leads to comprehending the occurrence of SNe Ic in coincidence with a family of long GRBs, presented in this article.

Section 2 recalls that the BdHN model assumes that the gravitational collapse of the CO core necessarily leads to an SN with 7–8$M_\odot$ ejecta and a millisecond spinning νNS of 1.5$M_\odot$, at its center. Both theoretical arguments and observational evidence for these assumptions are later justified in the article. In Section 2, we recall that ultrastripped binaries comprise 0.1%–1% of the total SNe, so the BdHN I population could be explained by a small subpopulation of 0.01%–0.1% of them (see, e.g., Fryer et al. 2015). It is then interesting to explore whether that branch could only occur under specific conditions in the last evolution stages of the binary evolution after the common-envelope phase. Our description of the multiwavelength phenomenology of long GRBs with the BdHN model predicts the formation of CO-NS binaries with orbital periods from hours to days (BdHN II and III) to minutes (BdHN I), with angular momentum playing a crucial role. These binaries could be eventually observed in the Galaxy or nearby galaxies by sensitive facilities, e.g., the James Webb Space Telescope (JWST). Additionally, thanks to cosmological time dilation, we have identified in BdHN at high redshift (e.g., GRB 220101A at $z = 4.2$, GRB 090423 at $z = 8.2$, GRB 090429B at $z = 9.4$) crucial information of the νNS-rise emission in Swift-XRT data (Bianco et al. 2023). JWST is also obtaining information on galaxies hosting high-redshift GRBs like the aforementioned ones. We have advanced that such νNS-rise emission identified in high-redshift sources could be observed coincident with GWs in nearby sources by a new satellite overcoming the 43 s gap between the GRB trigger and the Swift-XRT observations (see Bianco et al. 2023, for details).

This article addresses the identification of the separatrix properties of the CO core's gravitational collapse occurring in CO-NS binaries and leading, alternatively, to a single SN Ic or a similar SN Ic and a variety of long GRBs. It is shown that the most general BdHN, in addition to a standard Ic SN, leads to (1) an HN 10^3 times more energetic than a typical SN Ic, (2) to long GRBs, much more energetic than the SN Ic, in the range of 10^{49}–10^{54} erg, and (3) these long GRBs being subdivided into BdHN I, BdHN II, and BdHN III.

From observations and theoretical analysis, we illustrate in Section 2 the BdHN I with energies between 10^{52} and 10^{54} erg, the only BdHNe where the IGC process forms a BH, BdHN II with energies between 10^{50} erg and 10^{52} erg, and BdHN III with energies below 10^{50} erg. For each BdHN type, we have identified the typical CO-NS orbital period and the νNS spin: the former ranges from ∼4–5 minutes in BdHN I, ∼20 minutes in BdHN II, and to a few hours in BdHN III. The νNS spin ranges between 1 and 100 ms. A long-lasting X-ray afterglow is associated with *each* GRB and is present in *all* BdHN types. Specific examples are given in Sections 6–9.

An important conclusion can be inferred from these results, that BdHNe are intrinsically dominated by a large amount of rotational energy, detailed as follows:

1. The νNS spin inferred from the energetics of the X-ray afterglows has an initial dimensionless angular momentum $a/M = cJ/(GM^2)$, where J and M are the νNS angular momentum and mass, of ∼0.5 for BdHN I down to $\sim 10^{-3}$ in BdHN III. We have given an example of how the fast-spinning νNS in GRB 180720B initially follows a Jacobi ellipsoid sequence (Rueda et al. 2022a), an absolute first in relativistic astrophysics.
2. The BH is formed only in BdHN I by the IGC process due to the accretion of SN ejecta onto the companion NS. Also, in this case, an initial dimensionless parameter ∼0.5 of the BH has been inferred from the two BHs in BdHNI, GRB 180720B (see Section 6) and GRB 19014C (see Section 7).
3. As recalled above, the CO core gravitational collapse originates the entire energetics of the BdHN. Traditionally, the initial rotational energy of the CO core is assumed to be zero. Possibly the largest paradigm change introduced by the BdHN model has been to point out that the zero angular momentum traditionally assumed in the description of the collapse of the CO core is untenable. In the BdHN model, the CO core has to be close to corotation with the binary NS companion: this implies, for a binary companion NS of an ∼4 minute orbital period, a CO core with $a/m \sim 1$, assuming a radius $\sim 10^{10}$ cm and a mass $\sim 10 M_\odot$. All efforts should be directed at gaining observational evidence for this corotation and developing an SN explosion model consistent with this assumption.

In Section 3, we recalled relativistic transformations to evaluate the time measurement and the bolometric luminosities in the rest frame of the source. In Section 4, we presented a selected sample of 24 spectroscopically confirmed SN Ic and their associated long GRBs (see Table 1). The main outcome is that all observed SNe Ic have peak luminosities around an average value of 9.45×10^{42} erg s^{-1} independently of the source redshift (see Figure 2). The time of occurrence of the peak optical luminosity, measured from the GRB trigger, peaks at an average value of 1.16×10^6 s (see Figure 3), again independently of the redshift of the source.

The properties of the associated GRBs for the selected three BdHNe classes are correspondingly summarized as follows: (1) Figure 4 shows that the luminosity of the SN Ic has roughly the same value, BdHNe $E_{\rm iso}$ ranges from 10^{48} to 10^{54} erg; (2) Figure 5 shows that the time of occurrence of the peak luminosity of the SN Ic is also independent of the energetics of the associated BdHN; (3) the HN energy is 10^3 times larger than the common SN Ic. This decoupling between the GRBs and the Ic SN was highlighted in a pioneering work of Zeh et al. (2004) where this problem was announced, which we quantify and explain.

In Section 5, we indicated the BdHN approach in addressing the use of quantum and classical field theories; the conceptual description of a selected number of episodes were then subjected to observational scrutiny via a time-resolved spectral analysis in the rest frame of the BdHN. The case is presented for the necessity of introducing and verifying new physical laws, in extrapolating well-known physical laws already studied on Earth-bound experiments (see, e.g., Ruffini et al. 2010), now extended to new more extreme regimes encountered for the first time in extragalactic sources. This is the case for classical electrodynamics processes extended to overcritical fields. Equally important has been reviewing the introduction of new physical laws in the QED regimes to probe the process of rotational energy extraction from a nonstationary and nonasymptotically flat Kerr solution as explaining the high-energy GeV emission of GRBs. Particularly important has been the observational verification of the energy extraction process from a Kerr BH embedded in a fully ionized low-density plasma with a nonflat asymptotic solution given by a magnetic field aligned with the rotation axis of the Kerr solution. These new approaches, previously published in specific cases, are directly applied in interpreting *all* seven episodes of the most general BdHN, which we briefly recall below, the details of which are presented in Section 5.

Section 5.1: the SN-rise. We introduce, in this Episode (0), the first appearance of the CO core collapse and the SN explosion. This episode has been possibly observed in three BdHNe, i.e., GRB 160625B (Ruffini et al. 2021), GRB 221009A, and GRB 220101A (R. Ruffini et al. 2023, in preparation), and needs further examples to verify its spectrum unambiguously. What makes this episode's observation particularly difficult is its intrinsically low luminosity, with total energy $\sim 10^{52}$ erg, which in all three of the above BdHN I precedes, by a time interval between 1 and 100 s, the νNS-rise and the UPE, the first two episodes of the prompt radiation of energy 10^{53}–10^{54} erg (see also Ruffini et al. 2021).

Section 5.2: the νNS-rise. This episode is identifiable by CPL spectra and its time of occurrence, manifesting the early presence of rapidly spinning νNS. Their periods range from ∼1 ms in BdHN I to ∼100 ms in BdHN III. The νNS-rise occurs in all BdHN types. It is followed by the synchrotron emission emitted by the νNS interacting with the SN ejecta and leading to the three-component afterglow: in the X-ray, in the optical, and in the radio, further examined in Section 5.6. One of the main results obtained in the analysis of the νNS-rise in the two BdHN I, GRB 180720B and GRB 190114C, has been the first observations of an initial triaxial Jacobi ellipsoid evolving in a Maclaurin spheroid, with possible emission of gravitational waves. It is interesting that the presence of afterglows in *all* GRBs (observed in 380 BdHN I and all BdHN II and III) necessarily also implies the presence of νNS in *all* GRBs.

Section 5.3: the UPE phase. The SN accretion onto the binary NS companion, soon after the first observation of the νNS-rise, leads to the formation by the IGC process of a rapidly spinning Kerr BH whose presence is highlighted by the emission of the UPE. In this section, we present an extended introduction of the theoretical works developed to extend to overcritical fields, i.e., $E \geqslant E_c = m_e^2 c^3/(e\hbar) \approx 1.32 \times 10^{16}$ V cm^{-1}, to the multiyear theoretical works on vacuum polarization. This treatment is now finally reaching its observational verification in the GRBs. The overcritical field is due to an effective charge given by $Q_{\rm eff} = 2B_0 JG/c^3$, where B_0 is the magnetic field and J is the angular momentum of the Kerr BH. These verifications on two selected BdHNe I, GRB 190114C and GRB 180720B, have allowed us to explain the existence of detailed new spectral features with the presence of self-similarities and structures on ever-decreasing time intervals to 10^{-9} s. The UPE phase has allowed us to test observationally and verify the validity of the Christodoulou–Ruffini (Christodoulou 1970; Christodoulou & Ruffini 1971)–Hawking (Hawking 1971) mass-energy formula. This has allowed us to estimate the initial mass-energy of the Kerr BH and the associated magnetic field, B_0, in both BdHNe I examined.

Section *5.4: high-energy jetted (GeV) emission.* In this section, we study the high-energy GeV emission originating from the classical electrodynamics process that transitions from the overcritical field, characterizing the UPE phase, to an undercritical field. The theoretical analysis of the emission originated from a Kerr BH in the presence of a magnetic field of $\sim 10^{10}$–10^{11} G has allowed us to infer emission of the GeV radiation within a cone with a half-opening of $\approx 60°$ (Rueda et al. 2022b). This has been confirmed by the statistical analysis of the 54 BdHNe observed by Fermi-LAT. Only 25 emit GeV radiation, and the remaining 29 were confirmed to be unobservable given the beamed radiation (Ruffini et al. 2021). Equally important has been the specific temporal power-law behavior of the GeV luminosity, well evidenced in Section 6, dedicated to GRB 180720B, and Section 7, dedicated to GRB 190114C.

Section 5.5: the BH echoes. The cavity radiation, explained by the collision and partial reflection of the expanding e^+e^- with the cavity's wall, originated from the BH formation (Ruffini et al. 2019a), is evidenced for GRB 180720B in Section 6 and GRB 190114C in Section 7. The HXFs and SXFs, previously explained by the interaction of the expanding e^+e^- with the surrounding accretion matter, are observable in sources with observation angle in the equatorial plane of the BdHN (Ruffini et al. 2018g). These processes are identified in Section 6 for GRB 180720B. Neither HXF nor SXF is present in GRB 190114C, given the viewing angle orthogonal to the plane of orbit.

Section 5.6: multiwavelength (X, optical, radio) afterglow. In this section, the afterglow's multiwavelength X-ray, optical, and radio emissions are recalled with references to their theoretical treatments. We here recall that the afterglows are observed in *all* BdHN types, implying a large angle emission perfectly explained in terms of the synchrotron radiation emission process originating in a millisecond period of spinning νNS as described in Sections 6 and 7. The afterglow is observed in *all* BdHNe, implying that all of these GRBs originate from a CO-NS binary.

Section 5.7: the classic SN emission powered by nickel decay. In this section, we address the optical SN emission due to the nickel decay well expressed by the theoretical work of Nadyozhin (see, e.g., Nadyozhin's lectures, Nadyozhin 2011a, 2011b) and Arnett (Arnett 1982). The crucial point is to recall that SNe Ic are present in all BdHN types and observable with current telescopes for $z \lesssim 1$. New telescopes, e.g., JWST, should probe the presence of an SN, which is predicted to also exist for higher z-values, following the BdHN model. We refer to Table 1 for a summary.

We turn then to the two examples of BdHNe I. In Section 6, we have summarized the results of GRB 180720B, and in Section 7 of GRB 190114C. In Section 8, we provided the example of a BdHN II, GRB 190829A, and finally, in Section 9, the case of a BdHN III, GRB 171205A.

For each source, we have given: (1) the complete references to the observational papers we have utilized to perform the theoretical and the time-resolved spectral analysis; (2) a figure summarizing the luminosities for each episode as a function of the rest-frame time and concerning the specific instruments and bandwidths. The same figure shows the specific examples of the spectra of each episode; and (3) again, for each source, we present a table summarizing the names of the observed episodes. For each, we give the name of the event, the duration, the spectrum the corresponding $E_{\rm iso}$, and the underlying physical phenomena. A specific time-resolved spectral analysis of the UPE phase is exemplified in the case of GRB 190114C. In addition to the complete material for the description of two BdHN I, one BdHN II, and one BdHN III, we would like to mention that preliminary results have already been obtained for the UPE phase of two additional BdHN I, namely GRB 160626B and GRB 160509A (Li et al. 2023). There, one can find the detailed UPE analysis for GRB 160625B in Table 2, Figure 4, as well as Figure 5, and for GRB 160509 in Table 4, Figure 8, and Figure 9. We are currently working on the identification of the other six episodes present in both sources.

Following the above, we identify the primary energy source of all BdHN, independently of their type. The most remarkable property that has allowed us to understand the nature of GRBs has been the possibility of retracing back from the extraordinary observed spectral data the specific energy sources, and their fundamental new physics. This has been made possible by the guidance of the BdHN model. We refer to the Figures and the Tables in the text and the references to the data acquisitions we have performed.

In Section 10, we briefly highlight the three main topics in which the analysis of the BdHN has promoted new research perspectives with the discovery of new physical laws and the verification of existing laws in new regimes made possible by the unique GRBs and HNe observations. The study of rotating figures of equilibrium represents one of the topics of research in which the best intellectuals have addressed their attention for over two centuries: from the self-gravitating Maclaurin spheroids to the discovery of the triaxial Jacobi ellipsoids. Now, for the first time, we have given evidence that triaxial ellipsoids can play a fundamental role in relativistic astrophysics and be the most prominent source of gravitational waves (Rueda et al. 2022a). Furthermore, far from being a conclusion, this is just the beginning of a new era in relativistic astrophysics leading to a new understanding of the physics of gravitational collapse of the creation of new physical systems by gravitational fission, to a new physics of SN explosion based on quantum and classical electrodynamics process coupled to the rotational energy extraction.

Similarly, we have indicated the perspectives of classic and QED energy extraction processes from rotating NS and Kerr BHs. The examples of the UPE phase and the GeV emission are here recalled just as interesting prototypes to be further extended. But far from being self-exhaustive, the GRB observations still present new challenges via the observations of vast amounts of TeV radiation up to luminosities of 10^{52} erg s^{-1}. At the same time, these emissions have recently been observed, in very low fluxes, in Earth-based accelerators, e.g., at CERN. Possibly, the most exciting new perspective is that there is evidence that this most energetic emission *does not* originate from a rotating BH, as already shown in this article.

The interpretation of previous results on short GRBs using the knowledge acquired from the BdHN seven episodes looks equally promising, e.g., in GRB 140619B (Ruffini et al. 2015), GRB 090510 (Ruffini et al. 2016b), GRB 081024B, and GRB 140402A (Aimuratov et al. 2017).

Thus, we can return to explain the enormous energetic difference between an SN Ic and the associated HN and long GRB through the occurrence of seven specific episodes in the most general BdHN, leading to the following concluding remarks:

1. The associated SN Ic bolometric energy of 10^{49} erg originates from the nuclear physics process leading to the decay of a common amount of a fraction of $0.2\,M_\odot$ to $0.5\,M_\odot$ of nickel (see e.g., Arnett 1982; Nadyozhin 2011a, 2011b), remarkably similar in all BdHN sources. The same explanation regarding nuclear physics applies to explain the common time of occurrence of the SN peak emission, identified as soon as the relativistic corrections are implemented.
2. The HNe in BdHN have kinetic energies of 10^{52} erg originating from the kinetic energy of 7–8 $M_\odot$ ejecta, expanding mildly relativistically, observed in all BdHN types.
3. Both the above kinetic energy and the formation of a highly spinning millisecond νNS at the SN center should find an explanation in a CO core collapse, duly considering the contribution of the rotational energy, again observed in all BdHN types.

Turning now to the GRBs:

1. The X-ray, optical, and radio emission of the afterglow, present in all BdHN types, ranging from a few 10^{52} erg in BdHN I (GRB 190114C) down to 10^{49} erg in BdHN III (GRB 171205A), are powered by the synchrotron emission originating from the rotational energy of the νNS interacting with the SN ejecta. The νNS initial rotation period is 1–100 ms.
2. The MeV and GeV emissions observed in the prompt radiation phase, present only in BdHN I, ranging 10^{52}–10^{54} erg, are powered by quantum and classical electrodynamics process originating from the extractable rotational energy of a Kerr BH, embedded in a fully ionized low-density plasma. The Kerr solution is neither stationary nor asymptotically flat, but is in the presence of a magnetic field, B_0, aligned with its rotation axis and fulfilling the Christodoulou–Ruffini (Christodoulou 1970; Christodoulou & Ruffini 1971)–Hawking (Hawking 1971) mass-energy formula. For the latest developments, see Rueda and Ruffini (2023).
3. Only the MeV emission in the prompt radiation of BdHN II, of $\sim 10^{52}$ erg (see Table 5), originates from the accretion of the SN ejecta into the slowing rotating binary NS companion.

We can then conclude, generally, that SNe Ic associated with long GRBs originate from CO-NS binary progenitors.

We advance the hypothesis that most CO-NS binaries, with a binary period longer than a few hours, lead only to SNe Ic, without any associated pulsar, GRB, or HN. This point can be easily tested observationally. A CO core, with an initial $a/M \sim 1$, endowed with an initial magnetic field of $\sim 10^3$ G, and density of $\sim 10^4$ g cm^{-3}, can indeed lead, in the process of gravitational collapse, to a triaxial ellipsoid. The consequent fission, Roche lobe bifurcation, can lead to a fast-spinning νNS and a very powerful explosion. Like in the UPE phase, this process is expected to be driven by a quantum electrodynamical process originating from an overcritical "effective charge." This overcritical field can complete the comprehension of the GRB-SN connection and lead to a new understanding of some of the current open issues. This will undoubtedly mark a good starting point for approaching the yet unsolved problem of the SN explosion, mainly examined in the absence of rotation. But this brings us to a different topic: the multicentury works on the rotating equilibrium configurations, as recalled above, developed by Elie Cartan, Bernhard Riemann, James Hopwood Jeans, and summarized in a series of articles by Subrahmanyan Chandrasekhar (Chandrasekhar 1969), also in collaboration with Enrico Fermi (Chandrasekhar & Fermi 1953). These works are finally reaching the test of astrophysical observations in relativistic astrophysics, which is only partly this article's topic.

Acknowledgments

It has been a pleasure to collaborate with the knowledgeable anonymous referee who provided in-depth and constructive dialog with us. We are developing the BdHN model in a series of papers and are in continuous contact with many scientists and collaborators. Particularly important have been the discussions with Roy Patrick Kerr and with editors and referees: they have constructively contributed to finalizing the presentation of our research. We extend our heartfelt thanks to them all. L.M.B. is supported by the Vicerrectoría de Investigación y Extensión—Universidad Industrial de Santander Postdoctoral Fellowship Program No. 2023000107.

ORCID iDs

Y. Aimuratov https://orcid.org/0000-0001-5717-6523
L. M. Becerra https://orcid.org/0000-0002-3262-5545
C. L. Bianco https://orcid.org/0000-0001-7749-4078
C. Cherubini https://orcid.org/0000-0002-0542-5601
M. Della Valle https://orcid.org/0000-0003-3142-5020
S. Filippi https://orcid.org/0000-0003-1952-0834
Liang Li (李亮) https://orcid.org/0000-0002-1343-3089
R. Moradi https://orcid.org/0000-0002-2516-5894
J. A. Rueda https://orcid.org/0000-0003-4904-0014

R. Ruffini https://orcid.org/0000-0003-0829-8318
N. Sahakyan https://orcid.org/0000-0003-2011-2731
Y. Wang (王瑜) https://orcid.org/0000-0001-7959-3387

References

Abdalla, H., Adam, R., Aharonian, F., et al. 2019, Natur, 575, 464
Aimuratov, Y., Becerra, L., Bianco, C. L., et al. 2021, GCN, 31056, 1
Aimuratov, Y., Becerra, L., Bianco, C. L., et al. 2022a, GCN, 32780, 1
Aimuratov, Y., Becerra, L., Bianco, C. L., et al. 2022b, GCN, 32802, 1
Aimuratov, Y., Ruffini, R., Muccino, M., et al. 2017, ApJ, 844, 83
Ajello, M., Arimoto, M., Axelsson, M., et al. 2019, ApJ, 878, 52
Amati, L. 2006, MNRAS, 372, 233
Arnett, W. D. 1982, ApJ, 253, 785
Ashall, C., Mazzali, P. A., Pian, E., et al. 2019, MNRAS, 487, 5824
Atteia, J.-L. 2022, GCN, 31365, 1
Barthelmy, S. D., Barbier, L. M., Cummings, J. R., et al. 2005, SSRv, 120, 143
Barthelmy, S. D., Cummings, J. R., D'Elia, V., et al. 2017, GCN, 22184, 1
Becerra, L., Bianco, C. L., Fryer, C. L., Rueda, J. A., & Ruffini, R. 2016, ApJ, 833, 107
Becerra, L., Cipolletta, F., Fryer, C. L., Rueda, J. A., & Ruffini, R. 2015, ApJ, 812, 100
Becerra, L., Ellinger, C. L., Fryer, C. L., Rueda, J. A., & Ruffini, R. 2019, ApJ, 871, 14
Becerra, L., Guzzo, M. M., Rossi-Torres, F., et al. 2018, ApJ, 852, 120
Becerra, L. M., Moradi, R., Rueda, J. A., Ruffini, R., & Wang, Y. 2022, PhRvD, 106, 083002
Bellm, E. C., & Cenko, S. B. 2018, GCN, 23041, 1
Berger, E., Chornock, R., Holmes, T. R., et al. 2011, ApJ, 743, 204
Berger, E., Fox, D. B., Cucchiara, A., & Cenko, S. B. 2008, GCN, 8335, 1
Bianco, C. L., Mirtorabi, M. T., Moradi, R., et al. 2023, arXiv:2306.05855
Bianco, C. L., Ruffini, R., & Xue, S.-S. 2001, A&A, 368, 377
Bissaldi, E., & Racusin, J. L. 2018, GCN, 22980, 1
Blaauw, A. 1961, BAN, 15, 265
Bloom, J. S., Kulkarni, S. R., Price, P. A., et al. 2002, ApJL, 572, L45
Bolmer, J., Greiner, J., & Chen, T. W. 2019, GCN, 25651, 1
Breit, G., & Wheeler, J. A. 1934, PhRv, 46, 1087
Bright, J. S., Horesh, A., van der Horst, A. J., et al. 2019, MNRAS, 486, 2721
Bufano, F., Pian, E., Sollerman, J., et al. 2012, ApJ, 753, 67
Burrows, D. N., Hill, J. E., Nousek, J. A., et al. 2005, SSRv, 120, 165
Burns, E., Svinkin, D., Fenimore, E., et al. 2023, ApJL, 946, L31
Caito, L., Bernardini, M. G., Bianco, C. L., et al. 2009, A&A, 498, 501
Cano, Z., de Ugarte Postigo, A., Pozanenko, A., et al. 2014, A&A, 568, A19
Cano, Z., Wang, S.-Q., Dai, Z.-G., & Wu, X.-F. 2017, AdAst, 2017, 8929054
Cantiello, M., Yoon, S. C., Langer, N., & Livio, M. 2007, A&A, 465, L29
Cappellaro, E. 2022, NCimR, 45, 549
Cavallo, G., & Rees, M. J. 1978, MNRAS, 183, 359
Chandrasekhar, S. 1969, Ellipsoidal Figures of Equilibrium (New Haven, CT: Yale Univ. Press)
Chandrasekhar, S. 1970, ApJ, 161, 571
Chandrasekhar, S., & Fermi, E. 1953, ApJ, 118, 116
Chen, P., & Ruffini, R. 2015, ARep, 59, 469
Cherry, M. L., Yoshida, A., Sakamoto, T., et al. 2018, GCN, 23042, 1
Cherubini, C., Geralico, A., Rueda, H. J. A., & Ruffini, R. 2009, PhRvD, 79, 124002
Chincarini, G., Moretti, A., Romano, P., et al. 2007, ApJ, 671, 1903
Christodoulou, D. 1970, PhRvL, 25, 1596
Christodoulou, D., & Ruffini, R. 1971, PhRvD, 4, 3552
Cipolletta, F., Cherubini, C., Filippi, S., Rueda, J. A., & Ruffini, R. 2015, PhRvD, 92, 023007
Costa, E., Frontera, F., Heise, J., et al. 1997, Natur, 387, 783
Covino, S., & Fugazza, D. 2018, GCN, 23021, 1
Crouzet, N., & Malesani, D. B. 2018, GCN, 22988, 1
Cucchiara, A., & Fumagalli, M. 2013, GCN, 14207, 1
Cucchiara, A., Levan, A. J., Fox, D. B., et al. 2011, ApJ, 736, 7
Cucchiara, A., & Perley, D. 2013, GCN, 15144, 1
Darwin, G. H. 1886, RSPS, 41, 319
de Ugarte Postigo, A., Izzo, L., Thoene, C. C., et al. 2019, GCN, 25677, 1
D'Elia, V., Campana, S., D'Aì, A., et al. 2018, A&A, 619, A66
D'Elia, V., D'Ai, A., Lien, A. Y., & Sbarufatti, B. 2017, GCN, 22177, 1
D'Elia, V., D'Ai, A., Sbarufatti, B., et al. 2019, GCN, 23706, 1
Della Valle, M. 2011, IJMPD, 20, 1745
Della Valle, M., Chincarini, G., Panagia, N., et al. 2006a, Natur, 444, 1050
Della Valle, M., Malesani, D., Benetti, S., et al. 2004, in AIP Conf. Proc. 727, Gamma-Ray Bursts: 30 Years of Discovery, ed. E. Fenimore & M. Galassi (Melville, NY: AIP), 403
Della Valle, M., Malesani, D., Bloom, J. S., et al. 2006b, ApJL, 642, L103
Dessart, L., Yoon, S.-C., Aguilera-Dena, D. R., & Langer, N. 2020, A&A, 642, A106
Dewi, J. D. M., Podsiadlowski, P., & Sena, A. 2006, MNRAS, 368, 1742
Dichiara, S., Bernardini, M. G., Burrows, D. N., et al. 2019, GCN, 25552, 1
Dimmelmeier, H., Font, J. A., & Müller, E. 2002, A&A, 393, 523
Dirac, P. A. M. 1930, PCPS, 26, 361
Eichler, David, Livio, Mario, Piran, Tsvi, & Schramm, David N. 1989, Natur, 340, 126
Euler, H. 1936, AnP, 418, 398
Falcone, A. D., Morris, D., Racusin, J., et al. 2007, ApJ, 671, 1921
Fermi GBM Team 2019, GCN, 25551, 1
Ferrari, A., & Ruffini, R. 1969, ApJL, 158, L71
Feynman, R. P. 1948, RvMP, 20, 367
Feynman, R. P. 1949a, PhRv, 76, 749
Feynman, R. P. 1949b, PhRv, 76, 769
Fishman, G. J., Meegan, C. A., Parnell, T. A., & Wilson, R. B. 1982, in AIP Conf. Proc. 77, Gamma Ray Transients and Related Astrophysical Phenomena, ed. R. E. Lingenfelter et al. (Melville, NY: AIP), 443
Flores, H., Covino, S., Xu, D., et al. 2013, GCN, 14491, 1
Fox, D. W., Price, P. A., Soderberg, A. M., et al. 2003, ApJL, 586, L5
Fraija, N., Dichiara, S., Pedreira, A. C. C. d. E. S., et al. 2019, ApJ, 885, 29
Frederiks, D., Golenetskii, S., Aptekar, R., et al. 2016, GCN, 20323, 1
Frederiks, D., Golenetskii, S., Aptekar, R., et al. 2017, GCN, 22003, 1
Frederiks, D., Golenetskii, S., Aptekar, R., et al. 2018a, GCN, 23061, 1
Frederiks, D., Golenetskii, S., Aptekar, R., et al. 2018b, GCN, 23011, 1
Fruchter, A. S., Levan, A. J., Strolger, L., et al. 2006, Natur, 441, 463
Fryer, C. L., Mazzali, P. A., Prochaska, J., et al. 2007, PASP, 119, 1211
Fryer, C. L., & New, K. C. B. 2011, LRR, 14, 1
Fryer, C. L., Oliveira, F. G., Rueda, J. A., & Ruffini, R. 2015, PhRvL, 115, 231102
Fryer, C. L., Rueda, J. A., & Ruffini, R. 2014, ApJL, 793, L36
Fryer, C. L., Woosley, S. E., & Hartmann, D. H. 1999, ApJ, 526, 152
Fynbo, J. P. U., de Ugarte Postigo, A., D'Elia, V., Xu, D., & Malesani, D. 2012, GCN, 13477, 1
Galama, T. J., Vreeswijk, P. M., van Paradijs, J., et al. 1998, Natur, 395, 670
Ghirlanda, G., Ghisellini, G., & Lazzati, D. 2004, ApJ, 616, 331
Giacconi, R., & Ruffini, R. 1978, Physics and Astrophysics of Neutron Stars and Black Holes (Amsterdam: North Holland)
Golenetskii, S., Aptekar, R., Frederiks, D., et al. 2013, GCN, 14487, 1
Goodman, J. 1986, ApJL, 308, L47
Graham, J. F., & Fruchter, A. S. 2017, ApJ, 834, 170
Graham, J. F., & Schady, P. 2016, ApJ, 823, 154
Greiner, J., Mazzali, P. A., Kann, D. A., et al. 2015, Natur, 523, 189
Grieco, V., Matteucci, F., Meynet, G., et al. 2012, MNRAS, 423, 3049
Gropp, J. D., Kennea, J. A., Klingler, N. J., et al. 2019, GCN, 23688, 1
Guetta, D., & Della Valle, M. 2007, ApJL, 657, L73
Hamburg, R., Veres, P., Meegan, C., et al. 2019, GCN, 23707, 1
Hawking, S. W. 1971, PhRvL, 26, 1344
Heger, A., Fryer, C. L., Woosley, S. E., Langer, N., & Hartmann, D. H. 2003, ApJ, 591, 288
Heintz, K. E., Fynbo, J. P. U., Jakobsson, P., et al. 2019, GCN, 25563, 1
Heisenberg, W., & Euler, H. 1936, ZPhy, 98, 714
Hjorth, J., & Bloom, J. S. 2012, in Gamma-Ray Bursts, ed. C. Kouveliotou, R. A. M. J. Wijers, & S. Woosley (Cambridge: Cambridge Univ. Press), 169
Hoeflich, P., Wheeler, J. C., & Wang, L. 1998, arXiv:astro-ph/9807345
Hu, Y. D., Castro-Tirado, A. J., Kumar, A., et al. 2021, A&A, 646, A50
Infante, L., Garnavich, P. M., Stanek, K. Z., & Wyrzykowski, L. 2001, GCN, 1152, 1
Itoh, R., Murata, K. L., Tachibana, Y., et al. 2018, GCN, 22983, 1
Iwamoto, K., Mazzali, P. A., & Nomoto, K. 1999, in Japanese-German Workshop on High Energy Astrophysics, ed. W. Becker & M. Itoh (Garching bei Munchen: Max-Planck-Institut für Extraterrestrische Physik), 123
Iwamoto, K., Nomoto, K., Höflich, P., et al. 1994, ApJL, 437, L115
Izzo, L., de Ugarte Postigo, A., Maeda, K., et al. 2019, Natur, 565, 324
Izzo, L., Kann, D. A., de Ugarte Postigo, A., et al. 2018, GCN, 23040, 1
Izzo, L., Rueda, J. A., & Ruffini, R. 2012a, A&A, 548, L5
Izzo, L., Ruffini, R., Penacchioni, A. V., et al. 2012b, A&A, 543, A10
Izzo, L., Selsing, J., Japelj, J., et al. 2017, GCN, 22180, 1
Jacobi, C. G. J. 1834, AnP, 109, 229
Jeans, J. H. 1928, Astronomy and Cosmogony (Cambridge: Cambridge Univ. Press)

Jelinek, M., Strobl, J., Hudec, R., & Polasek, C. 2018, GCN, 23024, 1
Jordana-Mitjans, N., Mundell, C. G., Kobayashi, S., et al. 2020, ApJ, 892, 97
Kankare, E., O'Neill, D., Izzo, L., et al. 2017, GCN, 22002, 1
Kann, D. A., Izzo, L., & Casanova, V. 2018, GCN, 22985, 1
Kann, D. A., Thoene, C. C., Selsing, J., et al. 2019, GCN, 23710, 1
Kelly, P. L., Kirshner, R. P., & Pahre, M. 2008, ApJ, 687, 1201
Kennea, J. A., Sbarufatti, B., Burrows, D. N., et al. 2017, GCN, 22183, 1
Kerr, R. P. 1963, PhRvL, 11, 237
Kim, H.-J., Yoon, S.-C., & Koo, B.-C. 2015, ApJ, 809, 131
Klebesadel, R. W., Strong, I. B., & Olson, R. A. 1973, ApJL, 182, L85
Klose, S., Schmidl, S., Kann, D. A., et al. 2019, A&A, 622, A138
Kobulnicky, H. A., & Fryer, C. L. 2007, ApJ, 670, 747
Kocevski, D., Omodei, N., Axelsson, M., et al. 2019, GCN, 23709, 1
Kohri, K., Narayan, R., & Piran, T. 2005, ApJ, 629, 341
Kumar, A., Pandey, S. B., Gupta, R., et al. 2022, NewA, 97, 101889
Leiderschneider, E., & Piran, T. 2021, PhRvD, 104, 104002
Levan, A. J., Tanvir, N. R., Fruchter, A. S., et al. 2014, ApJ, 792, 115
Li, L. 2023, ApJS, 266, 31
Li, L., Rueda, J. A., Moradi, R., et al. 2023, ApJ, 945, 10
Lian, J.-S., Wang, S.-Q., Gan, W.-P., Li, J.-Y., & Liang, E.-W. 2022, ApJ, 931, 90
Lien, A., Sakamoto, T., Barthelmy, S. D., et al. 2016, ApJ, 829, 7
Lindner, C. C., Milosavljević, M., Shen, R., & Kumar, P. 2012, ApJ, 750, 163
Lipunov, V., Gorbovskoy, E., Tiurina, N., et al. 2018, GCN, 23023, 1
Lyman, J. D., Bersier, D., James, P. A., et al. 2016, MNRAS, 457, 328
MacFadyen, A. I., & Woosley, S. E. 1999, ApJ, 524, 262
MacLaurin, C. 1742, A Treatise of Fluxions: In Two Books (Edinburgh: Ruddimans)
Madau, P., & Dickinson, M. 2014, ARA&A, 52, 415
Maeda, K., Nomoto, K., Mazzali, P. A., & Deng, J. 2006, ApJ, 640, 854
MAGIC Collaboration, Acciari, V. A., Ansoldi, S., et al. 2019, Natur, 575, 455
Maity, B., & Chandra, P. 2021, ApJ, 907, 60
Mao, S., & Yi, I. 1994, ApJL, 424, L131
Margutti, R., Guidorzi, C., Chincarini, G., et al. 2010, MNRAS, 406, 2149
Martone, R., Guidorzi, C., Kobayashi, S., et al. 2018, GCN, 22976, 1
Mazzali, P. A., Deng, J., Pian, E., et al. 2006, ApJ, 645, 1323
Mazzali, P. A., Deng, J., Tominaga, N., et al. 2003, ApJL, 599, L95
Melandri, A., Izzo, L., D'Avanzo, P., et al. 2019, GCN, 23983, 1
Melandri, A., Izzo, L., Pian, E., et al. 2022, A&A, 659, A39
Mészáros, P. 2002, ARA&A, 40, 137
Meszaros, P., Laguna, P., & Rees, M. J. 1993, ApJ, 415, 181
Mészáros, P., & Rees, M. J. 2001, ApJL, 556, L37
Metzger, M. R., Djorgovski, S. G., Kulkarni, S. R., et al. 1997, Natur, 387, 878
Miller, B. D. 1974, ApJ, 187, 609
Milosavljević, M., Lindner, C. C., Shen, R., & Kumar, P. 2012, ApJ, 744, 103
Minaev, P. Y., & Pozanenko, A. S. 2019, MNRAS, 492, 1919
Mirzoyan, R., Noda, K., Moretti, E., et al. 2019, GCN, 23701, 1
Moradi, R., Li, L., Rueda, J. A., et al. 2021a, arXiv:2103.09158
Moradi, R., Rueda, J. A., Ruffini, R., et al. 2021c, PhRvD, 104, 063043
Moradi, R., Rueda, J. A., Ruffini, R., & Wang, Y. 2021b, A&A, 649, A75
Mulchaey, J., Kasliwal, M. M., Arcavi, I., Bellm, E., & Kelson, D. 2013, ATel, 5191, 1
Nadyozhin, D. K. 2011a, IRAP Ph.D. Erasmus Mundus Workshop - Les Houches https://www.icranet.org/images/stories/Meetings/LES-HOUCHES/presentations/Nadyozhin1.pdf
Nadyozhin, D. K. 2011b, IRAP Ph.D. Erasmus Mundus Workshop - Les Houches https://www.icranet.org/images/stories/Meetings/LES-HOUCHES/presentations/Nadyozhin2.pdf
Nakar, E., & Piran, T. 2017, ApJ, 834, 28
Narayan, R., Paczynski, B., & Piran, T. 1992, ApJL, 395, L83
Narayan, R., Piran, T., & Shemi, A. 1991, ApJL, 379, L17
Negoro, H., Tanimoto, A., Nakajima, M., et al. 2018, GCN, 22993, 1
Newton, I. 1687, Philosophiae Naturalis Principia Mathematica (London: Royal Society)
Nomoto, K., & Hashimoto, M. 1988, PhR, 163, 13
Nomoto, K., Maeda, K., Nakamura, T., et al. 2003, in Origin of Matter and Evolution of Galaxies 2000, ed. T. Kajino et al. (Singapore: World Scientific), 223
Ostriker, J. P., & Gunn, J. E. 1969, ApJ, 157, 1395
Paczynski, B. 1986, ApJL, 308, L43
Pandey, S. B., Anupama, G. C., Sagar, R., et al. 2003, A&A, 408, L21
Patat, F., Cappellaro, E., Danziger, J., et al. 2001, ApJ, 555, 900
Perley, D. A., & Cockeram, A. M. 2019a, GCN, 25623, 1
Perley, D. A., & Cockeram, A. M. 2019b, GCN, 25657, 1
Pian, E., Mazzali, P. A., Masetti, N., et al. 2006, Natur, 442, 1011
Piran, T. 2004, RvMP, 76, 1143
Piran, T., Shemi, A., & Narayan, R. 1993, MNRAS, 263, 861
Poolakkil, S., Preece, R., Fletcher, C., et al. 2021, ApJ, 913, 60
Podsiadlowski, Ph., Mazzali, P. A., Nomoto, K., Lazzati, D., & Cappellaro, E. 2004, ApJ, 607, L17
Price, D. J. 2011, SPLASH: An Interactive Visualization Tool for Smoothed Particle Hydrodynamics Simulations, Astrophysics Source Code Library, ascl:1103.004
Prochaska, J. X., Bloom, J. S., Chen, H. W., et al. 2003, GCN, 2482, 1
Ramirez-Ruiz, E., Celotti, A., & Rees, M. J. 2002, MNRAS, 337, 1349
Raskin, C., Scannapieco, E., Rhoads, J., & Della Valle, M. 2008, ApJ, 689, 358
Rastegarnia, F., Moradi, R., Rueda, J. A., et al. 2022, EPJC, 82, 778
Rees, M. J., & Meszaros, P. 1992, MNRAS, 258, 41P
Roberts, O. J., & Meegan, C. 2018, GCN, 22981, 1
Roming, P. W. A., Kennedy, T. E., Mason, K. O., et al. 2005, SSRv, 120, 95
Ronchi, M., Fumagalli, F., Ravasio, M. E., et al. 2020, A&A, 636, A55
Rossi, A., Izzo, L., Milvang-Jensen, B., et al. 2018, GCN, 23055, 1
Rueda, J. A. 2021, ARep, 65, 1026
Rueda, J. A., Li, L., Moradi, R., et al. 2022a, ApJ, 939, 62
Rueda, J. A., & Ruffini, R. 2012, ApJL, 758, L7
Rueda, J. A., & Ruffini, R. 2020, EPJC, 80, 300
Rueda, J. A., & Ruffini, R. 2023, arXiv:2303.07760
Rueda, J. A., Ruffini, R., Karlica, M., Moradi, R., & Wang, Y. 2020, ApJ, 893, 148
Rueda, J. A., Ruffini, R., & Kerr, R. P. 2022b, ApJ, 929, 56
Rueda, J. A., Ruffini, R., Li, L., et al. 2022, PhRvD, 106, 083004
Rueda, J. A., Ruffini, R., Li, L., et al. 2022a, PhRvD, 106, 083004
Rueda, J. A., Ruffini, R., Li, L., et al. 2022b, IJMPD, 31, 2230013
Rueda, J. A., Ruffini, R., Moradi, R., & Wang, Y. 2021, IJMPD, 30, 2130007
Rueda, J. A., Ruffini, R., Wang, Y., et al. 2018, JCAP, 2018, 006
Rueda, J. A., Ruffini, R., & Wang, Y. 2019a, Univ, 5, 110
Rueda, J. A., Ruffini, R., Wang, Y., et al. 2019b, JCAP, 2019, 044
Ruffini, R., Aimuratov, Y., Bianco, C. L., et al. 2018c, GCN, 23019, 1
Ruffini, R., Aimuratov, Y., Bianco, C. L., et al. 2018d, GCN, 23066, 1
Ruffini, R., Aimuratov, Y., Bianco, C. L., et al. 2018f, GCN, 23019, 1
Ruffini, R., Becerra, L., Bianco, C. L., et al. 2018g, ApJ, 869, 151
Ruffini, R., Bernardini, M. G., Bianco, C. L., et al. 2007, in ESA Special Publication 622, The 6th Integral Workshop—The Obscured Universe, ed. S. Grebenev et al. (Noordwijk: ESA), 561
Ruffini, R., Bianco, C. L., Enderli, M., et al. 2013, GCN, 14526, 1
Ruffini, R., Izzo, L., Muccino, M., et al. 2014b, A&A, 569, A39
Ruffini, R., Karlica, M., Sahakyan, N., et al. 2018a, ApJ, 869, 101
Ruffini, R., Li, L., Moradi, R., et al. 2019d, arXiv:1904.04162
Ruffini, R., Melon Fuksman, J. D., & Vereshchagin, G. V. 2019a, ApJ, 883, 191
Ruffini, R., Moradi, R., Aimuratov, Y., et al. 2019b, GCN, 23715, 1
Ruffini, R., Moradi, R., Rueda, J. A., et al. 2019c, ApJ, 886, 82
Ruffini, R., Moradi, R., Rueda, J. A., et al. 2021, MNRAS, 504, 5301
Ruffini, R., Muccino, M., Aimuratov, Y., et al. 2016b, ApJ, 831, 178
Ruffini, R., Muccino, M., Bianco, C. L., et al. 2014a, A&A, 565, L10
Ruffini, R., Muccino, M., Kovacevic, M., et al. 2015, ApJ, 808, 190
Ruffini, R., Rodriguez, J., Muccino, M., et al. 2018b, ApJ, 859, 30
Ruffini, R., Rueda, J. A., Muccino, M., et al. 2016a, ApJ, 832, 136
Ruffini, R., Vereshchagin, G., & Xue, S. 2010, PhR, 487, 1
Ruffini, R., Wang, Y., Aimuratov, Y., et al. 2018e, ApJ, 852, 53
Ruffini, R., & Wheeler, J. A. 1971, in Proc. The Astrophysical Aspects of Weak Interactions (Rome: Accademia Nazionale dei Lincei), 165
Salvaterra, R., Della Valle, M., Campana, S., et al. 2009, Natur, 461, 1258
Sana, H., de Mink, S. E., de Koter, A., et al. 2012, Sci, 337, 444
Sasada, M., Nakaoka, T., Kawabata, M., et al. 2018, GCN, 22977, 1
Sauter, F. 1931a, ZPhy, 69, 742
Sauter, F. 1931b, ZPhy, 73, 547
Schmalz, S., Graziani, F., Pozanenko, A., et al. 2018, GCN, 23020, 1
Schulze, S., Malesani, D., Cucchiara, A., et al. 2014, A&A, 566, A102
Schwinger, J. 1948, PhRv, 74, 1439
Schwinger, J. 1949a, PhRv, 75, 651
Schwinger, J. 1949b, PhRv, 76, 790
Selsing, J., Fynbo, J. P. U., Heintz, K. E., & Watson, D. 2019, GCN, 23695, 1
Sfaradi, I., Bright, J., Horesh, A., et al. 2018, GCN, 23037, 1
Shemi, A., & Piran, T. 1990, ApJL, 365, L55
Shivvers, I., Modjaz, M., Zheng, W., et al. 2017, PASP, 129, 054201
Siegel, M. H., Burrows, D. N., Deich, A., et al. 2018, GCN, 22973, 1
Smartt, S. J. 2009, ARA&A, 47, 63
Smartt, S. J. 2015, PASA, 32, e016
Smith, N., Li, W., Silverman, J. M., Ganeshalingam, M., & Filippenko, A. V. 2011, MNRAS, 415, 773
Sparre, M., Sollerman, J., Fynbo, J. P. U., et al. 2011, ApJL, 735, L24
Tanaka, M., Yamanaka, M., Maeda, K., et al. 2009, ApJ, 700, 1680

Tanvir, N. R., Fox, D. B., Levan, A. J., et al. 2009, Natur, 461, 1254
Tanvir, N. R., Kruehler, T., Wiersema, K., et al. 2016, GCN, 20321, 1
Tauris, T. M., Kramer, M., Freire, P. C. C., et al. 2017, ApJ, 846, 170
Tauris, T. M., Langer, N., & Podsiadlowski, P. 2015, MNRAS, 451, 2123
Tauris, T. M., & van den Heuvel, E. P. J. 2006, in Compact Stellar X-ray Sources, ed. L. Lewin & M. van der Klis (Cambridge: Cambridge Univ. Press), 623
Teffs, J., Ertl, T., Mazzali, P., Hachinger, S., & Janka, T. 2020, MNRAS, 492, 4369
Thöne, C. C., Greiner, J., Savaglio, S., & Jehin, E. 2007, ApJ, 671, 628
Tsvetkova, A., Golenetskii, S., Aptekar, R., et al. 2019, GCN, 25660, 1
Ulanov, M. V., Golenetskii, S. V., Frederiks, D. D., et al. 2005, NCimC, 28, 351
Valeev, A. F., Castro-Tirado, A. J., Hu, Y. D., et al. 2019, GCN, 25565, 1
van den Heuvel, E. P. J., & Heise, J. 1972, NPhS, 239, 67
Vergani, S. D., Flores, H., Covino, S., et al. 2011, A&A, 535, A127
Vreeswijk, P., Fruchter, A., Hjorth, J., & Kouveliotou, C. 2003, GCN, 1785, 1
Vreeswijk, P., Fynbo, J., & Melandri, A. 2011, GCN, 12648, 1
Vreeswijk, P. M., Kann, D. A., Heintz, K. E., et al. 2018, GCN, 22996, 1
Vurm, I., Hascoët, R., & Beloborodov, A. M. 2014, ApJL, 789, L37
Wang, Y., Becerra, L. M., Fryer, C. L., Rueda, J. A., & Ruffini, R. 2023, ApJ, 945, 95
Wang, Y., Rueda, J. A., Ruffini, R., et al. 2019, ApJ, 874, 39
Wang, Y., Rueda, J. A., Ruffini, R., et al. 2022, ApJ, 936, 190
Watson, A. M., Butler, N., Becerra, R. L., et al. 2018, GCN, 23017, 1
Woosley, S. E. 1993, ApJ, 405, 273
Woosley, S. E., & Bloom, J. S. 2006, ARA&A, 44, 507
Xu, D., Yu, B. Y., Zhu, Z. P., et al. 2019, GCN, 25555, 1
Yamazaki, R., Yonetoku, D., & Nakamura, T. 2003, ApJL, 594, L79
Yoon, S.-C. 2015, PASA, 32, e015
Yoon, S.-C., Woosley, S. E., & Langer, N. 2010, ApJ, 725, 940
Yüksel, H., Kistler, M. D., Beacom, J. F., & Hopkins, A. M. 2008, ApJL, 683, L5
Zapartas, E., de Mink, S. E., Justham, S., et al. 2019, A&A, 631, A5
Zeh, A., Klose, S., & Hartmann, D. H. 2004, ApJ, 609, 952
Zhang, B. 2018, The Physics of Gamma-Ray Bursts (Cambridge: Cambridge Univ. Press)
Zhang, B. 2019, Natur, 575, 448
Zhang, W., Woosley, S. E., & Heger, A. 2004, ApJ, 608, 365
Zheng, W., & Filippenko, A. V. 2018, GCN, 23033, 1

Draft version September 26, 2023
Typeset using LaTeX **preprint** style in AASTeX63

Probing electromagnetic-gravitational wave emission coincidence in type I binary-driven hypernova family of long GRBs at very-high redshift

C. L. Bianco,[1,2,3,4] M. T. Mirtorabi,[1,5] R. Moradi,[1,2,6] F. Rastegarnia,[1,7] J. A. Rueda,[1,2,8,9,4] R. Ruffini,[1,2,10] Y. Wang (王瑜),[2,1,6] M. Della Valle,[11,1] Liang Li (李亮),[1,2,6] and S. R. Zhang (张书瑞)[1,8,12,13]

[1] ICRANet, Piazza della Repubblica 10, I-65122 Pescara, Italy
[2] ICRA, Dip. di Fisica, Sapienza Università di Roma, Piazzale Aldo Moro 5, I-00185 Roma, Italy
[3] Université de Nice Sophia-Antipolis, Grand Château Parc Valrose, Nice, CEDEX 2, France
[4] INAF, Istituto di Astrofisica e Planetologia Spaziali, Via Fosso del Cavaliere 100, 00133 Rome, Italy
[5] Department of Fundamental Physics, Faculty of Physics, Alzahra University, Tehran, Iran
[6] INAF – Osservatorio Astronomico d'Abruzzo, Via M. Maggini snc, I-64100, Teramo, Italy
[7] Department of Physics, Faculty of Physics and Chemistry, Alzahra University, Tehran, Iran
[8] ICRANet-Ferrara, Dip. di Fisica e Scienze della Terra, Università degli Studi di Ferrara, Via Saragat 1, I–44122 Ferrara, Italy
[9] Dip. di Fisica e Scienze della Terra, Università degli Studi di Ferrara, Via Saragat 1, I–44122 Ferrara, Italy
[10] INAF, Viale del Parco Mellini 84, 00136 Rome, Italy
[11] INAF - Osservatorio Astronomico di Capodimonte, Salita Moiariello 16, I-80131, Napoli, Italy
[12] School of Astronomy and Space Science, University of Science and Technology of China, Hefei 230026, China
[13] CAS Key Laboratory for Research in Galaxies and Cosmology, Department of Astronomy, University of Science and Technology of China, Hefei 230026, China

(Received ddmmyyyy; Revised September 26, 2023; Accepted ddmmyyyy; Published ddmmyyyy)

Submitted to ApJ

ABSTRACT

Due to the technical time delay of the XRT instrument on board the Neil Gehrels Swift Observatory satellite, we cannot observe the X-ray emission less than ~ 40 s after a gamma-ray burst (GRB) trigger. We here indicate a new strategy of using the cosmological time dilatation in high redshift GRBs to observe the earliest X-ray emission by Swift/XRT. We use 354 GRBs with a cosmological redshift from the Swift catalog, including short and long GRBs. We first analyze the redshift distributions of the long GRBs of the different binary-driven hypernova (BdHN) families. We infer that the further evolution of BdHNe II and III may be short GRB progenitors. We then compare and contrast the time delay between the GRB trigger and the first observation by Swift/XRT, measured in the observer frame (OTD), and the corresponding delay measured in GRBs' cosmological rest-frame (RTD). We consider as prototypes three BdHNe I: GRB 090423 at $z = 8.2$ with an RTD of 8.2 s, GRB 090429B at $z \sim 9.4$ with an RTD of 10.1 s, GRB 220101A at $z = 4.61$ with an RTD of 14.4 s. This opens a new possibility for probing Episode (1) of BdHNe, linked to the newborn neutron star (νNS) early appearance. In all three cases, we evidence a first regime related to the νNS spin-up by the supernova ejecta fallback and a second regime leading to the νNS slowing down by the X-ray, optical, and radio synchrotron emission. These two phases may be separated by a very short gravitational wave emission due to a fast spinning νNS triaxial configuration.

1. INTRODUCTION

Interestingly, important astronomical breakthroughs are often marked by the possibility of studying events occurring in the nearby universe. There are several prominent examples, e.g., SN 1987A; its proximity has allowed the first detection of neutrinos (Hirata et al. 1987; Alexeyev et al. 1988; Bionta et al. 1987) and the observation of the shock-breakout (Arnett et al. 1989). Another example is GRB 980425 and SN 1998bw, the prototype of GRB-SN connection (Galama et al. 1998; Patat et al. 2001), which occurred at about 40 Mpc. It is still the closest case of GRB-SN connection observed so far. More recently, we expect important results from

ruffini@icra.it

the observation of SN 2023ixf exploded at only ~ 6 Mpc in M101 (Perley et al. 2023), whose explosion time was constrained, due to its proximity, to about 1 h (Yaron et al. 2023). The problem of the GRB-SN connection has been addressed in Aimuratov et al. (2023), where the BdHN model has been illustrated. Unlike the cases briefly illustrated above, in this work, we show how the observation of GRBs at very high redshift, by exploiting the time dilatation factor $(1+z)$, can allow us to enter the "terra incognita" of the very early GRB X-ray emission currently inaccessible in nearby events. Paradoxically, they would be more suitable to be studied, but the significant delay in the observer's rest frame prevents their early X-ray emission observations.

Our analysis has been made possible by the GRB binary-driven hypernova (BdHN) model (see Sec. 2). We used a sample of 354 GRBs present in the Swift GRB database (see https://swift.gsfc.nasa.gov/archive/grb_table/) with a measured redshift (see Sec. 3), which includes both short and long GRBs. We first analyze the redshift distributions of the long GRBs belonging to the different BdHN families, and we infer that the further evolution of BdHNe of types II and III may be progenitors of short GRBs (see Sec. 3). We then define the observed time delay (OTD) as the time after the GRB trigger needed by Swift/XRT to repoint the source measured in the observer frame[1] (for details see Sec. 4 and, e.g., E. Troja, "The Neil Gehrels Swift Observatory Technical Handbook Version 17.0", https://swift.gsfc.nasa.gov/proposals/tech_appd/swiftta_v17.pdf, as well as Gehrels et al. 2004). The minimum OTD in our sample is 43.88 s from GRB 140206A at redshift $z = 2.73$ (marked by a horizontal green line in the plot). It is then clear that Swift/XRT is generally technically unable to observe the X-ray emission in the first tens of seconds after the GRB trigger. Hence, the X-ray emission occurring within ~ 40 s of the GRB trigger remains unobservable, making this time interval an uncharted new X-ray territory. This large OTD can be circumvented by considering the cosmological corrections presented in this article and turning to the cosmological rest-frame time delay (RTD, see Sec. 4).

After introducing in Sec. 5 the k-correction and the 0.3–10 keV luminosity light curves, in Sec. 6 special attention is dedicated to the three prototypes of BdHNe I: GRB 220101A at $z = 4.61$ (Fu et al. 2022; Perley 2022; Fynbo et al. 2022); GRB 090423 at $z = 8.2$ (Salvaterra et al. 2009; Tanvir et al. 2009; Ruffini et al. 2014); as well as GRB 090429B at a photometric redshift $z \sim 9.4$ (Cucchiara et al. 2011). They set the record for the smallest RTD values. Their excellent data creates the condition to analyze the new physics just after the SN-rise, giving for the first time the opportunity to identify the physical processes occurring in the νNS-rise as announced in Aimuratov et al. (2023); Rueda et al. (2022c).

[1] Namely, the column "XRT Time to First Observation [sec]" in the Swift GRB catalog, see https://swift.gsfc.nasa.gov/archive/grb_table/.

2. THE BINARY DRIVEN HYPERNOVA (BDHN) MODEL

Within the BdHN model, long GRBs have a common progenitor: a binary comprising a carbon-oxygen (CO) star and a neutron star (NS) companion with binary periods ranging from minutes to hours. The CO core collapse generates a newborn NS (νNS) and the Supernova (SN). The latter triggers the GRB emission episodes through physical processes, leading to seven episodes with spectral signatures in the precursor, MeV prompt, GeV and TeV emissions, X-optical-radio afterglow, and optical SN emission. They involve the physics of the early SN, NS accretion, black hole (BH) formation, synchrotron radiation, BH gravitomagnetism, and quantum and classic electrodynamics processes to extract the BH rotational energy.

Three different types of BdHNe have been defined, corresponding to the diversity of long GRBs:

1. BdHNe I are the most extreme with energies 10^{52}–10^{54} erg. Their orbital periods are about 5 minutes. In these sources, the material ejected in the SN is easily accreted by the NS companion, so it reaches the point of gravitational collapse, forming a rotating BH. As we point out in this article, in Sec. 3, such BdHNe of type I do follow the cosmic star-formation rate very closely (see, e.g., Madau & Dickinson 2014).

2. BdHNe II have orbital periods of 20–40 minutes and emit energies 10^{52}–10^{54} erg. The accretion is lower, so the NS remains stable.

3. BdHN III have orbital periods of hours, and the accretion is negligible. They explain GRBs with energies lower than 10^{50} erg.

In Ruffini et al. (2018b), the idea that BdHNe II and III may end up in remnant binary systems that, in turn, can later become progenitors of short GRBs has been advanced. This hypothesis is supported by analyzing the redshift distributions of the different GRB families presented in Sec. 3.

A representative (but incomplete) set of references of the BdHN model is Rueda & Ruffini (2012); Fryer et al. (2014, 2015); Becerra et al. (2016); Ruffini et al.

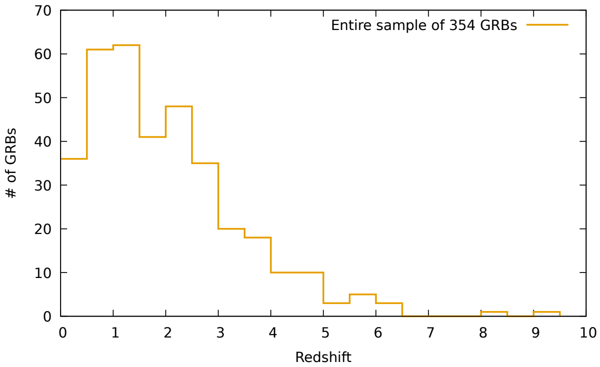

Figure 1. The distribution of the redshifts of the 354 GRBs in our sample (see Table 1).

(2018c,a); Becerra et al. (2019); Ruffini et al. (2019); Rueda & Ruffini (2020); Moradi et al. (2021); Ruffini et al. (2021); Rueda et al. (2022b,a); Wang et al. (2022); Rueda et al. (2022c); Becerra et al. (2022); Li et al. (2023), and we refer the reader to Aimuratov et al. (2023) for the latest discussion and novelties of the model.

As indicated in Aimuratov et al. (2023), we have identified a sequence of seven Episodes in the most general BdHN. These seven episodes start with an *episode zero*, Episode (0), representing the onset of the SN (SN-rise), originated in the CO core collapse. Coeval with the SN-rise is the νNS appearance (νNS-rise), i.e. Episode (1), in which the fallback accretion of SN ejecta spins up the νNS. The νNS-rise can be only observed in the X-rays by Swift/XRT. The further evolution of the νNS leads to the X-ray afterglow originating from the synchrotron radiation, also emitted in the optical and radio bands by the spinning νNS. We refer to Aimuratov et al. (2023) and references therein for details. To study the CO core collapse and the birth process of the νNS, it is essential to have more early data to identify the νNS-rise and its temporal evolution into the afterglow, which is indeed the topic of this paper. This article aims to introduce a new methodology for analyzing the earliest Swift/XRT data in the rest frame of the source, taking advantage of the case of GRBs with large cosmological redshift z.

3. THE SAMPLE OF 354 GRBS AND THEIR REDSHIFT DISTRIBUTION

Our sample comprises 354 GRBs observed by Swift/XRT (see Table 1) and has been built by including all GRBs that respect the following three criteria:

1. The GRB is present in the Swift GRB database (see https://swift.gsfc.nasa.gov/archive/grb_table/).
2. The GRB has a measured redshift reported in the Swift GRB database.
3. The GRB has XRT observations with a measured delay between the GRB trigger time and the moment of the first Swift/XRT observation.

In Fig. 1, we present the distribution of the redshifts of the 354 GRBs in our sample (see Table 1). It has a double-peak structure, with one peak around $z \sim 1$ and another between $z \sim 2$ and $z \sim 2.5$.

To investigate the reason behind this double-peak structure, we emphasize that our sample of 354 GRBs includes every possible kind of GRB (long, short, etc.). The only requirement is the matching of the above-mentioned three criteria. Within the BdHNe model, there are identified several different GRB families (Aimuratov et al. 2023, and references therein), each one with a different kind of progenitor system and, therefore, in principle, with a different redshift distribution. A detailed analysis of the redshift distribution of all the different GRB families implied by the BdHNe model is outside the scope of the present paper. Here, we are presenting only a very preliminary analysis of our sample of 354 GRBs to justify the presence of the double-peak in Fig. 1. We have that:

- Ruffini et al. (2021) made a catalog of all BdHNe I exploded until December 2018. Our sample has 50 GRBs out of the 354 detected after December 2018. Therefore, for the moment, we are excluding these 50 from the analysis of the redshift distribution, and we are left with 304 GRBs.
- Of these 304 GRBs, 216 are catalogued as BdHNe I by Ruffini et al. (2021), while the other 88 are not.
- Of these remaining 88 GRBs, 21 have an observed prompt emission duration $T_{90} < 2$ s, then they can be classified as short GRBs. They are too few to be further divided among the different families of short GRBs implied by the BdHN model. Therefore, we are considering together the redshift distribution of all these 21 short GRBs.
- Of the remaining 67 GRBs, 3 have no observed T_{90} duration in the Swift catalog and are therefore excluded from the analysis. We are left with 64 GRBs with an observed prompt emission duration $T_{90} > 2$ s which are not cataloged by Ruffini et al. (2021) as BdHNe I and which therefore are either BdHNe II or BdHNe III. A further division of these 64 GRBs into BdHNe II and BdHNe III requires an extra analysis of each of them, which is outside

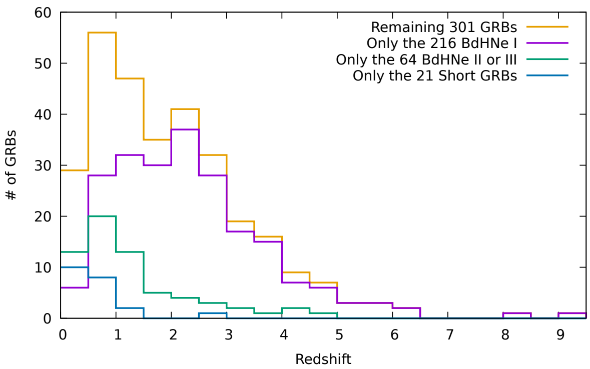

Figure 2. The distributions of the redshifts of the selected 301 GRBs in our sample, divided into the different GRB families indicated by the BdHNe model.

the paper's scope. Then, we consider the redshift distribution of all these 64 GRBs together.

In summary, among our sample of 354 GRBs, 53 sources have to be excluded from this preliminary analysis of the redshift distribution of each GRB family for the above-mentioned reasons, while the 301 remaining GRBs can be divided as follows:

- 216 GRBs are BdHNe I;
- 64 GRBs are BdHNe II or BdHNe III;
- 21 GRBs are short GRBs.

Figure 2 shows the distributions of the redshifts of each of these three groups and all 301 GRBs together. We can see that the redshift distribution of all 301 GRBs together presents the same double-peak structure of the entire sample of 354 GRBs plotted in Fig. 1. We can also see that the redshift distribution of BdHNe I presents a single peak between $z \sim 2$ and $z \sim 2.5$ and appears to follow the cosmic star-formation rate very closely (see, e.g., Madau & Dickinson 2014), while the distribution of BdHNe II and III presents a single peak around $z \sim 1$ and that of short GRBs presents a single peak for $z < 0.5$. This last fact supports the idea, advanced in Ruffini et al. (2018b), that BdHNe II and III may end up in remnant binary systems that, in turn, can later become progenitors of short GRBs. We can then conclude that the double peak structure in the redshift distribution of our sample of 354 GRBs is due to the superposition of the different redshift distributions of the different GRB families.

4. THE NEIL GEHRELS SWIFT/XRT OBSERVED TIME DELAY (OTD) COMPARED AND CONTRASTED WITH THE COSMOLOGICAL REST-FRAME TIME DELAY (RTD)

We now focus on examining the Swift/XRT time delays in our sample of 354 GRBs as a function of their cosmological redshift. We define the observed time delay (OTD) as the time after the GRB trigger needed by Swift/XRT to repoint the source measured in the observer frame[2] (see Gehrels et al. 2004, for more information) and we plot this quantity in Fig. 3. The minimum OTD in our sample is 43.88 s from GRB 140206A at redshift $z = 2.73$ (marked by a horizontal green line in the plot). The OTD for most GRBs lies between 50 s and 150 s and peaks at ~ 80 s, as shown in the upper panel of Fig. 4. Table 1 presents the complete list of the 354 GRBs in our sample and their OTD in seconds.

It is then clear that Swift/XRT is generally unable to observe the X-ray emission in the first 43 seconds after the GRB trigger. This is because it takes at least between 10 s and 20 s for the Swift satellite to automatically realize that a Swift/BAT trigger condition occurred, to compute the coordinates of the source, to check if a slewing to those coordinates is possible, and to start slewing to put the source in the Swift/XRT field of view; the actual slewing time is between 20 s and 75 s (for details see, e.g., E. Troja, "The Neil Gehrels Swift Observatory Technical Handbook Version 17.0", https://swift.gsfc.nasa.gov/proposals/tech_appd/swiftta_v17.pdf, as well as Gehrels et al. 2004). Hence, X-ray events occurring within ~ 40 s of the GRB trigger remain unobservable by Swift/XRT, making this time interval an uncharted new territory in X-ray. Our knowledge during this phase, which corresponds to the prompt emission of GRBs, is confined to fewer than 100 detections made by BeppoSAX and HETE-2 (see, e.g., Tamagawa et al. 2003; Costa & Frontera 2011; Frontera 2019).

Interestingly, this large OTD can be circumvented by considering the cosmological corrections presented in this article and turning to the cosmological rest-frame time delay (RTD) in seconds. This procedure has been routinely applied in our approach (see, e.g., Ruffini et al. 2021, and references therein). Due to the cosmological time dilation, a time interval Δt measured on Earth corresponds to a time interval $\Delta t/(1+z)$ in the cosmological source rest-frame, where z is its cosmological redshift. In other words, a phenomenon appearing to our instruments on the Earth to last 50 s may last 10 s if the source is at $z = 4$, like if we were observing the phenomenon in slow motion.

[2] Namely, the column "XRT Time to First Observation [sec]" in the Swift GRB catalog, see https://swift.gsfc.nasa.gov/archive/grb_table/.

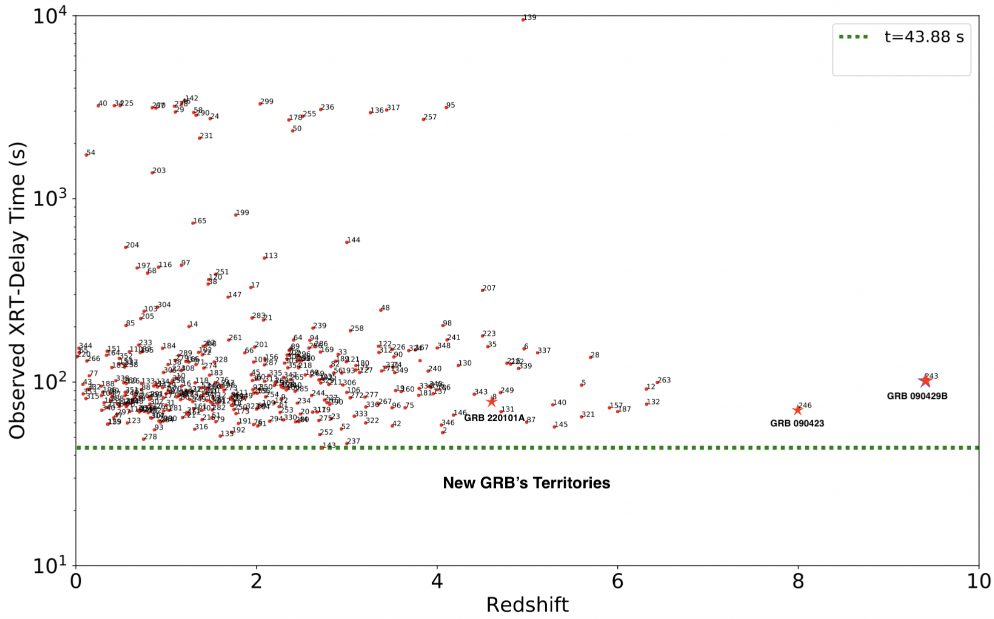

Figure 3. The Swift/XRT time delay in the observer's frame (OTD). Red stars mark GRB 220101A at $z = 4.61$, GRB 090423 at $z = 8.2$, and GRB 090429B at $z \sim 9.4$.

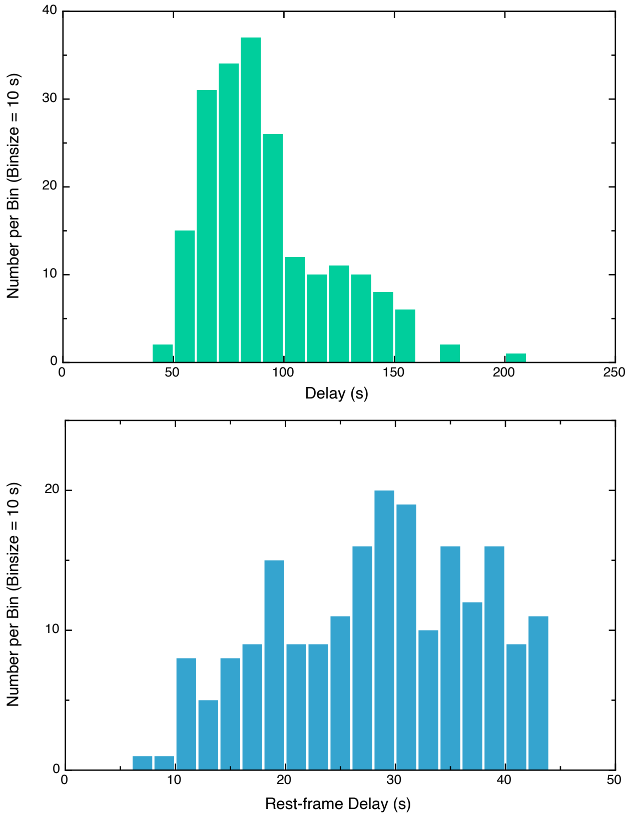

Figure 4. The histogram of Swift-XRT time delays in the observer's frame (OTD, upper panel) and the cosmological rest-frame (RTD, lower panel).

Therefore, the OTD needed by Swift/XRT to start its observations after the GRB trigger may correspond to a much shorter actual RTD for sources with a large redshift z, exactly by a factor $(1 + z)$. If, e.g., XRT starts to observe a GRB 60 s after the trigger in the observer frame, it is observing the X-ray signals emitted $60/(1 + z)$ s after the trigger in the rest-frame of the source. This corresponds to the possibility of observing 10 s after the trigger for a GRB with $z = 5$: the higher the GRB redshift, the shorter the time Swift/XRT can observe the source after the GRB trigger.

This is clearly shown in Fig. 5, where we present the time delays of the upper panel converted in the cosmological rest frame of each source; see also Table 1 where we compare and contrast OTD and RTD. The green line still marks the 43.88 s minimum OTD, and the red line corresponds to this minimum OTD rescaled as a function of the redshift of the source: $43.88/(1 + z)$ s. Many sources, which were observed by Swift/XRT with an OTD greater than 43.88 s, would not have been deemed interesting from the early X-ray emission point of view. However, thanks to their large cosmological redshift, when looking at their RTD, it is clear that they have been observed 10 s after the trigger and allow us to observe the new physical process in Episode (1) related to the νNS-rise of GRBs.

After this conversion of the time delays in the cosmological rest-frame of each source, the recorded minimum RTD in the sample of 354 GRBs is $\sim$ 8 s from

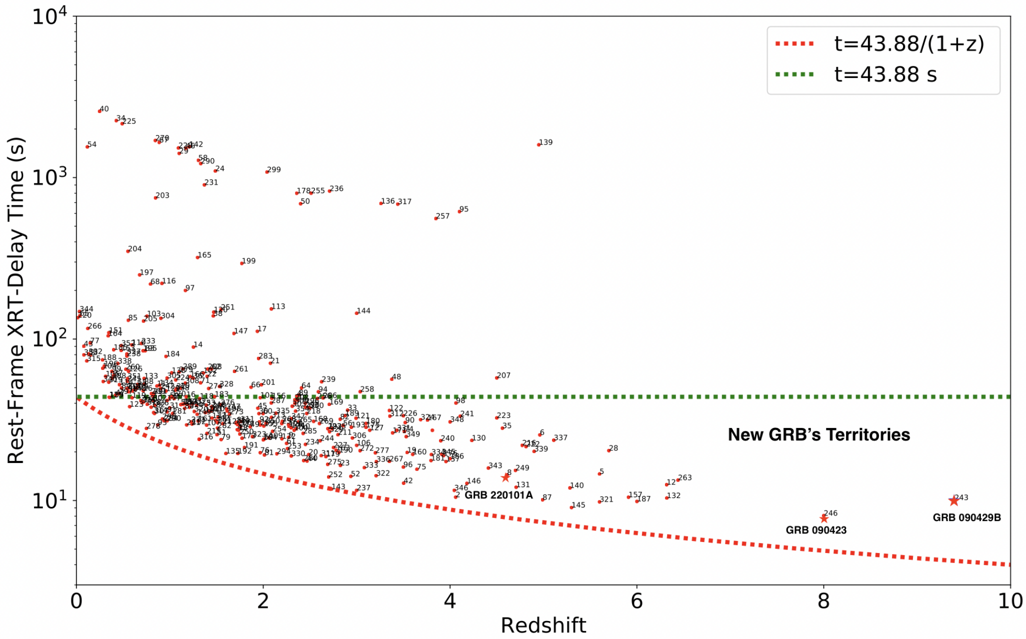

Figure 5. The Swift/XRT time delay in the cosmological rest-frame (RTD). Red stars mark GRB 220101A at $z = 4.61$, GRB 090423 at $z = 8.2$, and GRB 090429B at $z \sim 9.4$.

GRB 090423 at redshift $z = 8.2$. The RTD range for most of the bursts is between 10 s and 45 s, with a peak at ~ 30 s, as shown in the lower panel of Fig. 4.

Therefore, observing GRBs with large values of z represents an invaluable tool for exploring transient X-ray regimes, which occur after the GRB trigger time and the SN-rise described in Episode 0, to unveil the physical processes taking place during the νNS-rise (Episode 1).

5. K-CORRECTION AND 0.3–10 KEV LUMINOSITY LIGHT CURVES

The photon index during the early afterglow of a GRB sometimes exhibits significant variations, especially in the steep decay or X-ray flare periods, where the photon index can deviate from the average value of ~ 2 in the afterglow, evolving between approximately 1 and 4. When calculating the GRB luminosity based on the observed flux, we need to consider the k-correction, a function of the photon index. Therefore, we must consider time-resolved k-correction when dealing with early afterglow data. For some bursts, the shape of the luminosity light curve of the early afterglow generated by time-resolved k-correction differs from that generated by time-integrated k-correction (see details in Ruffini et al. 2018c; Wang et al. 2023).

6. THE PROTOTYPICAL CASES OF GRB 220101A, GRB 090423, GRB 090429B

We now analyze specifically our prototypical cases:

- GRB 220101A has a redshift $z = 4.61$, the OTD is 80.78 s corresponding to an RTD of 14.40 s. Swift/XRT 0.3–10 keV luminosity is shown in Fig. 6. The orange strip marks the data before ~ 45 s, which is observable only thanks to the high source redshift. The best-fit parameters of the decaying part are $A_{\rm X} = (1.80 \pm 0.11) \times 10^{53}$ erg/s, and $\alpha = -1.26 \pm 0.01$ representing the X-ray afterglow.

- GRB 090423 has a redshift $z \sim 8.2$, the OTD is 72.48 s corresponding to an RTD of ~ 8 s. Swift-XRT 0.3–10 keV luminosity is shown in Fig. 7. The orange strip marks the data before ~ 45 s, which is observable only thanks to the high source redshift. The best-fit parameters of the decaying part are $A_{\rm X} = (2.18 \pm 0.49) \times 10^{52}$ erg/s, and $\alpha = -1.37 \pm 0.03$ representing the X-ray afterglow.

- GRB 090429B has a photometric redshift $z \sim 9.4$. The OTD is 104.69 s, corresponding to an RTD of ~ 10.1 s. Swift-XRT 0.3–10 keV luminosity is shown in Fig. 8. The orange strip marks the data before ~ 45 s, which is observable only thanks to the high source redshift. The best-fit parameters of the decaying part are $A_{\rm X} = (1.05 \pm 0.13) \times 10^{52}$ erg/s, and $\alpha = -1.28 \pm 0.19$ representing the X-ray afterglow.

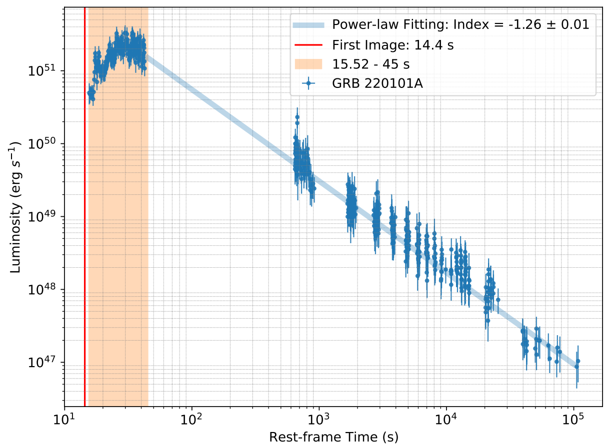

Figure 6. The Swift-XRT 0.3–10 keV luminosity of GRB 220101A in the cosmological rest-frame. The red line at 14.4 s corresponds to the first observation by XRT while still in Image mode before switching to Windowed Timing (WT) mode (for details, see, e.g., E. Troja, "The Neil Gehrels Swift Observatory Technical Handbook Version 17.0", https://swift.gsfc.nasa.gov/proposals/tech_appd/swiftta_v17.pdf, as well as Gehrels et al. 2004). The orange strip, which extends from 15.52 s to 45 s, indicates the data observable thanks to the cosmological effect at $z = 4.61$ duly considered in this article. There are other data points between 13.3 s and 14.4 s corresponding to observations performed while Swift was still slewing to the source location, and has not been considered in this paper. The blue line is a power-law fitting function of the form $A_X t^\alpha$ whose best-fit parameters are: $A_X = (1.80 \pm 0.11) \times 10^{53}$ erg/s, and $\alpha = -1.26 \pm 0.01$.

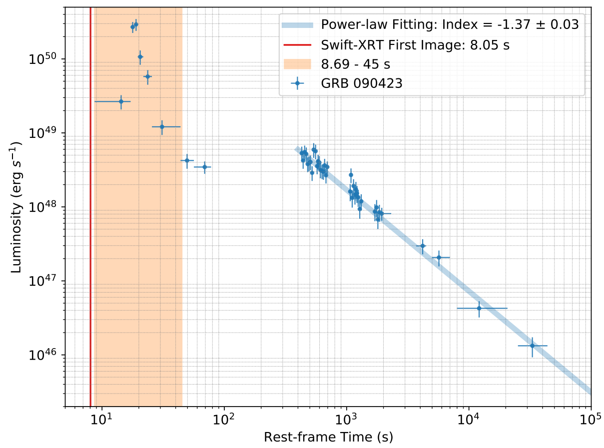

Figure 7. The Swift-XRT 0.3–10 keV luminosity of GRB 090423 in the cosmological rest-frame. The red line corresponds to the first observation by XRT while still in Image mode before switching to Windowed Timing (WT) mode (for details, see, e.g., E. Troja, "The Neil Gehrels Swift Observatory Technical Handbook Version 17.0", https://swift.gsfc.nasa.gov/proposals/tech_appd/swiftta_v17.pdf, as well as Gehrels et al. 2004). The orange strip, which extends from 8.69 s to 45 s, indicates the data observable thanks to the cosmological effect at $z = 8.2$ duly considered in this article. The blue line is a power-law fitting function of the form $A_X t^\alpha$ whose best-fit parameters are: $A_X = (2.18 \pm 0.49) \times 10^{52}$ erg/s, and $\alpha = -1.37 \pm 0.03$.

7. CONCLUSION

We can summarize three main conclusions:

1. In this article, we have introduced the use of the time dilation in high-redshift GRBs for the first time to overcome the observed instrumental time delay, greater than 43 s, between the GRB trigger time and the first X-ray observations by Swift/XRT. This time delay has traditionally hampered the observations of Episode (1) in BdHNe (see, e.g., Aimuratov et al. 2023). The methodology has been developed using a sample of 354 GRBs, reported in Table 1, all with an identified redshift. When measured in the observer frame, the time delay (OTD) between the earliest X-ray emission and the GRB trigger time is always larger than 40 s (see Fig. 3 and Fig. 4). In contrast, a substantially shorter time delay is observed in the rest frame of the source (RTD, see Fig. 4 and Fig. 5). This new methodology, focused on three BdHNe I at high redshift, has allowed us to unveil the occurrence of the νNS emission increasing with time, preceding the traditional X-ray afterglow emission decreasing in time with a specific power-law index.

2. Equally important is the byproduct of analyzing the redshift distribution of all the 354 GRBs of the sample, and in particular of the 216 BdHN I, of the 64 BdHNe II and III and of the 21 short GRBs contained in the sample, as presented in Fig. 1 and Fig. 2. The distribution of the 354 sources presents two peaks: the first at $z \sim 1$ and the second, dominated by the BdHN I component, at $z = 2$ reminiscent of the cosmic star-formation rate (Madau & Dickinson 2014). The similarity between the redshift distribution of BdHNe II and III and that of short GRBs supports the idea, advanced in Ruffini et al. (2018b), that BdHNe II and III may end up in remnant binary systems that, in turn, can later become progenitors of short GRBs.

3. The most eloquent example is the case of one of the most powerful GRBs ever detected, GRB 220101A, at $z = 4.61$. This source allows the identification of all the seven episodes of a BdHN, except for the late radioactive decay of the SN ashes, given the source's high redshift.

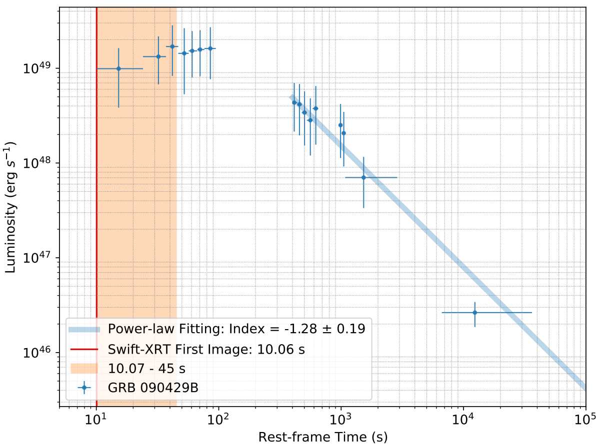

Figure 8. The Swift-XRT 0.3–10 keV luminosity of GRB 090429B in the cosmological rest-frame. The red line corresponds to the first observation by XRT while still in Image mode before switching to Windowed Timing (WT) mode (for details, see, e.g., E. Troja, "The Neil Gehrels Swift Observatory Technical Handbook Version 17.0", https://swift.gsfc.nasa.gov/proposals/tech_appd/swiftta_v17.pdf, as well as Gehrels et al. 2004). The orange strip, which extends from 10.07 s to 45 s, indicates the data observable thanks to the cosmological effect at $z = 9.4$ duly considered in this article. The blue line is a power-law fitting function of the form $A_X t^{\alpha}$ whose best-fit parameters are: $A_X = (1.05 \pm 0.13) \times 10^{52}$ erg/s, and $\alpha = -1.28 \pm 0.19$.

In particular, GRB 220101A shows the SN-rise (Episode 0) triggering the entire GRB (Ruffini et al., 2023, in preparation). Especially significant are the unexpected high-quality data associated with the Swift/XRT observations of the νNS-rise (Episode 1). As shown in Fig. 6, the X-ray emission observed by Swift/XRT starts 14.4 s after the trigger, following the end of the SN-rise and indicating the spin-up phase of the νNS by the fallback accretion of matter initially ejected by the SN, followed by the slowing down phase corresponding to the decaying part of the X-ray afterglow (Wang et al. 2023; Rueda et al. 2022a; Becerra et al. 2022; Rueda et al. 2022c). The unexpected very high quality of the Swift/XRT data also applies to GRB 090423 at $z = 8.2$ (see Fig. 7) and GRB 090429B at $z = 9.4$ (see Fig. 8): in both cases the first Swift/XRT data shows the νNS spin-up phase, extending up to 10^2 s and followed by the slowing down phase corresponding to the decaying part of the X-ray afterglow. One of the key questions to be addressed is the possibility that these two phases can be separated by a very short-time process of gravitational wave emission due to a triaxial configuration of the fast spinning νNS.

Indeed, a fantastic opportunity exists for new missions with wide field-of-view soft X-ray instruments designed to simultaneously observe the GRB X-ray and gamma-ray emissions from 0.3 keV to 10 MeV since the moment of the GRB trigger and without any time delay, such as, e.g., THESEUS (Amati et al. 2018, 2021).

ACKNOWLEDGMENTS

We express our gratitude to an anonymous referee whose suggestions greatly improved the presentation of our results. We are grateful to B. Cenko and J. Kennea for their important clarifications on the timing of the Swift automatic slew system. We are also grateful for the fruitful discussions with Y. Aimuratov, L. Amati, L. M. Becerra, C. Cherubini, and N. Sahakyan, which have led to these new results.

Table 1. List of GRBs observed by Swift/XRT and their observed time delay (OTD) and cosmological rest-frame time delay (RTD) in seconds. The delay time is between the initial burst detection and the start time of the first XRT observation. The XRT start time data is sourced from https://swift.gsfc.nasa.gov/archive/grb_table/. The bold GRB names in this table indicate GRBs with an RTD of less than 43.9 s, namely shorter than the minimum OTD.

#	GRB	redshift	OTD (s)	RTD (s)
1	**221226B**	2.694	102.93	27.86
2	**221110A**	4.06	53.05	10.48
3	221009A	0.151	91.6	79.58
4	220611A	2.3608	149.22	44.4
5	**220521A**	5.6	96.34	14.6
6	**220117A**	4.961	151.94	25.49
7	220107A	1.246	26700.0	11887.8
8	**220101A**	4.61	80.78	14.4
9	**211207A**	2.272	80.5	24.6
10	211024B	1.1137	105.0	49.68
11	211023B	0.862	95.3	51.18
12	**210905A**	6.318	91.7	12.53
13	**210822A**	1.736	74.56	27.25
14	210731A	1.2525	200.92	89.2
15	**210722A**	1.145	84.84	39.55
16	**210702A**	1.1757	95.5	43.89
17	210619B	1.937	328.05	111.7
18	**210610B**	1.13	83.92	39.4
19	**210610A**	3.54	89.95	19.81
20	**210517A**	2.486	67.05	19.23
21	210504A	2.077	218.0	70.85
22	210420B	1.4	141.0	58.75
23	**210411C**	2.826	63.14	16.5
24	210321A	1.487	2730.62	1097.96
25	**210222B**	2.198	95.87	29.98
26	210210A	0.715	82.09	47.87
27	**201221D**	1.046	87.42	42.73
28	**201221A**	5.7	136.48	20.37
29	201216C	1.1	2966.8	1412.76
30	**201104B**	1.954	102.0	34.53
31	**201024A**	0.999	74.89	37.46
32	201021C	1.07	101.97	49.26
33	**201020A**	2.903	141.53	36.26
34	201015A	0.426	3214.07	2253.91
35	**201014A**	4.56	156.0	28.06
36	200829A	1.25	128.71	57.2
37	200522A	0.4	83.42	59.59
38	200205B	1.465	342.71	139.03
39	**191221B**	1.19	86.25	39.38
40	191019A	0.248	3210.93	2572.86
41	**191011A**	1.722	74.78	27.47
42	**191004B**	3.503	57.66	12.8
43	190829A	0.0785	97.31	90.23
44	**190719C**	2.469	60.93	17.56
45	**190627A**	1.942	109.76	37.31
46	190324A	1.1715	3297.89	1518.72
47	190114C	0.42	63.95	45.04
48	190114A	3.3765	246.63	56.35
49	**190106A**	1.86	81.79	28.6
50	181213A	2.4	2342.83	689.07
51	**181110A**	1.505	63.99	25.54
52	**181020A**	2.938	55.57	14.11
53	**181010A**	1.39	93.05	38.93
54	180728A	0.117	1730.81	1549.52
55	180720B	0.654	86.45	52.27
56	**180624A**	2.855	112.24	29.12
57	**180620B**	1.1175	83.16	39.27
58	180510B	1.305	2950.1	1279.87
59	**180404A**	1.0	86.46	43.23
60	**180329B**	1.998	103.59	34.55
61	**180325A**	2.25	73.38	22.58
62	180314A	1.445	159.29	65.15
63	**180115A**	2.487	131.07	37.59
64	171222A	2.409	169.7	49.78
65	171205A	0.0368	144.69	139.55
66	171020A	1.87	144.45	50.33
67	170903A	0.886	3117.48	1652.96
68	170714A	0.793	392.71	219.02
69	**170705A**	2.01	72.29	24.02
70	170607A	0.557	73.41	47.15
71	170604A	1.329	124.72	53.55
72	**170531B**	2.366	140.9	41.86
73	170519A	0.818	80.4	44.22
74	**170405A**	3.51	120.6	26.74
75	**170202A**	3.645	72.49	15.61
76	**170113A**	1.968	58.73	19.79
77	161219B	0.1475	108.25	94.34
78	161129A	0.645	81.99	49.84
79	**161117A**	1.549	60.83	23.86
80	**161108A**	1.159	80.33	37.21
81	**161017A**	2.0127	57.66	19.14
82	**161014A**	2.823	121.8	31.86
83	160804A	0.736	147.0	84.68
84	160624A	0.483	73.72	49.71
85	160425A	0.555	203.44	130.83
86	**160410A**	1.717	82.89	30.51
87	**160327A**	4.99	60.5	10.1
88	160314A	0.726	90.95	52.69
89	160227A	2.38	151.85	44.93
90	**160203A**	3.52	137.28	30.37
91	**160131A**	0.97	69.68	35.37
92	**160121A**	1.96	91.05	30.76
93	**160117B**	0.87	54.97	29.4
94	151215A	2.59	169.12	47.11
95	151112A	4.1	3141.04	615.89

Table 1 *continued*

Table 1 *(continued)*

Table 1 *continued*

Table 1 *(continued)*

#	GRB	redshift	OTD (s)	RTD (s)
96	**151111A**	3.5	72.48	16.11
97	151031A	1.167	433.62	200.1
98	**151027B**	4.063	203.39	40.17
99	151027A	0.38	87.0	63.04
100	**151021A**	2.33	90.71	27.24
101	**150915A**	1.968	128.69	43.36
102	150910A	1.359	145.3	61.59
103	150821A	0.755	243.26	138.61
104	150818A	0.282	84.45	65.87
105	150727A	0.313	77.18	58.78
106	**150424A**	3.0	87.87	21.97
107	**150423A**	1.394	70.12	29.29
108	150413A	3.2	303300.0	72214.29
109	**150403A**	2.06	74.7	24.41
110	150323A	0.593	146.55	92.0
111	**150314A**	1.758	85.12	30.86
112	**150301B**	1.5169	82.44	32.75
113	150206A	2.087	474.54	153.72
114	150120A	0.46	76.2	52.19
115	150101B	0.093	139200.0	127355.9
116	141225A	0.915	423.51	221.15
117	**141221A**	1.452	79.47	32.41
118	**141220A**	1.3195	99.16	42.75
119	**141212A**	0.596	69.11	43.3
120	141121A	1.47	362.43	146.73
121	**141109A**	2.993	129.18	32.35
122	**141026A**	3.35	157.0	36.09
123	**141004A**	0.57	59.89	38.15
124	**140907A**	1.21	83.59	37.82
125	**140903A**	0.351	59.0	43.67
126	140710A	0.558	98.42	63.17
127	**140703A**	3.14	112.82	27.25
128	**140629A**	2.275	94.25	28.78
129	140622A	0.959	93.4	47.68
130	**140614A**	4.233	123.25	23.55
131	**140518A**	4.707	69.0	12.09
132	**140515A**	6.32	75.79	10.35
133	140512A	0.725	98.38	57.03
134	140506A	0.889	97.9	51.83
135	**140430A**	1.6	50.82	19.55
136	140423A	3.26	2943.48	690.96
137	**140419A**	3.956	86.49	17.45
138	140318A	1.02	124.75	61.76
139	140311A	4.95	9500.0	1596.64
140	**140304A**	5.283	75.18	11.97
141	**140301A**	1.416	86.07	35.62
142	140213A	1.2076	3425.34	1551.61
143	**140206A**	2.73	43.88	11.76
144	140114A	3.0	577.5	144.38
145	**131227A**	5.3	57.0	9.05
146	**131117A**	4.18	66.11	12.76
147	131105A	1.686	290.93	108.31
148	131103A	0.599	76.26	47.69
149	**131030A**	1.293	78.36	34.17

Table 1 *continued*

Table 1 *(continued)*

#	GRB	redshift	OTD (s)	RTD (s)
150	**131004A**	0.717	69.97	40.75
151	130925A	0.347	147.39	109.42
152	**130907A**	1.238	66.59	29.75
153	130831A	0.4791	125.8	85.05
154	**130701A**	1.155	85.47	39.66
155	**130612A**	2.006	86.97	28.93
156	**130610A**	2.092	132.97	43.0
157	**130606A**	5.91	72.43	10.48
158	130604A	1.06	99.27	48.19
159	**130603B**	0.356	59.05	43.55
160	**130514A**	3.6	88.83	19.31
161	**130511A**	1.3033	71.58	31.08
162	**130505A**	2.27	96.37	29.47
163	**130427B**	2.78	77.37	20.47
164	130427A	0.34	140.19	104.62
165	130420A	1.297	735.33	320.13
166	130418A	1.218	129.7	58.48
167	**130408A**	3.758	149.89	31.5
168	**130131B**	2.539	109.46	30.93
169	**121229A**	2.707	145.9	39.36
170	121211A	1.023	89.52	44.25
171	**121201A**	3.385	115.07	26.24
172	**121128A**	2.2	77.17	24.12
173	**121027A**	1.773	67.38	24.3
174	**121024A**	2.298	93.0	28.2
175	**120922A**	3.1	116.42	28.4
176	**120909A**	3.93	93.42	18.95
177	**120907A**	0.97	82.02	41.63
178	120815A	2.358	2686.79	800.12
179	**120811C**	2.671	68.67	18.71
180	**120805A**	3.1	123.11	30.03
181	**120802A**	3.796	84.78	17.68
182	**120729A**	0.8	68.12	37.84
183	120724A	1.48	109.1	43.99
184	120722A	0.9586	152.97	78.1
185	120714B	0.3984	120.07	85.86
186	**120712A**	4.0	90.86	18.17
187	**120521C**	6.0	69.11	9.87
188	120422A	0.28	95.07	74.27
189	**120404A**	2.876	130.02	33.54
190	**120327A**	2.81	75.61	19.85
191	**120326A**	1.798	59.54	21.28
192	**120119A**	1.728	53.29	19.53
193	**120118B**	2.943	112.09	28.43
194	**111229A**	1.3805	83.28	34.98
195	111228A	0.714	145.07	84.64
196	111225A	0.297	88.14	67.96
197	111209A	0.677	418.89	249.79
198	**110503A**	1.613	93.63	35.83
199	110422A	1.77	814.5	294.04
200	**110213A**	1.46	91.74	37.29
201	110205A	1.98	155.4	52.15
202	**110128A**	2.339	140.47	42.07
203	101225A	0.847	1383.04	748.8

Table 1 *continued*

Table 1 *(continued)*

#	GRB	redshift	OTD (s)	RTD (s)
204	101219B	0.5519	542.7	349.7
205	101219A	0.718	221.92	129.17
206	**100906A**	1.727	80.24	29.42
207	100902A	4.5	316.15	57.48
208	100901A	1.408	156.97	65.19
209	100816A	0.8034	82.85	45.94
210	**100814A**	1.44	87.31	35.78
211	**100728B**	2.8	97.05	25.54
212	**100728A**	1.567	76.72	29.89
213	**100724A**	1.288	88.9	38.85
214	100621A	0.542	76.03	49.31
215	**100615A**	1.398	62.4	26.02
216	**100513A**	4.772	126.77	21.96
217	**100425A**	1.755	78.81	28.61
218	**100424A**	2.465	119.81	34.58
219	100418A	0.6235	79.13	48.74
220	100316D	0.014	137.67	135.77
221	**100316B**	1.18	64.09	29.4
222	**100302A**	4.813	125.47	21.58
223	**100219A**	4.5	178.56	32.47
224	091208B	1.063	115.14	55.81
225	091127	0.49	3214.62	2157.46
226	**091109A**	3.5	150.68	33.48
227	**091029**	2.752	79.88	21.29
228	091024	1.092	3192.0	1525.81
229	**091020**	1.71	81.5	30.07
230	**091018**	0.971	61.49	31.2
231	090927	1.37	2136.98	901.68
232	**090926B**	1.24	88.76	39.62
233	090814A	0.696	159.3	93.93
234	**090812**	2.452	76.82	22.25
235	**090809**	2.737	104.02	27.84
236	090726	2.71	3061.74	825.27
237	**090715B**	3.0	46.25	11.56
238	090618	0.54	120.9	78.51
239	090529	2.625	197.09	54.37
240	**090519**	3.9	114.92	23.45
241	**090516A**	4.109	170.0	33.27
242	090510	0.903	94.1	49.45
243	**090429B**	9.4	104.69	10.07
244	**090426**	2.609	84.62	23.45
245	090424	0.544	84.46	54.7
246	**090423**	8.0	72.48	8.05
247	**090418A**	1.608	96.1	36.85
248	**090407**	1.4485	93.04	38.0
249	**090205**	4.7	87.61	15.37
250	**090113**	1.7493	70.91	25.79
251	090102	1.547	387.21	152.03
252	**081222**	2.7	51.75	13.99
253	**081221**	2.26	68.4	20.98
254	**081203A**	2.1	83.1	26.81
255	081121	2.512	2813.2	801.03
256	**081118**	2.58	153.3	42.82
257	081029	3.8479	2702.93	557.55

Table 1 *continued*

Table 1 *(continued)*

#	GRB	redshift	OTD (s)	RTD (s)
258	081028A	3.038	190.7	47.23
259	**081008**	1.9685	87.15	29.36
260	081007	0.5295	99.35	64.96
261	080928	1.692	169.7	63.04
262	**080916A**	0.689	70.21	41.57
263	**080913**	6.44	99.49	13.37
264	**080906**	2.0	71.27	23.76
265	**080905B**	2.374	103.21	30.59
266	080905A	0.1218	130.38	116.22
267	**080810**	3.35	76.0	17.47
268	**080804**	2.2045	99.04	30.91
269	**080721**	2.602	108.03	29.99
270	080710	0.845	3131.59	1697.34
271	**080707**	1.23	68.29	30.62
272	**080607**	3.036	82.13	20.35
273	**080605**	1.6398	90.39	34.24
274	080604	1.416	119.29	49.38
275	**080603B**	2.69	61.77	16.74
276	**080520**	1.545	99.53	39.11
277	**080516**	3.2	82.9	19.74
278	**080430**	0.75	48.87	27.93
279	080413B	1.1	131.25	62.5
280	**080413A**	2.433	60.67	17.67
281	**080411**	1.03	70.15	34.56
282	**080330**	1.51	70.54	28.1
283	080319C	1.95	223.69	75.83
284	**080319B**	0.937	60.47	31.22
285	**080310**	2.4266	89.21	26.03
286	**080210**	2.641	157.12	43.15
287	**080207**	2.0858	124.05	40.2
288	071227	0.383	79.09	57.19
289	071122	1.14	139.8	65.33
290	071117	1.331	2848.0	1221.79
291	071112C	0.823	83.6	45.86
292	**071031**	2.692	102.8	27.84
293	**071021**	2.452	130.5	37.8
294	**071020**	2.145	61.24	19.47
295	071010B	0.947	92631.04	47576.29
296	**070802**	2.45	137.92	39.98
297	070724A	0.457	66.76	45.82
298	**070714B**	0.92	61.37	31.96
299	070611	2.04	3287.17	1081.31
300	**070529**	2.4996	130.96	37.42
301	070521	0.553	76.89	49.51
302	**070508**	0.82	75.92	41.71
303	**070506**	2.31	126.99	38.37
304	070429B	0.904	256.26	134.59
305	070419A	0.97	112.89	57.3
306	**070411**	2.954	96.48	24.4
307	**070318**	0.836	63.58	34.63
308	070208	1.165	115.48	53.34
309	**070129**	2.3384	133.69	40.05
310	**070110**	2.352	93.44	27.88
311	**070103**	2.6208	68.63	18.95

Table 1 *continued*

Table 1 *(continued)*

#	GRB	redshift	OTD (s)	RTD (s)
312	**061222B**	3.355	145.08	33.31
313	**061222A**	2.088	101.02	32.71
314	**061217**	0.827	64.0	35.03
315	061201	0.111	81.32	73.2
316	**061121**	1.314	55.4	23.94
317	061110B	3.44	3042.21	685.18
318	**061110A**	0.758	69.22	39.37
319	061021	0.3463	72.79	54.07
320	**061007**	1.261	80.45	35.58
321	**060927**	5.6	64.72	9.81
322	**060926**	3.208	59.95	14.25
323	**060908**	1.8836	71.68	24.86
324	**060906**	3.685	148.51	31.7
325	**060904B**	0.703	68.81	40.41
326	**060814**	0.84	71.54	38.88
327	060729	0.54	124.39	80.77
328	060719	1.532	128.76	50.85
329	**060714**	2.71	99.0	26.68
330	**060708**	2.3	62.3	18.88
331	**060707**	3.43	120.51	27.2
332	060614	0.13	91.4	80.88
333	**060607A**	3.082	65.2	15.97
334	**060605**	3.8	92.39	19.25
335	**060604**	2.1357	108.83	34.71
336	**060526**	3.21	73.23	17.39
337	**060522**	5.11	144.4	23.63
338	060512	0.4428	101.77	70.54
339	**060510B**	4.9	118.81	20.14
340	060502B	0.287	70.27	54.6
341	**060502A**	1.51	76.29	30.39
342	**060418**	1.49	77.97	31.31
343	**060223A**	4.41	85.93	15.88
344	060218	0.0331	153.08	148.18
345	**060210**	3.91	94.95	19.34
346	**060206**	4.045	58.35	11.57
347	**060124**	2.3	106.12	32.16
348	**060116**	4.0	153.52	30.7
349	**060115**	3.53	112.62	24.86
350	**060108**	2.03	91.4	30.17
351	051221A	0.547	88.0	56.88
352	051117B	0.481	134.78	91.01
353	051109B	0.08	86.22	79.83
354	**051109A**	2.346	119.66	35.76

REFERENCES

Aimuratov, Y., Becerra, L. M., Bianco, C. L., et al. 2023, ApJ, 955, 93, doi: 10.3847/1538-4357/ace721

Alexeyev, E. N., Alexeyeva, L. N., Krivosheina, I. V., & Volchenko, V. I. 1988, Physics Letters B, 205, 209, doi: 10.1016/0370-2693(88)91651-6

Amati, L., O'Brien, P., Götz, D., et al. 2018, Advances in Space Research, 62, 191, doi: 10.1016/j.asr.2018.03.010

Amati, L., O'Brien, P. T., Götz, D., et al. 2021, Experimental Astronomy, 52, 183, doi: 10.1007/s10686-021-09807-8

Arnett, W. D., Bahcall, J. N., Kirshner, R. P., & Woosley, S. E. 1989, ARA&A, 27, 629, doi: 10.1146/annurev.aa.27.090189.003213

Becerra, L., Bianco, C. L., Fryer, C. L., Rueda, J. A., & Ruffini, R. 2016, ApJ, 833, 107, doi: 10.3847/1538-4357/833/1/107

Becerra, L., Ellinger, C. L., Fryer, C. L., Rueda, J. A., & Ruffini, R. 2019, ApJ, 871, 14, doi: 10.3847/1538-4357/aaf6b3

Becerra, L. M., Moradi, R., Rueda, J. A., Ruffini, R., & Wang, Y. 2022, PhRvD, 106, 083002, doi: 10.1103/PhysRevD.106.083002

Bionta, R. M., Blewitt, G., Bratton, C. B., et al. 1987, PhRvL, 58, 1494, doi: 10.1103/PhysRevLett.58.1494

Costa, E., & Frontera, F. 2011, Nuovo Cimento Rivista Serie, 34, 585, doi: 10.1393/ncr/i2011-10069-0

Cucchiara, A., Levan, A. J., Fox, D. B., et al. 2011, ApJ, 736, 7, doi: 10.1088/0004-637X/736/1/7

Frontera, F. 2019, Rendiconti Lincei. Scienze Fisiche e Naturali, 30, 171, doi: 10.1007/s12210-019-00766-z

Fryer, C. L., Oliveira, F. G., Rueda, J. A., & Ruffini, R. 2015, Physical Review Letters, 115, 231102, doi: 10.1103/PhysRevLett.115.231102

Fryer, C. L., Rueda, J. A., & Ruffini, R. 2014, ApJL, 793, L36, doi: 10.1088/2041-8205/793/2/L36

Fu, S. Y., Zhu, Z. P., Xu, D., Liu, X., & Jiang, S. Q. 2022, GRB Coordinates Network, 31353, 1

Fynbo, J. P. U., de Ugarte Postigo, A., Xu, D., et al. 2022, GRB Coordinates Network, 31359, 1

Galama, T. J., Vreeswijk, P. M., van Paradijs, J., et al. 1998, Nature, 395, 670, doi: 10.1038/27150

Gehrels, N., Chincarini, G., Giommi, P., et al. 2004, ApJ, 611, 1005, doi: 10.1086/422091

Hirata, K., Kajita, T., Koshiba, M., et al. 1987, PhRvL, 58, 1490, doi: 10.1103/PhysRevLett.58.1490

Li, L., Rueda, J. A., Moradi, R., et al. 2023, ApJ, 945, 10, doi: 10.3847/1538-4357/acb20b

Madau, P., & Dickinson, M. 2014, ARA&A, 52, 415, doi: 10.1146/annurev-astro-081811-125615

Moradi, R., Rueda, J. A., Ruffini, R., & Wang, Y. 2021, A&A, 649, A75, doi: 10.1051/0004-6361/201937135

Patat, F., Cappellaro, E., Danziger, J., et al. 2001, ApJ, 555, 900, doi: 10.1086/321526

Perley, D. A. 2022, GRB Coordinates Network, 31357, 1

Perley, D. A., Gal-Yam, A., Irani, I., & Zimmerman, E. 2023, Transient Name Server AstroNote, 119, 1

Rueda, J. A., Li, L., Moradi, R., et al. 2022a, ApJ, 939, 62, doi: 10.3847/1538-4357/ac94c9

Rueda, J. A., & Ruffini, R. 2012, ApJL, 758, L7, doi: 10.1088/2041-8205/758/1/L7

—. 2020, European Physical Journal C, 80, 300, doi: 10.1140/epjc/s10052-020-7868-z

Rueda, J. A., Ruffini, R., & Kerr, R. P. 2022b, ApJ, 929, 56, doi: 10.3847/1538-4357/ac5b6e

Rueda, J. A., Ruffini, R., Li, L., et al. 2022c, PhRvD, 106, 083004, doi: 10.1103/PhysRevD.106.083004

Ruffini, R., Karlica, M., Sahakyan, N., et al. 2018a, ApJ, 869, 101, doi: 10.3847/1538-4357/aaeac8

Ruffini, R., Izzo, L., Muccino, M., et al. 2014, A&A, 569, A39, doi: 10.1051/0004-6361/201423457

Ruffini, R., Rodriguez, J., Muccino, M., et al. 2018b, ApJ, 859, 30, doi: 10.3847/1538-4357/aabee4

Ruffini, R., Wang, Y., Aimuratov, Y., et al. 2018c, ApJ, 852, 53, doi: 10.3847/1538-4357/aa9e8b

Ruffini, R., Moradi, R., Rueda, J. A., et al. 2019, ApJ, 886, 82, doi: 10.3847/1538-4357/ab4ce6

—. 2021, MNRAS, 504, 5301, doi: 10.1093/mnras/stab724

Salvaterra, R., Della Valle, M., Campana, S., et al. 2009, Nature, 461, 1258, doi: 10.1038/nature08445

Tamagawa, T., Kawai, N., Yoshida, A., et al. 2003, in International Cosmic Ray Conference, Vol. 5, International Cosmic Ray Conference, 2741

Tanvir, N. R., Fox, D. B., Levan, A. J., et al. 2009, Nature, 461, 1254, doi: 10.1038/nature08459

Wang, Y., Becerra, L. M., Fryer, C. L., Rueda, J. A., & Ruffini, R. 2023, ApJ, 945, 95, doi: 10.3847/1538-4357/acb771

Wang, Y., Rueda, J. A., Ruffini, R., et al. 2022, ApJ, 936, 190, doi: 10.3847/1538-4357/ac7da3

Yaron, O., Bruch, R., Chen, P., et al. 2023, Transient Name Server AstroNote, 133, 1